

Characterisation of Multipotential Stromal Cells (MSCs) from Subchondral
Bone in Ankle Osteoarthritis and their Biological Modulation Towards
Chondrogenesis Enhancement

William G. Jones

Submitted in accordance with the requirements for the degree of Doctor of Philosophy

The University of Leeds

Faculty of Mechanical Engineering

June 2021

The candidate confirms that the work submitted is his own, except where work which has formed part of jointly authored publications has been included. The contribution of the candidate and the other authors to this work has been explicitly indicated below. The candidate confirms that appropriate credit has been given within the thesis where reference has been made to the work of others. The work in Chapter 3 and 4 of the thesis have appeared in publication as follows:

Multipotential stromal cells in the talus and distal tibia in ankle osteoarthritis - Presence, potency and relationships to subchondral bone changes. *Journal for Cellular and Molecular Medicine*. January 2021.

I was responsible for: Conceptualization (equal); Data curation (lead); Formal analysis (equal); Funding acquisition (equal); Investigation (lead); Methodology (lead); Software (equal); Validation (equal); Visualization (equal); Writing-original draft (Lead); Writing-review & editing (equal)

Work attributed to others: Conceptualisation (JEJ, CLB, EJ) Methodology (Supporting, LK) Software (Supporting, LK) Data Curation (JEJ, EJ) Resources (JEJ, IK, EJ) Supervision (JEJ, CLB, EJ) Writing and Editing (JEJ) Project Administration (CLB, EJ), Formal Analysis (EJ), Funding Acquisition (EJ), Writing-original draft (EJ, supporting); Writing-review & editing (EJ).

This copy has been supplied on the understanding that it is copyright material and that no quotation from the thesis may be published without proper acknowledgement.

© 2021 The University of Leeds and William Jones

List of Figures

Figure 1.1.1 Medial view of the lower leg, with nomenclature of the bones.	25
Figure 1.1.2 Anterior view of the bones of the lower leg.	26
Figure 1.1.3 Facets of articulation and Anatomical Landmarks of Talus and Tibia..	27
Figure 1.1.4 Zonal Variation of Hyaline Articular Cartilage.....	28
Figure 1.1.5 Typical Structure of the Proteoglycan-Hyaluronan complex.	32
Figure 1.2.1 The Oblique Transverse Axis of the Talocrural Joint.....	34
Figure 1.2.2 Illustration of the 6 Major Rotations of the Ankle.....	34
Figure 1.2.3 The Typical Human Gait Cycle.....	35
Figure 1.3.1 The differentiation pathways of the MSC, including formation of muscle, bone, cartilage, fat and other tissues.	37
Figure 1.5.1 Arthroscopic debridement of osteochondral lesion of the talus.....	45
Figure 1.5.2 Microfracture with healthy cartilage border	47
Figure 1.5.3 Apparatus used in immobile ankle joint distraction aiming to hold the tibia and talus in place to prevent opposing articular surface contact.	48
Figure 1.6.1 The Diamond Concept for Regenerative Therapies.	53
Figure 2.3.1 MSC Extraction Process of Talar and Tibial MSCs.	66
Figure 2.4.1 Haemocytometer view under microscope, showing counting squares	67
Figure 2.6.1 Simplified qPCR Process.....	70
Figure 3.2.1 Calculation of BA/TA. Safranin O stained images are converted into black and white in ImageJ..	90
Figure 3.2.2 Demonstration of CD271 Area of Total Area Measurements, and alignment with Bone Area of Total Area Measurements.	93
Figure 3.2.3 Porcine Tissue Dissection and Experimental Protocol for Method Development for Mechanical Testing of Human Explants from Ankle Fusion surgery.....	96
Figure 3.2.4 Calibration Charts for Indentation Apparatus.	98
Figure 3.2.5 Indentation Rig Example	98
Figure 3.2.6 Indentation Rig for Cartilage Needle Indentation	99
Figure 3.2.7 Resistive Load Profile of Cartilage During Needle Indentation.....	99
Figure 3.3.1 The Distal Tibia and Talus – Retrieved Sample Morphology.	102
Figure 3.3.2 Morphological changes of OA visible by mCT on proximal talus and distal tibia.	103
Figure 3.3.3 Quantification of mCT of Talus and Distal Tibia in OA and Health	104
Figure 3.3.4 Decalcification Rates of Formalin-Fixed Tibia and Talar Segments in EDTA.....	106
Figure 3.3.5 The Morphological OA Changes seen in Distal Tibia and Talus Samples Retrieved from Ankle Fusion Surgery, Shown by Haematoxylin and Eosin Staining.	107

Figure 3.3.6 OA Morphological Changes in Distal Tibia and Talus by Safranin O Staining in End-Stage Osteoarthritis.....	108
Figure 3.3.7 Evaluation of OA Ankle Sample Histology by OARSI Scoring.	109
Figure 3.3.8 Relationships between Cartilage and Bone Changes Between High and Low Grade Damage Regions in OA Talus and Tibia.....	110
Figure 3.3.9 CD271 Antibody Positive Topography in the Distal Tibia and Talus.	112
Figure 3.3.10 High Magnification Images of CD271 Immunohistochemistry of MSCs and Association with Cartilage and Bone Changes, comparing bone regions of grade 3 or grade 5 cartilage damage between talus and tibia.....	113
Figure 3.3.11 Relationships between CD271-Positive Cells and Bone Behaviour.	114
Figure 3.3.12 Quantified Analysis of CD271+ Staining for Endogenous Multipotential Stromal Cells with the Osteoarthritic Human Talus and Tibia.	115
Figure 3.3.13 Osteoclast Behaviour in the Osteoarthritic Talus and Tibia by Tartrate Resistant Acid Phosphatase staining.	116
Figure 3.3.14 Representative Picosirius Red Staining (A) and Analysis (B and C) of Proximal Talus of ankle OA.....	117
Figure 3.3.15 Picosirius Red Analysis of Proximal Talus of ankle OA patients	118
Figure 3.3.16 Investigation of Potential Cells Involved in New Bone Synthesis through CD56 and E11.	119
Figure 3.3.17 Assessment of Cartilage Displacement in Porcine Talar Samples with Minimal Bone.	120
Figure 3.3.18 Assessment of Cartilage Thickness in Porcine Talar Samples with Minimal Bone. Control and freeze-thaw samples had a minimum of 6cm underlying bone, as typical in cartilage thickness studies.	121
Figure 4.2.1 ImageJ Selection of Adipocytes.	141
Figure 4.3.1 MSCs 2D in culture following isolation from bone..	143
Figure 4.3.2 Changes to Talar and Tibial Plastic-Adherent Cell Morphology During P0-P3 Culture..	144
Figure 4.3.3 Cell Egression from Enzymatically Treated Bone.....	145
Figure 4.3.4 Colony Forming Unit Fibroblast Assay of Plastic-Adherent Putative MSCs from Talus, Tibia and IC Enzymatic Digests.....	146
Figure 4.3.5 Estimation of Plastic-Adherent Putative MSC Content in Surgically-Retrieved Bone Samples of Talus, Tibia and IC by CFU-F Assay	147
Figure 4.3.6 Colony Characteristics of Plastic-Adherent Putative MSCs Isolated from Distal Tibia, Talus and IC.....	148

Figure 4.3.7 Population Doubling Times of Plastic-Adherent Putative MSCs from Passage 0 to Passage 3 from Distal Tibia, Talus and IC.....	149
Figure 4.3.8 Gating Strategy for Characterisation of Surface Phenotype of Cultured Cells Isolated by Enzymatic Extraction from Talar, Tibial and IC Bone. Red events denote cellular events, and purple the isotype control events.....	150
Figure 4.3.9 Surface phenotype of isolated cells from talus, tibia and IC after culture to passage 2 by flow cytometry	151
Figure 4.3.10 Morphology of Adipogenic and Osteogenic Differentiation Cultures at 21 Days of Culture in Osteogenic and Adipogenic Media of Distal Tibia, Talus and IC MSC cultures.....	152
Figure 4.3.11 Alkaline Phosphatase (ALP) Activity in Talar, Tibial and IC Cultures Initiated by Passage 3 Putative MSCs Grown in either Osteogenic or Expansion Media after 14 Days Culture	153
Figure 4.3.12 Alizarin Red Staining of Cultures from Distal Tibia, Talus and IC from Putative MSCs after 21 Days Growth in Osteogenic or Expansion (negative control) Media	154
Figure 4.3.13 Quantitative Assessment of Calcium Deposition of MSCs from Distal Tibia, Talus and IC Cultures after 21 Days Culture of Putative MSCs in Osteogenic or Expansion (negative control) Media	155
Figure 4.3.14 Oil Red O Staining of Talar, Tibial and IC Cultures After 21 Days Culture in Adipogenic Medium or Negative Expansion Control of Putative MSCs	156
Figure 4.3.15 Nile Red Staining of Talar, Tibial and IC Cultures After 21 Days Culture in Adipogenic Medium or Negative Expansion Control of Putative MSCs..	157
Figure 4.3.16 Quantification of Adipogenesis by Putative MSCs from Distal Tibia, Talus and IC after 21 Days Culture in Adipogenic Medium or Expansion Media as Negative Control	159
Figure 4.3.17 Chondrogenic Pellets After 21 Days of Talar, Tibial or IC Putative MSC Culture in Chondrogenic Media or Negative Control in Expansion Media.....	160
Figure 4.3.18 Diameter of Putative MSC pellets from Talus, Tibia and IC After 21 Day Culture in Chondrogenic Medium or Negative Control Expansion Media	160
Figure 4.3.19 GAG Concentration of Talar, Tibial and IC Cultures After 21 Day Growth in Chondrogenic Medium or Negative Control Expansion Media	161
Figure 4.3.20 Relationships of Relative Differentiation Capacity for Adipogenesis, Chondrogenesis and Osteogenesis in Tibia, Talus and IC.	162
Figure 5.1.1 Extraction of PRP from human blood.	174
Figure 5.2.1 Preconditioning methodology including revival, adherence, culture and testing steps.....	178
Figure 5.3.1 Effects of Different Biological Stimulants upon Cellular Morphology After 7 Days Preconditioning.....	181

Figure 5.3.2 The Effect of Different Biological Stimulants Upon MSC Circularity after 7-day culture.....	182
Figure 5.3.3 Changes in ALP Expression by IC MSC Colonies after 14 Day Preconditioning with Different Stimulants as a Comparator for Differentiation Capacity.	183
Figure 5.3.4 ALP Staining of MSCs after Preconditioning in Various Biological Stimulants Under Microscope.....	184
Figure 5.3.5 Comparison of ALP-Positive MSC Integrated Density Between IC MSCs Treated with Different Stimuli.....	185
Figure 5.3.6 Toluidine Blue Staining of ALP-Stained IC MSC Colonies after 14 Day Stimulation with Various Biological Stimulants.....	186
Figure 5.3.7 Quantification of Toluidine Blue Stained MSC Colonies Between IC MSCs Treated with Different Stimuli.	187
Figure 5.3.8 Assessment of ALP Colony Area of Toluidine Blue Area to Estimate Relative Differentiation Potential of MSCs after Preconditioning in Different Media.	188
Figure 5.3.9 Estimation of Isolated RNA Concentration Following Preconditioning in Various Biological Stimuli.....	189
Figure 5.3.10 Expression of Genes Related to Chondrogenesis in IC MSCs after 14 Day Preconditioning in Various Stimulants.....	191
Figure 5.3.11 Expression of Genes Related to Osteogenesis in IC MSCs after 14 Day Preconditioning in Various Stimulants.....	193
Figure 5.3.12 Expression of Genes Related to Osteogenesis in IC MSCs after 14 Day Preconditioning in Various Stimulants.....	194
Figure 6.3.1 Fibrin Alginate Bead Structure After Synthesis.....	214
Figure 6.3.2 FA Bead Diameter and Sphericity	215
Figure 6.3.3 Characterising the Swelling Ratio of Fibrin Alginate by Weight After Freeze-Drying in PBS	215
Figure 6.3.4 Fibrin Alginate Structure During Culture Over 14 Days in DMEM..	216
Figure 6.3.5 Figure 6.3.1 Change in FA Weight Over Culture	216
Figure 6.3.6 Effect of Fibrin Alginate on MSC Viability by Indirect Toxicity Assay.....	217
Figure 6.3.7 FA Bead and MSC Behaviour after 48 Hour Culture in StemMACS	218
Figure 6.3.8 MSC Appearance in Fibrin Alginate Beads Grown in C, PL or K at 7 Days after 14 Day Preconditioning in C, PL, or K.....	219
Figure 6.3.9 Analysis of Burst FA Cultures	220
Figure 6.3.10 Methylene Blue Staining of FA Beads After 14 Days Culture.....	221
Figure 6.3.11 Toluidine Blue Staining of FA Beads.....	222

Figure 6.3.12 Pellet and Media from IC MSCs Preconditioned in K or PL for 14 Days Before 3D Culture in Pellets in K, PL or C	224
Figure 6.3.13 Toluidine Blue Staining of Chondrogenic Pellets Demonstrating GAG Deposition	225
Figure 6.3.14 Diameter of IC Pellets after 2 Week Preconditioning with K or PL, and 3 Week 3D Culture with K, PL or C	226
Figure 6.3.15 GAG Content of IC MSC Pellets after K or PL Preconditioning for 2 Weeks and Differentiation in C, K or PL in Pellets for 3 Weeks	227
Figure 6.3.16 GAG Content of Media from IC MSC Cultures after K or PL Preconditioning for 2 Weeks and Differentiation in C, K or PL in Pellets for 3 Weeks	228
Figure 6.3.17 Ratio of GAGs Retained in the Pellet to Total GAG in IC MSC Cultures, after K or PL Preconditioning for 2 Weeks and Differentiation in C, K or PL in Pellets for 3 Weeks	229
Figure 6.3.18 Gene Expression of IC MSCs Preconditioned for 2 Weeks PL and Differentiated in PL or C	230
Figure 6.3.19 The Effect on Gene Expression of IC MSCs after PL or K Preconditioning followed by Pellet Culture in C	231
Figure 6.3.20 The Effect on Gene Expression of Preconditioning in PL or K followed by Pellet Culture in PL or C for Donor RC071	232
Figure 6.3.21 Talar and Tibial MSC Chondrogenic Pellets After Preconditioning in K or PL, and 3D treatment in C, K or PL	234
Figure 6.3.22 Pellet Diameter of Distal Tibial and Talar MSC Cultures, after K or PL Preconditioning for 2 Weeks and Differentiation in C, K or PL for 3 Weeks	235
Figure 6.3.23 GAG Content of Pellets from Distal Tibial and Talar MSC Cultures, after K or PL Preconditioning for 2 Weeks and Differentiation in C, K or PL for 3 Weeks	236
Figure 6.3.24 GAG Content of Media from Distal Tibial and Talar MSC Cultures, after K or PL Preconditioning for 2 Weeks and Differentiation in C, K or PL in Pellets for 3 Weeks	237
Figure 6.3.25 Ratio of GAGs Retained in the Pellet to Total GAG in Distal Tibial and Talar MSC Cultures, after K or PL Preconditioning for 2 Weeks and Differentiation in C, K or PL in Pellets for 3 Weeks	238

List of Tables

Table 1.1 Regenerative Therapies for OA	50
Table 1.2 The Effect of Mechanical Stimulation Upon MSCs	56
Table 2.1 Distal Tibia and Talus Sample Characteristics Retrieved from Ankle Fusion	60
Table 2.2 Distal Tibia and Talus Sample Characteristics from Healthy Donor Tissue	61
Table 2.3 Fresh Iliac Crest Sample Characteristics	61
Table 2.4 Frozen Iliac Crest Sample Characteristics	61

Table 2.5 Paraffin Embedding Process.....	63
Table 2.6 Deparaffinisation and rehydration protocol	64
Table 2.7 Dehydration and Cover slipping.....	65
Table 2.8 Reverse Transcription Protocol.....	72
Table 2.9 TaqMan Probes Pooled for Pre-Amplification	73
Table 2.10 Pre-Amplification Protocol.....	73
Table 2.11 qPCR Protocol.....	74
Table 2.12 Choice of Statistical Test for Each Dataset.....	76
Table 3.1 Distal Tibia and Talus Sample Characteristics Retrieved from Ankle Fusion	83
Table 3.2 Distal Tibia and Talus Sample Characteristics Of Non-Diseased Donor Tissue	83
Table 3.3 Haemotoxylin and Eosin Staining Process.....	85
Table 3.4 Safranin O Staining Process.....	86
Table 3.5 OARSI Stage of Osteoarthritis Assessment	87
Table 3.6 Cartilage Histopathology Grade Assessment	87
Table 3.7 CD271 Immunohistochemistry Staining Process	92
Table 3.8 Tartrate-Resistant Acid Phosphatase Staining Process.....	94
Table 3.9 Picrosirius Staining Process	95
Table 3.10 Average Size of Non-Diseased Human Ankle Samples.....	101
Table 3.11 Average Size of Human OA Ankle Fusion Samples.....	101
Table 4.1 Distal Tibia and Talus Sample Characteristics Retrieved from Ankle Fusion	132
Table 4.2 Fresh IC Sample Characteristics	132
Table 4.3 Flow Cytometry Antibody Details	136
Table 4.4 Choice of Statistical Test for Each Dataset.....	142
Table 5.1 Donor Information for MSCs used in Preconditioning Experiments.....	176
Table 5.2 Donor Information for Pooled Human Serum.....	177
Table 5.3 Culture Condition Shorthand and Media Composition.....	178
Table 5.4 Genes Measured by qPCR of Preconditioned Samples.....	180
Table 6.1 Common Biomaterials Used for Cartilage Synthesis.....	202
Table 6.2 Distal Tibia and Talus Sample Characteristics Retrieved from Ankle Fusion	206
Table 6.3 IC Sample Characteristics Used for Preconditioning with 3D Treatment	206
Table 6.4 Preconditioning and Differentiation Media for IC, Talar and Tibial MSCs	210
Table 6.5 Genes used for qPCR of 3D Treatments.....	212
Table 6.6 Toluidine Staining Protocol	213
Table 6.7 Summary of IC Pellet Chondrogenic Results After Preconditioning and Differentiation	244
Table 6.8 Summary of Talocrural Pellet Chondrogenic Results.....	247

1. Table of Contents

1. Chapter 1 Introduction	24
1.1. Anatomy of the Ankle	25
1.1.1. Whole Structure.....	25
1.1.2. The Talocrural Joint.....	26
1.1.3. The Subtalar Joint.....	26
1.1.4. The Talonavicular Joint	26
1.1.5. The Tibio-Fibular Syndesmosis.....	27
1.1.6. Talocrural Joint Bone Anatomy.....	27
1.1.7. Cartilage	28
1.1.8. Subchondral Bone	30
1.1.9. Extracellular Matrix Proteins	32
1.2. Biomechanics of the Ankle.....	34
1.2.1. Common Biomechanics.....	34
1.2.2. Prevalent Loading and Abnormalities.....	35
1.3. MSC Characteristics, Localisation and Roles	37
1.4. OA of the Ankle	40
1.4.1. Prevalence.....	40
1.4.2. Current Understanding of Progression	41
1.5. Treatments of Ankle OA.....	44
1.5.1. Conservative and Early-Stage Therapies.....	44
1.5.2. Non-Regenerative Surgical Treatments	45
1.5.3. Regenerative Therapies	47
1.5.4. Potential MSC Based Treatments	51
1.6. Current Areas of Regenerative Therapy Development for MSC Enhancement	53
1.6.1. Impact of the Scaffold on MSC Behaviour	53
1.6.2. Growth Factors in MSC Differentiation.....	54

1.6.3.	Mechanical Stimulation Effect on MSCs	55
1.7.	Current Challenges of the Research Area	57
1.8.	Thesis Aims and Objectives.....	58
2.	Chapter 2 - General Materials and Methods	59
2.1.	Sample Retrieval and General Processing	60
2.2.	Sample Processing for Histology.....	62
2.2.1.	Decalcification Process.....	62
2.2.2.	Tissue Processing and Paraffin and Embedding.....	62
2.2.3.	sectioning and Baking	63
2.2.4.	Deparaffinisation and Rehydration.....	64
2.2.5.	Dehydration and Application of Coverslips.....	64
2.3.	Cell Extraction from Bone using Collagenase	65
2.3.1.	Sterilisation of Solutions and Equipment.....	65
2.3.2.	Collagenase Extraction of MSCs.....	65
2.4.	General Cell Techniques.....	67
2.4.1.	Cell Seeding.....	67
2.4.2.	Counting of Cells by Haemocytometer	67
2.4.3.	Trypsinisation of Adherent MSCs.....	67
2.4.4.	Freezing of Enzymatically Released MSCs for Long-term Storage.....	68
2.4.5.	Freezing of Cultured MSCs for Long-Term Storage.....	68
2.4.6.	Passaging of Enzymatically Released MSCs in Culture.....	68
2.4.7.	Thawing of Cultured Cells	69
2.4.8.	Thawing of Primary Uncultured Cells.....	69
2.5.	Assessment of Genomic Content using the Nanodrop.....	69
2.5.1.	DNA Content	69
2.5.2.	RNA Content.....	69
2.6.	Reverse Transcribed Real-time Polymerase Chain Reaction	70
2.6.1.	General Theory.....	70
2.6.2.	Cell Lysis	71

2.6.3.	RNA Extraction	72
2.6.4.	Reverse Transcription	72
2.6.5.	Pre-amplification.....	73
2.6.6.	Performing qPCR Using the Fluidigm/BioMark System	73
2.6.7.	Post-qPCR Run Analysis.....	74
2.7.	Imaging.....	75
2.7.1.	Gross Tissue	75
2.7.2.	Histological Sections	75
2.7.3.	Live Cell Imaging During Culture and Cell Culture Image Scans	75
2.8.	Statistics	76
2.8.1.	Assessment of Normality	76
2.8.2.	Choice of Statistical Test	76
3.	Chapter 3 – Characterisation of Osteoarthritic Changes to the Distal Tibia and Talus of the Ankle Joint, and the Relationship between Bone, Cartilage and Cell Behaviour.....	78
3.1.	Introduction	79
3.2.	Specific Methods.....	82
3.2.1.	Sample Information	82
3.2.2.	mCT of Tissues.....	83
3.2.3.	Haemotoxylin and Eosin Staining.....	85
3.2.4.	Safranin O Staining.....	86
3.2.5.	OARSI Scoring for the Degree of Cartilage Damage.....	86
3.2.6.	Bone Area of Total Area Measurements	89
3.2.7.	Subchondral Bone Plate Thickness Measures.....	90
3.2.8.	CD271 Staining	91
3.2.9.	CD271 Localisation Measurements	93
3.2.10.	Tartrate-Resistant Acid Phosphatase Staining.....	94
3.2.11.	Picrosirius Red Staining	95
3.2.12.	CD56 and E11 Staining	95
3.2.13.	Collection of Osteochondral Plugs from Porcine Tissue	95

3.2.14.	Indentation of Ankle Cartilage to Measure Cartilage Properties.....	97
3.2.15.	Needle Indentation of Ankle Cartilage to Measure Cartilage Thickness	98
3.3.	Results.....	100
3.3.1.	Morphological Changes during OA of the Talus and Distal Tibia.....	100
3.3.2.	Investigating Relationships Between Bone Changes and Cellular activity	111
3.3.3.	Uncovering the Driving Force of New Bone Formation in OA Talus and Tibia .	116
3.3.4.	Developing Methods to Quantify Cartilage Quality in OA Talus and Distal Tibia 120	
3.4.	Discussion.....	122
4.	Chapter 4 In vitro Characterisation Talocrural Joint Mesenchymal Stem Cells.....	128
4.1.	Introduction: The Need for an Endogenous Repair Source	128
4.2.	Methods.....	132
4.2.1.	Relevant Sample Information (IC and ankle)	132
4.2.2.	MSC Isolation	133
4.2.3.	Measuring Egression of Cells from Digested Bone	133
4.2.4.	Colony Forming Unit Fibroblast Assay	133
4.2.5.	Area and Density Analysis of CFU-F Colonies.....	134
4.2.6.	Growth Rate Analysis	134
4.2.7.	Flow Cytometry for cultured MSCs.....	134
4.2.8.	Osteogenic Differentiation.....	137
4.2.9.	Chondrogenic Differentiation	139
4.2.10.	Adipogenic Differentiation.....	140
4.2.11.	Measuring Correlations between Differentiation Lineage Propensity	142
4.2.12.	Statistics	142
4.3.	Results.....	143
4.3.1.	Growth and Morphology of Tibial and Talar Plastic-Adherent Cells in Culture	143
4.3.2.	Measuring Putative MSC Frequency, Colony Behaviour and Growth Characteristics.....	146
4.3.3.	Proving MSC Identity by Surface Protein Expression.....	150

4.3.4.	Multi-Lineage Capacity of Talocrural MSCs in Comparison to IC MSCs	152
4.4.	Discussion.....	163
5.	Chapter 5 – Biological Enhancement of MSCs of the Talocrural Joint.....	170
5.1.	Introduction	171
5.2.	Methods	176
5.2.1.	Sample Information	176
5.2.2.	Choice and Development of Biological Stimulants	177
5.2.3.	Design of Culture Process	177
5.2.4.	Culture in Hypoxia.....	179
5.2.5.	Imaging.....	179
5.2.6.	Alkaline Phosphatase Staining	179
5.2.7.	Toluidine Blue	179
5.2.8.	Cell Size Analysis	180
5.2.9.	Colony Analysis	180
5.2.10.	Real-Time Reverse Transcribed Polymerase Chain Reaction.....	180
5.3.	Results.....	181
5.3.1.	The Effects of Short-Term Stimulant Effect Upon IC MSC Behaviour.....	181
5.3.2.	The Effect of Biological Stimulants Upon MSC Gene Expression.....	189
5.4.	Discussion.....	196
6.	Chapter 6 – The Ability of PL and KGN to Act as Chondrogenic Inducers in a 3D Model in Combination with Preconditioning	200
6.1.	Introduction	201
6.2.	Methods	206
6.2.1.	Sample Information	206
6.2.2.	Minimal Cell Culture and Processing	207
6.2.3.	Alginate Synthesis	207
6.2.4.	Image Capture of Preconditioning and Alginate Beads	208
6.2.5.	Bead Diameter	208
6.2.6.	Sphericity	208

6.2.7.	Swelling Ratio	209
6.2.8.	Degradation Rate	209
6.2.9.	Encapsulating IC and Talocrural MSCs within FA, and Pellet Culture	209
6.2.10.	XTT Assay.....	211
6.2.11.	Measuring Effects of Pellet Culture on MSC Expression by qPCR.....	211
6.2.12.	Glycosaminoglycan Content	213
6.2.13.	Snap-freezing of Pellets	213
6.2.14.	Cryo-sectioning of Pellets	213
6.2.15.	Toluidine Blue Staining of Pellets.....	213
6.3.	Results.....	214
6.3.1.	Mechanical Properties of FA Bead Hydrogels.....	214
6.3.2.	IC MSC Behaviour in in 3D FA or Pellet Culture after PL or K Preconditioning .	218
6.3.3.	Preconditioning and 3D Culture Effect on Talar and Tibial MSC Chondrogenesis	233
6.4.	Discussion.....	239
7.	Chapter 7 – Discussion and Conclusions.....	250
8.	APPENDIX.....	256
8.1.	Undecalcified Resin Histology.....	256
8.1.1.	Dehydration and Infiltration	256
8.1.2.	Embedding of Sample into Resin	256
8.1.3.	Preparation of Embedding Sample for sectioning	257
8.1.4.	Cutting of Thick Sample Sections.....	257
8.2.	Separated Preconditioning and Differentiation Results for Talus and Tibia.....	258
8.3.	Reagents, Stocks and Buffers.....	260
8.3.1.	Antibodies	260
8.3.2.	Reagents.....	261
8.3.3.	Solutions and Buffers	264
8.3.4.	Consumables.....	266
8.3.5.	Equipment.....	268

9. Work-cited Publications.....	274
---------------------------------	-----

List of Jointly Authored Publications

Jones, W.G., El-Jawhari, J.J., Brockett, C.L., Koria, L., Ktistakis, I., Jones, E. (2021). Multipotential stromal cells in the talus and distal tibia in ankle osteoarthritis - Presence, potency and relationships to subchondral bone changes. *Journal for Cellular and Molecular Medicine*. 25(1):259-271. doi: 10.1111/jcmm.15993.

Ilas, D.C., Baboolal, T., Churchman, S.M., **Jones, W.G.**, Giannoudis, P.V., Bühring, H., McGonagle, D. and Jones, E. The osteogenic commitment of CD271+CD56+ bone marrow stromal cells (BMSCs) in osteoarthritic femoral head bone. *Scientific Reports*. 10(1):11145. doi: 10.1038/s41598-020-67998-0.

El-Jawhari, J.J., Ilas, D.C., **Jones, W.**, Cuthbert, R., Jones, E. and Giannoudis, P.V. (2020). Enrichment and preserved functionality of multipotential stromal cells in bone marrow concentrate processed by vertical centrifugation. *European Cells and Materials*. 40:58-73. doi: 10.22203/eCM.v040a04.

List of Abbreviations

2D 2-Dimensional

ACAN Aggrecan

ACI Autologous Chondrocyte Implantation

ADAMT A Disintegrin and Metalloproteinase

ADAMTS A Disintegrin and Metalloproteinase with Thrombospondin Motifs

ALP Alkaline Phosphatase

BA/TA Bone Area of Total Area

BMC Bone Marrow Concentrate

BMP Bone Morphogenic Protein

BV/TV Bone Volume of Total Volume

C ChondroDIFF

CaCl₂ Calcium Chloride

CCL C-C Motif Chemokine Ligand

CD Cluster of Differentiation

cDNA Complementary DNA

CFUF Colony Forming Unit Fibroblast Assay

COL Collagen

COMP Cartilage Oligomatrix Protein

Ct Cycle Threshold

CXCL C-X-C Motif Chemokine Ligand

DAB 3,3'-diaminobenzidine tetrahydrochloride

DAPI 4',6-diamidino-2-phenylindole

dH₂O Distilled Water

DMEM Dulbecco's Modified Eagle Medium

DMP	Dentin Matrix Acidic Phosphoprotein
DNA	Deoxyribonucleic acid
DNase	Deoxyribonuclease
dNTP	deoxyribonucleotide
DPX	Distyrene Plasticiser Xylene
E11	Podoplanin
ECM	Extracellular Matrix
EDTA	Ethylenediaminetetraacetic acid
FABP	Fatty acid binding protein
FACS	Fluorescence assisted cell sorting
FCS	Fetal calf serum
FITC	Fluorescein isothiocyanate
GAG	Glycosaminoglycan
GAPDH	Glyceraldehyde 3-phosphate dehydrogenase
GSK	Glycogen synthase kinase-3
H&E	Haemotoxylin and Eosin
HGF	Hepatocyte Growth Factor
HIF	Hypoxia Inducible Factor
HPRT	Hypoxanthine Phosphoribosyltransferase 1
HRP	Horse Radish Peroxidase
HS	Human Serum
IC	Iliac Crest
IGF	Insulin Growth Factor
ISCT	International Society for Cellular Therapy
K	Kartogenin
KREMEN	Kremen Protein 1 Receptor

LEF	Lymphoid Enhancer Binding Factor
LEPR	Leptin Receptor
LVDT	Linear Variable Distance Transformer
MACI	Matrix-Induced Autologous Chondrocyte Implantation
mCT	micro Computer Tomography
MMP	Matrix Metalloproteinase
MRI	Magnetic Resonance Imaging
MSC	Multipotential Stromal Cell
NDC	Non-Diseased Control
NICE	National Institute for Health and Care Excellence
NSAID	Non-steroidal anti inflammatory drug
OA	Osteoarthritis
OAFAS	American Orthopaedic Foot & Ankle Society
OARSI	Osteoarthritis Research Society International
OAT	Osteochondral Autologous Transplantation
OPG	Osteoprotegerin
PBS	Phosphate Buffered Saline
PD	Population Doubling
PE	Phycoerythrin
PerCP	Peridinin-Chlorophyll-Protein
PL	Platelet Lysate
PPARG	Peroxisome Proliferator Activated Receptor Gamma
PRP	Platelet Rich Plasma
PTH LH	Parathyroid Hormone Like Hormone
PTPR	Protein Tyrosine Phosphate Receptor
PTPRC	Protein Tyrosine Phosphate Receptor Type C

qPCR	Real-time Reverse Transcription Polymerase Chain Reaction
RANK	Receptor activator of nuclear factor κ B
RANKL	Receptor activator of nuclear factor κ B ligand
RNA	Ribonucleic Acid
RNase	Ribonuclease
RUNX2	Runt-Related Transcription Factor
SBP	Subchondral Bone Plate
SFRP	Secreted Frizzled-related proteins
sGAG	Sulphated Glycosaminoglycan
SM	StemMACS
SOX9	Sry- Box 9
SPHK1	Sphingosine Kinase
TAR	Total Ankle Replacement
TBS	Tris-Buffered Saline
TGF	Transforming Growth Factor
TGFR	Transforming Growth Factor Receptor
TIMP	Tissue Inhibitor of Metalloproteinases
TNFSR1	Tumour Necrosis Factor alpha soluble receptor 1
TRAP	Tartrate Resistant Acid Phosphatase
U	Unit
VAS	Visual Analogue Score
VEGF	Vascular Endothelial Growth Factor
WNT	Wingless Int-1

Acknowledgements

I would like to thank my supervisors, Dr. Elena Jones, Dr Jehan El-Jawhari, Dr. Claire Brockett and Dr. Hazel Fermor for all the support and insightful input they have given me throughout my PhD. I would like to especially thank Elena for her incredible commitment with rapid, thorough feedback, for always encouraging me when I was struggling with progressing to the next level of my research, and helping me achieve the best in both my research and my own personal progression. I would also like to give specific thanks to Jehan for her expert experimental advice and constant encouragement, and to Claire for always being responsive and finding time to support not only my research ideas but also my personal development, and my ideas for improving diversity, equality and inclusion in the University. I would also like to thank Hazel for her thoughtful multidisciplinary insight, and for being a kind ear since the very start of my integrated PhD which helped me to find the confidence to be myself.

I am thankful for my research group who made research more enjoyable and for their critical analysis of my approach to help me develop my ideas to the next level. I would especially like to mention Lekha Koria, Dr. Dragos Ilas, Dr. Heather Owston and Dr. Payal Ganguly for their expert advice and kind support.

I am grateful to the research staff at the University of Leeds for their above and beyond support throughout my research, especially to Dr. Rekha Parmer, Dr. Rae Cowie, Dr. Sophie Stephenson, Dr. Daniel Thomas, Dr. Nicola Conway, Dr. Mike Shires and Dr. Joanna Koch, each of whom always greeted me with a smile and offered expert advice when I was developing my experimental design.

I also would like to acknowledge the EPSRC for funding this work through the Centre for Doctoral Training Program, which provided me with a peer network of multidisciplinary researchers and friends which gave me support that built my confidence and my research ability. I would like to thank the CDT directly for their excellent support, and fantastic provision of personal development opportunities.

I would like to thank Dr. Mary Murphy for hosting me at the REMEDI institute to investigate multipotential stromal cell development for the whole bench to bedside approach, in the laboratory, industry and clinical settings, and everyone who helped me during the placement.

I would like to express my gratitude to the LGBT Staff Society, and everyone involved in the Northern Power Inclusion Matters project, for helping me develop my confidence and my own approach to E&I.

I would also like to give special thanks to my friends Dr Camille Laporte, Dr. Pier Pischedda, Ahranee Camden, Dr. Juan-Pablo Gevaudan and Dr. Pablo Caramés-Mendéz who provided me with critical advice to develop my own ability in academia, and at the same time helped me improve my confidence.

In addition, I would like to give thanks to my friends and family for always believing in me and pushing me to do my best, but also reminding me to give myself the time to recover when needed.

Finally, I give special thanks to my partner Ayham Khazna for his constant love and support which has meant so much while working under lockdown conditions during this pandemic.

Abstract

Osteoarthritis (OA) of the ankle is unique in that it has an early onset and is often post-traumatic. Surgical treatments of ankle OA are less effective than in other joints due to its anatomical and biomechanical complexity, whereas joint-preserving treatments, which rely on endogenous multipotential stromal cells (MSCs), show good outcomes of up to 2 years, but degenerate subsequently. The aims of this study are: 1) To develop understanding of OA progression in the talus and tibia of the ankle through micro computed tomography, histology with cartilage damage grade scoring (Osteoarthritis Research Society International cartilage histopathology assessment (OARSI)) and immunohistochemistry, with a focus on resident reparative cells, CD271+ MSCs. 2) Assess the presence and potency of resident MSCs in OA talus and tibia in comparison to non-diseased, iliac crest (IC) MSCs, utilising standard *in vitro* methods 3) Develop two-dimensional expansion methods of MSC preconditioning for chondrogenesis enhancement, using clinically relevant, xeno-free biological stimulants, Kartogenin (K) and Platelet Lysate (PL) 4) Investigate preconditioning and 3D culture for synergetic enhancement of MSC chondrogenic differentiation in non-diseased IC MSCs, and OA talar and tibial MSCs, utilising fibrin alginate and pellet culture methods for GAG deposition and gene expression.

In non-diseased bone, the tibia presented a significant, 2.5-fold higher bone volume of total volume ($p=0.001$) than the talus. In OA, the subchondral bone plate of talus and tibia thickened 1.3-to-2.5-fold compared to non-diseased controls, with bone volume of total volume increasing within 2 mm from the subchondral bone plate, but falling below non-diseased controls after 2 mm in OA in both talus and tibia. The subchondral bone plate thickened 3-7 fold under damaged cartilage (OARSI grade 5) cartilage compared to grade 3 in both talus and tibia ($p=0.003$, 0.0003 respectively), and bone volume of total volume increased 2-fold in tibia under grade 5 compared to grade 3 cartilage ($p=0.002$), but not in talus. MSCs appeared to associate with cartilage damage, with CD271+ positive staining correlating significantly with overlying cartilage damage grade in tibia ($p=0.008$ between grade 3 and 6), with a trend also clear in the talus. CD271+ MSCs were also found in similar areas as CD56+ osteoprogenitors and E11+ osteocytes, suggesting a link between MSCs and new bone formation. Plastic adherent, colony-forming MSCs were found in both OA tibia and talus, with a significant 30-fold higher MSC proportion of total cells than IC ($p=0.005$, 0.013 respectively). OA talar and tibial MSCs showed 1.5-3-fold increased osteogenesis by calcium deposition, and 2-fold increased chondrogenesis by GAG production, significant in the talus ($p=0.012$). Talar MSCs showed a 10-fold reduction in adipogenesis compared to IC and tibial MSCs by Oil Red O staining normalised to DAPI ($p=0.049$). Preconditioning with xeno-free 10 %human serum (HS) and biological stimulants 10 μ M K and 10% PL showed increased proliferation in IC MSCs compared to the positive control

ChondroDIFF. Treatment with K led to increased expression of chondrogenic gene ACAN, but reduced COMP, COL2 and SOX9 compared to ChondroDIFF, whereas PL did not elevate expression of any chondrogenic gene. Subsequent differentiation in 3D culture showed a trend for elevated GAG production and retention after preconditioning with K/10% HS, and differentiation in K/50% HS relative to other conditions, suggesting this as the most successful combination for cartilage regeneration. PL treatment alone led to the majority of GAG not being retained, and elevated expression of osteogenic genes, as such appears unsuited for chondrogenic preconditioning of OA talar and tibial MSCs. Ankle OA cultures showed reduced GAG retention in comparison to IC, and far more variance in GAG production, suggesting OA has an impact on the chondrogenic ability of MSCs following biological stimulation.

Overall, OA induced profound changes in talar and tibial cartilage and bone structure, likely impacting on joint biomechanics. MSCs are present within bone and are consistent with therapies which rely on endogenous cells, e.g. microfracture, however their association with bone-forming cells indicated a predominantly osteogenic phenotype. In standard conditions, these MSCs are capable of chondrogenesis to a greater extent than IC, but require stimulants which block osteogenesis whilst enhancing chondrogenesis to be targeted clinically. Preconditioning with K/10% HS demonstrated the ability to initiate chondrogenesis, and subsequent differentiation in K/50% PL shows enhanced GAG production and reduced RUNX2 expression, making this a suitable candidate for a clinically suitable drug to enhance chondrogenesis in combination with microfracture.

1. Chapter 1 – Introduction

Osteoarthritis (OA) of the talocrural joint of the ankle is a distinct and intricate clinical entity, due to the complex nature of the ankle joint, and how this affects both disease progression and available treatment options. The ankle is more prone to post-traumatic osteoarthritis compared to the hip or knee, as such is more common in younger patients, with symptomatic OA onset at an average age of 52, compared to 67 in the hip¹. However, the complex biomechanics of the ankle make total joint replacement only last 10 years, in comparison to the knee or hip where these can last 30 years¹. As such, replacement is only employed in older patients, on average at 67 years old^{1,2}. As such, conservative regenerative therapies are employed until joint fusion or replacement will last the lifetime of the patient. However, these therapies show limited success, only retaining strong outcomes for up to 2 years after treatment, after which there is progressive degradation of the joint. To prevent topics being discussed without explaining relevant concepts, this chapter will introduce anatomy and biomechanics of the ankle, and then the building blocks of joint repair, before and then OA in general and in the ankle, in order to provide a comprehensive overview of the area.

1.1. Anatomy of the Ankle

1.1.1. Whole Structure

The foot itself is composed of twenty-six individual bones, which cumulates into thirty-three individual joints when including the long bones of the lower leg. The ankle “joint” is formed of three articulations excluding the metatarsals. This includes the talocrural joint (of the talus and tibia), subtalar joint (of the talus and calcaneus) and the transverse tarsal joint (of the calcaneus and cuboid, and talus with navicular) (Fig. 1.1.1). The interactions between each joints is essential for joint function³.

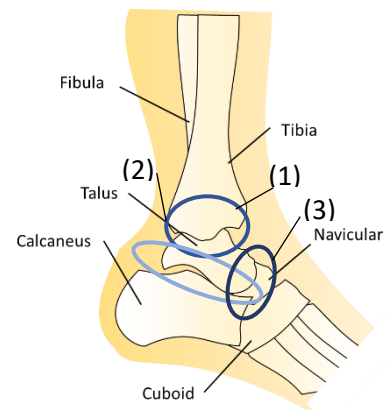


Figure 1.1.1 Medial view of the lower leg, with nomenclature of the bones. (1) Talocrural Joint. (2) Subtalar Joint. (3) Transverse tarsal joint. Adapted from Neumann 2016⁴.

1.1.2. The Talocrural Joint

The talocrural joint sits at the distal end of both the talus and tibia, with the load bearing region at the interface. The talus has no muscular connections, and instead gains stability from both various ligaments and how the joint is structured. As such it is a diarthrosis joint. The talus is constrained by the medial malleolus of the tibia, and the lateral malleolus of the fibula, as shown in Fig. 1.1.2,

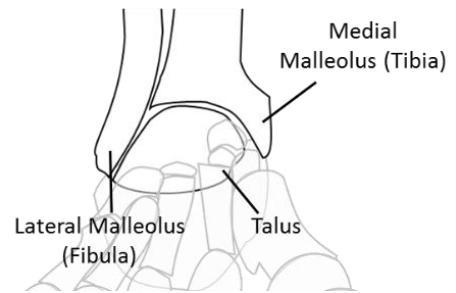


Figure 1.1.2 Anterior view of the bones of the lower leg. The talus is constrained by the mortise of the malleoli of both the tibia and fibula.

presenting a hinge-joint structure. However, the cone shaped trochlea of the tibia suggests movement atypical to a hinge joint. The talus is widest from the anterior orientation for strength and stability during dorsiflexion (raising the front of the foot towards the shin). A thin capsule covers the joint, connecting to the tibia and fibula malleoli, and articular surface of the talus^{3,5}.

The Talocrural joint forms the crux of this project due to a large proportion of ankle trauma occurring at this location, suggesting a higher rate of OA at this specific joint⁶⁻⁸. However, current treatments are sub-optimal, and do not last more than 10 years.

Due to the risk of OA in neighbouring joints when natural biomechanics are altered, each joint of the ankle needs to be considered when investigating the disease. The talocrural joint is cited as the most likely location for osteochondral lesions in the ankle, as it is prone to injury from excessive landing force leading to bone rotation, as only ligaments hold the talus in place^{7,9}. This leads to the increased rate of lesions in the talocrural joint^{9,10}. This makes the talocrural joint a frequent site for regenerative therapies, and therefore a key focus of this thesis.

1.1.3. The Subtalar Joint

The subtalar joint is comprised of the superior, concave surface of the Calcaneus, and inferior convex surface of the talus. This enables most of the eversion and inversion of the foot. This is an arthrodial joint, as such only allows gliding motion between two thirds of the anterior calcaneus and lower side of the talus³.

1.1.4. The Talonavicular Joint

The talonavicular joint is composed of the posterior portion of the navicular, and below the middle and anterior portion of the talus. This joint moves by rotation about an axis through the talus, in a forward and downward slant in the medial direction. This enables engagement in both inversion and eversion, with two muscles for inversion, the tibialis anterior and posterior, and three of eversion, the peronei, which insert in front of the transverse tarsal joint³.

1.1.5. The Tibio-Fibular Syndesmosis

A syndesmosis refers to a joint of two bones connected by ligaments and a strong membrane. This is the nature of the joint between the distal tibia and fibula. This acts to secure the tibiofibular mortise upon the talus. This type of joint permits 1 mm of motion when transferring from plantar flexion to dorsiflexion³.

Despite the many joints within the ankle, as the talocrural joint was the focus of this work, from this point forward the ankle joint refers to the talocrural joint specifically.

1.1.6. Talocrural Joint Bone Anatomy

As mentioned as Sections of joints above, the major bones involved in the ankle joint include the Tibia, Talus, Calcaneus, Navicular and Cuboid. However, as this project focuses on explants removed during fusion of the talocrural joint, the talus and tibia shall be explained here.

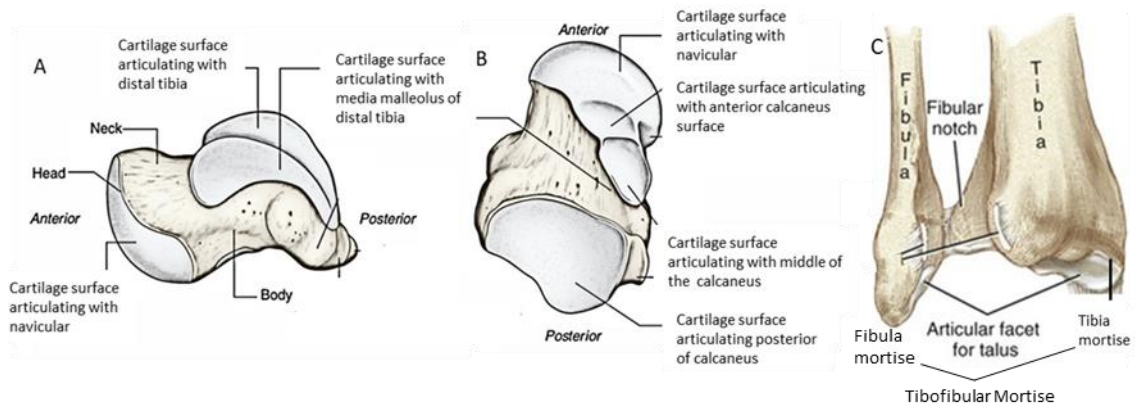


Figure 1.1.3 Facets of articulation and Anatomical Landmarks of Talus and Tibia. A Medial view of the talus. B Anterior view of the talus. C Anterior lateral view of the tibia. Adapted from Neumann 2016⁴.

The talus, as shown in Fig. 1.1.3, bears resemblance to a snail, with a rounded head at the end of the short neck, with a larger posterior body. The anterior of the talus is domed to enable articulation with the corresponding concave surface of the navicular. The superior side of the talus is again domed to enable articulation within the distal ends of the tibia and lateral malleolus of the fibula. As the fibula extends further than the tibia distally, the corresponding articular cartilage of the talus extends further than that which interacts with the tibia^{3,11,12}.

The distal tibia interacts with the talus, with the tibiofibular mortise restricting its rotation (Fig. 1.1.3). The tibia extends less than the fibula in this mortise, as such further rotation is permitted in the medial direction. Where the tibia interfaces with the talus, there is a concave curvature covered by cartilage to enable smooth rotation^{5,13,14}.

1.1.7. Cartilage

The cartilage of the ankle is of hyaline nature, existing on the articular surfaces. This helps disperse load during movement, with cartilage mostly dealing with shear forces¹⁵. Articular cartilage is both aneural and avascular due to the load-bearing nature of the tissue, instead receiving nutrients and hydration from the synovial fluid for superficial cartilage, or from the subchondral bone for deep cartilage¹⁶. This lack of vasculature and neural behaviour is

thought to inhibit the repair of cartilage¹⁷. Hyaline cartilage is composed of 4 zones, shown in Fig. 1.1.4. The surface is the superficial zone, composed of collagen fibres orientated parallel to the surface, supporting chondrocytes with little proteoglycan. The chondrocytes of this zone secrete superficial zone protein¹⁸. Within the ankle most of the cells are paired, with only 25% found singularly, unlike in other joints which tend to larger groups of cells, with less distance between chondrocytes¹⁹. The intermediate zone holds randomly orientated collagen and sparse chondrocytes. The deep zone contains collagen oriented perpendicular to the surface and clusters of 2-3 chondrocytes, and the calcified zone is where mineralisation begins to occur, with a few hypertrophic chondrocytes root-like type X collagen structures reaching into the calcified zone from the deep zone²⁰. This zone connects to the subchondral bone, with a rapid change into calcified bone with no chondrocytes and change from type 2 to type 1 collagen¹⁷. The area where the articular cartilage starts to become calcified is termed the tidemark (shown on Fig. 1.1.4), due to the rapid progression of cartilage from a demineralised tissue to a calcified one, whilst also denoting the change in nutritional source from synovial fluid to subchondral bone for the chondrocytes. This tidemark can be visually distinguished by histochemical staining, however the reason for its existence is still argued between three theories. Firstly, as a leftover of the subchondral ossification growth-plate, secondly, as a junction between the pliant hyaline cartilage and rigid calcified tissue, and thirdly as a by-product of the chondrocyte life cycle. Evidence shows chondrocytes slowly migrate to the tidemark from the articular surface altering the extracellular matrix (ECM) as it goes, before undergoing apoptosis at the tidemark²¹. In OA, this tidemark is duplicated, thought to be due to the progression of bone into the cartilage^{21,22}.

The calcified cartilage is preceded by subchondral bone, with a subchondral bone plate formed of a 1-3 mm plate of cortical bone, followed by and with metabolically active trabecular bone distal to this²³.

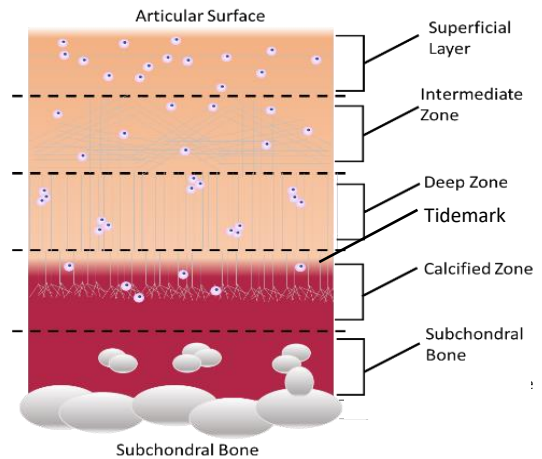


Figure 1.1.4 Zonal Variation of Hyaline Articular Cartilage. Adapted from Gray 2009³.

Collagen, the major load-bearing macromolecule of cartilage, forms 60% of the dry weight. This is mostly formed of fibrillar type II collagen (90-95%), with a minority of collagen types VI, IX and XI²⁴. The second major macromolecule is proteoglycans, which trap water within its hydrophilic glycosaminoglycan (GAG) side chains to allow cartilage to resist compressive load. As such, water forms up to 80% of cartilage wet weight²⁰. By weight, the most abundant proteoglycan is aggrecan, followed by decorin, biglycan and fibromodulin. Chondroitin sulphate is the most common GAG, with aggrecan binding up to 100 of these as side chains¹⁷. This forms large aggregates via link proteins to bind hyaluronan, holding large amounts of water to resist load²⁵.

As mentioned, cartilage of the ankle is different from the hip or knee. Firstly, the cartilage is both thinner and more uniform. The cartilage within the talocrural joint is 1.0 to 1.6 mm thick on average, but thinner on the talar dome, where it measures between 0.9 and 1.7 mm. In comparison, the cartilage within the knee joint measures between 1.69 and 2.55 mm in thickness. Proportionally, the superficial layer of the ankle is much greater than the knee, so much so that despite the difference in total cartilage thickness, the superficial layers are similar thicknesses²⁶.

Additionally, there is a higher degree of congruency in the ankle, with a load-bearing area of 11-13cm², although this is still lower than the knee due to the small nature of the ankle^{5,27}. The cartilage is thought to be more able to repair, due to the enhanced ability of chondrocytes to synthesize proteoglycans, as well as a higher stiffness and decreased permeability due to its higher GAG content, with just under twice as much GAG per wet weight in the ankle than in the knee²⁸.

Thirdly, the aggregate modulus, a measure of stiffness of the tissue at equilibrium when all fluid flow has ceased, is higher²⁹.

$$H_a = \frac{E(1 - \nu)}{[(1 + \nu)(1 - 2\nu)]}$$

Equation 1.1.1 Calculation of Aggregate Modulus. E = Young's Modulus. ν = Poisson's Ratio

The aggregate modulus is calculated using Young's Modulus (E) and Poisson's Ratio (ν). The ankle has an aggregate modulus of 1 MPa, compared to 0.6 MPa in the knee, meaning there is less deformation under load within the ankle^{18,28}. These properties of cartilage are thought to be a large part of the reason why the ankle is less prone to primary OA³⁰.

Another difference in the ankle compared to other joints such as the knee is cited to be a difference in profile of molecule synthesis (catabolism), and molecule degradation (anabolic) focus between the joints. The ankle has an anabolic phenotype, whereas the knee presents more catabolic activity. As such, ankles show increased synthesis markers such as C-terminal type-II

procollagen pro-peptide and of Aggrecan turnover³¹. Additionally, there is less response to catabolic markers such as interleukin-1 β and fibronectin fragments, with no evidence of matrix metalloproteinase (MMP) 8 mRNA which has been found to enhance OA progression in the knee³²⁻³⁴. MMPs are a family of ECM degrading proteins, which include accompanying inhibitors termed Tissue Inhibitors of Metalloproteinase (TIMPs), as well as the specific proteins of the same family, A Disintegrin and Metalloproteinase (ADAM) and ADAM with Thrombospondin Motifs (ADAMTS). These have all be found key in the progression of OA.

The evidence of ankle OA being a distinct clinical entity compared to knee was also shown by interleukin-1 stimulation, a glycoprotein involved in immune response modulation. Cartilage in the knee stimulated with interleukin-1 showed an increased loss of GAG content, however the ankle showed no changes¹⁸. Further research into the different factors involved in OA progression of the ankle is required to build a 'library' of factors, and further characterise the degeneration of this joint. Additionally, it needs to be confirmed if these changes are limited to the post-traumatic model of OA or is also found in primary OA. Some studies exist of the various anabolic and catabolic inducing factors involved in OA; however, these combine results from the ankle, knee and hip, and as such do not provide reliable information for individual joints.

The talocrural joint is less susceptible to cartilage damage, explained by the increased joint congruency, and better cartilage mechanical properties as discussed earlier³⁰. To better understand why cartilage therefore becomes unable to repair after trauma, a better understanding of changes to cartilage in OA is required, both morphologically and mechanically.

1.1.8. Subchondral Bone

Distal to the articular surface and beneath the calcified layer of deep cartilage lies the subchondral bone. This is 1-3 mm of cortical plate with subsequent trabecular bone and bone marrow³. This cortical plate is partially porous, with blood vessels and nerves extending tendrils into the calcified cartilage³⁵. Subchondral bone, conversely to cartilage, is highly neurovascular tissue. This is due to the bone not having the same compressive function as the cartilage, as such the vessels are protected. The localisation of these vessels within the cortical plate is concentrated at the area under most loading, and the number of these vessels tend to increase with age, shown in the hip³⁶. In comparison to the cortical plate, the trabecular bone is much more porous and metabolically active. The trabecular subchondral bone provides the majority of mechanical support in shock absorption. The structure of the trabeculae is non-homogenous and anisotropic, meaning the structure is built in the direction of force, in order to best resist loading. Within the trabeculae also lies the bone marrow, providing a stock of cells. The

subchondral bone is a highly dynamic structure, with the level and location of mechanical load controlling the remodelling of the tissue.

The major cells types of the bone include monocytes, osteoclasts, osteoblasts and osteocytes³⁷. Bone which undergoes little mechanical loading will induce monocytes differentiation into osteoclasts, which resorb the surrounding bone³⁸. This prevents wastage of material as well as helping the bone be modelled to best resist force. When bone is needed to be built, osteoblasts lay down new bone by secreting ECM proteins including osteocalcin, osteopontin and dense cross-linked collagen, to form a pre-bone scaffold called the osteoid. Cells trapped within the bone are termed osteocytes. Whilst these cells no longer secrete bone-forming proteins, they act as mechanosensory units which can send signals to the surface of the bone³⁹. Osteoblasts are generated from Mesenchymal Stromal Cells (MSCs) which typically form connective tissues, and will be described in more detail at a later point in this literature review⁴⁰.

Osteocytes within the bone interact with each-other through dendritic processes. The filopodia to perform this are extended into canaliculi, connecting between osteocytes via gap junctions. These act to sense both mechanical and systemic stimuli⁴¹.

Microfracture to the trabeculae of the subchondral bone leads to a reduction in the elastic modulus of the structure, which also affects the loads cells will undergo. Microdamage to the cortical bone results in apoptosis of osteocytes and an increase in osteoclast-mediated remodelling in rats⁴². This association of microdamage with bone resorption offers a potential cause for post-traumatic OA, considering cartilage viewed arthroscopically after injury appears undamaged.

1.1.9. Extracellular Matrix Proteins

The extracellular matrix (ECM) of a tissue forms a mechanical structure on which cells can attach, aiding both rest and migration of these cells. These also provide surface signals, with the strength of a material influencing the differentiation of a cell as well as its migration ^{43,44}. Additionally, the ECM acts as a growth factor store. Within the cartilage, as earlier mentioned, the major constituents of the ECM are collagen (II,VI,IX and XI) and proteoglycans (Aggrecan, Lubricin).

Proteoglycans are composed of a protein core, with many sugar side chains, which by their hydrophilic nature allow the entrapment of water within its structure. These often contain link proteins at the base of the protein component, which act to bind the proteoglycan to a larger complex through hyaluronan, this is shown within Figure 1.1.5.

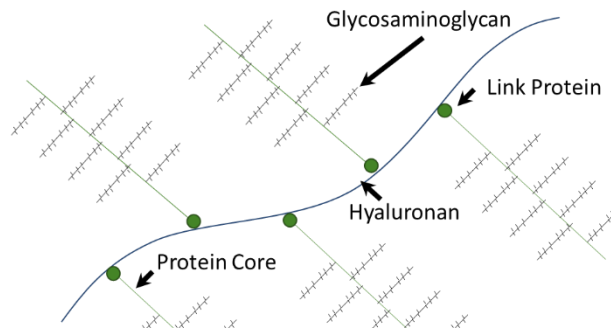


Figure 1.1.5 Typical Structure of the Proteoglycan-Hyaluronan complex. Adapted from Roughley & Mort 2014²⁵.

Degradation of the extracellular matrix leads to perturbation of resident cells. The degradation products of hyaluronan lead to proliferation of chondrocytes as well as their apoptosis ⁴⁵. OA is at least perpetuated by overexpression of inflammatory factors and ECM degrading components which leads to a vicious cycle of degradation⁴⁶.

In the bone, the extracellular matrix is termed the bone matrix. This matrix acts to separate osteocytes from each-other. The matrix is formed of fibronectin, collagen, laminin and proteoglycans. Cells can adhere to these proteins through integrin- β 1, which binds to the extracellular matrix via RGD-domains (arginine, glycine aspartic acid), which enables cell adhesion and migration, whilst also enabling downstream signals through focal-adhesion kinases and vinculin ^{47,48}. Disruption of these signals such as by the use of antibodies causes cell apoptosis ⁴⁹. Collagen of the bone is typically formed of type-I collagen, which is also a fibril-forming collagen. In comparison to type-II collagen, type-I has a lower content of both hydroxylysine and glycosyl/galactosyl residues ⁵⁰. However, this type itself is stronger ⁵¹. Whilst the matrix of these two tissues show some similarity as well as differences, their close proximity suggests the dependence of the two tissues on each other.

1.1.10. The Osteochondral Junction and Bone Cartilage Crosstalk

There is now a large body of evidence for cross-talk between subchondral bone and cartilage both in healthy and unhealthy joints, including the ankle⁵². This is mediated by the relatively high vasculature and abundance of osteocytes. As OA progress, there is widening of the connections between the two tissues, due to microfractures, perforation, vascular invasion of bone and cartilage damage, leading to an increase in signalling between the two tissues as well as hydraulic conductance^{53,54}.

Molecules thought to be involved in this molecular crosstalk include Osteoprotegerin (OPG), Receptor Activator of Nuclear Factor κ B (RANK), RANK ligand (RANKL), Hepatocyte Growth Factor (HGF) and Hypoxia-Inducible Factor 2 α (HIF-2 α). OPG acts to inhibit binding of the RANK-RANKL complex, the complex being essential for bone resorption. RANKL is expressed by both osteoblastic lineages as well as chondrocytes, implicating cartilage in the signalling process. In early human OA, the ratio of RANKL to OPG is increased, suggesting bone resorption, but decreased in late OA, giving reason for the thickening of subchondral bone in late-stage OA⁵⁵. There is a large body of evidence for crosstalk between the cartilage and bone, however the complex events involved means the potential mechanism of action is still unknown.

The complexity of this joint leads to various differences in biomechanics, affecting OA progression and the types of treatments that can be employed. These are investigated next.

1.2. Biomechanics of the Ankle

1.2.1. Common Biomechanics

The axis of rotation of the ankle is complex. Some researchers state the ankle has a single axis, with an oblique transverse axis, as shown in Figure 1.2.1, however others hypothesize there is a shift in the axis of rotation of the talocrural joint during plantarflexion (whenever the heel raises relative to the toes), shifting from anterior to posterior^{2,3,11}. A study in 2014 by Siegler *et al.* directly compared the geometry of the talocrural joint to the degree of congruency, to test the theories. They found the trochlear surface of the talus is skewed inwardly, as such there is no axis of symmetry, which implies a varying axis of rotation, which matches results of numerous other studies⁵⁶. Sturnick *et al.* performed gait analysis of cadaveric ankles using reflective markers attached to the tibia and talus, and physiological load applied to the extrinsic tendons for simulated gait cycles. This again showed a varying axis rotation. However, as this was performed on cadaveric tissue, it is difficult to prove that this is the ankle behaves in a healthy human⁵⁷. Lundberg *et al.* used roentgen stereophotogrammetry to measure the axis of rotation in 8 healthy patients. Projections were made after 10-degree steps in each motional direction, again showing a moving axis of rotation. However, roentgen stereophotogrammetry is based off markers within a replacement prosthesis, as such movement will be abnormal⁵⁸.

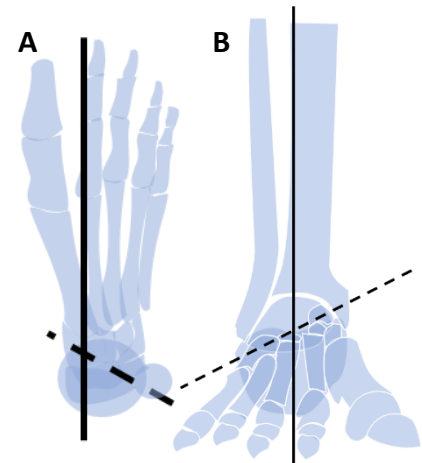


Figure 1.2.1 The Oblique Transverse Axis of the Talocrural Joint. Dashed line shows the transverse axis in both A and B, which is not completely horizontal. A show the superior view. B shows the anterior view. Adapted from Neumann 2016⁴.

Before discussing joint rotation, biomechanical rotations of the ankle need to be defined. The rotations are described within Figure 1.2.2, with plantarflexion and dorsiflexion relating to the elevation and depression, adduction and abduction relating to medial or lateral rotation and eversion/inversion relating to rotation of the sole inwards or outwards. Plantarflexion and

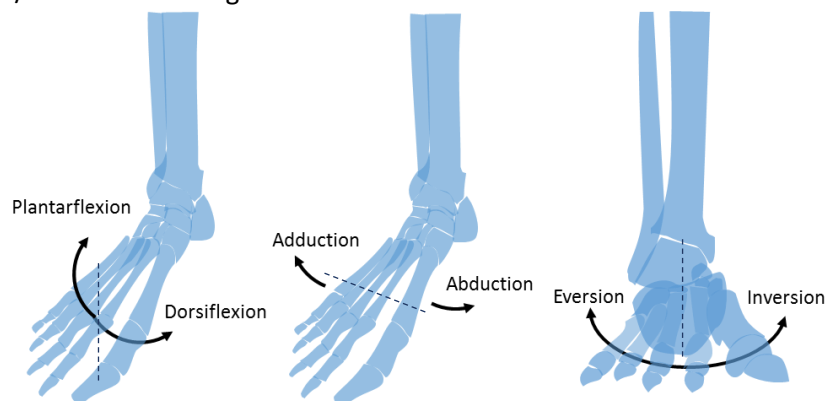


Figure 1.2.2 Illustration of the 6 Major Rotations of the Ankle. Adapted from Neumann 2016⁴.

dorsiflexion are largely controlled by the gastrocnemius (the muscle connecting the femur to the Achilles tendon), contracting for plantar flexion and relaxing in dorsiflexion ^{5,11}.

Inversion and eversion denote the sole of the foot turning inward and outward respectively. During inversion the ankle will undergo dorsiflexion, and vice versa for eversion ^{5,11}. Abduction describes medial movement of the lower foot and adduction lateral movement ^{5,11}. A further two movements are described as supination and pronation, in the ankle describing combination of the above movements, supination being plantarflexion, inversion and adduction, resulting in the sole facing medially, and pronation the inverse ^{5,11}. A combination of these movements is required to enable walking, which are described by the gait cycle (Fig. 1.8).

During a typical gait cycle, the two phases are swing and stance, shown in Figure 1.8. The stance phase is split into four Sections for the ankle, heel-strike, flat foot, mid-stance and heel off. This begins with plantarflexion of the foot as the heel strikes the ground, then relaxing until mid-stance. Dorsiflexion occurs until heel-off, maintained until toe-off. During swing phase, the ankle undergoes dorsiflexion to allow the foot to clear the ground, whilst returning to plantarflexion for heel strike ⁵.

1.2.2. Prevalent Loading and Abnormalities

The natural movement of a joint during walking is termed the gait cycle. For the ankle, the typical gait cycle is shown in Fig. 1.2.3.

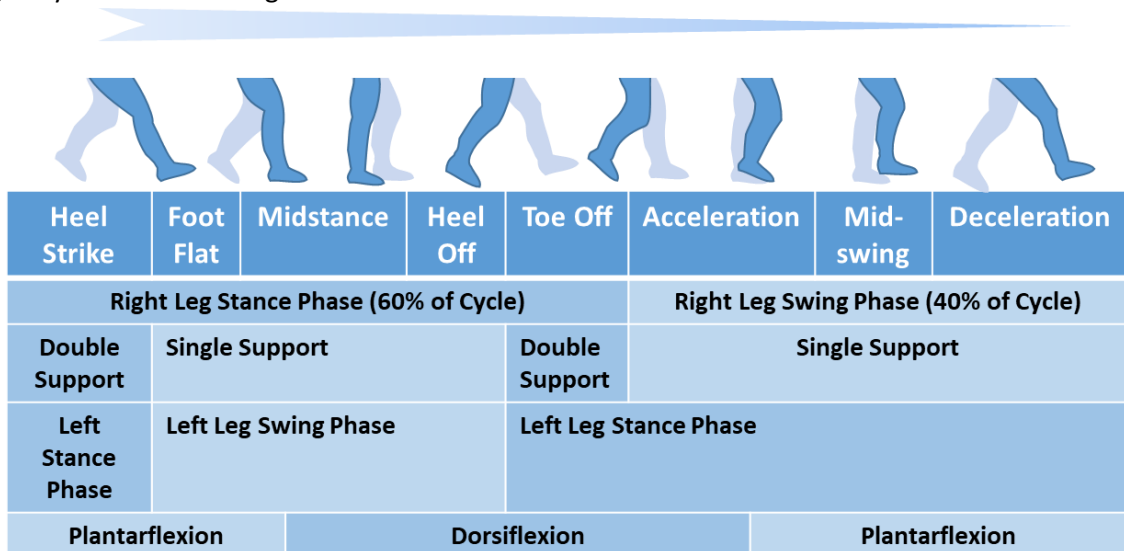


Figure 1.2.3 The Typical Human Gait Cycle. Adapted from Valderrabano *et al.* 2007⁶⁴.

The typical load through the ankle during normal gait is believed to be 4.5-5 times bodyweight at its highest, during the heel-off phase of the gait cycle, with 0.36 times body weight exhibited through shear forces, that is two surfaces moving past each other by unaligned, opposite forces. When running, this load increases up to 13 times bodyweight⁵⁹. These numbers are greater than

that of the hip or knee, with the hip showing 1.5 to 2.5 times bodyweight during walking⁶⁰. Each ankle carries around 49.3% of body weight, with the remainder carried by the rest of the foot, through 11-13 cm² of weight-bearing surface in each ankle. Of this, 83% is through the talocrural joint and 17% through the fibula⁶¹. As the contact surface area of the ankle is higher than that of the hip or knee, the load transmission is lower relative to the hip or knee¹⁴. However, the distribution of this load changes throughout motion. For example, Panero et al. found that during normal stance, 20% of load is placed through the forefoot and 30% on the hindfoot, however during squatting this changes to 40% on the hindfoot and 10% on the forefoot⁶².

During OA, the biomechanics of movement change greatly. As the patients no longer want to place weight upon the injured tissue, there is a shift in movement pattern, causing abnormal loading. This may promote further degeneration of the ankle and potentially further post-traumatic OA⁶³. When using the Musculoskeletal Functional Assessment questionnaire, patients with end-stage ankle OA reported significant reduction in range of motion and their quality of life as well as general disability and other complications⁶⁴. Dyrby *et al.* showed in 6 patients that overall range of motion of the ankle is reduced by 38%, with most of this being accounted for by a loss in inversion, although interestingly the degree of eversion increased compared to the control⁶⁵. The loss of motion is clear from the fact the two bones are fixed together, however the alteration in both biomechanics, joint structure and reduction in pain may allow for a greater amount of eversion, such as a reduction in the size of the mortise, since the tibia is made flat during the fusion surgery. Horisberger *et al.* showed that end-stage osteoarthritic patients show an increase in the average maximum force and peak pressure placed on the ankle, as well as a reduction in pressure on the forefoot with more being placed on the forefoot. Additionally, when pressure was applied the patients minimised contact area between the back and midfoot, with an increased period spent with load upon the forefoot. However, these values did not correlate with clinical scores of the patient⁶³.

To better understand changes in OA to the talus, the general understanding of OA and specific changes identified in the talus and tibia are discussed next.

1.3. MSC Characteristics, Localisation and Roles

This Section will introduce the roles and functions of Multipotential Stromal Cells (MSCs), particularly within bone behaviour and cartilage repair, as well as describe the current understanding of the talus and tibia of the ankle, the effects of osteoarthritis (OA), and current therapies available for treatment. First, this will focus on MSCs and their relevance to regenerative therapy.

Stem cells define cells which can form multiple cell types whilst maintaining their own population. The type of cells formed depends on the type of stem cell. For example, an early embryonic cell (up to three days) is termed 'totipotent', as these cells are capable of forming any cell type within the body. MSCs are an example of a cell with a more constrained potency, termed multipotent, as they only form cells of mesenchymal origin *in vivo*. Primarily this includes bone (osteogenic), cartilage (chondrogenic), fat (adipogenic) cell types, but with correct stimuli give rise to connective tissue, shown in Fig. 1.3.1⁶⁶.

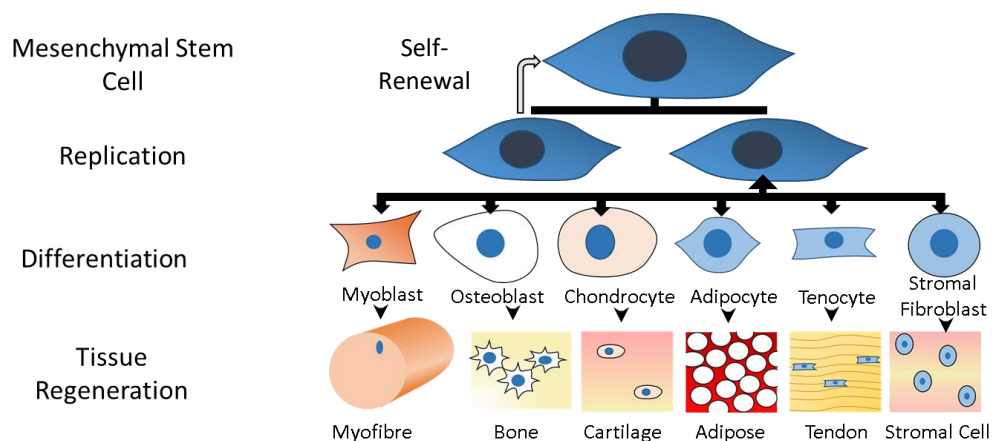


Figure 1.3.1 The differentiation pathways of the MSC, including formation of muscle, bone, cartilage, fat and other tissues. Adapted from Caplan 1991⁷³.

MSCs are highly proliferative cells with limited replication, showing 20-40 population doublings *in vitro* compared to 8 identified in most fibroblasts, although this varies in the literature due to culture conditions and source tissue⁶⁷⁻⁶⁹. MSCs are rare in that whilst compared to most adult stem cells, they are able to form cells of many lineages *in vivo* and *in vitro*, particularly of osteochondral lineages, as well as having immunomodulatory effects, making them one of the best studied cells within the regenerative medicine field^{70,71}. They are potent osteochondral agents, and whilst originally identified within the bone marrow, they do not form cells of haemopoietic lineage. Subsequently, MSCs have been observed in many locations within the body, including bone, skin, muscle and adiposal tissue. Within cancellous bone, MSCs form around 1% of all cells following enzymatic digestion of the tissue⁷².

A confounding factor within the MSC field is that they are referred to by many names. MSCs were first isolated in 1974 and then defined as multipotential stem cells in 1991 by A.I. Caplan^{73,74}. However, these cells were unable to show 'stemness', as despite being able to form multiple lineages and reproduce themselves *in vitro*, the third criteria, the ability for *in vitro* self-renewal following serial transplantations, is not met, as earlier shown they cannot replicate indefinitely⁷⁵. However, there is some evidence that some MSC subpopulations can meet this criteria⁷⁶. This led to recommendation of the International Society for Cellular Therapy to redefine these cells as multipotent stromal cells, to retain the same acronym but account for these new properties, with the additional rule that a subset of these MSCs isolated directly from bone marrow showing true stemness should retain mesenchymal stem cells nomenclature⁷⁷. However, MSCs were also termed Medical Signalling Cells due to them showing significant paracrine effects to reduce inflammatory responses^{78,79}. This immunomodulatory effect occurs in part due to live MSC activity, as well as after apoptosis of MSCs after injection which releases suppressing factors^{80,81}. However, the recruitment of endogenous MSCs rather than injection may prevent the apoptotic response seen^{71,82}. Despite being given the name medical signalling cells, MSCs have shown significant therapeutic benefit in cartilage repair, with proven cartilage formation by MSCs *ex vivo* in human explant models, and evidence of *in vivo* repair^{71,83,84}. In this work I will also show evidence of MSCs being involved in bone sclerosis, and therefore I strongly believe the name multipotential stromal cells is more suitable^{82,83,85}.

MSCs exist in multiple niches within the joint, including within the subchondral bone, synovial fluid, synovium and adiposal tissue⁸⁶⁻⁸⁸. Bone marrow MSCs are the best characterised, which co-exist with haemopoietic stem cells within the bone marrow, with exhibiting multiple effects over the other⁸⁹. This gives the bone-resident MSC multiple roles, both to control haemopoietic stem cell function, maturation and movement into circulation, as well as controlling host tissue-remodelling, bone repair after fracture and homeostasis of adiposal tissue in bone. MSCs were originally identified as rare bone marrow cells to adhere to plastic and proliferate to form fibroblastic colonies⁹⁰. Now better characterized, these bone MSCs are isolated through their Cluster of Differentiation (CD) antigens, with CD73, CD90 and CD271 being examples of the bone MSC markers⁹¹. To assist with this CD45 and CD31, markers of haemopoietic and endothelial cells, are used as negative markers⁹¹. These bone MSCs are found as a MSC perivascular population, as well as in stromal reticular niche, associating with venous sinusoids, which explains why, despite not being found in circulation, are able to rapidly home locally to where they are required^{86,92}.

Synovial MSCs can be found both in synovial fluid, and within synovial tissue projections, which has since been proven in the hip and knee by harvesting synovium during arthroscopy^{93,94}.

However the hip population was unable to be cultured *in vitro*, although the knee MSCs grew normally⁹⁴. This study also grew MSCs harvested from synovial fluid, which formed colonies in both tissues⁹⁴. Synovial MSCs are cited for their enhanced chondrogenic ability, thought to be related to their resident site being near cartilage⁹⁵. Synovial MSCs have been isolated from the talus of the ankle, and demonstrated standard requirements for MSC behaviour, however as this was not compared other MSC sites, relative differentiation capacity cannot be assessed⁹⁶.

Another common source of MSCs is from adiposal tissue, however these MSCs do not form osteogenic or chondrogenic tissue as readily as bone marrow MSCs⁹⁷. Within the ankle, 3 studies of adiposal MSC injection were identified, two from the subcutaneous buttocks, and one being lipoaspirate⁹⁸⁻¹⁰⁰.

MSCs have been shown to be elevated within the OA hip joint relative to a healthy joint, however do not initiate repair, with subchondral bone MSCs showing reduced mineralisation and altered migration⁵⁵. Additionally, CD271, a native MSCs marker, has shown their accumulation in bone near cartilage defects in immunohistochemistry, associating with CD56, a marker of bone forming cells, osteocytes^{85,101}. Furthermore, whilst in some cases of regenerative therapies cartilage has been reformed, the new cartilage does not integrate with the existing cartilage within the joint¹⁰². This leaves a potential for endogenous repair after correction of these.

MSCs are not generally believed to be found in cartilage, as such this is rarely targeted for cartilage repair, however there is some evidence in animal models. Archer *et al.* found that bromodeoxyuridine staining of chondrocytes indicated that chondrocytes are likely replenished from the superficial zone of cartilage, with a following study of the same group identifying an MSC-like population in the same location^{103,104}. Chondrocytes have shown the potential to de-differentiate into an MSC-like state. This was shown by isolation of cartilage chondrocytes and inducing growth of pellets, which showed formation of a marrow cavity by endochondral myelogenesis, which a chondrocyte would be unable to perform. This may however have been due to MSCs from within cartilage, should they exist within the tissue¹⁰⁵. Each of these studies may explain the other; however, there is no evidence in favour either.

MSCs are found in proximity to the OA disease site, as such provide a key target for regenerative therapies. However, there still remain barriers to clinical success. A key target of regenerative therapies is the ankle, due to its complexity which makes surgical treatments which retain function less effective in the long term. This is explored next.

1.4. OA of the Ankle

1.4.1. Prevalence

OA represents one of the largest medical economic burdens to current society, with an estimated cost estimation of \$89 to \$99 billion (in 2001 and 2006 respectively) to the USA annually ^{106,107}. Additionally, it is the fourth greatest loss in quality of life by disability in the UK, with a pain level equivalent to that of sufferers of end-stage kidney disease or congestive heart failure ^{108,109}. Between 2004 and 2010, 2.10 million, 4.72 million and 1.56 million consultations of OA for the hips, knees and hands were performed respectively. Interestingly however, 101,651 hip replacements and 108,713 knee replacements were performed, presumably due to the high success rate of hip replacements ^{1,110}. The majority of OA is age-related, particularly within the hands, hips, knees and spine, with the average age of patients receiving replacement being 70 years old ^{110,111}. Younger cases of OA within these joints are largely due to genetic predisposition, particular of matrix proteins within the cartilage such as collagen ¹¹².

The incidence of ankle OA is comparatively lower to that of the hip or knee. Between 2004 and 2010, 1.77 million patients received consultation regarding OA of the foot and ankle, as recorded by the Consultations in Primary Care Archive, forming 20% of consultations in this time period¹. Additionally, there is a lesser degree of total joint replacement in the ankle, with 839 procedures in 2016, compared to 100,000 hip replacement procedures. This is partially due to the preference of fusion over replacement in the ankle, but also as ankle OA is less common. However, this is a 15% rise in total ankle replacement (TAR) since last year, compared to the 3.5% increase in hip replacement ¹¹⁰. Additionally, the average age of patients who receive ankle replacement is 69.4, although the average age of patients reporting pain is only of 51.5 years of age ^{110,113}.

The ankle is mostly different from other joints due to the majority of cases occurring post-traumatically, with reports suggesting that this attributes to 70-90% of cases, whilst only 12% of all hip, knee and ankle OA cases are post-traumatic ^{106,113,114}. This may be due in part to the ankle being the joint most-often injured in sports, with one study finding 22.6% of all cases of injury being of the ankle, however participation in sport itself is not associated with arthritis ^{115,116}. Saltzman *et al.* studied 639 patients from a tertiary orthopaedic centre, and found that only 7% of all ankle OA cases were primary OA, and 70% were post-traumatic. As not all ankle injuries are reported, this may be an underestimation ¹¹³.

Primarily ankle OA is diagnosed in patients by examining the joint for signs of swelling, followed by an x-ray to look for evidence of joint-space narrowing or osteophytes. This will be confirmed by magnetic resonance imaging (MRI) to look for osteochondral lesions, or arthroscopy to

identify these lesions, visible by their yellow or grey discolouration from white, as well as fibrillation or detached cartilage. Whilst MRI is typically used to determine if a patient has ankle OA, the sensitivity is not perfect. Sugimoto *et al.* found that when arthroscopic evaluation was performed of patients with prolonged lateral instability of the ankle, 77% of ankles without abnormalities detected by radiography or MRI had subchondral lesions identified during surgery¹¹⁷. Additionally, a second study found with 3T MRI a sensitivity of 71% and specificity of 74%, and a third study a sensitivity of only 46% using 1.5T MRI for osteochondral lesions^{118,119}. This suggests the incidence of ankle OA may be higher than that currently reported.

Currently there is much less literature regarding ankle OA than that of the hip or knee. Results from the studies of the ankle are used alongside studies of other joints and compared directly to controls. This means that ankle OA is rarely studied as its own entity, which hinders both our understanding of ankle OA, as well as understanding within other osteoarthritic joints and their treatment.

1.4.2. Current Understanding of Progression

OA is a complex disease with multiple potential causes, progression pathways and initiation sites, as such its understanding is constantly evolving. The majority of OA originates from the articular cartilage of the joint, however, particularly in the case of post-traumatic OA, accelerated progression and MRI evidence suggests otherwise. Injury is most likely within the ligaments of the ankle, with the majority of these cases resulting in OA down the line¹¹⁵. Additionally, MRI of these injuries in the subsequent months often provide early predictors of OA onset¹¹⁹. The joints of the body include numerous structures, including bone, cartilage, tendon, synovium and in some joints the menisci, all of which undergo changes during OA, and it may be one or a combination of these from which OA progression initiates¹²⁰. The most common form of ankle injury is to the ligament; however there is importance to the fact that during injury, cartilage and bone fragments will potentially be removed from opposing surfaces from the force of impact, and so the point of origin for post-traumatic disease is more difficult to determine^{115,121,122}.

1.4.3. OA Progression in Cartilage

On the macro scale, during OA the cartilage undergoes fibrillation, the splitting of superficial layers, occurring horizontally aligned with the cartilage fibres at the beginning and slowly progressing to deeper layers. This creates clefts within the cartilage which can reach all the way to the bone, as well as leading to thinning of the cartilage. However, OA has a much more varied impact at the molecular level. As the cartilage of the joint is relatively acellular, as well as avascular and aneural to prevent vessel damage during compression, the extracellular matrix changes are key during the progression of OA^{20,120}. One of the changes to the cartilage associated with both old age and OA includes the tidemark being duplicated. This is evidence of mineralisation moving further towards the superficial layer, which increases the aggregate modulus and thus hindering the ability of the tissue to resist force¹²³. Additionally, the major component of cartilage to resist force, proteoglycans, are degraded during the process of OA, with loss in Aggrecan causing the most notable change, as defined by the earlier Sections. This reduces the amount of water which can be retained, further weakening the tissue. In addition, there is degradation of collagen fibrils, especially of type 2, which is central to forming the meshwork which holds GAGs in place.

On a cellular level, chondrocytes are found to die rapidly within the area of damage, and slowly cells of the surrounding areas undergo cell death after 48 hours. Additionally, whilst the high degree of MSC proliferation enables new synthesis of cartilage, this does not integrate with existing cartilage¹²⁴.

Garrido *et al.* applied an impulse of 1 Ns to an *ex vivo* human talus using a 4 mm diameter indenter in order to replicate injury, with peak forces in the range of 600N. This induced 70% cell death in the superficial layer on average, and around 35% in the middle and deep layers on average. After 48 hours, surrounding cells began to die, with 60% cell viability after 14 days¹²⁵. Whilst not a long-term study nor progression to OA, this shows a clear risk to the joint after injury. Shapiro *et al.*, as mentioned earlier, found that after injury there was a reduction in cell viability, although MSCs increased in number and aided new cartilage synthesis, however was unable to attach with the existing matrix, with fibrillation worsening after 36 weeks¹²⁴.

1.4.4. OA Progression in Bone

Compared with the midshaft of the long bones, subchondral bone of the joints contains less cortical bone and higher cancellous bone. This allows greater shock absorbance to protect the cartilage. This close relationship may account for why the subchondral bone is often affected during disease processes. Typically during early OA the subchondral plate becomes thicker, with bone growth and osteophyte formation. This is associated with increased vascular invasion, as well as formation of bone marrow lesions and subchondral bone cysts, leading to thinning of the cancellous tissue¹²⁶. A bone marrow lesion defines regions of bone beneath cartilage with tissue oedema, fibrosis and necrosis, whereas a subchondral bone cyst refers to a cavitory lesion within the bone^{35,127}. There is increased mineralisation, of almost five-fold in early stages²³. There is also micro-damage to the subchondral bone with breakage of the trabeculae and subsequent sclerosis³⁵. In late-stage OA, there is a reduced rate of bone mineralisation, as well as thickening of the subchondral plate. As such, OA is considered to be split into two phases, early resorptive and late bone anabolic¹²⁸.

Similar processes have been found within the ankle. Scintigraphy using 740MBq of 99mTechnetium labelled 3,3-diphosphono-1,2-propanodicarboxylic acid, which selectively binds mineralized bone, showed increased uptake in the tibia of 67% and talus of 33% in OA compared to healthy controls⁵². In the talus this increased uptake was associated with subchondral cysts, with uptake in both being local to the subchondral bone-cartilage interface. Additionally, staining of the areas without increased uptake within the subchondral bone marrow showed more features indicative of fatty tissue with more blood vessels and fat cells with few bone-lining cells. Staining of the increased uptake areas showed a fibrovascular morphology with high cell counts and significantly more osteoblasts, as well as increased collagen⁵².

OA progression specifically in the talus and tibia still remains poorly explored, as such became a key target of this work. To better guide a clinically relevant research process, existing treatments and their relevance to specific OA behaviours in the ankle were next investigated.

1.5. Treatments of Ankle OA

1.5.1. Conservative and Early-Stage Therapies

The first advice offered by doctors to patients diagnosed with symptomatic early-stage OA includes increasing their level of exercise and attempting weight loss to help to reduce pain. Early stage treatment includes the use of thermotherapy, electrotherapy or assistive devices, such as a brace, or manual therapy¹²⁹.

Those who suffer from OA will first be offered painkillers such as topical non-steroidal anti-inflammatory drugs (NSAIDs) or paracetamol¹²⁹. These have high efficacy, with a systematic review in hip OA of 58,451 patients finding clinical significance in all cases¹³⁰. If ineffective, oral NSAIDs, opioids or intra-articular corticosteroid injections are offered, however these have greater side-effects with debatable increase in efficacy. Corticosteroid injections showed significant improvement in 82% of ankle OA patients, however 30% of these required surgery within 2 years, with only 12% of patients still successfully being treated at 2 years¹³¹.

Injection of biological stimulants is another aspect considered. Clinically, hyaluronic acid and platelet rich plasma (PRP) have been areas of recent focus, with another, Kartogenin (K) showing strong benefits for cartilage formation by MSCs, however has not reached the clinical trial stage yet. Local hyaluronan injections are not recommended by National Institute of Health and Care Excellence (NICE) for the treatment of ankle OA, however are still used for research¹²⁹. Hyaluronan injections aim to restore proteoglycan content of the joint, however it does not remain in the tissue. The outcomes are debated, with some studies finding significant benefits, whilst others finding no difference from saline injections^{132,133}. As this targets cartilage directly, this was not considered for this work. PRP is concentrated blood extract, and therefore contains concentrated levels of growth factors and platelets, although red blood cells are removed. Injection of PRP into the ankle joint has shown a reduction in visual analogue pain score from 59.7 to 39.7 after 4 weeks, however the pain returned to 42.4 after 12 weeks, returning patients to the moderate pain category, showing similar effects to typical regenerative therapies¹³⁴. PRP has shown good outcomes *in vitro*, with the ability to enhance chondrogenesis by MSCs. However, it has also been attributed with bone formation, and there is a large amount of variation into the literature for its effectiveness¹³⁵⁻¹³⁸. Whilst this may in part be due to the variation in its composition, as PRP simply defines that platelets are concentrated in plasma, and so can have very different levels of platelets or growth factors between groups. This leaves a large body of research that still needs to be undertaken, and studies should use well defined PRP composition. For use *in vitro*, platelets in PRP are lysed by freeze-thawing to produce Platelet Lysate (PL), in order to enable its use long term, as platelets are not stable external to

the body for more than a day¹³⁹. As a supplement with the potential for increasing GAG production by MSCs by 6-fold, this became a stimulant of interest for this study¹⁴⁰. The second stimulant, Kartogenin, was identified in 2012, and is cited for its ability to induce chondrogenesis whilst inhibiting osteogenesis, therefore directly targeting the differentiation pathway of interest¹⁴¹. This stimulant has shown the ability to pre-commit MSCs towards chondrogenesis during preconditioning, as well as enhance chondrogenic differentiation during 3D culture, and increase release of extracellular vesicles with chondrogenic growth factors by MSCs^{142,143}. However, other studies have found K to produce no GAG unless combined with other, clinically unusable factors¹⁴⁴. To better understand the capabilities of K, this also became a key focus for inducing MSC differentiation in this work.

1.5.2. Non-Regenerative Surgical Treatments

Non-regenerative treatments of ankle OA include debridement, fusion of the talocrural joint, and Total Ankle Replacement (TAR).



Figure 1.5.1 Arthroscopic debridement of osteochondral lesion of the talus. Adapted from Medda *et al.* 2017¹⁴⁵.

Debridement is performed during arthroscopy, where a small incision into the anterior of the joint is performed, allowing use of small tools and a camera (Fig. 1.5.1). Should the signs of OA be identified, the damaged cartilage is removed through debridement, until a stable border of healthy cartilage has been reached. This allows integration of newly synthesized cartilage with the existing tissue, which cannot occur naturally due to

denatured proteins¹⁴⁵. Debridement is often combined with regenerative therapies.

Ankle fusion has long been the gold-standard for treatment of end-stage ankle OA. The procedure acts to simply prevent the joint from moving, thus preventing pain. The surgery typically involving flattening the tibia and talus to enable them to be fused onto one another, removing small amounts of bone from the tibia of dimensions around 25 x 18 x 8.2 (mm) and talus of 35 x 33 x 5.7 (mm)¹⁴⁶. As the gold-standard treatment, outcomes are typically very good. A level 2 trial of 107 fused ankles showed a 19.5±24.3 reduction in Ankle OA score (AOS) from 53 to 33, sufficient for satisfactory outcome. This was compared to 281 patients who received TAR for the same period, who showed a greater reduction of 25.7, however there was a much lesser rate of complication within the fusion group, as well as a longer survivorship. Of the fusion group, 7% failed within 5 years, mostly due to malalignment, whereas 19% of the replacement group failed due to aseptic loosening, fracture or deep infection¹⁴⁷. It is known that the largest

complications to ankle fusion include malalignment, which has been improving in recent years, however the change in biomechanics also leads to progressive adjacent joint OA, such as increases in biomechanical stress within the talonavicular and midfoot of around 50% with a shift in stress towards the medial side¹⁴⁸. A study by Ebalard *et al* of 72 fusions with minimum follow-up of 10 years found the rates of early-stage adjacent joint OA to be 73% tibiotalar, 58.3% subtalar, 65.8% talonavicular and 53.5% calcaneocuboid¹⁴⁹. However, the rate of this is also dependent on the alignment of the implant. The same study had normal alignment in 45% of cases, 22% varus and 33% valgus alignment, with malalignment correlated to the rate of adjacent joint OA¹⁴⁹. The complications of ankle fusion however are more-so than surgical outcomes but also complaints from patients from a lesser ability to perform tasks such as walking on an incline¹⁵⁰. As such the satisfaction with fusion perceived by the patient was mostly satisfactory, with 55% of patients considering the treatment good, although only 19% of patients in the study by Ebalard *et al*. found the outcome very good or better¹⁴⁹.

TAR is a technique that came about more recently due to the success of joint replacements elsewhere, with 93,000 primary replacements in both the hip and knee in 2016¹¹⁰. Whilst at first the outcomes were very poor due to the complex nature of the joint both complicating the design of a replacement and the surgical method, this treatment is now considered, at least, on par with ankle fusion, and is in preference for older patients with the average age of surgery being 67^{110,151}. This surgery is currently less common than fusion however, with only 839 replacements in 2016¹¹⁰. The goal of ankle replacement is to remove the pain of OA from the patient whilst also mimicking the biomechanics of the natural ankle, thus preventing adjacent OA, loss of movement, or balance in patients. Current outcomes are poor in comparison to other joints, with recent long-term survivorship rates of 78-86% at 10 years, 63% at 15 years and 55% at 19 years^{152,153}. These treatments do however show a higher patient satisfaction, range of motion and a lesser degree of adjacent-joint OA than ankle fusion, however, a higher rate of surgical complication, failure as well as pain scores remaining within the mild region¹⁵¹.

1.5.3. Regenerative Therapies

Current regenerative therapies for ankle replacement are typically applied in conjunction with debridement. These include microfracture, osteochondral autologous transplant (OAT), and autologous chondrocyte implantation (ACI). Whilst not performed arthroscopically, joint distraction of the ankle is also of note, as the method aims to spare the joint of load to enable endogenous repair by resident reparative cells. Each of these shall be discussed in this Section.

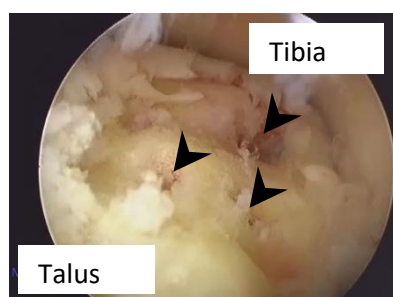


Figure 1.5.2 Microfracture with healthy cartilage border. Arrows show microfractures. Adapted from Medda *et al.* 2017¹⁴⁵.

Microfracture, visualised in Fig. 1.5.2, usually occurs after debridement of the damaged cartilage, with the access to a stable cartilage border being essential for repair. Small holes into the exposed bone are gouged after the debridement, typically 3-4 mm apart. This releases blood and cells from the subchondral bone, which then coagulate within the defect. These cells are able to adhere to the rough surface of the microfractures. Following microfracture there is initiation of repair, typically forming durable cartilaginous tissue within 2-6 months, with repair continuing over 2 years¹⁵⁴. However, after 2 years, cartilage gradually turns into fibrocartilage, and clinical outcome measures gradually fall¹⁵⁵. This leaves opportunity for enhancement of this surgery, such as use of biological stimulants to better improve outcomes such as PRP. When this treatment fails, microfracture is usually repeated until underlying bone becomes necrotic from repeated drilling and invasive surgical approaches are required³⁰. Additional methods such as nanofracture have been suggested, to better preserve surrounding tissue and elicit a cartilage repair response⁸⁴.

Osteochondral autologous transplantation involves the transplantation of cartilage from a donor-site articular surface to replace the lost cartilage removed during debridement. In the ankle OA, this is taken from the non-weight bearing regions of the knee or femoral head¹⁵⁶.

Randomized controlled trials have shown each of these treatments effective. One study compared microfracture with debridement against debridement only and OAT. Microfracture patients showed significant improvement in American Orthopaedic Foot & Ankle Society ankle-hindfoot score (AOFAS) score and Tegner Score (a measure of sporting activity) as well as reduction in visual analogue scale (VAS) of pain in comparison to arthroscopic debridement alone. Additionally there was an improvement in the range of motion of around 24°. The results of microfracture were very similar to patients who received an OAT (Table 1.1)¹⁵⁷.

ACI has been in use since 1994 and is considered one of the gold-standards for treating osteochondral lesions. The original technique involved taking a biopsy of healthy cartilage, and subsequent enzymatic digestion to release the chondrocytes. These cells are then cultivated for 11 days before releasing the cells from culture and injection of the cultured cells into a periosteal flap sutured over the lesion¹⁵⁸. Within the ankle, the modern approach has adapted to be purely arthroscopic, preventing the morbidities with open surgery, however requires the use of a scaffold to substitute the periosteal flap⁶. Long term results from a study of 5-7 years of 20 patients showed an increase in AOFAS score 60 months postoperatively, increasing after 87.2 months (Score changes presented in Table 1.1) However, the results of a small patient group, and results are skewed towards lower values. This suggests that whilst a majority have good outcomes, some patients see no improvement and require further surgery¹⁵⁹.

Joint distraction is a less invasive method of treating OA, aiming to greatly reduce load from the joint in order to allow space for repair, although this is conflicting with evidence suggesting mechanical stimulation is central for natural osteochondral homeostasis. This treatment is not recommended by NICE, except in the case of research, as positive outcomes have yet to be proven¹⁶⁰. The treatment is typically undertaken for a year or more, creating a gap of

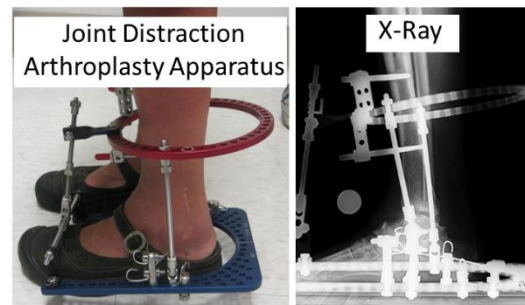


Figure 1.5.3 Apparatus used in immobile ankle joint distraction aiming to hold the tibia and talus in place to prevent opposing articular surface contact. Adapted from Bernstein *et al* 2017¹⁰.

up to 5 mm between the tibia and talus, with the aim of partial regeneration of the joint once the apparatus is removed¹⁶⁰. Typical immobilisation apparatus is shown in Fig. 1.5.3. A systematic review of 249 patients showed variable outcomes, with most of the studies being of small case study groups. Overall, the rate of good outcome varied from 73% to 91%, however patients between 6.2% and 44% requiring further surgical intervention, such as TAR or fusion. The study subsequently recommended a minimum of 5.8 mm distraction gap for optimum outcome, to maintain no contact between articular surfaces during full weight bearing, in line with Fragomen *et al.*'s cadaveric study results, but converse with the typical "up to" 5 mm distraction gap used¹⁶⁰⁻¹⁶². In one of the studies included, Nguyen *et al.* reported an improved outcome in those with earlier stage OA, as well as in patients of older age¹⁶³. However, the OA had worsened after 8 years in most cases^{163,164}. A recent study reported significant improvements in pain, level of disability and AOFAS score following 3 months of 1 mm distraction¹⁶⁵. A more recent approach has been combining joint distraction with other approaches. Within a study combining microfracture with joint distraction, 46 patients

underwent ankle distraction alone and 50 with microfracture as well as distraction. Both didn't require further surgery and improved pain and AOFAS scores, both being slightly further improved with additional microfracture, which whilst significant, was only of an additional 20% improvement (presented in Table 1.1) ¹⁶⁶.

Each these regenerative therapies aims to create an environment where the tissue can repair itself. However, they lack the addition of biological stimulants or scaffolds to better help resident reparative cells regenerate the tissue. Some treatments exist to take advantage of this, such as the addition of bone marrow concentrate, or the use scaffold in a process termed matrix-assisted chondrocyte implantation (MACI) ^{167,168}. However, as yet, these still show similar outcomes to other regenerative therapies, with progressive cartilage degeneration after 2 years ¹⁶⁸. Better understanding of resident reparative cell potency will aid improvements of these therapies, by being better able to direct MSC differentiation, and focus on additional stimulants to mitigate morphological changes in bone and cartilage structure, as well as MSC behaviour.

Table 1.1 Regenerative Therapies for OA

Author, Year, Ref	Treatment	Patients	Mean Age	Length of Treatment	Mean Follow-up (Months)	Clinical Result	Rate of Failure
Sun (2016) ¹⁵⁷	Debridement	48	34.6	N/A	27.4	AOFAS: 53.7 to 64.9 VAS: 7.5 to 5.2 10.6 improvement in ROM Score	NR
	Debridement and Microfracture	53	34.5	N/A	27.4	AOFAS: 52.4 to 76.7 VAS: 7.6 to 2.7 24.5 improvement in ROM Score	NR
	Debridement and OAT	52	33.2	N/A	27.4	AOFAS: 54.5 to 79.6 VAS: 7.5 to 5.2 26.2 improvement in ROM Score	NR
Pagliazzi (2017) ¹⁵⁹	ACI	20	35	N/A	87.2	AOFAS: 58.7 ± 15.7 to 90.9 ± 12.7	NR
Ploegmakers (2005) ¹⁶⁹	Joint Distraction	27	NR	3 Months	10 ± 2.5	AOS: 74 ± 5% to 32 ± 7%	27%
Tellisi (2009) ¹⁷⁰	Joint Distraction	25	43	3 Months	30	AOFAS: 55 to 74 10-point gain in ROM	8%
Intema (2011) ¹⁷¹	Joint Distraction	26	NR	3 Months	24	AOS: 60.3 ± 3% to 35.4 ± 4%	NR
Saltzman (2012) ¹⁶⁴	Joint Distraction	36	NR	3 Months	25	AOS: 63 ± 11% to 34 ± 19%	NR
Marijnissen (2014) ¹⁷²	Joint Distraction	25	NR	3 Months	8.1 ± 5.1	Data was only presented statistically	44%
Nguyen (2015) ¹⁶³	Joint Distraction	29	41.5	3 Months	8.3 ± 2.2	AOS: 60 to 33 in treatments which did not fail	45%

AOFAS – American Orthopaedic Foot and Ankle Society Score, OAT – Osteochondral Autologous Transplant, AOS – Ankle OA Score, NR – Not Reported

1.5.4. Potential MSC Based Treatments

MSC therapy for ankle OA is a logical step, considering they already exist within the musculoskeletal system, can produce bone, cartilage and fat of the joint, and can play an immunomodulatory role, as explained earlier in the chapter (Section 1.3). Current treatments include the injection of a form of MSCs into the OA joint with a biological agent to assist growth. Culture expanded MSCs or bone-marrow concentrate (BMC) have been shown within ankle OA patients to have no risk within human application⁹⁸. One study of autologous bone-derived MSC injection into patients with moderate to severe OA of the hip, knee and ankle revealed that the treatment was safe, whilst also reducing pain and showing both cartilage repair and functional improvement, although pain measured by VAS returned to baseline level after 30 months¹⁷³. As such, whilst these treatments exist, they have yet to provide long term clinical benefits, or pass clinical trials.

An additional method of MSC application includes the use of bone marrow concentrate (BMC). By taking MSCs from the source, the expensive nature of cell culture can be avoided, as well as the complex legal regulation of expanded cells. This also allows inclusion of growth factors naturally found in bone marrow such as Transforming Growth Factor- β (TGF- β), Bone Morphogenic Protein-2 (BMP-2) and Vascular Endothelial Growth Factor (VEGF)¹⁶⁷. A study by Hauser *et al.* showed multiple local deliveries of BMC combined with hyperosmotic dextrose for ankle OA treatment both reduced pain and improved function, however only had one case of ankle OA. The patient did not report quantitative pain outcomes, although the patient regained the ability to stand and walk for long period of time without pain and improved range of motion¹⁷⁴. Combination of this BMC with a scaffold enriched with platelet-rich fibrin which acts as a source of growth factors, showed an outcome equal to with ACI, whilst also only requiring a single-step procedure⁸. Again, results of using BMC within OA have only been shown short term, at a maximum period of two years. Additionally, bone cysts and symptoms persist in a proportion of treatments, whilst successful treatment provides only minimal benefits to established ones such as ACI.

MSCs can also be derived from adiposal tissues, with one study showing improved cartilage repair with adiposal MSC injection in combination with microfracture compared to microfracture alone, with improved VAS and AOFAS scores, although VAS scores still remained at around 5 in 1-10 scale, suggesting the patient remains in the mild region of pain¹⁷⁵. As such, the treatment does not fully restore activity to the patient. This study was only conducted over a short period, of one year, and as such longer-term studies would be required to determine the success of treatment. Additionally, AOFAS scores were lower than existing treatments including ACI¹⁵⁹.

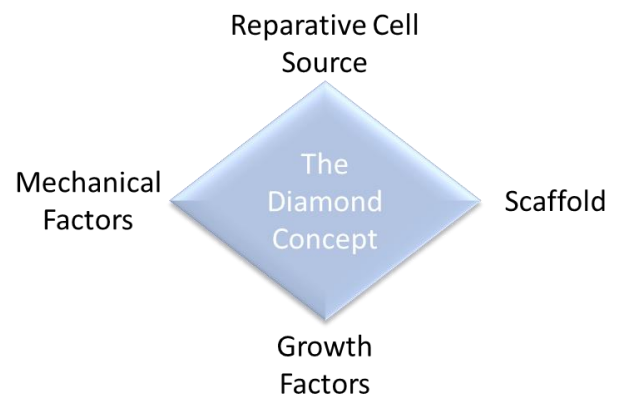
The lack of long-term improvements from existing treatments, as well as poor outcomes in early-stage treatments suggest a need for new approaches. It has been shown that MSCs have the potential for regeneration, however their culture before re-implantation is expensive, with high risk of cell infection, and addition to complex regulation of cultured cells. Whilst removal of autologous MSCs for treatment has already been performed, there still remains a myriad set of issues. Expanded cells lose their innate behaviour, including a reduction in chondrogenicity compared to native cells¹⁷⁶. Furthermore, the source of cells remain an issue, considering that MSCs can be difficult to isolate in large numbers from the bone or synovium, cells are often taken from adiposal tissue, which have their own differentiation pathways in comparison to bone marrow-MSCs¹⁷⁷. Additionally, whilst bone marrow-MSCs have been shown to form cartilage, this is typically of a fibrocartilage nature, formed with collagen type 1. Whilst this is how cartilage typically forms during development, full regeneration of hyaline cartilage would require type 2 collagen¹⁷⁸.

Regenerative therapies are one of the most common employed approaches to treatment of osteochondral lesions of the ankle, aiming to treat the disease before OA progresses to a severe level which requires irreversible surgical treatment. However, regenerative therapies show declining outcomes after 2 years, which is less than ideal. This Section will next discuss methods that these regenerative therapies could be enhanced through.

1.6. Current Areas of Regenerative Therapy Development for MSC Enhancement

So far, this chapter has shown that the ankle joint is a common target for regenerative therapies, and it is likely that MSCs are localised within the tissue, if not yet proven. MSCs are a common target of these regenerative therapies as a source of endogenous repair, although this is not always specifically cited. Despite these regenerative therapies showing some success, their long-term outcomes are hindered by the formation of fibrocartilage preventing successful repair. This chapter will next discuss the use of stimulants for better improving repair, with a particular focus on MSCs as a likely candidate for mediating endogenous repair.

Regenerative therapies have long cited the 'diamond' concept for factors which effect repair, shown in Fig. 1.6.1. Whilst proposed for bone fracture repair, the same factors are key for cartilage repair as well¹⁷⁹. The reparative cell source will affect repair in terms of differentiation capacity and response to the



environment, with the case for MSCs already being explained earlier (Section 1.3). The choice of scaffold will affect MSC differentiation based on its material properties and any biologically active components. Growth factors can direct MSC differentiation or control their proliferation^{144,176}. Lastly, mechanical factors such as compression affect cell signalling through rearranging the MSC cytoskeletal system, which will also change MSC behaviour¹⁸⁰. As such, therapies both need to consider the effect of these, and if needed develop suitable conditions for each to best program repair. As current therapies mostly target just the release of MSCs or the addition of the scaffold, there are many avenues to develop MSC-enhanced repair.

Figure 1.6.1 The Diamond Concept for Regenerative Therapies. Adapted from Giannoudis *et al.*¹⁷⁹.

1.6.1. Impact of the Scaffold on MSC Behaviour

Scaffold effect on MSC behaviour has been well explored. Scaffolds can affect MSC behaviour in 3 major ways. Biomaterials used for MSC differentiation utilise synthesised materials, which in cartilage repair mostly focuses on soft materials. This is because the mechanical properties of the scaffold effect MSC differentiation. Scaffolds with higher Young's moduli direct MSCs towards bone, whereas lower Young's moduli induce chondrogenesis of MSCs^{181,182}. Material strength changes depending on the base material(s) chosen, synthesis method, degree of cross-linking, gelation speed and even the temperature during synthesis, resulting in scaffolds which are highly tuneable to the specific need^{181,183,184}. Softer material substrates showed increased

GAG production and reduced stress-related fibres such as α -actin, suggesting a lower stiffness promotes chondrogenic differentiation⁴³.

Secondly, MSC behaviour is affected by any bioactive components of the scaffold^{185,186}. Whilst some scaffolds do not have any biological activity, preventing interaction with MSCs, some have innate interactions with MSCs such as collagen-based scaffolds, which can enhance MSC attachment, or fibrin-based scaffolds where fibrinogen domains during synthesis can enhance MSC homing^{83,187}. Additionally, scaffolds can be enhanced with biofunctionalization, with some common examples including RGD-domains to enhance cell adhesion, or addition of calcium phosphate to improve osteogenic differentiation^{185,188}. A major point is also that the scaffold is biocompatible, which can have a range of meanings. In terms of cartilage repair, biocompatible means that the scaffold does not raise an immunogenic response, supports both cartilage synthesis and integration with patient tissue, and the material is resorbed by the human body once mechanically competent cartilage has been synthesised and natural tissue biomechanics have been restored¹⁸⁹. Within the talocrural joint, MACI, as described earlier (Section 1.5.3) utilises scaffolds, but has a focus on chondrocytes¹⁹⁰. The most common scaffold is a type I/III blended hydrogel, with a prominent clinical example being Chondro-Gide^{®168}. Whilst this technique is, like other regenerative therapies, effective for 2 years, there is a steady decline in outcome as shown in a systematic review by Shaikh *et al.*, falling by half of the 'best' value seen at 2-year follow up at the 4 year follow-up¹⁶⁸.

The range of requirements and effects of scaffolds create a large degree of complexity and cost to MSC therapy, which also needs to be considered for developing cartilage regenerating treatments which enhance endogenous repair. As such, the focus should be on a scaffold which is biocompatible, mechanically favours cartilage, encourages homing of resident MSCs, and lastly improves repair without overcomplicating scaffold design to minimise cost and prevent masking of other scaffold effects. The various materials utilised, clinical examples, and their impact will be investigated further in the relevant chapter (Chapter 6).

1.6.2. Growth Factors in MSC Differentiation

The third key part of MSC differentiation is growth factors. Growth factors are bioactive polypeptides produced by cells to stimulate cellular activities such as growth or differentiation, which induce synthesis of key ECM components such as type II collagen, aggrecan or cartilage oligomatrix protein (Section 1.2.7)¹⁹¹. Key growth factors utilised for cartilage repair include transforming growth factor (TGF- β 1), bone morphogenic protein (BMP-2, BMP-7), insulin growth factor (IGF-1), fibroblast growth factor (FGF-2) and platelet derived growth factor (PDGF) among others^{191,192}. The addition of these as biological stimulants however is more complicated,

as they may have effects off target, such as TGF- β inducing fibrosis in synovium¹⁹³. As such, biological stimulants are also employed, which may contain an assortment of growth factors or other bioactive compounds. Examples of these commonly used clinically in cartilage repair of the ankle include platelet rich plasma (PRP), for their own effects on cartilage repair. PRP showed significantly improved outcomes up to 16 months in a systematic review of clinical trials, with reduction in pain by VAS score and improved AOFAS score, however still showed a decline in function over time as seen in most studies of regenerative therapies for cartilage repair in the ankle¹⁹⁴. These will again be investigated in more depth in the relative chapter (Chapter 5).

1.6.3. Mechanical Stimulation Effect on MSCs

The fourth cited crux of MSC differentiation includes the effects of mechanical forces. Application of mechanical forces to MSCs includes compression, tension, shear forces (perpendicular frictional force) or hydrostatic pressure (gravitational force of water). A study of cyclical mechanical compression of synovial-derived MSCs showed an increase in BMP-2 levels during both osteo- and chondrogenic differentiation, with knock-out of BMP-2 removing expression chondrogenic and osteogenic factors. This was found at a compressive stress of 2.3 Pa, 0.33 Hz frequency, and 8% strain¹⁹⁵. Using multi-axial load, Gardner *et al.* found activation of latent TGF- β , which drove chondrogenic differentiation of bone marrow-MSCs grown on a fibrin-poly(ester-urethane) scaffold. In this study, the cells were exposed to 20 1-h cycles of 10% compression superimposed on a 10% pre-strain and shear loading ($\pm 25^\circ$) at 1 Hz for 1 h a day five times a week for 4 weeks¹⁹⁶. Lin *et al.* performed dynamic loading of bone marrow-MSCs upon a methacrylated hyaluronic acid scaffold after chondrogenic preconditioning with chondrogenic medium. The results showed that the healing of osteochondral lesions within a rat model was greatly enhanced after both preconditioning and dynamic loading compared to free-loading, with 62.3% more GAG and 35.9% more collagen¹⁹⁷. Carroll *et al.* exposed porcine bone marrow-MSCs loaded on a fibrin scaffold to uniaxial cyclic tensional strain, with strain of 10% at 0.5Hz frequency for 4 hours each day over 7 days This demonstrated increased alignment of MSCs and synthesis of collagen, with no visible chondrogenic differentiation¹⁹⁸. Summary results of various studies for the effects of mechanical stimulation upon MSCs is summarised in Table 1.2. Both mechanical stimulation and scaffold stiffness seemed to activate similar factors, and should aim to produce TGF- β for chondrogenesis and BMP-2, Run Runt-Related Transcription Factor 2 (RUNX2), Osteoprogenin (OPN) and alkaline phosphatase (ALPL) for osteogenesis, although additional genes were expressed after mechanical stimulation, including collagen.

Table 1.2 The Effect of Mechanical Stimulation Upon MSCs

Author, Year and Reference	Cell Type Used	Force Applied	ECM Changes	Signalling Factor Changes
Fu <i>et al.</i> 2017 ¹⁹⁵	Synovial- MSCs	Cyclical Compression	-	BMP-2 Increase
Gardner <i>et al.</i> 2017 ¹⁹⁶	Bone Marrow- MSCs	Multi-axial Loading and shear stress	-	TGF- β increase
Lin <i>et al.</i> 2017 ¹⁹⁷	Bone Marrow- MSCs	Dynamic Compression	60% increase in GAG, 30% increase in collagen	-
Carrol <i>et al.</i> 2017 ¹⁹⁸	Bone Marrow- MSCs	Uniaxial Tension	COL1A1, COL10A1, OPN, ALPL increases	BMP-2, RUNX2 increase
MSC - MSC, BM - Bone-Marrow Derived, BMP – Bone Morphogenic Protein, TGF – Transforming Growth Factor, RUNX2 – Runt-related transcription factor 2				

Within the ankle, mechanical stimulation of MSCs has not been performed, however it has been performed upon cells isolated from the iliac crest and subsequently cultured on a collagen scaffold using pulsed electromagnetic fields, which may have included MSCs in the tissue mix. This was performed as a clinical trial as an addition to bone marrow derived cell transplantation during debridement of an osteochondral lesion. Results showed significantly higher AOFAS scores compared to patients without the added mechanical stimulation, as such showing the mechanical stimulation itself provided some form of benefit¹⁹⁹. However, iliac crest cells include cells of many functions, including immunomodulation and haematopoiesis. As such the mechanical stimulation may have played some role in controlling these tissues as well²⁰⁰. Additionally, mechanical stimulation is known to be essential in cartilage homeostasis, with rapid reductions in its properties when immobilized, and as such the mechanical stimulation may not have improved the outcome due to the impact on the cells themselves²⁰¹. Investigating if the mechanical stimulation is likely to have improved MSC behaviour, and its mechanism of action, may provide new methods or treatments to improve the outcomes of early-stage ankle OA interventions.

1.7. Current Challenges of the Research Area

Currently, there is a lack of literature within the ankle for OA, with the existing knowledge being that ankle OA is mostly post-traumatic, and a distinct clinical entity from OA in the hip or knee. In evidence of this is the increased anabolic response as well as the thinner cartilage structure. An understanding of the changes in cartilage within ankle OA needs to be defined separately from other joints, with current knowledge being increased sulphated GAGs, lower water content, and higher synthesis and turnover of both proteoglycans and collagen²⁸. A better understanding of OA progression within the ankle to reveal potential targets for regeneration. Existing treatments for ankle OA all show individual merits to the patient, however, present low patient satisfaction and relatively short-term benefits of less than 20 years. Application of the diamond concept in repair, including consideration of resident MSC potency, and application of scaffolds, biological stimulants and mechanical forces will lead to enhancements of existing regenerative therapies, which already employ the tools required, but not in combination. Microfracture allows access to resident cells, MACI describes addition of a scaffold, and joint distraction offers the ability to control the mechanical environment, in addition to chondrogenic biological stimulants that are currently being researched.

When looking at MSCs as a potential treatment option, the outcomes of clinical trials using cultured MSCs have shown good benefits, however the cost of bringing such a product to market is extensive and will not benefit a large majority of patients at current pricing, as such the use of autologous cells is beneficial. Current isolation of MSCs is a slow process, and production of enough cells for autologous treatment of many OA patients would require a mass-production technique which reduces the complexity and cost of cell culture whilst also reducing risk of cell infection. As such scaffolds which recruit existing MSCs of the patient to the wound site (*in situ* regeneration) would be ideal, whilst also only requiring a single step. The MSC homing could either be enhanced by including growth factors within the scaffold itself or additional factor supply such as from soaking the scaffold in platelet-rich plasma. Additionally, the growth of MSCs could be enhanced by use of the novel techniques of mechanical stimulation, which has previously shown enhancement in both osteogenesis and chondrogenesis. However, a method that could be performed within the patient would be required, which also allows both tensile strain for bone formation, and compressive strain to aid cartilage formation. MSCs would be sourced from the subchondral bone, possibly through use of microfracture. Additionally, a scaffold which varied in stiffness to mimic the transition from bone to cartilage would also be ideal.

1.8. Thesis Aims and Objectives

The overall aim of this study was to further improve understanding of OA within the talus and tibia, and investigate the ability for endogenous repair by resident, reparative cells, MSCs by the use of biological stimulants. As the talus and tibia are tissues with specific structure and biomechanics which may lead to different behaviour compared to other joints and create specific challenges for repair. The presence of reparative cells, MSCs was assessed based on standardised criteria and investigated in relation to other joints to identify, if any, changes specific to the OA ankle. Information gleaned from this was then used to guide development of a 2-step clinically relevant treatment process to direct MSCs taken from OA bone towards chondrogenesis, to identify if there was possibility for endogenous repair of the ankle by talocrural MSCs, and the extent to which different biological stimulants could enable this. This investigation has been conducted through:

- To perform computed tomographic, histological and immunohistochemical analysis of OA tissue from human osteochondral explants retrieved from ankle fusion surgery for end-stage OA (Chapter 3)
- To extract and prove MSCs identity of cells enzymatically extracted from human osteochondral explants retrieved from ankle fusion surgery using standard ISCT criteria for MSCs, and investigation of their specific differentiation properties in relation to non-diseased iliac crest control MSCs (Chapter 4)
- To develop a preconditioning method for MSCs to both increase small numbers of isolated MSCs and direct them towards a chondrogenic stage, whilst inhibiting osteogenic differentiation (Chapter 5)
- To develop 3D culture methods for induction of chondrogenic differentiation of talar and distal tibial MSCs, utilising xeno-free biological stimulants, to work synergistically with preconditioning to best guide chondrogenesis (Chapter 6)
- To compare the effect of preconditioning and 3D differentiation of iliac crest, talar and distal tibial MSCs to investigate viability of biological stimulants Kartogenin and platelet lysate as chondrogenic inducers for clinical translation (Chapter 6)

2. Chapter 2 - General Materials and Methods

2.1. Sample Retrieval and General Processing

Reagents, Solutions, Buffers and Equipment are detailed in the appendix (Supplementary Tables 8.3.1-8.3.5).

Ethical approval for human ankle tissue collection (07/Q1205/27), and control Iliac Crest (IC) tissue collection (06/Q1296/127) was obtained from NREC Yorkshire and Humberside National Research Ethics Committee, in compliance with the Helsinki Declaration of ethical principles for medical research involving human subjects. Seven ankle OA patients (median age 66 years, range 34-73, 4 male 3 female) were included after signed consent was received. Each patient underwent fusion of the talocrural joint for OA. Inclusion criteria included patients between 18 and 85 years old, undergoing ankle fusion. Exclusion criteria included Rheumatoid arthritis or septic arthritis. IC bone from 3 donors was obtained from patients undergoing orthopaedic surgery for metal removal following previous fracture, who were otherwise healthy. Samples were placed immediately into saline post-surgery and transferred to the laboratory. Inclusion criteria included patients aged 13-80, undergoing surgery at Leeds General Infirmary. Exclusion criteria was that patients were not under 13. Non-diseased human cadaveric ankles (age 40-60 years, all-male, no evidence of ankle OA) were obtained from Medcure, USA, under local university ethics, and stored at -80°C before distal tibia and talus were removed for imaging. Inclusion criteria was that were patients were between 30 and 60 years of age. Exclusion criteria was history of lower limb or trauma surgery, or diabetes. Porcine legs of 6-month-old pigs were obtained from a local accredited abattoir, within 24 hours of slaughter.

Table 2.1 Distal Tibia and Talus Sample Characteristics Retrieved from Ankle Fusion

Sample ID	Experimental Use	Donor Age (Years)	Donor Sex
WJ001	Histology	70	M
WJ002	Histology	46	M
WJ003	Histology	46	M
WJ004	mCT	75	F
WJ005	mCT	64	M
WJ008	mCT	57	M
WJ011	MSC Isolation	58	F
WJ012	MSC Isolation	34	F
WJ013	MSC Isolation	66	M
<i>Averages</i>	<i>N/A</i>	<i>57</i>	<i>66% male 33% Female</i>

All samples were washed in sterile PBS upon arrival, and either frozen at -80°C for storage before mCT, placed into ethanol for histology, or the sample digestion process begun, described further in the relevant Sections. Characteristics of samples are described in Tables 2.1.1-2.1.3.

An additional 6 donors of Iliac Crest (IC) MSCs were used to optimise MSC preconditioning and 3D differentiation for chondrogenesis after preconditioning experiments. These were from a separate ethics for previously isolated IC MSCs, and are shown in Table 2.1.4 (06/Q1296/127).

Table 2.2 Distal Tibia and Talus Sample Characteristics from Healthy Donor Tissue

Sample ID	Experimental Use	Donor Age (Years)	Donor Sex
LK01	mCT	43	M
LK02	mCT	50	M
LK03	mCT	57	M
<i>Averages</i>	<i>N/A</i>	<i>50</i>	<i>100% male</i>

Table 2.3 Fresh Iliac Crest Sample Characteristics

Sample ID	Experimental Use	Donor Age	Donor Gender
ICC1	MSC Isolation	32	M
ICC2	MSC Isolation	42	F
ICC3	MSC Isolation	41	M
<i>Averages</i>	<i>N/A</i>	<i>38</i>	<i>66% Male, 33% Female</i>

Table 2.4 Frozen Iliac Crest Sample Characteristics

Sample ID	Experimental Use	Donor Age	Donor Gender
TRBM10	Preconditioning	44	F
GCBM11	Preconditioning	28	M
BM140207	Preconditioning	19	M
<i>Average</i>	<i>N/A</i>	<i>30</i>	<i>66% Male 33% Female</i>
RC071	Chondrogenic induction		
GCBM11	Chondrogenic induction	28	M
BM313	Chondrogenic induction		
<i>Averages</i>	<i>N/A</i>	<i>38</i>	<i>66% Male, 33% Female</i>

2.2. Sample Processing for Histology

2.2.1. Decalcification Process

Whole talus and distal tibial Sections from 4 ankle OA patients were fixed in 3.7% formaldehyde for 1 week, and subsequently decalcified in 0.5 M EDTA for at least 3 months, with EDTA replaced, as necessary. Specifically, this was daily for the first week, every two days for the second week, and then once per week, as decalcification slows over time due to accessibility of the calcium within bone. Decalcification was confirmed using dental X-ray²⁰². Once decalcified, samples were fixed for a further 48 hours in 3.7% formaldehyde, and then embedded in paraffin blocks. This process is explained further in Section 2.2.2.

2.2.2. Tissue Processing and Paraffin and Embedding

Once fully decalcified, samples were embedded in paraffin to allow flat, 5µm Sections to be taken. Once the bone had fully decalcified, the sample was fixed in 250 ml 3.75% formaldehyde for 2 days, after which the formaldehyde was removed, sample washed in 50 ml PBS and placed in 250 ml 70% ethanol. The sample was subsequently embedded in paraffin over two weeks using the Leica ASP200 Embedding system, according to Table 2.2.1 Once this was completed, the samples were placed into a mould and covered in paraffin, which was solidified at 4°C on the embedding system. Samples were orientated perpendicular to the cartilage surface.

Table 2.5 Paraffin Embedding Process

Process	Step	Solutions and Reagents	Time (Hours)	Temperature (°C)
Paraffin Embedding	1	70% Ethanol (in water)	1.00	37
	2	80% Ethanol	2.00	37
	3	90% Ethanol	2.00	37
	4	95% Ethanol	3.00	37
	5	100% Ethanol	12.00	37
	6	100% Ethanol	12.00	37
	7	100% Ethanol	12.00	37
	8	Xylene	12.00	37
	9	Xylene	24.00	37
	10	Xylene	24.00	37
	11	Paraffin Wax	12.00	65
	12	Paraffin Wax	24.00	65
	13	Paraffin Wax	24.00	65

2.2.3. sectioning and Baking

Embedded samples were placed on ice to cool prior to sectioning. From the embedded samples, 5µm Sections were taken by microtome and left to flatten in a water bath heated to 45°C for 10 seconds. These were lifted onto HISTOBOND® Supa Mega White charged microscope slides for large whole ankle fusion OA samples, or Histobond® + S White microscope slides for all other samples. These were then dried overnight at 28°C and baked for 4 hours at 45°C on a hotplate.

2.2.4. Deparaffinisation and Rehydration

Prior to staining, Sections must be deparaffinised and rehydrated to allow dyes to permeate and stain the Sections. This was performed by repeated submersion in xylene and different grades of ethanol as described in Table 2.2.2.

Table 2.6 Deparaffinisation and rehydration protocol

Process	Step	Solutions and Reagents	Time (mins)
Dewaxing	1	Xylene	3:00
	2	Xylene	3:00
	3	Xylene	3:00
	4	Xylene	3:00
Rehydration	5	100 % Ethanol	3:00
	6	100 % Ethanol	3:00
	7	100 % Ethanol	3:00
	8	100 % Ethanol	3:00
	9	75 % Ethanol	3:00
	10	50 % Ethanol	3:00
	11	25 % Ethanol	3:00
	12	Running tap water	1:00

2.2.5. Dehydration and Application of Coverslips

Once staining had been performed, Sections were dehydrated, and coverslip added for long term storage. This is simply an inverse process of the rehydration process, followed by placing Distyrene Plasticiser Xylene (DPX) on a coverslip and adhering it to the slide, as described in Table 2.2.3

Table 2.7 Dehydration and Cover slipping

Process	Step	Step	Time (mins)
Dehydration	1	Dehydrate with 3 changes of 95% EtOH	1:00 per change
	2	Dehydrate with 2 changes of 100% EtOH	1:00 per change
Clearing	3	Xylene	3:00
	4	Xylene	3:00
	5	Xylene	3:00
Coverslip	6	DPX	N/A

Table 2.2.3 is a continuation of most staining processes described in other chapters

2.3. Cell Extraction from Bone using Collagenase

2.3.1. Sterilisation of Solutions and Equipment

Where not mentioned, tools used for cell culture were purchased as sterile disposables. Equipment used for breaking down bone such as the Rongeurs were sprayed with Distel and left for 1 minute, wiped with ethanol, then rinsed with water and then autoclaved at 121°C, 1ATM for 30 minutes prior to use. Preparation of sterile solutions is listed in the solutions table in the appendix (Supplementary Table 8.3.1-8.3.3), however in all cases was performed by sterile filtration through 0.22µm filters.

2.3.2. Collagenase Extraction of MSCs

Firstly, cells were isolated from bone, using field specific practice⁷². In sterile conditions, talus and distal tibia samples of 3 ankle OA patients were washed three times in PBS, and then articular cartilage and soft tissue were removed using a scalpel, and subsequently discarded. Submerged in 25 ml of dPBS to keep the tissue hydrated, subchondral bone was mechanically minced into small fragments using a rongeur, and then transferred to a falcon tube with known weight of dPBS for weighing. Samples were digested for 4 hours at 37°C in 600 U/ml collagenase with 5 ml per gram of bone, with agitation every 30 minutes. The liquid fraction was then filtered through a 44 µm pore filter, followed by running dPBS through the filter after all liquid was filtered in order to ensure all cells were collected. This was then repeated for the filtrate in a 22 µm pore filter, as the original sample would have not passed through a 22 µm filter. The filtered solution was then spun by centrifuge at 13 g and transferred into a new 50 ml falcon to remove

fat and remaining debris. This solution was then centrifuged at 500 g for 10 minutes, and the supernatant disposed of²⁰³. The cell pellet was typically re-suspended in 5 ml 1% P/S StemMACS media, depending on the pellet size. Cells were then counted using haemocytometer (Section 2.4.2) and used for CFU-F assay (Section 4.2.3) or culture expansion (Section 2.4.5).

IC MSCs were isolated and expanded with the same method except that the removal of cartilage and soft tissue was not necessary. The overall process is detailed in Fig. 2.3.1

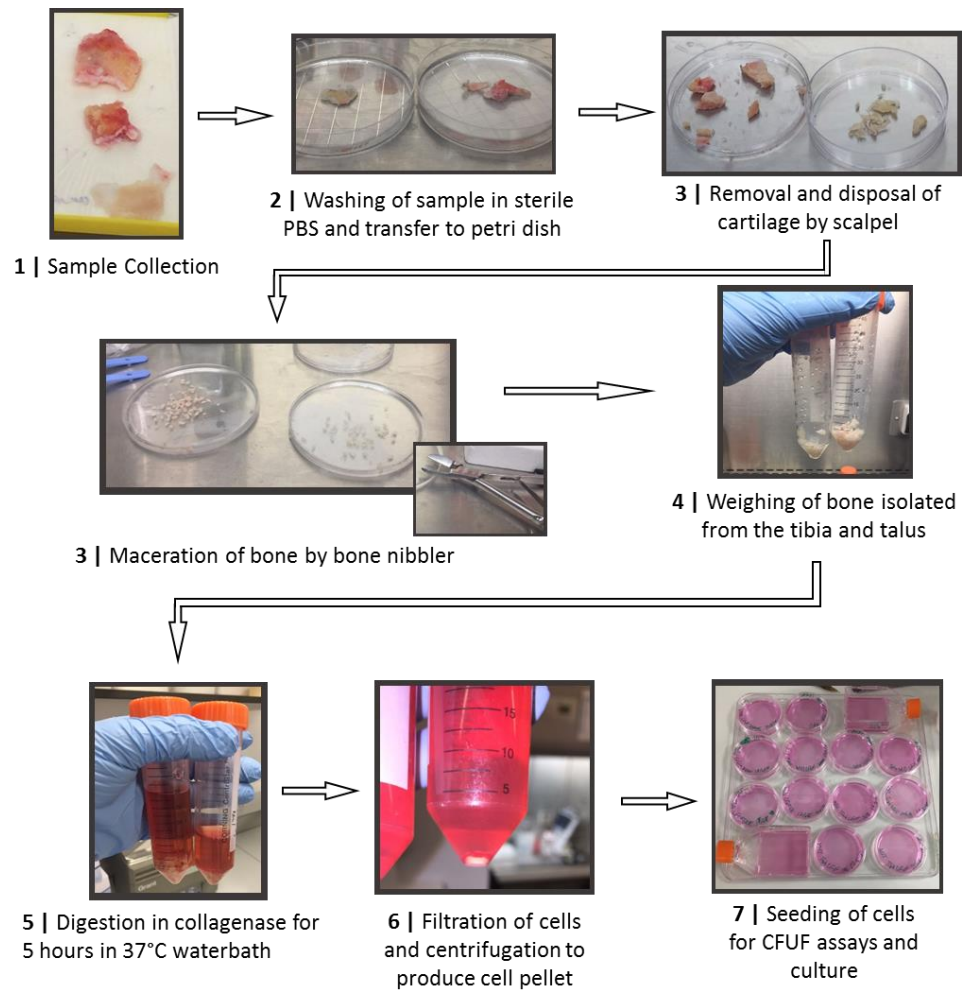


Figure 2.3.1 MSC Extraction Process of Talar and Tibial MSCs.

2.4. General Cell Techniques

2.4.1. Cell Seeding

To generate putative MSC cultures, as well as to produce enough cells for further experiments, cells were grown in culture. Approximately 1×10^6 enzymatically released cells isolated from the bone (Section 2.4.1, 2.4.2, counted according to 2.4.2) were taken from the 5 ml suspension and transferred into a 25 cm² tissue culture flask (Corning). The volume was made up to 5 ml by adding the corresponding StemMACS™ MSC Expansion Media (SM) supplemented with 1% penicillin/streptomycin (P/S) (Final concentration of 100 U/ml Penicillin, 100 µg/ml Streptomycin) prior to cells being added, and adherent cells grown to passage 0 (Section 2.4.6).

2.4.2. Counting of Cells by Haemocytometer

To count cells, 10 µl of cell suspension was mixed with 10 µl of 0.4% trypan blue to exclude dead cells from the count. In healthy cells, trypan blue is unable to enter live cells due to the lipid bilayer, but stain dead cells as the bilayer is compromised. From this mix, 10 µl was pipetted into a haemocytometer (Hawksley) (Fig. 2.4.1). Cells were counted from all 4 of the white 4x4 Sections with the top left borders included and bottom right borders excluded. Counts were divided by 4 to average the cell count. This was then multiplied by the dilution factor, the volume the cells were suspended in and by 1×10^4 (to account for the known volume of a haemocytometer counting square) to estimate the total cells in the solution.

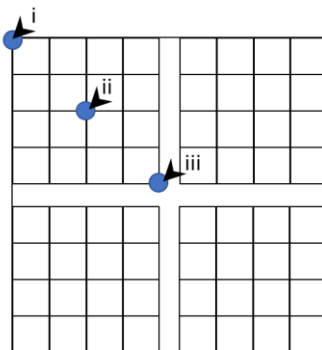


Figure 2.4.1 Haemocytometer view under microscope, showing counting squares. Arrows demonstrate method for counting cells. i – cell include as square '1', ii – cell included as square 11, iii – cell excluded from the count.

2.4.3. Trypsinisation of Adherent MSCs

Once cells reach around 80% confluency, MSCs need to be trypsinized to allow their detachment from the plastic flasks such that they can be removed and used for further growth or other experiments, as higher confluency will induce senescence. Firstly, the media was removed, and the cells washed in 3 ml sterile PBS to remove any remaining media, which would deactivate the trypsin. To remove the cells, 2 ml of trypsin was added, and the sample left in the 37°C incubator (Sanyo) for 5 minutes. Following this, the flask was agitated to detach the cells and

checked under light microscope to confirm a change to an unattached rounded morphology. To this, 3 ml of DMEM with 10% FCS was added to deactivate the trypsin, and the cell solution was transferred from the tissue culture flask to a 15 ml falcon tube. The solution was mixed, and 10 μ l was taken for cell counting (Section 2.5.2). The falcon tube was then spun by centrifugation at 500 g for 10 minutes to pellet the cells. After this, the supernatant was disposed of, and the cell pellet was re-suspended in StemMACS and counted, with 100,000 being seeded for further culturing and the remainder frozen (Section 2.5.4) or re-suspended in PBS for flow cytometry (Section 4.2.6).

2.4.4. Freezing of Enzymatically Released MSCs for Long-term Storage

Once cells had been seeded for CFUF assay (Section 4.2.3) or culture (Section 2.4.6), the remaining enzymatically released cells were frozen for use in future experiments. For each 1×10^6 cells in the pellet, 1 ml of freezing medium (10% DMSO in FCS) was used to re-suspend the pellet, and 1 ml of the mixture added to separate 1.8 ml cryovials. Following this, the cryovials were transferred to a CoolCell freezing container. This was then stored in a -80°C freezer for a minimum of 24 hours. The cryovials were then transferred to long term storage inside liquid nitrogen storage unit.

2.4.5. Freezing of Cultured MSCs for Long-Term Storage

Once cells had been trypsinized, counted and seeded for further culture (Sections 2.4.5, 2.4.2 and 2.4.4), the remainder of cells were prepared for freezing by centrifugation at 500 g for 10 minutes, after which the supernatant was disposed of, and cells re-suspended in 1 ml of freezing media per 1×10^6 cells. Subsequently, 1 ml of the cell suspension was placed into 1.8 ml cryovials which was transported for freezing (Section 2.4.6)

2.4.6. Passaging of Enzymatically Released MSCs in Culture

Passaging of cells was completed to reach standard passage numbers MSCs are characterised at, most importantly for flow cytometry and differentiation assays (Chapter 4). Once seeded or after media changes, flasks or wells were placed into an incubator at 37°C with 5% O_2 and 5% CO_2 . After 48 hours following the seeding of enzymatically-released cells (Section 2.4.1), the media was removed and the adherent cells washed in sterile PBS, with 5 ml StemMACS media added subsequently to 25 cm^2 flask once the PBS was disposed of. Media was subsequently changed every 3 days until the cells reached 80% confluency. Once confluent, cells were trypsinized (Section 2.4.3). From this suspension, 1×10^5 cells were cultured in 5 ml of SM in a subsequent 25 cm^3 flask to passage 1 and the remainder frozen (Section 2.4.5). Media was changed every 3 days until the cells grew to 80% confluency, and once again trypsinized (Section 2.4.3). Again, 1×10^5 cells were grown in 5 ml of SM in a new 25 cm^3 tissue flask, and the

remainder frozen. Media was again changed every 3 days until 70% confluence was reached, at which point the cells were trypsinized (Section 2.4.5) and phenotyped by flow cytometry (Section 4.2.6).

2.4.7. Thawing of Cultured Cells

For cells to be revived, the frozen vials were removed from long term storage and taken to tissue culture. Frozen vials were thawed in 37°C water bath until returned to liquid state, and then pipetted drip-wise into a separate 15 ml falcon tubes containing 5 ml pre-warmed 1% P/S, 10% FCS DMEM media (37°C). This mixture was then centrifuged at 453 g for 10 minutes to pellet the cells, the supernatant discarded, and the pellet re-suspended in StemMACS media.

2.4.8. Thawing of Primary Uncultured Cells

Primary uncultured cells are not pure MSC cultures, and so are more susceptible to 'clumping' which prevents their successful revival. To prevent this, 10 µl of 1 mg/ml of DNase was added to the 10 ml of 1% P/S, 10% FCS DMEM media prewarmed to 37°C, and cells revived as before (Section 2.4.6).

2.5. Assessment of Genomic Content using the Nanodrop

2.5.1. DNA Content

To be certain enough cDNA is available for qPCR experiments, or as a basic assessment of cell number in certain differentiation experiments (Chapters 4, 5 and 6), DNA was measured using the nanodrop. Once RNA had been isolated and cDNA solutions were prepared, they were kept on ice and taken to the Nanodrop. The nanodrop software was loaded and the DNA setting was selected. The system was first loaded and run 1µl with nuclease-free water, and then blanked using the same buffer that DNA had been placed into. DNA content was then assessed from 1 µl of the test solution.

2.5.2. RNA Content

RNA content was measured to test that pure RNA of high enough quantity had been isolated to allow qPCR from lysed cells. Following RNA extraction using the Norgen Biotek Single Cell RNA extraction kit (process explained in detailed methods for that Section), RNA was assessed similarly to DNA, instead using the single-stranded RNA programme setting.

2.6. Reverse Transcribed Real-time Polymerase Chain Reaction

2.6.1. General Theory

Reverse transcribed real-time polymerase chain reaction (RT-qPCR) allows a 'snapshot' of gene expression by cells to be measured at any time, by measuring RNA of specific genes from the instant that cells were lysed. This has been critical to scientific research as it provides direct information on not only what activities the cells were likely to be engaged in, but also the effect of different scenarios on early stages of gene expression, before relevant proteins may have been produced. As key proteins in MSC differentiation pathways are understood, investigating expression of differentiation-related genes is regularly performed. The original process of normal PCR works to rapidly replicate small amounts of DNA to exponentially larger amounts. However, the addition of a fluorophore and quencher to specific gene primers used can extend this process to allow the expression of specific sequences to be measured. The general method is described in Fig. 2.6.1 and described below.

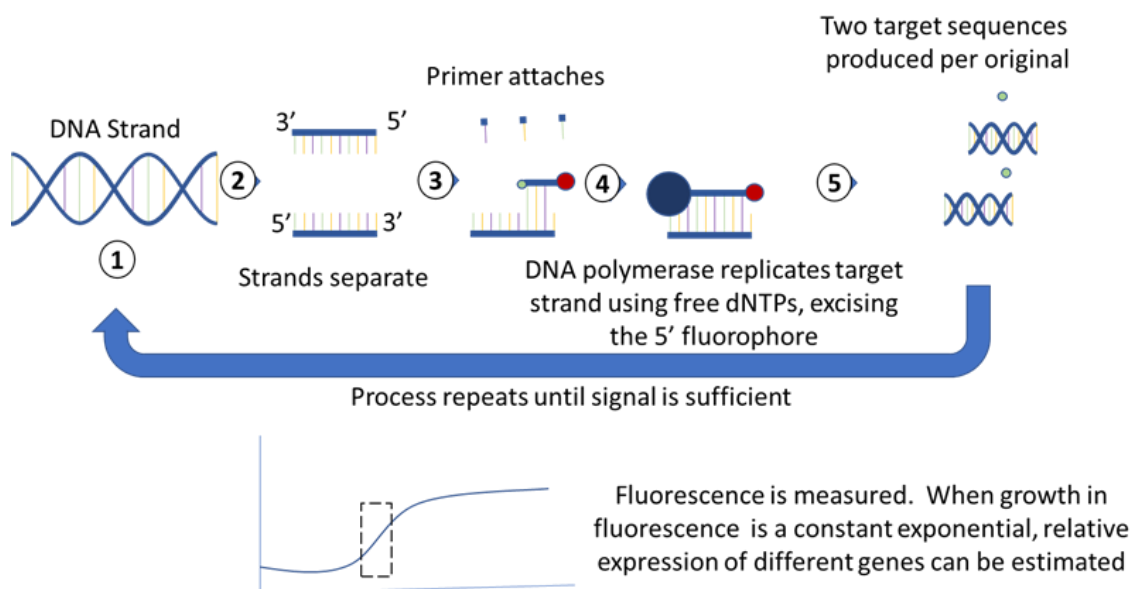


Figure 2.6.1 Simplified qPCR Process. 1 – cDNA. 2 – Heat-induced denaturation at 90°C. 3+4 – DNA Polymerization by DNA polymerase using free dNTPs. 5 – Production of 2 cDNA complexes.

As RNA cannot be read and duplicated by DNA polymerase, firstly, RNA needs to be extracted from the sample and reverse-transcribed into DNA (Section 2.6.2). For qPCR, the DNA, primers (single-strand versions of the usual double stranded helix DNA, usually targeting the beginning and end of the sequence to be replicated), and a DNA polymerase (to enable replication) are mixed. This mix is then heated to 94-98°C for 30 seconds to denature the DNA and break the double-stranded helix into single strands. This is cooled to 50°C for 20-40 seconds to anneal the single strands with the primers, which bind a short but specific sequence at the 3' end of the DNA strand, with a primer for each strand. This will then be heated to the temperature the DNA polymerase enzyme functions at, commonly 72°C, and DNA synthesised from the free

deoxyribonucleotides (dNTPs), with the primer-DNA sequence acting as a template for DNA synthesis in the 5'-3' direction. This process is then repeated from the denaturation step as many times as is needed to get the DNA required, with growth being exponential, as the amount of DNA will double each time. In real-time PCR, this method is modified with the addition of a fluorescent reporter to the 5' of the primer, and a fluorescence quencher to the 3' end. As DNA replicates, the polymerase will excise the 5' end from the primer, separating it from the quencher and activating the fluorescence, which can be measured. With each PCR cycle, the level of fluorescence should double, due to the exponential increase in DNA. By measuring this level of fluorescence at a threshold of when exponential growth is constant, a relative assessment of gene expression per DNA can be made. If there is more active gene per DNA sample, the exponential growth phase will be more rapid relative to another, less expressed gene. This is termed the threshold cycle (Ct). This is then converted into delta Ct, as the difference in relative DNA value to the housekeeping gene.

2.6.2. Cell Lysis

To investigate gene expression of cells, firstly RNA needed to be isolated from cells. RNA extraction was performed using the Norgen Biotek single cell RNA purification kit according to manufacturer's instructions. For RNA extraction, media was removed from the well plates, and then the plate washed twice with sterile PBS. PBS was removed with care to remove all remaining liquid. Plates were placed onto ice to keep cold during extraction. Cell lysis buffer was prepared (Buffer RL) with 10 μ l β -mercapthanol added per ml of lysis buffer. To each well, 350 μ l of cell lysis buffer was added. Cells were roughly agitated and scraped using a pipette tip to ensure everything was collected. The lysate was then aspirated into a tube. Another 350 μ l of cell lysis buffer was added to the well, and the well-plate vortexed, before the lysate was added again to the same tube. RNA content of the sample was then measured by nanodrop using 5 μ l of solution (Section 2.5.2). This was then stored at -80°C until RNA was extracted.

For isolation of RNA from chondrogenic pellets instead of from the 2D well plates, media was removed from the screw-top Eppendorf and pellets washed twice with sterile PBS. Pellets were then removed and crushed between two slides. This was then added back to the screw-top Eppendorf and 350 μ l cell lysis buffer added (with 10 μ l β -mercapthanol per ml). The Eppendorf was then agitated using a pipette and vortexed thoroughly to ensure RNA was extracted. Again, 5 μ l was used to measure RNA by nanodrop (Section 2.5.2) and then stored at -80°C until extracted.

2.6.3. RNA Extraction

As cell lysis simply leaves all remnants of lysis, additional steps are required to purify the RNA. Samples were thawed from -80°C and kept on ice. To each sample $200\ \mu\text{l}$ of 96% ethanol in dH_2O was added and briefly vortexed to mix. A spin column was assembled within a collection tube, and $600\ \mu\text{l}$ of lysate was added to the spin column. This was centrifuged for 1 minute at $3,500\ \text{g}$. The content of the collection tube was disposed of, and the process repeated with remaining sample. DNase type I solution was prepared using $15\ \mu\text{l}$ of $0.25\ \text{units}/\mu\text{l}$ DNase type I in $100\ \mu\text{l}$ of enzyme incubation buffer and mixed by inverting. To wash the sample, $400\ \mu\text{l}$ of wash solution A was added to the spin column and centrifuged for 2 minutes at $14,000\ \text{g}$. Flow through was discarded, and $100\ \mu\text{l}$ of the DNase I solution was added to the column. This was centrifuged for 1 minute at $14,000\ \text{g}$. The flow through was added back to the spin column and left for 15 minutes at 25°C . Washing was repeated twice more with $400\ \mu\text{l}$ of Wash solution A added to the spin column, centrifugation at $14,000\ \text{g}$, and flow through discarded. After this, the column was spun at $14,000\ \text{g}$ for 2 minutes to dry the resin, and the collection tube was discarded. The column was reassembled in a $1.7\ \text{ml}$ elution tube, and RNA was then eluted by adding $10\ \mu\text{l}$ of elution solution A and centrifuging at $200\ \text{g}$ for 1 minute, and then $14,000\ \text{g}$ for 2 minutes. RNA content was again measured by nanodrop (Section 2.5.2). This was then stored at -80°C until reverse transcription.

2.6.4. Reverse Transcription

As qPCR can only be performed on DNA, RNA was first put through reverse transcription. For all qPCR steps, the Fluidigm FlexSIX protocol was used according to manufacturer's instructions. Prepared in a 96 well plate, for each sample $1\ \mu\text{l}$ of RT MasterMix was added per well. RNA was diluted in RNase-free water so that RNA concentration was below $50\ \text{ng}/\mu\text{l}$ for each sample, and then $4\ \mu\text{l}$ of sample added per well. This was then run through a nexus cycler L/R/G with the protocol given in Table 2.6.1 to generate complementary DNA (cDNA).

Table 2.8 Reverse Transcription Protocol

Step	Process	Temperature ($^{\circ}\text{C}$)	Time (minutes)
1	Stabilise Temperature	25	5
2	Reverse Transcribe	42	30
3	Denature Enzyme	80	5
4	Hold	4	-

2.6.5. Pre-amplification

When low amounts of RNA can be obtained, preamplification is used to increase the amount of cDNA to measurable levels. In this case, 18 duplications by pre-amplification were chosen. Firstly, a pooled TaqMan assay probe mix was created using 2 μ l of the 12 genes being tested for, and 2 μ l of 38 other TaqMan assays for similar genes, and then 100 μ l of purified water. For the testing of the 96 genes in Chapter 6, 2 μ l of the TaqMan's for genes being tested was added, and then 2 μ l of LEF1, BMP2, DMP1 and GSK3B were added. To this, 200 μ l of TE buffer was added. This list is given in Table 2.6.2. In a new 96 well plate, 2.5 μ l of pooled TaqMan mix was added per well, as well as 2 μ l of Pre-amplification Master Mix, and 5.5 μ l of cDNA from reverse transcription (Section 2.6.4). This was again run in the Nexus cycle, with the protocol given in Table 2.6.3. Following preamplification, 20 μ l of TE buffer was added per well.

Table 2.9 TaqMan Probes Pooled for Pre-Amplification

ALP	HPRT	PTPRC	TGFBR3	CCL5	GAPDH	GSK3B
RUNX2	COL2A1	THY-1	COL1A2	COL10A1	TGFB1	WNT10B
FABP4	ACAN	MMP1	TGFBR2	CXCL12	PTPR21	KREMEN1
PPARG	COMP	COL1A1	SFRP4	TNFSRF1	BMP2	SPHK1
SOX9	VEGFA	MMP14	PTH LH	LEF1	DMP1	TIMP1

Table 2.10 Pre-Amplification Protocol

Step	Process	Temperature ($^{\circ}$ C)	Time (minutes)	Repeats
1	Initial Denaturation	90	2	-
2	Denaturation	95	0:15	18x
3	Anneal/Extend	60	4	
4	Hold	4	-	

2.6.6. Performing qPCR Using the Fluidigm/BioMark System

qPCR was performed using the FlexSIX PCR chip as earlier mentioned, following manufacturer's instructions. This chip was chosen due to the accuracy and simplicity of the Fluidigm system, as well as the convenience of being able to use individual partitions at a time rather than all at once, as there was only a small sample number. Before first use the chip was primed using the

96.96 control line fluid followed by the 'Prime Chip' script on the HX loader. The chip was then loaded. To the assay portion of the chip, 2µl of the TaqMan for the gene being tested was mixed with 2µl of assay loading reagent, and then 3µl loaded to a well on the chip. This was done for the 12 genes being assayed, repeated in a second partition as there were a total of 24 samples. To the component portion of the chip, 2µl of TaqMan universal MasterMix, 0.2µl of GE sample loading reagent, and 1.8µl of cDNA from a sample was mixed. Per sample, 3µl of this was added per well of the chip. The 'Load and Mix (153x)' protocol was then run on the HX loader. The BioMark system was then used to run qPCR. The protocol for this is given in Table 2.6.4. Following the run, the 'Post-Run (153x)' script was run on the HX loader.

Table 2.11 qPCR Protocol

Step	Process	Temperature (°C)	Time (minutes)	Repeats
1	Thermal Mix	25	30	-
2		70	60	-
3	UNG & Hot Start	50	2	-
4		95	10	-
5	PCR (40 Cycles)	95	0:15	40x
6		60	1	

2.6.7. Post-qPCR Run Analysis

To quantify differences in gene replication rate, BioMark outputs were loaded into the Fluidigm Digital PCR analysis software (v4.3.1). The cycle threshold (Ct) was calculated by drawing a threshold at the point where gene replication was constant for each individual gene. Where there was no clear exponential growth or no growth in fluorescence at all, it was considered below detection (BD) This value was then normalised to the housekeeping gene (HPRT) by the following equation.

$$\Delta Ct = Ct_{Target\ Gene} - Ct_{Housekeeping\ Gene}$$

Equation 2.6.1 Calculation of Change in Cycle Threshold Value. Ct = Cycle Threshold.

This was then converted into relative expression using the next equation.

$$\text{Relative Expression} = 2^{-\Delta CT}$$

Equation 2.6.2 Calculation of Relative Expression using the Delta Ct method. Ct = Cycle Threshold.

This method was chosen over the double-delta method which compares the change in expression in each condition to the 'gold-standard' treatment, for two reasons. Firstly, there were 3 control methods, and both C treatment or SM treatments would've been valid choices, however their effectiveness in 2D conditions was unknown, and therefore may not have been an optimal comparisons. As such, using the delta-Ct method allowed the controls to be assessed, as well as visualise differences to both negative and positive controls in the treatment media.

2.7. Imaging

2.7.1. Gross Tissue

Whole tissue was obtained from surgery with anatomical directions marked by the surgeon on the sample pot. Images were taken with careful care to keep tissues sterile and hydrated, using a ruler to measure size. Images were taken using an iPhone 7 camera.

2.7.2. Histological Sections

Haemotoxylin and Safranin O were imaged using an infinity 1 camera on a GX microscope using the Infinity Image Acquisition Software (version 6.5.6, Lumenera). Picrosirius red staining was imaged under brightfield and polarised light using an Axiolmager 2, and tiled using the Zen software. Toluidine blue images were taken on the Axiolmager 2 using brightfield light using the Zen software. Immunohistochemistry for CD271 was Images were taken on a Nikon Eclipse Ti2-E camera.

Whole slides were scanned at 10x using the Leica Aperio T2 and images captured at 25x-200x magnification were taken from these scans using Aperio Imagescope v12.4.0.5043, and scale bars applied using the software.

2.7.3. Live Cell Imaging During Culture and Cell Culture Image Scans

Cell images were taken using an EVOS FL imaging system from 40x-200x magnification, using the intrinsic software (v1.4) to add scale bars . Well plates were imaged by scanner, at 1400 DPI, using the Windows Fax and Scan software (v2004).

2.8. Statistics

2.8.1. Assessment of Normality

For a group to first be considered normal, an N number of at least 10 was first required. As no more than 3 samples were used for any experiment, all data sets were considered not normally distributed, with a statistical rule being 10 or more samples can be representative of a sample population. In the case of repeated measures being taken from one donor (individual colonies), only the true patient N was considered.

2.8.2. Choice of Statistical Test

Statistical tests were chosen based on the number of groups being tested and the data being analysed, as well as if they were normally distributed and/or paired. Statistics were performed using Graphpad Prism 9 (v9.0.1). The choice of statistics is listed in Table 2.8.1. For 2 groups, matched data was tested with the non-parametric Wilcoxon Matched Pairs Signed Rank test, and unmatched data the Mann-Whitney U test. For 3 or more groups, the non-parametric Friedmann's test with Dunn's multiple comparisons test was used for paired samples, or Kruskal-Wallis for unpaired samples. As talus and tibia were obtained from the same donor, these were considered paired. However as iliac crest samples came from separate donors, these were unpaired and tested against talus and tibia as such. In Chapters 5 and 6, tests were considered paired as same donors with different treatments were being compared. Significance was set at * = $P < 0.05$, ** $P < 0.01$, *** $P < 0.001$, **** $P < 0.0001$.

Table 2.12 Choice of Statistical Test for Each Dataset

Chapter	Figure	Test Chosen	Groups
3	3.3.3A,B	Friedmann's with Dunn's multiple comparisons	4 (2x2)
	3.3.3C-E	Wilcoxon Matched Pairs Signed Rank	2
	3.3.4A-E	Wilcoxon Matched Pairs Signed Rank	2
	3.3.7	Wilcoxon Matched Pairs Signed Rank	2
	3.3.8	Friedmann's with Dunn's multiple comparisons	4-8
	3.3.12A	Wilcoxon Matched Pairs Signed Rank	2

Table 2.12 Choice of Statistical Test for Each Dataset

	3.3.12B,C	Friedmann's with Dunn's multiple comparisons	4-8
	3.3.15A	Wilcoxon Matched Pairs Signed Rank	2
	3.3.15B	Friedmann's with Dunn's multiple comparisons	4
	3.3.17C	Wilcoxon Matched Pairs Signed Rank	2
	3.3.18	Friedmann's with Dunn's multiple comparisons	3
	4.3.6-8	Kruskal-Wallis with Dunn's multiple comparisons	3
4	4.3.13	Kruskal-Wallis with Dunn's multiple comparisons	3-6
	4.3.16	Kruskal-Wallis with Dunn's multiple comparisons	3-6
	4.3.18,19	Kruskal-Wallis with Dunn's multiple comparisons	6
	5.3.5	Friedmann's with Dunn's multiple comparisons	6
5	5.3.8	Friedmann's with Dunn's multiple comparisons	6
	5.3.1-16	Friedmann's with Dunn's multiple comparisons	6
	6.3.6	Friedmann's with Dunn's multiple comparisons	6
	6.3.14A-C	Wilcoxon Signed Rank	2
6	6.3.14D	Friedmann's with Dunn's multiple comparisons	6
	6.3.15-17A,B	Wilcoxon Signed Rank	2
	6.3.15-17C	Friedmann's with Dunn's multiple comparisons	6
	6.3.22-25	Friedmann's with Dunn's multiple comparisons	4-6

All datasets had N of 3, as such all could not be assumed to be normally distributed

3. Chapter 3 – Characterisation of Osteoarthritic Changes to the Distal Tibia and Talus of the Ankle Joint, and the Relationship between Bone, Cartilage and Cell Behaviour

3.1. Introduction

As mentioned at the start of Chapter 1, Ankle osteoarthritis (OA) is potentially distinct from OA of other joints such as hip or knee, due to its high post-traumatic incidence¹⁰⁶. As such a key starting point for this research was to examine the tissue to look for key differences in OA progression relative to existing literature from other joints. Additionally, these changes were linked with resident stem cells to investigate if endogenous cells instigate a repair response, and to what extent Multipotential Stromal Cells (MSCs) are involved. The rate of post-traumatic ankle OA is estimated to be anywhere from 5-95%, mostly reported in the higher range, compared to 12-50% in the knee and around 1% in the hip, with around 12% of all OA cases being post-traumatic^{106,113,204}. There is currently very little gross or histological information on cartilage changes within the ankle. Whilst it has previously been reported there are minor differences such as “tram-track lesions” (grooves from high stress activity rotations), a deep investigation through histological and links with cell behaviour has yet to be completed²⁰⁵.

Treatment of ankle OA is unique in that joint-sparing regenerative strategies are more likely to be employed than other joints and show more positive outcomes. Treatments such as microfracture show good to excellent results in up to 96% of patients, compared to 75% in knee, and other regenerative treatments showing similar short to mid-term success up to 10 years^{6,206-208}. This has yet to be fully explored, but may be related to increased miRNA and increased anabolism observed in the ankle, which is lower in the knee and lowest in the hip, correlating with overall success rates for similar treatments in the three joints²⁰⁹. Otherwise, it could be related to ankle biomechanics through the high congruency, increased cartilage uniformity or other anatomical factors compared to the knee^{30,113}. However, regenerative therapies of the ankle are generally perceived to start failing after 5 years, at which point fibrocartilage formation leads to mechanical incompetency of cartilage^{168,210}. Whilst there is little research in the ankle describing the resident cells responsible for this repair, MSCs are often cited as a potential source, as such were a key focus of this chapter²¹¹. MSCs have been investigated in OA for both hip and knee and have shown potential for cartilage and bone differentiation, particularly with higher chondrogenesis than niches such as the IC^{85,101}. As such it seems likely MSCs are key to the repair process, however if they improve the outcome of regenerative treatments such as microfracture in the ankle more than other joints is an area that needs investigation.

Prior research associates MSCs with both new cartilage formation and with OA bone sclerosis, and so investigating this balance may lead to improvements in treatments for both the ankle or other joints^{85,101}. A key point for this repair however is that after 5 years, this seemingly successful microfracture does not lead to hyaline cartilage formation, and instead fibrocartilage production eventually fails due to suboptimal mechanical performance, and can no longer

prevent pain for the patient. Microfracture is then repeated to attempt repair again, until this is no longer successful and instead joint replacement or fixation is chosen, as earlier discussed. One opinion on why microfracture stops being successful is that this repeated surgery leads to necrosis of the underlying bone, preventing further drilling⁷. By removing the need for repeating the microfracture by improving the outcome of prior treatments would avoid or delay invasive surgeries with low patient satisfaction, this would need to be driven by understanding the joint-resident reparative response and developing techniques to enhance this.

Local MSCs are implicated in these treatments as the major regenerative cell within the joint, however their behaviour is poorly understood within the ankle compared to other joints like hip and knee²¹². As MSCs are unlikely to be transported by blood, resident cells from subchondral bone, synovial fluid or synovium are considered to be the main MSC tissue sources within joints which may directly participate in cartilage repair²¹³⁻²¹⁵. In ankle OA, MSCs have been isolated from the synovial fluid of patients, however MSC presence in talocrural subchondral bone, from which reparative cells released by microfracture would come from, remains unexplored⁹⁶. Synovial fluid cells presented MSC surface expression and differentiation capacity, proving their presence. Unfortunately, there was no comparison to other tissue other than gene expression for 5 genes to prove they were not bone MSCs. This showed expression of osteogenic-related genes SMOC2, SFRP4 and OGN, as well as intraarticular related genes ECRG4 and PRELP, however this does little to compare their relative ability for joint repair⁹⁶. No existing study has compared resident subchondral bone MSC topography with joint changes between talus and distal tibia in ankle OA patients. A clear understanding of resident MSCs behaviour, and how tissue damage affects their function, from both biological and mechanical standpoints, is of major importance for the development of novel regenerative medicine strategies to treat ankle OA or osteochondral lesions²¹⁶.

In the hip, MSCs have been investigated both *in vivo* through immunohistochemistry and *in vitro* through culture. The hip is a simple ball and socket joint, between the femur and acetabulum, therefore is very different to the ankle in structure. Therefore, the mechanical forces and OA processes may be significantly different. It has been previously shown that underlying damage such as bone marrow lesions aligned with overlying cartilage defects, and in particular, bone marrow lesions were seen far more frequently in samples with more greatly damaged cartilage¹⁰¹. Staining for CD271, a marker of MSCs, showed association with bone lining, and again correlated with regions of cartilage damage¹⁰¹. A second study then further identified these CD271+ MSCs into different subsets, including the osteogenically committed CD271+/CD56+ subtype, which presented an osteogenically committed with a 100-fold increased expression of osteo-related genes such as osteopontin and osteocalcin⁸⁵. As such, an

MSC response to OA damage has previously been identified, with associated with cartilage damage, however not only in a cartilage-reparative response. MSC also showed subsets with increased bone formation associated with sclerotic bone. This shows that MSCs are engaged with a repair response, but need modulating to ensure that correct repair occurs. Treatment of hip OA is mostly restricted to hip replacement at late stage, however early-stage treatments include typical OA treatments such as painkillers or intra-articular injections of corticosteroids. Alternative therapies include stem cell injections, such as MSCs. Attempts of treatments used in the ankle just as microfracture show results equivalent to that seen in simple debridement, suggesting that resident reparative cells such as MSCs are not as capable as repair as in the ankle, potentially relating to different biomechanical cues or different resident cell behaviour²¹⁷. However, by further understanding manipulation of MSCs in the ankle, this may be adapted for the hip to better improve outcomes.

The knee is a slightly more complex joint compared to the hip. It is considered a hinge joint, however, is slightly more complex in that, being made of three bones, the patella, the distal femur and the proximal tibia, as well as the soft tissue structure the meniscus. As such, the movement of the joint is not that reminiscent of a hinge, instead there is both a small amount of lateral and medial rotation as well as flexion and extension. This specific lateral and medial rotation lends some similarity to the ankle joint, and as such standard protocol for ankle testing is to use an inverted knee simulator, as ankle simulators are yet to be widespread. Whilst the biomechanics are altered, this takes advantage of similarities between the two joints. For example, the distal femur forms a convex shape, like the proximal talus, and that the proximal tibia a concave structure, similar to the distal tibia. MSCs have again been investigated within the knee. It has already been shown that despite MSCs increasing in synovial fluid in OA, this did not lead to cartilage repair, as such there is still a level of incompetent repair response²¹⁸. Again, MSCs correlated with areas of cartilage damage, as well as increased gene expression of bone turnover related genes as seen in the hip. There is extensive, continued evidence that MSCs are bone-resident in multiple types of OA, and that there is an increase in their number, particularly in a localised response to cartilage damage^{101,219,220}. As such, there is a great need for further understanding resident behaviour of these MSCs and what can be done to direct them towards cartilage repair.

Research in this chapter was designed to characterise major difference between the talus and tibia in both health and OA, and compare this to what is known in other joints. In this, it was hypothesised that talus and tibia would present OA with similar presentation to that of other joints, with cartilage loss, subchondral bone plate thickening and increased bone turnover.

Additionally, that there would be increased chondrocyte hypertrophy and loss of organisation, and increase in cellularity. Specifically, this chapter aimed to:

- Perform a basic assessment of overall 3D structural changes using micro-computed tomography (mCT) to investigate OA changes in relation to non-diseased tissue
- Study specific structural changes using basic histological techniques for bone and cartilage to understand bone, cartilage and cellular level changes
- Investigate the role of resident cell types such as MSCs, Osteoblasts and Osteocytes using immunohistochemistry, and their relationship with hallmark OA changes
- Develop methods of characterising mechanical changes to cartilage in extremely small samples

3.2. Specific Methods

3.2.1. Sample Information

For this study, OA human distal tibia, proximal talus as well as non-diseased human distal tibia and talus samples were used. Samples used in this chapter are listed in Tables 3.2.1 and 3.2.2. Retrieval methods were described in general methods (Section 2.1.1). To reiterate, ethical approval for human ankle tissue collection (07/Q1205/27) was obtained from NREC Yorkshire and Humberside National Research Ethics Committee, in compliance with the Helsinki Declaration of ethical principles for medical research involving human subjects. In this chapter, six ankle OA patients (median age 58 years, range 46-75, 5 male and 1 female) were included after signed consent was received. Unfortunately, whether or not OA was post-traumatic was not known. Each patient underwent fusion of the talocrural joint for OA, and were ambulatory prior to surgery, with the general patient characteristics given in Table 3.2.1. Once retrieved, samples were washed 3 times in 50 ml PBS until water was clean. PBS was removed and samples were wrapped in PBS-soaked filter paper before being frozen at -80°C. Non-diseased human cadaveric ankles (age 40-60 years, all-male, no evidence of ankle OA) were obtained from Medcure, USA, under local university ethics (MEEC 18-027), and stored at -80°C before distal tibia and talus were removed for imaging, with sample information given in Table 3.2.2. Freezing meant that cadaveric samples were unsuitable for subsequent cell analysis.

Table 3.1 Distal Tibia and Talus Sample Characteristics Retrieved from Ankle Fusion

Sample ID	Experimental Use	Donor Age (Years)	Donor Sex
WJ001	Histology	70	M
WJ002	Histology	46	M
WJ003	Histology	46	M
WJ004	mCT	75	F
WJ005	mCT	64	M
WJ008	mCT	57	M
<i>Median</i>	<i>N/A</i>	<i>60</i>	<i>83% male 17% Female</i>

Table 3.2 Distal Tibia and Talus Sample Characteristics Of Non-Diseased Donor Tissue

Sample ID	Experimental Use	Donor Age (Years)	Donor Sex
LK01	mCT	43	M
LK02	mCT	50	M
LK03	mCT	57	M
<i>Median</i>	<i>N/A</i>	<i>50</i>	<i>100% male</i>

3.2.2. mCT of Tissues

Firstly, the general structure of the ankle in both health and OA needed to be understood, to investigate if the usual effects of OA, such as bone thickening and subchondral bone plate thickening occurred as expected. Three pairs of ankle OA talar and distal tibial osteochondral samples (approximately 35 mm x 25 mm x 9 mm; and 28 mm x 2 mm x 7.8 mm from distal tibia and talus respectively (Width, height, depth)) were retrieved and stored at -80°C. Samples were defrosted by fully submerging in PBS and then left in a fridge 4°C for 24 hours. In the case of samples having multiple segments, segments were kept together and defrosted and scanned together. Once defrosted, samples were placed into a 50 ml falcon tube made up to 50 ml with PBS, or in a heat-sealed bag in PBS (should the sample be too large), and imaged using mCT according to standard practice²²¹. Samples were orientated with the loading surface aligned, and

in the case of multiple segments, each individual sample was orientated as such, and positioned in the scanner so the scan would be taken along the coronal plane.

For scanning of OA samples, a SkyScan 1278 mCT was used to scan at an 18 μ m isotropic resolution for non-diseased human tissue (65 kVP, 270 μ A, 380 ms integration time), with samples submerged in PBS in either heat-sealed bag or falcon tube. Image data was extracted directly to the TIFF image format. Each scan took approximately 20 minutes to 2 hours, depending on the size of the sample.

The cadaveric, non-diseased ankle bones were obtained and scanned by another researcher (Ms. Lekha Koria) in a different laboratory, meaning scans were performed in another machine, but it was attempted to keep scans relatively similar. Non-diseased ankle bones were scanned at a 16 μ m isotropic resolution (70 kVP, 114 μ A, 250 ms integration time) using a Micro-CT100. Scans were exported in the ISQ format, which was converted into normalised TIFFs (0-255 grayscale, 8-bit) using a MATLAB script designed in house by that researchers' group. This script converts all negative Hounsfield units to 0, and the maximum theoretical Hounsfield unit to 255. These took on average 40 minutes to 2 hours, again depending on sample size.

Anatomic areas were matched between the talus and tibia for both OA and health, selecting regions of loading, the apex of the talus and distal arch of the tibia, reflecting the regions removed during surgery.

Bone volume of total volume (BV/TV) and subchondral bone plate (SBP) thickness were measured according to standard methods²²¹⁻²²³. BV/TV was measured using the BoneJ²²³ plugin (v1.4.2) for NIH ImageJ²²² (US National Institutes of Health (v1.4.2)), up to 3 mm depth from the SBP. In order to do this, the image cube was loaded ('File>Import>Image Stack'), the stacks were selected for a depth applicable for all samples, as well as for depth-dependent measures by selecting the number of stacks that represent the set depth (0.8 mm was chosen, as this was 50 slices of a 16 μ m isotropic resolution stack). The threshold was optimised using the intrinsic BoneJ tool (Plugins>BoneJ>Optimise Threshold) after seeing the best results compared to other methods of analysis. BV/TV of the whole stack was measured using the 'Plugins>BoneJ>Volume Fraction' tool. Stacks were then duplicated and 0.8 mm segments created using the 'Image>Stacks>Set Slice' tool, and then volume fraction measured in order to make depth dependent measurement. BV/TV per sample was compared using a Friedman test with Dunn's multiple comparison test and follow-up. It was expected that the talus would have a higher BV/TV in health than tibia due to its high loading, increasing further in OA.

SBP thickness was measured by re-orientating the image to a transverse view and measuring the perpendicular distance from the beginning of bone to the first visible trabecular gap.

Measurements were taken at twenty random slices for each bone, and averaged. The average measurement for each technical replicate was averaged, and then for each biological replicate this was compared for statistical analysis using a Friedman test with Dunn's multiple comparison test as follow-up. It was expected that the talus would have a higher subchondral bone plate thickness due to its high-loading and involvement in 3 loading-regions, increasing further in OA.

3.2.3. Haemotoxylin and Eosin Staining

To understand basic morphology of bone, cartilage and resident cells in the distal tibia and talus in OA, Haemotoxylin and Eosin staining was used, as is standard practice²²⁴. Processing prior to staining is given in Chapter 2 (Sections 2.2.1-2.2.4). Haemotoxylin is a basic, cationic dye which stains the basophilic nucleic acids of the nuclei blue, and Eosin is a acidic, anionic dye which stains the basic cytoplasm and proteins red. Specific steps are shown in Table 3.2.3. Staining was followed by addition of a coverslip detailed in Section 2.2.5 for long term storage.

Table 3.3 Haemotoxylin and Eosin Staining Process

Process	Step	Solutions and Reagents	Time (mins)
Haemotoxylin and Eosin Stain	13	Mayer's Haematoxylin	2:00
	14	Running tap water	1:00
	15	Scott's tap water	2:00
	16	Running tap water	1:00
	17	Eosin	2:00
	18	Running tap water	1:00

Table 3.2.6 is a continuation of the process described in Table 3.2.4, as such starts at step 13, and is followed by dehydration and coverslip application (Table 3.2.5).

3.2.4. Safranin O Staining

Safranin O staining was additionally used to distinguish between cartilage and bone, allowing relationships between the two in OA to be investigated, as is standard practice²²⁴. Processing prior to staining is given in Chapter 2 (Sections 2.2.1-2.2.4). Safranin O is a cationic dye, and binds carboxyl and sulphate groups glycosaminoglycans in cartilage, staining them red. The counterstain, fast-green, is anionic, and stains bone blue. This technique is commonly used in investigation of OA²²⁴. Specific steps are shown in Table 3.2.4. Staining was followed by addition of a coverslip detailed in Section 2.2.5 for long term storage.

Table 3.4 Safranin O Staining Process

Process	Step	Solutions and Reagents	Time (mins)
Safranin O	13	Stain with Weigert's Iron Haematoxylin Working Solution for 10 minutes	10:00
	14	Wash in running tap water for 10 minutes	10:00
	15	Counterstain in 0.02% Fast Green	5:00
	16	Rinse quickly with 1% Acetic Acid	0:15
	17	Stain in 0.1% Safranin O solution	5

Table 3.2.7 is a continuation of the process described in Table 3.2.4, as such starts at step 13, and is followed by dehydration and coverslip application (Table 3.2.5).

3.2.5. OARSI Scoring for the Degree of Cartilage Damage

To assess the level of cartilage damage in both talus and distal tibia from ankle OA patients, the OARSI OA cartilage histopathology scoring system was used, according to standard practice^{225,226}. Two independent observers (Author W.J. and supervisor Dr. Elena Jones) assessed the score for whole tissues using the whole tissue scans of safranin O staining of tiled images taken at 10x magnification. From each sample, the OARSI scoring method was used to select cartilage of different grades and segment it with the underlying bone, to create plugs of all the different levels of cartilage damage within each sample for downstream analysis of cartilage and bone damage relationships²¹⁹. This was novel to this work to directly compare overlying cartilage with bone changes. To compose the score, the grade of damage is measured according to Table 3.2.5, and the stage, or area of tissue with that level of damage is also measured, according to Table 3.2.6. To then get the overall score, the two measures are multiplied together^{225,226}.

Table 3.5 OARSI Stage of Osteoarthritis Assessment

Stage	% Involvement (Area)
0	None
1	<10%
2	10-25%
3	25-50%
4	>50%

Stage – Extent of joint involvement

Table 3.6 Cartilage Histopathology Grade Assessment

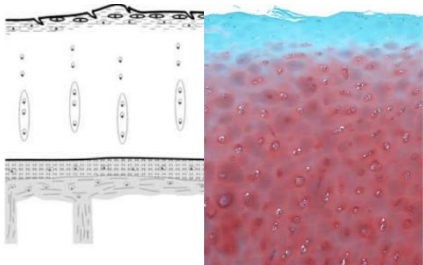
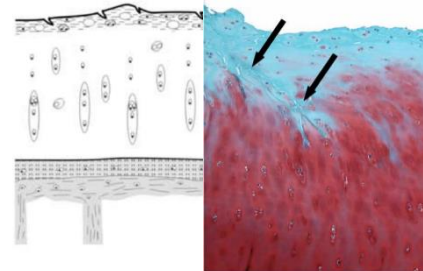
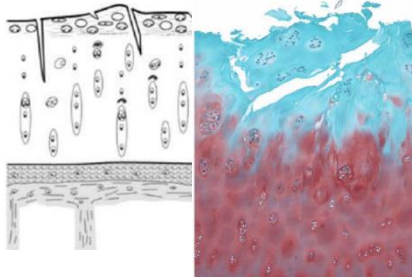
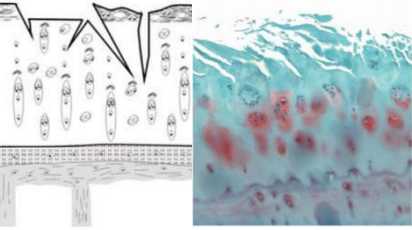
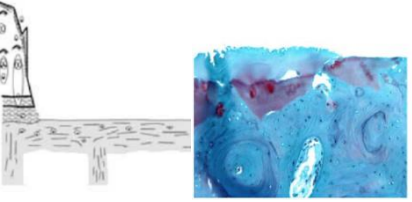
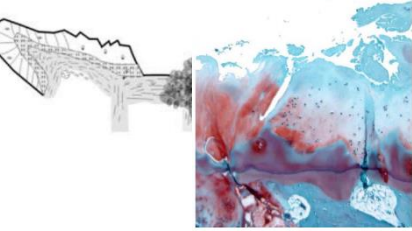
Grade	Criteria (Tissue Reaction)	Example Image
Grade 0	Matrix: normal architecture Cells: intact, appropriate orientation	N/A
Grade 1	Matrix: superficial zone intact, oedema and/or superficial fibrillation (abrasion), focal superficial matrix condensation Cells: death, proliferation (clusters), hypertrophy, superficial zone Reaction must be more than superficial fibrillation only	
Grade 2	As above; Matrix discontinuity at superficial zone (deep fibrillation) Cationic stain matrix depletion (Safranin O or Toluidine Blue) upper 1/3 of cartilage. Focal perichondral increased stain (mid zone). Disorientation of chondron columns Cells: death, proliferation (clusters), hypertrophy	

Table 3.6 Cartilage Histopathology Grade Assessment

Grade 3	<p>As above; Matrix vertical fissures into mid zone, branched fissures Cationic stain depletion (Safranin O or Toluidine Blue) into lower 2/3 of cartilage (deep zone) New collagen formation (polarized light microscopy, Picrosirius Red stain) Cells: death, regeneration (clusters), hypertrophy, cartilage domains adjacent to fissures</p>	
Grade 4	<p>Cartilage matrix loss: delamination of superficial layer, mid layer cyst formation Excavation: matrix loss superficial layer and mid zone</p>	
Grade 5	<p>Surface: sclerotic bone or reparative tissue including fibrocartilage within denuded surface. Microfracture with repair limited to bone surface</p>	
Grade 6	<p>Bone remodelling (more than osteophyte formation only). Includes: microfracture with fibrocartilaginous and osseous repair extending above the previous surface</p>	

Grade – Depth of Progression into Cartilage. Images are Safranin O. Adapted from ²²⁷.

3.2.6. Bone Area of Total Area Measurements

Bone area of Total Area (BA/TA) was measured from Safranin O images for comparison to cartilage changes (Section 3.2.4), as well as to compare CD271 immunohistochemistry matched images to relate CD271+ staining area to bone changes such as BV/TV (Section 3.2.9). A direct comparison between the two has not been performed previously, however BV/TV and CD271 are both heavily implicated in OA changes^{85,228}. Both overall, and depth dependent behaviour was measured using ImageJ. This was a novel method to this study to relate the basic science setting to clinical computed tomographic settings, and relate bone changes to cartilage changes.

For both processes, a sample image was loaded into ImageJ, image clarity optimised manually using the 'Image>Adjust>Brightness/Contrast' function to reduce debris and enhance bone. A scale was applied using the scale bar on the image, using the 'Analyse>Set Scale' function, to be used for depth dependent measures and subchondral bone plate thickness. The 'Analyse>Set measures' function was set to 'Measure Area' so that total bone area could be measured. The image was then converted into an 8-bit image. A polygon region-of-interest tool was used to select the total area, starting at where the subchondral bone plate ended, as defined earlier, set to be where the first trabecular space is beneath the bone plate. The selected area continued to the maximum depth attainable in all bone tissue for consistency. The excluded region was cleared using the 'Edit>Clear Outside' function to remove irrelevant areas of the image such as cartilage or around the sample. A binary threshold was then applied, selecting pixels of grayscale value between two set values and then converting these into a binary image, using the 'Image>Adjust>Threshold' function, and manually set to select bone in black, and exclude stromal tissues in trabecular spaces, leaving the background white. The image was then duplicated ('Image>Duplicate') for the following measurements and to select specific areas. For overall BA/TA, the 'Analyse>Analyse Particles tool' was applied, with 'Show Outlines' active to ensure selected regions were correct. The value for total area was taken, as well as the area of bone (black region), and the latter divided by the former to derive BA/TA. For depth dependent BA/TA, duplicated images were taken, and split into 1 mm segments, starting from the subchondral bone plate. This process is described in Figure 3.2.1.

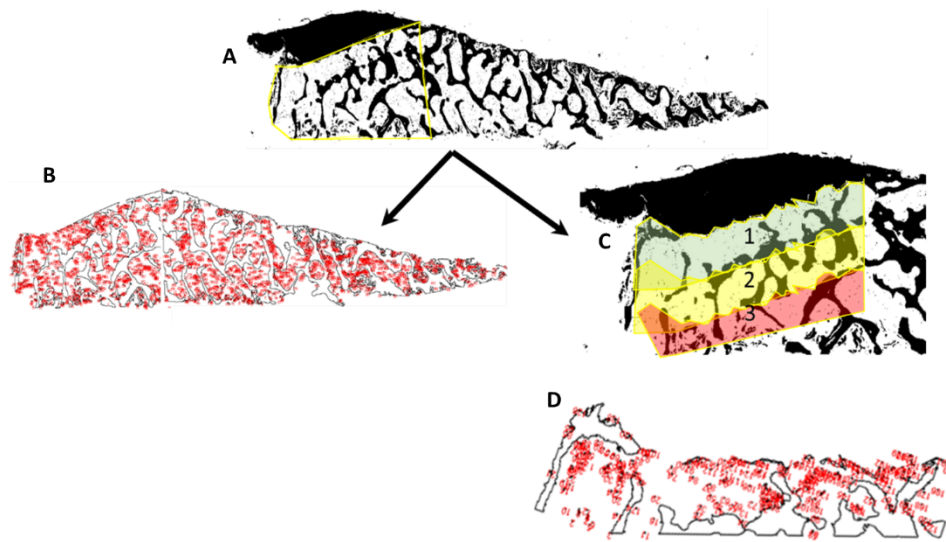


Figure 3.2.1 Calculation of BA/TA. Safranin O stained images are converted into black and white in ImageJ. Bone area of total area is calculated from all bone once cartilage is manually excluded (Shown by yellow outline in A, or B. Specific depth regions were also measured (C – 1, 2 & 3 for 0-1 mm, 1-2 mm and 2-3 mm respectively). Individual segments were duplicated, and then bone area and total area measured again (shown in D for 1) and then duplicated in order to segment that area only, and bone area of total area measured. Red numbers on each image mark every unconnected segment of bone measured (Refer to many red dots within the image due to small bone fragments).

3.2.7. Subchondral Bone Plate Thickness Measures

To further understand specific bone changes in OA and if it varies between joints, the subchondral bone plate thickness was analysed as having previously been implicated in OA progression²²¹. The subchondral bone plate was defined as the distance from the tidemark (in the case of duplication, the earliest point), to the first trabecular space within the bone, as common in literature, using standard methods²²⁹. Subchondral bone plate thickness was taken from both Safranin O images, and mCT, again using ImageJ²²². SBP thickness was measured by re-orientating the image to a transverse view and measuring the perpendicular distance from the beginning of bone (the tidemark) to the first visible trabecular gap. Measurements were taken at twenty points for each bone, and averaged. Similar to BA/TA measurements (Section 3.2.6), the scale was applied within the program using the scale bar.

3.2.8. CD271 Staining

Immunohistochemistry for CD271-positive cells, a broadly used marker of in vivo bone-resident MSCs, was used to analyse MSC location in relation to bone and cartilage changes, using methods standard to the research group^{101,215}. The CD271 monoclonal mouse anti-human antibody at 1:200 dilution in antibody diluent solution was used followed by incubation with the EnVision+ Dual Link System-HRP including Horse Radish Peroxidase (HRP) and 3,3'-diaminobenzidine tetrahydrochloride(DAB) kit. A negative control without antibody was used. Positive controls were performed previously by the group with this antibody clone and so this was not repeated. The kit included dual endogenous enzyme block, labelled polymer, substrate and chromogen solutions. Haematoxylin was stained for to show cells in the background (Section 3.2.3, steps 13-16). As samples were of varying sizes, the volume of solution used was dependent. For the first TBS wash, via pipette, 10 µl aliquots were gradually added until sample was covered. Total volume was then used for subsequent incubations. The staining process is detailed in Table 3.2.7. The stain utilises the chromogen 3,3'-Diaminobenzidine (DAB), which is catalysed by the HRP conjugated to the antibodies. This creates the visible staining at the antibody target antigen site under brightfield light microscopy. Positive controls have been completed by other lab group members and so were not performed for this study as the group uses this antibody frequently^{72,101}. This staining follows sample processing (Section 2.2.1-2.2.4). Images were taken on a Nikon Eclipse Ti2-E camera (Nikon, Tokyo, Japan) and analysed using the Nuance Multispectral Imaging System as detailed in Section 3.2.9, and bone area of total area was measured as detailed in Section 3.2.6 using matched images from the CD271 analysis instead of safranin O images. Afterwards, coverslips were again applied (Section 2.2.5).

Table 3.7 CD271 Immunohistochemistry Staining Process

Process	Step	Solutions and Reagents	Time (mins)
CD271 IHC	13	Use a PAP pen to draw hydrophobic circles around samples	N/A
	14	Wash with Tris-Buffered Saline (TBS)	1:00
	15	Wash with TBS	5:00
	16	Tap off TBS and incubate with block endogenous enzyme with Dual Endogenous Enzyme Block solution	10:00
	17	Rinse with TBS from wash bottle then wash in TBS	5:00
	18	Incubate with antibody diluent	
	19	Tap off TBS and add primary antibody or negative controls and incubate at room temperature in the dark	60:00
	20	Rinse with TBS from wash bottle then wash in TBS	5:00
	21	Tap off TBS and apply Labelled Polymer	30:00
	22	Rinse with TBS from wash bottle then wash in TBS	5:00
	23	Tap off TBS and apply substrate/chromogen solution, and incubate in dark at room temperature	5:00-10:00
	24	Collecting run off in hazardous waste container, rinse samples with water	2:00
	25	Immerse slides in aqueous haematoxylin	2:00
	26	Rinse in tap water	1:00
	27	Immerse sides in Scott's Tap Water Substitute	2:00
	28	Rinse with tap water	1:00

Table 3.2.10 is a continuation of the process described in Table 3.2.4, as such starts at step 13, and is followed by dehydration and coverslip application (Table 3.2.5).

3.2.9. CD271 Localisation Measurements

CD271+ staining was measured in order to relate resident MSC behaviour to bone changes. The Nuance Multispectral Imaging System was used to analyse the CD271 stained images (Section 3.2.8), again using methods specific to the research group. Firstly, stained samples were imaged, and the real component analysis function used to compute and unmix spectra, in order to create a library-spectra for DAB staining, to identify CD271+ staining. A region stained only with haemotoxylin was defined as one colour, a region with both DAB staining and haemotoxylin of a dual-stained cell was taken to define mixed staining, and a pure DAB spectra was defined using the manual compute spectra tool. This was then saved as a spectral library for image analysis. Then, samples were imaged for analysis. These were again converted to optical density unmixed using the real component analysis function, and the previous spectral library created used to define regions stained with each dye. A threshold was manually applied to appropriate identify DAB+ area, and the 'manual draw regions' tool used to apply regions of interest of trabecular spaces and bone-lining cells to only measure DAB in this area. This is demonstrated in Fig. 3.2.2. The measured value for DAB area is divided by total region-of-interest area to calculate DAB stained area of total area. Bone area of total area was taken from matched images in ImageJ, using the same method detailed in Section 3.2.10, using the same tile of CD271 instead of Safranin O images.

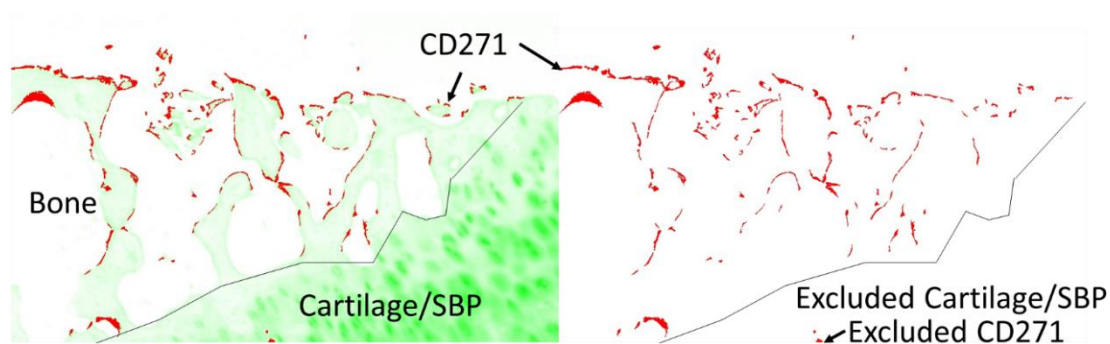


Figure 3.2.2 Demonstration of CD271 Area of Total Area Measurements, and alignment with Bone Area of Total Area Measurements. Separated spectral libraries allowed selection of DAB CD271+ stained areas (red). Counterstain was coloured green, allowing bone to be identified and visual exclusion of cartilage and SBP could be performed as shown. Individual tiles had CD271+ area calculated, and then bone area of total was calculated after non-bone lining CD271 was excluded, allowing direct correlation per tile. This was performed for all tiles as well as correlated with OARSI grade.

3.2.10. Tartrate-Resistant Acid Phosphatase Staining

To further characterise cellular relationships to bone changes, TRAP staining was used to identify osteoclasts, according to standard methods²³⁰. In OA, bone remodelling is disturbed, typically with bone resorption in early OA, turning towards bone synthesis at later stages of OA²²¹. Therefore, it was expected there would be elevated presence of osteoclasts within the OA human ankle tissues within more damaged sites²³¹. This dye stains osteoclasts red-violet, and fast-green counterstains the background blue. The process following rehydration (Section 2.2.4) is shown in Table 3.2.8 below. DPX cannot be used for coverslips on TRAP staining as it needs to remain hydrated, and so water-soluble Leica Mounting Media (Leica Biosystems) was used to mount the sample, also shown in Table 3.2.8²³².

Table 3.8 Tartrate-Resistant Acid Phosphatase Staining Process

Process	Step	Process	Time (mins)
Tartrate-Resistant Acid Phosphatase	13	TRAP Staining Solution pre-warmed to 37°C (incubate during staining at 37°C)	30:00-45:00
	14	Wash gently in dH ₂ O	4 Changes
	15	Counterstain in 0.02% Fast Green	0:30
	16	Quickly wash in dH ₂ O	4 Changes
	17	Air dry overnight	Overnight
	18	Mount with water soluble media (Leica Mounting Media)	0:30

Table 3.2.8 continues the process described in Table 2.2.2, starting at step 13.

3.2.11. Picrosirius Red Staining

To investigate the possibility and quality of bone repair, picrosirius red staining was used to identify collagen fibre alignment and orientation. This dye stains collagen fibres red, but under polarised light, birefringence identifies collagen maturity from a scale of green for mature fibres, red for immature disorganised fibres, and yellow in between the two. As OA induces rapid bone turnover, it was theorised this would show increased disorganised immature fibres, and picrosirius was performed following standard methods^{224,233}. This staining process follows Section 2.3.4 and is demonstrated in Table 3.2.9. Coverslips were applied as in Section 2.3.5.

Table 3.9 Picrosirius Staining Process

Process	Step	Process	Time (mins)
Picrosirius Red	13	Stain in Picrosirius Red	60:00
	14	Wash in two changes of 0.5% Acidified Water	4 Changes

Table 3.2.9 is a continuation of the process described in Table 2.2.2, as such starts at step 13, and is followed by dehydration and coverslip application Table 2.4.5

3.2.12. CD56 and E11 Staining

CD56 and E11 are markers for osteoblasts and early-embedding osteocytes respectively⁸⁵. As sclerotic bone forms in end-stage OA, it was expected that E11/CD56+ cells would be present, particularly in relation to the wound site. Additionally, as MSCs are a common source of osteoblasts, correlation with CD271+ MSCs was performed to investigate if these cells are related to the disease process, particularly in relation to bone formation. This method follows similar work performed by another member of the research group^{220,234}. Immunohistochemistry for CD56 and E11 was completed similarly to CD271 stains, as in Section 3.2.8, and Table 3.2.7. Antibodies used were: CD56 and E11. These titrations were previously optimised by other researchers within the group⁸⁵.

3.2.13. Collection of Osteochondral Plugs from Porcine Tissue

Specifically, it was important to learn if firstly, cartilage properties of osteochondral plugs can be accurately measured in surgical tissue explants from ankle fusion surgery, as well as the effect of freeze thawing. Porcine cartilage was indented to investigate the mechanical properties of a relevant animal model to develop methods to test human tissue, particularly considering that bone segments were extremely thin. Changes to cartilage of the ankle during OA are poorly understood as such this work had aimed to investigate this, however not enough tissue samples

were obtained to complete this work. Additionally, non-diseased human control tissue was obtained from America, as such would need to be frozen and defrosted, firstly for transport, and then for preparation for testing. This represented method development for future studies. Extra-skeletal tissues were removed using scalpel and forceps to expose the talocrural joint. During dissection, exposed cartilage was kept moistened using phosphate-buffered saline (PBS) using a spray or wrapped in PBS-soaked paper towels. Talus and tibia were fully removed and then secured by bench-top vice with additional PBS-soaked towels to secure it, and then an $\varnothing 8$ mm corer hammered in to extract osteochondral plugs of 5 cm depth with a flat cartilage surface (Fig. 3.2.3). These were separated into groups for the purpose of testing. Group A went through 3 freeze-thaw cycles, whereas B did not, to investigate effects of freeze/thaw on small tissues.

Secondly, samples of 5 cm bone depth were indented under a constant load of 50N for half an hour. These were then shaved to 2 mm to mimic the samples obtained from surgery and left in PBS for 2 hours to regain mechanical properties, and then indented again. An additional control group without shaving was used to verify that second indentation provided similar results to the first round. Following this indentation, samples were moved for needle indentation to assess cartilage thickness, then retrieved for histology. Dissection and experimental process is summarised in Fig. 3.2.3.

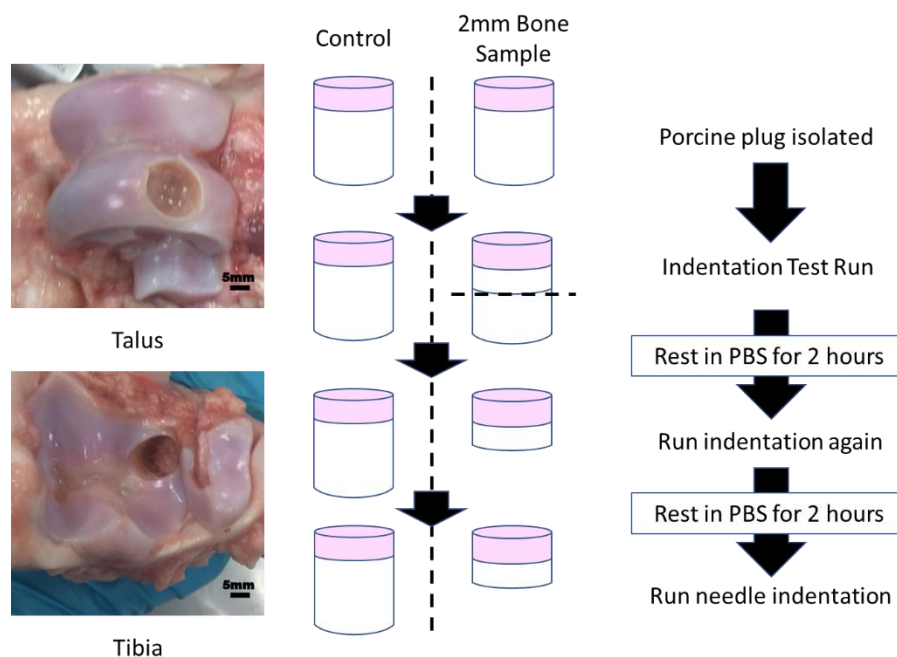


Figure 3.2.3 Porcine Tissue Dissection and Experimental Protocol for Method Development for Mechanical Testing of Human Explants from Ankle Fusion surgery. Porcine tissues were dissected from sacrificed 6 month old pigs, ligaments and tendons were removed and then synovial membrane broken to separate the two bones. Plugs of 8 mm \varnothing were removed using a corer with as flat cartilage as possible for testing. Control samples were of approximately 5mm depth, with duplicate test samples cut to 2 mm to mimic human samples after the first indentation test. Scale bars are 5mm.

3.2.14. Indentation of Ankle Cartilage to Measure Cartilage Properties

By understanding the osteoarthritic changes to cartilage quality, the functional behaviour of repair cartilage that MSCs had been induced to form could better be qualified. The 8 mm diameter porcine osteochondral plugs, taken from distal tibia and talus (Section 3.2.13), were placed into a custom-made holder, tightened to prevent displacement of the whole sample, and submerged in PBS. This was then placed into an indentation rig. A continuous load of 0.5N was applied perpendicular to the cartilage through a rigid, hemispherical indenter of 2.5 mm diameter over a period of half an hour, which first compresses the cartilage, and then over time will push the water out, until there is a point the tissue will deform no further, which can be used to calculate the permeability of the tissue. The hemispherical indenter was used to account for surface curvature, as to be accurate indentation data must be used upon a flat surface^{235,236}. A linear variable differential transducer (LVDT, linear error $\pm 0.5\%$ of full scale) located on top of the shaft detected linear displacement of the shaft and a piezoelectric force transducer (error ± 0.1 mm) measured the resistive force. The data from both the LVDT, and the force transducer were visualised on an analogue-digital converter connected to a desktop computer. Force and displacement output data was displayed and recorded using LabView 8 software.

The procedure for calibration was developed by previous researchers at the University of Leeds²³⁷. Calibration procedures for both the LDVT and force transducer were performed prior to testing to determine calibration factors, by which to convert voltage outputs into millimetres and newtons respectively. For LVDT calibration, voltage was measured at 0mm displacement, then incrementally changed from 0.005 mm to a maximum of 2 mm. Voltage was plotted against height, and the linear trend plotted. From this line, the equation for calibration factor was produced (Fig. 3.2.4A). The force transducer calibration was performed in a similar manner, starting with 0 g load, and then 10 g increments until 50 g, and voltage measured at each weight (Fig. 3.2.4B). Again, a linear trend was plotted, and the calibration factor equation calculated.

Each porcine cartilage pin was placed within a collet, and secured in a specimen holder, which was tightened to prevent non-linear movement of the plug. This was then secured to the indentation apparatus. The specimen holder was filled with PBS to keep the sample hydrated. A 2.5 mm diameter hemispherical indenter was chosen to minimise edge-loading effects. The indenter was raised 1 mm above the sample before release to minimise initial impact force. The rig is displayed in Figure 3.2.5.

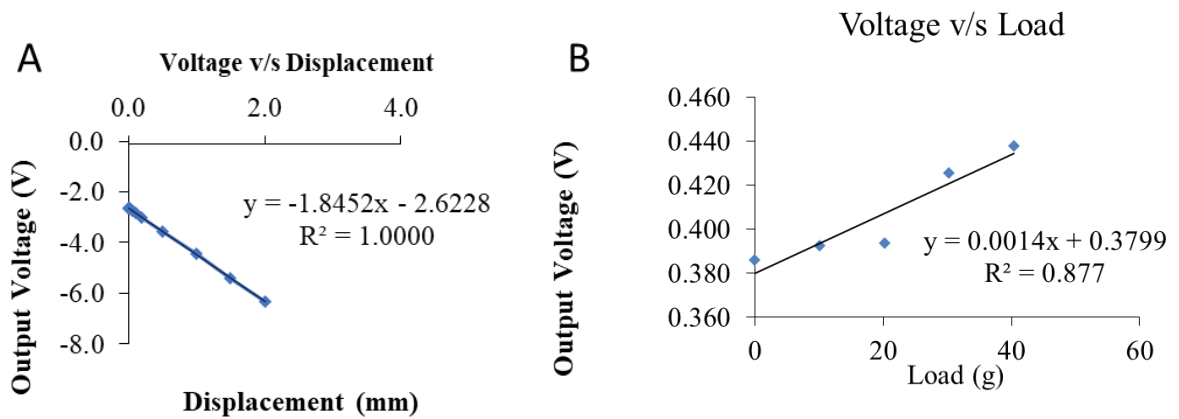


Figure 3.2.4 Calibration Charts for Indentation Apparatus. Calibration plots were used to calculate permeability of samples by converting the voltage output into displacement by measuring voltage changes over set distances (A) and load by measuring voltage changes against set loads (B). Equations of the line of best fit and R2 values were calculated to calibrate the experiment.



Figure 3.2.5 Indentation Rig Example

3.2.15. Needle Indentation of Ankle Cartilage to Measure Cartilage Thickness

Needle indentation was used to approximate the thickness of porcine ankle cartilage¹³. Osteochondral plug specimens following indentation, of both control 5 mm and test 2 mm bone depth, were placed into a collet. This was tightened into a sample holder and loaded into an Instron testing machine, with the set up shown in Figure 3.2.6.

The next logical step from this would be to calculate permeability or aggregate modulus, using the results of cartilage thickness (Section 3.2.14) and indentation (Section 3.2.13). These two values would then be applied to a computational biphasic model to estimate both Young's modulus and the Poisson ratio, to find values which match the measured maximum indentation and cartilage thickness, as given by the equation in Section 1.1.8. This would allow direct comparison to existing studies to identify differences in cartilage between the ankle and other joints. Due to time constraints, ongoing development of the model, and loss of critical staff, this work could not be completed.



Figure 3.2.6 Indentation Rig for Cartilage Needle Indentation

Cartilage plugs were tested perpendicularly to the cartilage surface, in 3 locations approximately 2 mm apart, by adjusting the rig, using a needle of 0.5 mm diameter. The needle was positioned 1 mm above the cartilage before being driven into the cartilage by the Instron at a constant speed of 4.5 mm/minute. Stiffness was measured continuously during insertion, with three gradually more resistant materials, air, cartilage penetration and bone penetration. The needle was manually stopped when the needle had entered bone with reasonable clearance as detected by changes in stiffness. Cartilage thickness was measured by plotting stiffness (N) against displacement (mm), and identifying the points of cartilage entry and bone entry and measuring the displacement distance between the two. The stiffness profile is shown in Figure 3.2.7. This is changed from previous similar work which used the term resistive force, which is not what is truly being measured here.

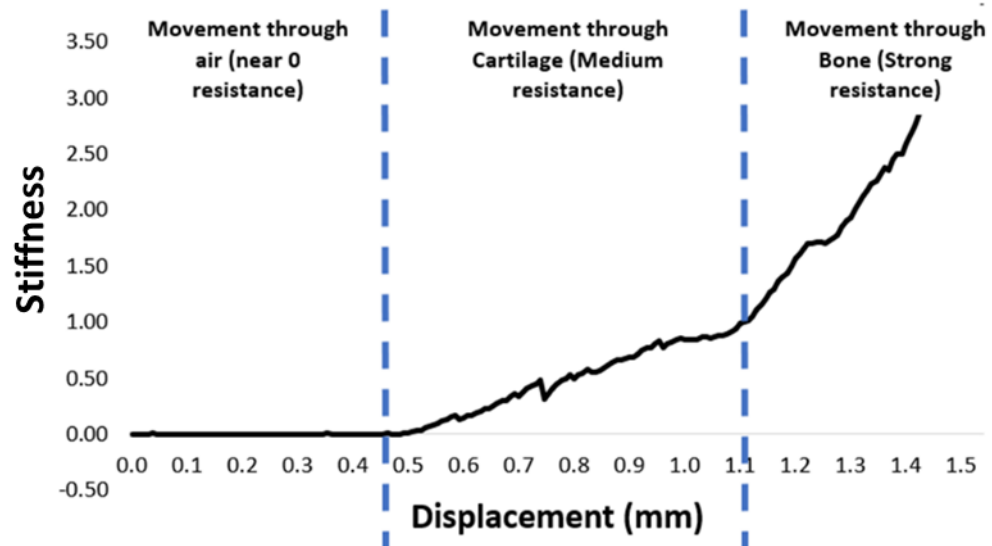


Figure 3.2.7 Resistive Load Profile of Cartilage During Needle Indentation. Resistive force is split into 3 segments – Air, which will provide near 0 resistance, cartilage, which will have some, and bone which will show heavy resistance. By measuring the displacement in the second segment, cartilage thickness can be calculated.

3.3. Results

3.3.1. Morphological Changes during OA of the Talus and Distal Tibia

Of importance in this work was first to see if there were differences between the non-diseased or OA ankle, and to secondly see if there were key anatomical differences between distal tibia and talus. Cadaveric human tissues were investigated first (Fig. 3.3.1, Table 3.3.1). Samples presented smooth, shiny white cartilage without exposed subchondral bone, typical of what is expected from non-diseased cartilage²³⁸. When size was investigated, the talus and tibia had similar width (defined by medial-lateral anatomical length of the sample), but the talus was longer (Defined by anterior to posterior anatomical length), due to its involvement in other joints. When the cartilage only regions were investigated, the talar dome and tibial pilon both showed similar size. Next, osteochondral OA samples were examined, which were osteochondral specimens retrieved from talocrural joint fusion surgery (Section 3.2.1), of which there is little documentation of the amount of tissue removed. Surgeons revealed that this varies based on the preference of the surgery – however they prioritise removing as little bone as possible to prevent leg length inequality. From the distal tibia, as shown (Fig. 3.3.1B), multiple segments were typically obtained. Comparison to 3D images and information from surgeons showed these were from the medial edge of the distal tibia, at the base of the curve leading to the malleolus, which allows a flat corner to be left behind to insert the talus in before adding screws (Fig. 3.3.1) (demonstrated by red boxes in Fig. 3.3.2). In comparison, the talus was usually in one part, and included the top of both medial and lateral domes of the proximal portion of the talus (Fig. 3.3.1). Sizes of samples rarely exceeded 5 mm depth (range 5 mm-16 mm) in both talus and tibia, and surface area typically 30mm by 30mm (range 20 mm-49 mm) (Table 3.3.2). Tibia samples were on average larger than talar segments. Samples were separated into 3 main pathways, for mCT, histology (both Chapter 3) or cell work (Chapter 4) (N=3 for each). Samples presented with the typical white colour of cartilage, however the surface was frayed, with subchondral bone exposed in all samples and no shiny, smooth cartilage in any sample. In some regions (first talar segment Fig. 3.3.1B) cartilage had worn away to a translucent thickness, indicative that this is indeed end-stage OA. To gain a 3-dimensional understanding of talus and tibial structure, mCT was next performed.

Table 3.10 Average Size of Non-Diseased Human Ankle Samples

	Length (mm)	Width (mm)	Height (mm)
Talus (N=1)	590	450	200
Tibia (N=1)	420	450	800
Talar Dome (N=1)	370	400	190
Tibial Pilon (N=1)	420	400	800

As N=1, no standard deviation is given. Samples were not all measured on arrival so could only be completed for 1 sample.

Table 3.11 Average Size of Human OA Ankle Fusion Samples

	Length (mm)	Width (mm)	Height (mm)
Talus (N=3)	27.5±8.7	27±4.8	7.8±2.6
Tibia (N=3)	34.8±7.4	25.2±7.4	8.8±0.5

In cases of multiple segments, individual segments were measured and then summarised to estimate the total sample size. Medians are given and ± denotes standard error

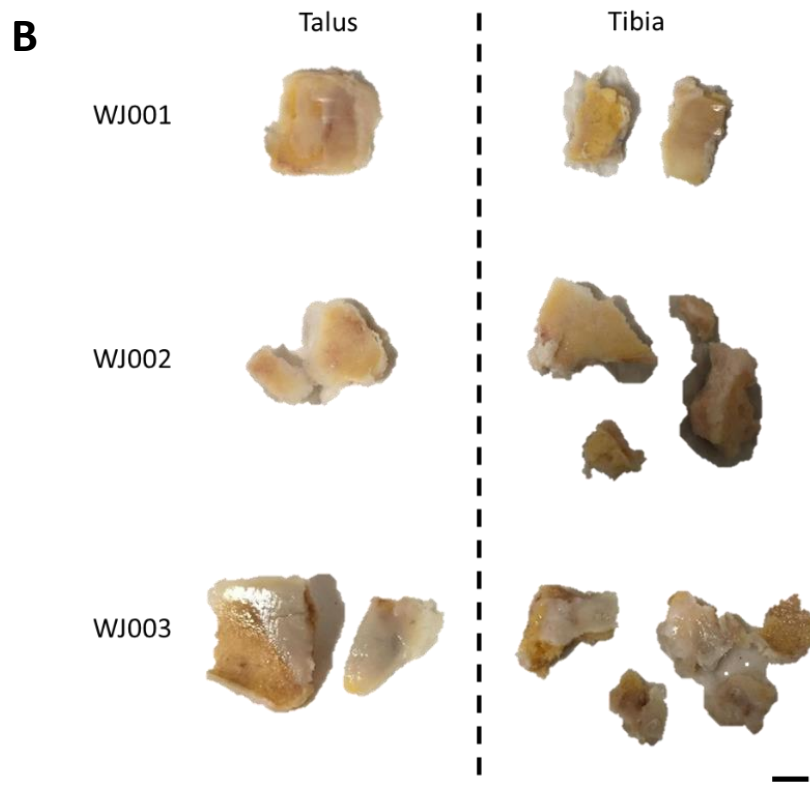
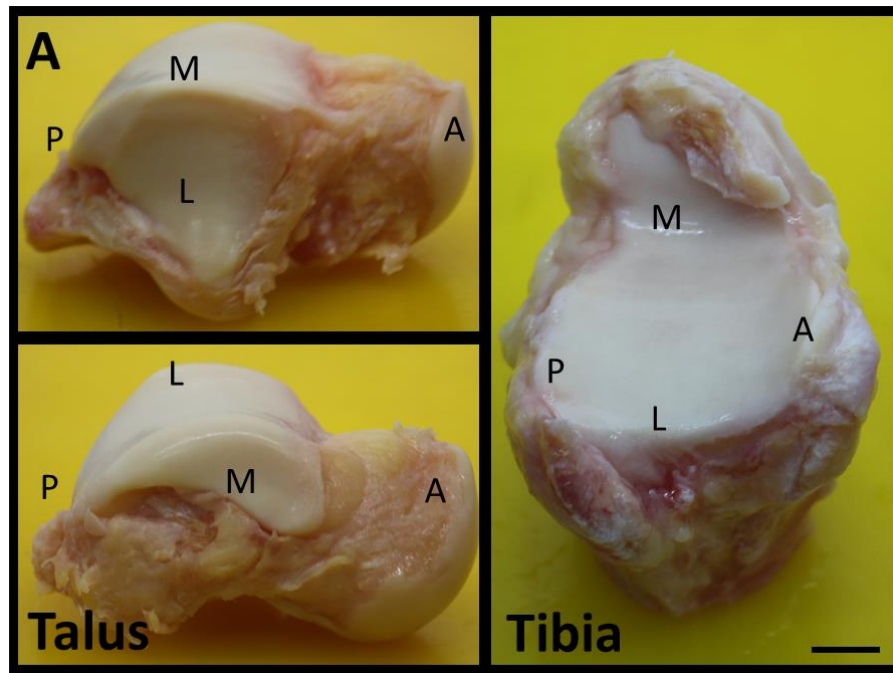


Figure 3.3.1 The Distal Tibia and Talus – Retrieved Sample Morphology. A Non-diseased cadaveric human donor tissue. Each sample shows white shiny cartilage without exposed subchondral bone. M – Medial, L – Lateral, A – Anterior, P – Posterior. Scale bar is 100mm. B Specimens of Talar and Tibia Bone Excised Following Talar Fusion from 3 donors. Samples show frayed cartilage with exposed subchondral bone and no healthy cartilage. Pictures were taken following washing in PBS and 48 hour fixation in formaldehyde. Images were captured cartilage side up. Scale bar is 10mm.

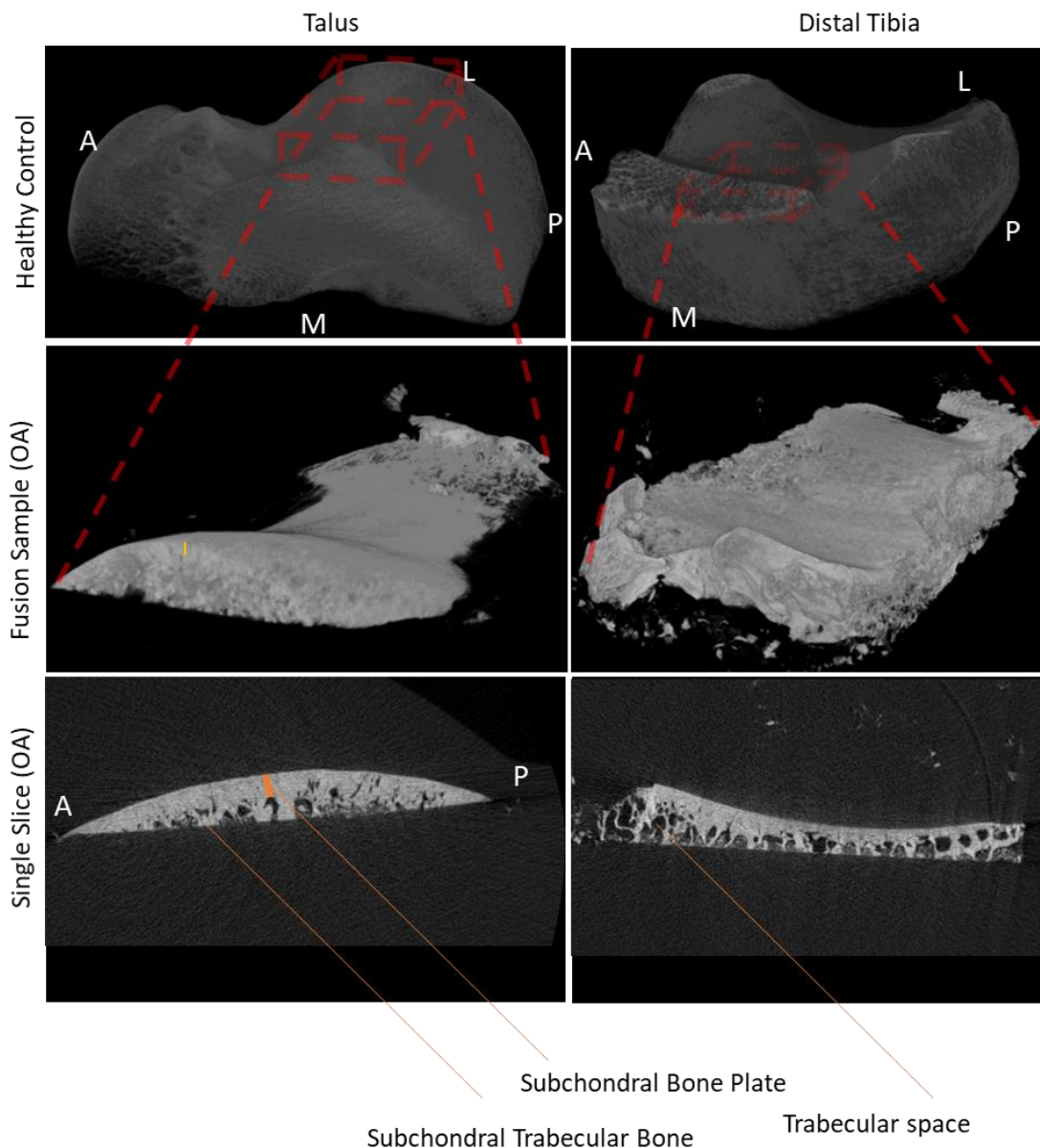


Figure 3.3.2 Morphological changes of OA visible by mCT on proximal talus and distal tibia (N=3 OA patients compared to n=3 don-diseased controls, (NDC). All samples are orientated in the same way. A – anterior, P – posterior, M – medial, L – lateral. The OA talus and tibia are far smaller due to the minimal amount of bone removed from surgery, with approximate anatomical region described by the red region on non-diseased samples.

To investigate the specific subchondral bone behavioural changes in OA-affected bones of the ankle, mCT was performed and compared to non-diseased control cadaveric samples from approximately same anatomic regions (Fig. 3.3.2, red regions for controls). Firstly, OA samples were far smaller than non-diseased controls, with red squares showing approximate matched regions in controls to OA samples (Fig. 3.3.2). The SBP (shown by orange line) was visibly larger in OA than health, with apparent bone thickening towards the surface of samples in OA. These changes were then quantified to understand specific changes in OA.

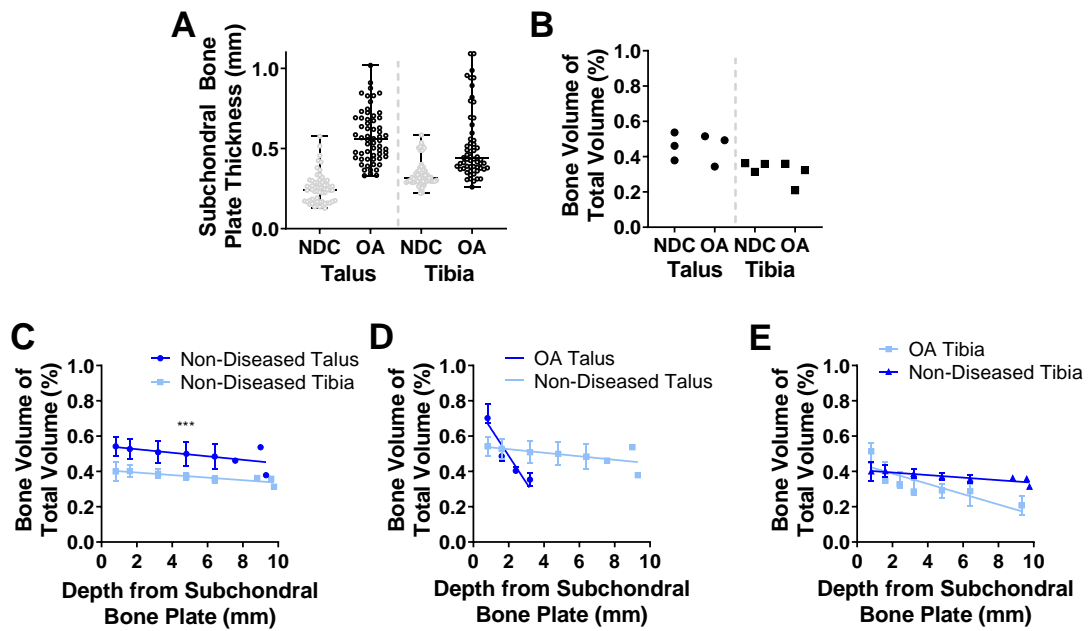


Figure 3.3.3 Quantification of mCT of Talus and Distal Tibia in OA and Health (N=3). A Change in subchondral bone plate (SBP) thickness in OA (data shows all 20 repeats per donor from 3 donors for each condition). B Change in Bone Volume of Total Volume (BV/TV) in the analysed regions in OA talus/tibia (symbols represent individual donors). C Change in BV/TV by depth in non-diseased control talus/tibia. D Change in BV/TV by depth from the SBP in talus. OA talus samples are measured to 4 mm depth due to thinner samples being removed during surgery. E Change in BV/TV by depth from SBP in tibia. Symbols and error bars on D-F show medians \pm interquartile range for 1 analysis per donor for 3 donors, with a minimum of 200 slices per depth interval. C was tested using the Wilcoxon rank test. Significance was set at: *** $p < 0.001$.

Quantification of SBP thickness (Fig. 3.3.3A) revealed an apparent increase in OA compared to non-diseased tissue in both talus and distal tibia, consistent with prior research in the ankle (SBP thickness was measured as the distance to the first trabecular space (demonstrated in orange on Fig. 3.3.2))²³⁹. The overall volume as a fraction of total volume (BV/TV) was unchanged between health and OA, measured to 3 mm depth from the SBP (Fig. 3.3.3B). The talus appeared to have higher BV/TV than tibia in both OA and health, consistent with prior work²⁴⁰. To investigate if BV/TV in OA changed by depth from the joint surface, samples were segmented in millimetre depths up to 3 mm, and BV/TV measured for each 1 mm. In health, the tibia and talus measurements showed a similar gradual decrease in BV/TV as the depth increased, with the tibia being significantly thinner than the talus at each depth ($p=0.001$)(Fig. 3.3.3C). In OA, the talus showed much greater BV/TV increases near the SBP than in the tibia (Fig. 3.3.3D), but also a depth-dependent loss in BV/TV which fell below that of the non-diseased talus at 2 mm. The tibia showed a similar trend (Fig. 3.3.3E), whilst not as severe as the talus, but more so than the non-diseased control. These microstructural changes in OA talus and distal tibia indicated the predominant bone formation near the joint surface by the SBP thickening and up to 2 mm

beneath it. This appears to suggest that whilst talus and tibia show similar trends, they have different capacity to resist these changes in SBPT.

To further investigate these changes, OA samples were placed into EDTA to begin decalcification, to allow histological analysis as a crux of this work. Additional techniques would have been required to allow any investigation of cartilage in mCT, in order to sufficiently differentiate its density from cartilage, such as the use of a contrast agent or increased resolution, however neither was possible in this work. Non-diseased tissues were provided by another researcher, and had subsequent destructive plans for their work. Additional samples could not be obtained and so could not be used for histology.

To help planning of future studies, decalcification rate based on sample size was investigated. Typically bone plugs are used, and so investigating the change in rate for whole samples was of interest. X-ray images at time 0 show individual trabeculae at the surface clearly, whereas at endpoint these disappear and a basic grey shape is shown (Fig. 3.3.4A). Average weight of samples was measured following fixation and placement in EDTA. As samples in tibia were typically larger, the tibial samples showed on average a higher mass (Fig. 3.3.4B). Decalcification rate was apparently slower within the talus by mass, weight and size compared to tibia (Fig. 3.3.4C-E). Average time to decalcification of such large samples was expectedly slow, taking a median average of around 236 days in talus and 146 in tibia, likely due to the increased BV/TV seen in the talus which would result in a comparatively higher surface area and reduced bone content in tibia (Fig. 3.3.4F). Once decalcification was complete, histology was commenced.

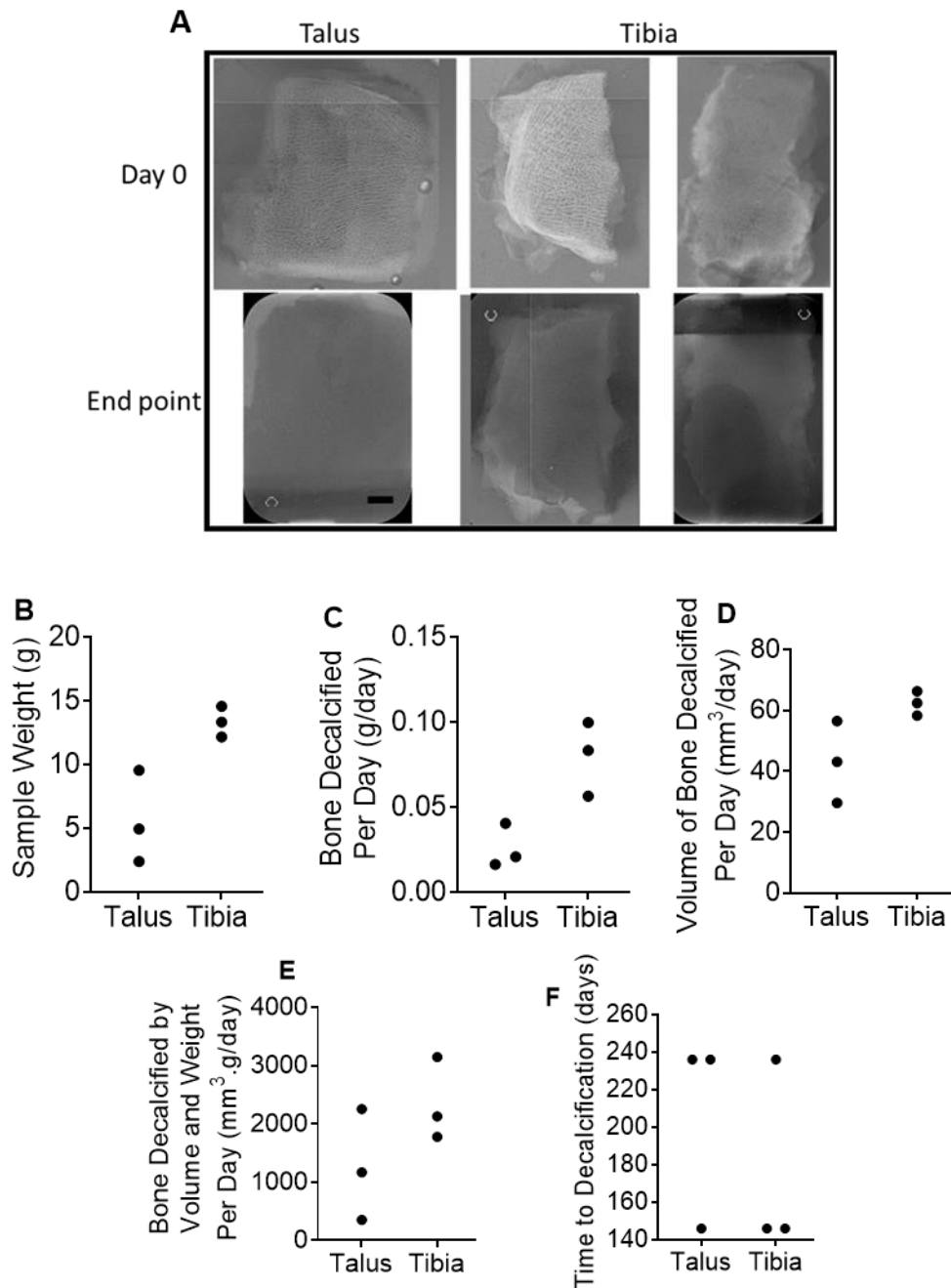


Figure 3.3.4 Decalcification Rates of Formalin-Fixed Tibia and Talar Segments in EDTA. A X-rays taken of bones before EDTA decalcification, and once endpoint was reached, showing the loss of calcium from the bone. B Average weight of tissue sample. C Rate of decalcification by mass. D Rate of decalcification by volume. E Rate of decalcification by mass per volume. F Total time taken for decalcification. Data shown is median and range with all datapoints.

H&E staining was performed first to investigate general morphological changes to osteochondral tissues, and compare to previous research of OA progression in other joints (Fig. 3.3.5) (Section 3.1). It was clear that osteochondral injury was not the same across the whole bone in both tissues, as seen in whole donor bone images, with areas of cartilage (i) or fully exposed subchondral bone (ii). This is similar to morphological changes seen in end-stage OA as in other joints, with extreme bone sclerosis (iii), cartilage loss (iv), and loss of trabecular organisation (v). Areas of damage were visibly matched between overlying cartilage and underlying bone. Between the tibia and the talus, there were few visually obvious differences. Under higher magnification, visible changes included fibrillation of the cartilage surface (panel 1), cartilage loss up to the tidemark (panel 2), loss of chondrocyte organisation and hypertrophy (panel 3), tidemark duplication (panel 4) and cell aggregation near thickening bone (panel 5). However cellularity remained unchanged within stromal tissues (panel 6). These are typical changes seen with OA of other joints. To further understand changes, closer examination to see cellular changes under specific osteochondral stains for comparison was needed.

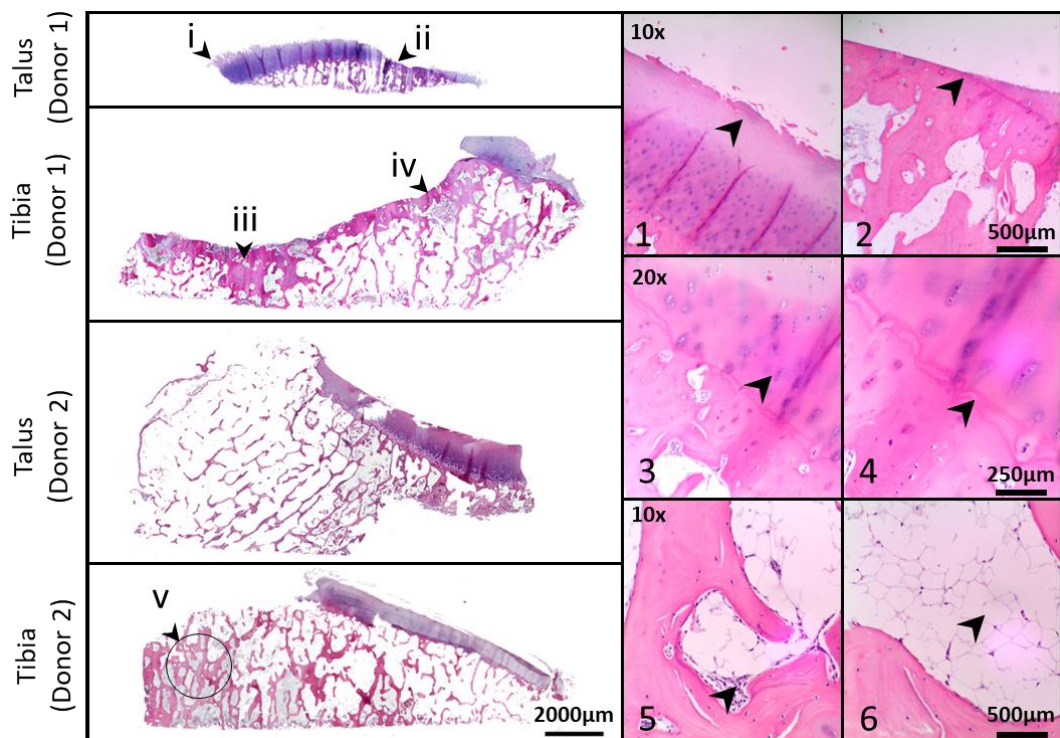


Figure 3.3.5 The Morphological OA Changes seen in Distal Tibia and Talus Samples Retrieved from Ankle Fusion Surgery, Shown by Haematoxylin and Eosin Staining. i – Cartilage, ii – Exposed subchondral bone iii – thickened subchondral bone iv - cartilage ablation, v – loss of bone organisation. Panel 1 – cartilage fibrillation Panel 2 – Cartilage loss up to the tidemark Panel 3 – Chondrocyte loss of alignment and hypertrophy. Panel 4 - tidemark duplication Panel 5 - stromal cell association with thickened subchondral bone, Panel 6 – stromal cells.

To reiterate, Safranin O stains GAGs red, and bone blue, allowing direct comparison between changes to cartilage and the underlying bone, in relation to morphological changes, which Haemotoxylin and Eosin does not allow. Whole tissue samples were stained in order to allow comparison between talus and tibia (Fig. 3.3.6). The level of whole tissue damage was visually more or less the same between both tissues, which included general hallmarks of OA such as cartilage fibrillation (i), cartilage thinning (ii), subchondral bone thickening (iii), complete cartilage ablation and subchondral bone plate thickening (iv), duplication of the tidemark (v) and glycosaminoglycan depletion (vi). More rare abnormalities included regions of seemingly random repair with evidence of both cartilage and bone growing about the previous surface (vii), and cellularised gaps within the subchondral bone plate (viii), the former of which may potentially be due to repeated microfracture.

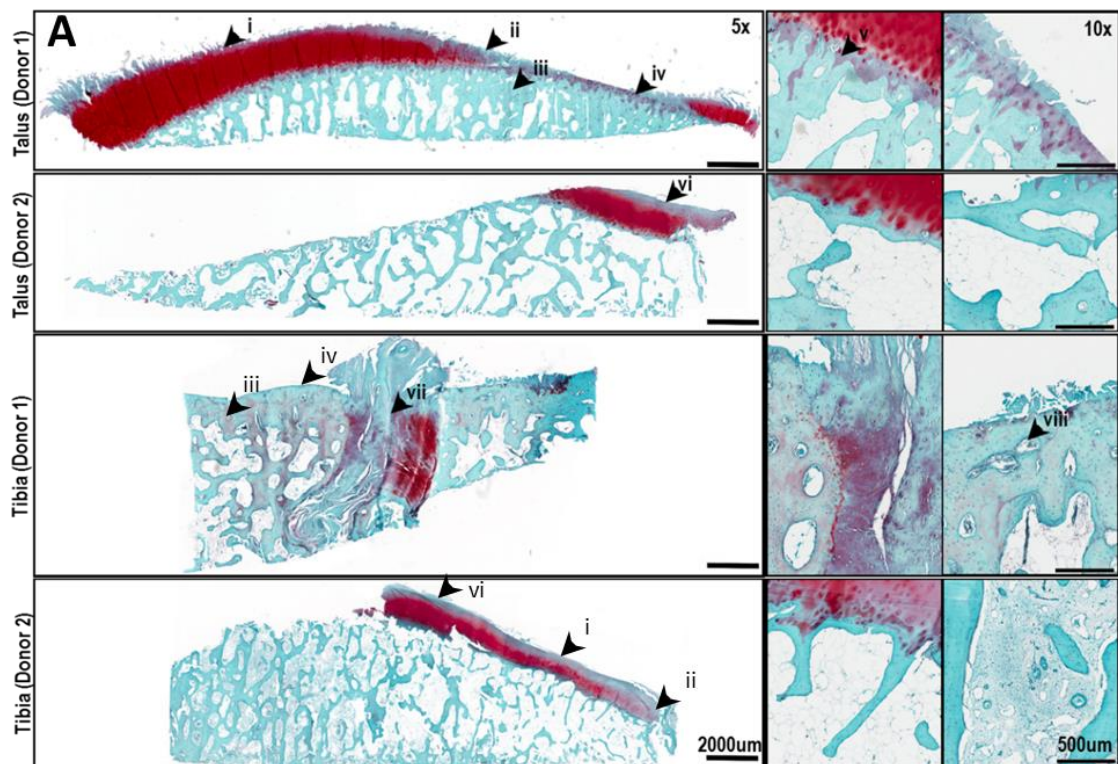


Figure 3.3.6 OA Morphological Changes in Distal Tibia and Talus by Safranin O Staining in End-Stage Osteoarthritis. Safranin O histology of talus or tibial Sections obtained from ankle fusion (i – cartilage with minor fibrillation, ii – thinned cartilage, iii – thickened subchondral bone, iv – bone with denuded cartilage, v – duplication of the tidemark, vi – loss of glycosaminoglycan at the cartilage surface, vii – fibrocartilaginous and osseous repair extending above the previous surface, viii – cellular activity within cracks within the subchondral bone plate).

In order to assess tissue changes in relation to overlying cartilage damage, OARSI scoring was performed first on whole tissues for overall score, and then on segmented regions to allow comparison with other features. On whole tissues, there was no differences between grade (severity of damage), stage (region of damage) or score (Grade multiplied by Stage) (Fig. 3.3.7). Samples presented at least grade 3 damage, with GAG loss and minor fibrillation, and generally up to grade 5 damage, with complete cartilage denudation. More rarely, grade 6 regions were present. Once segmented, these regions were used to compare morphological changes such as bone thickness or BA/TA between tissues.

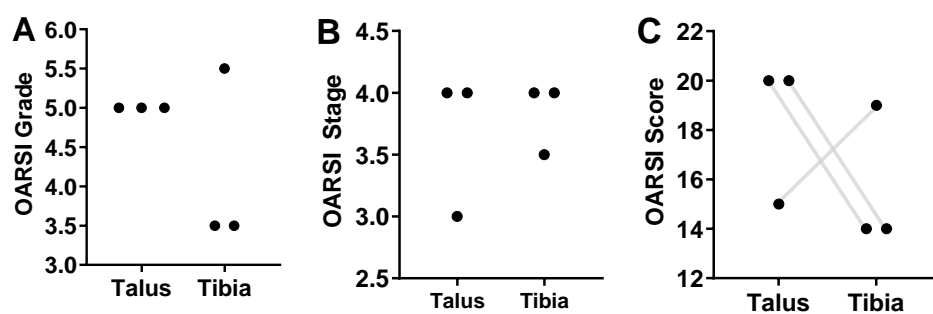


Figure 3.3.7 Evaluation of OA Ankle Sample Histology by OARSI Scoring. A OARSI Grade, defining the maximum damage grade identified in the tissue. B OARSI Stage, defining the size of the tissue which received the highest grade. C OARSI score (Grade multiplied by Stage). Lines represent tibia and talus donor pairs. Lines show paired donors. Differences of 0.5 reflect different observer values being averaged.

'Plugs' of grade 3 and grade 5 tissues were segmented out of whole tissues with an example comparison shown in Figure 3.3.8A. Overall, grade 5 tissues in comparison to grade 3 tissues presented a visually much thicker SBP (Figure 3.3.8A), as well as underlying subchondral bone (grades described in Table 3.2.6, results Figure 3.3.8A).

To investigate if bone formation correlated with regions requiring chondral repair, the pattern of cartilage damage was investigated in relation to the subchondral bone changes. Indeed, SBP thickness increased significantly (3-7-fold) with increasing cartilage damage in both talus and tibia (for grade 3 compared to grade 6, $p=0.003$ and 0.0003 for talus and tibia respectively)(Fig. 3.3.8B). In tibia, there was a similar significant relationship ($p=0.002$) between cartilage damage and subchondral bone density, measured as bone area as a fraction of total area (BA/TA), but not so in the talus (Fig. 3.3.8C). In line with the mCT data (shown in Fig. 3.3.4D and 3.3.4E), there was a significant reduction in BA/TA in deeper areas from the SBP, being 50% lower between 3 mm and 4 mm compared to 0 mm-1 mm ($p=0.043$, $p=0.003$ in talus and tibia respectively) (Fig. 3.3.8D).

BA/TA as a function of distance from the SBP, was next compared between greatly damaged, grade 5 regions, to less damaged grade 3 regions. In both talus (Fig. 3.3.8E) and tibia (Fig. 3.3.8F), grade 5 regions displayed higher BA/TA at both depths measured, however these trends were only statistically significant in tibia ($p=0.0064$, 0.00196 for Grade 3 and 5 respectively)(Figure 3.3.8F), suggesting that sclerosis in relation to cartilage loss may be stronger in tibia than in talus. Combined with mCT work, these data indicated that bone sclerotic changes happen most near the joint surface, with increased SBP thickness and higher BV/TV closer to the joint surface.

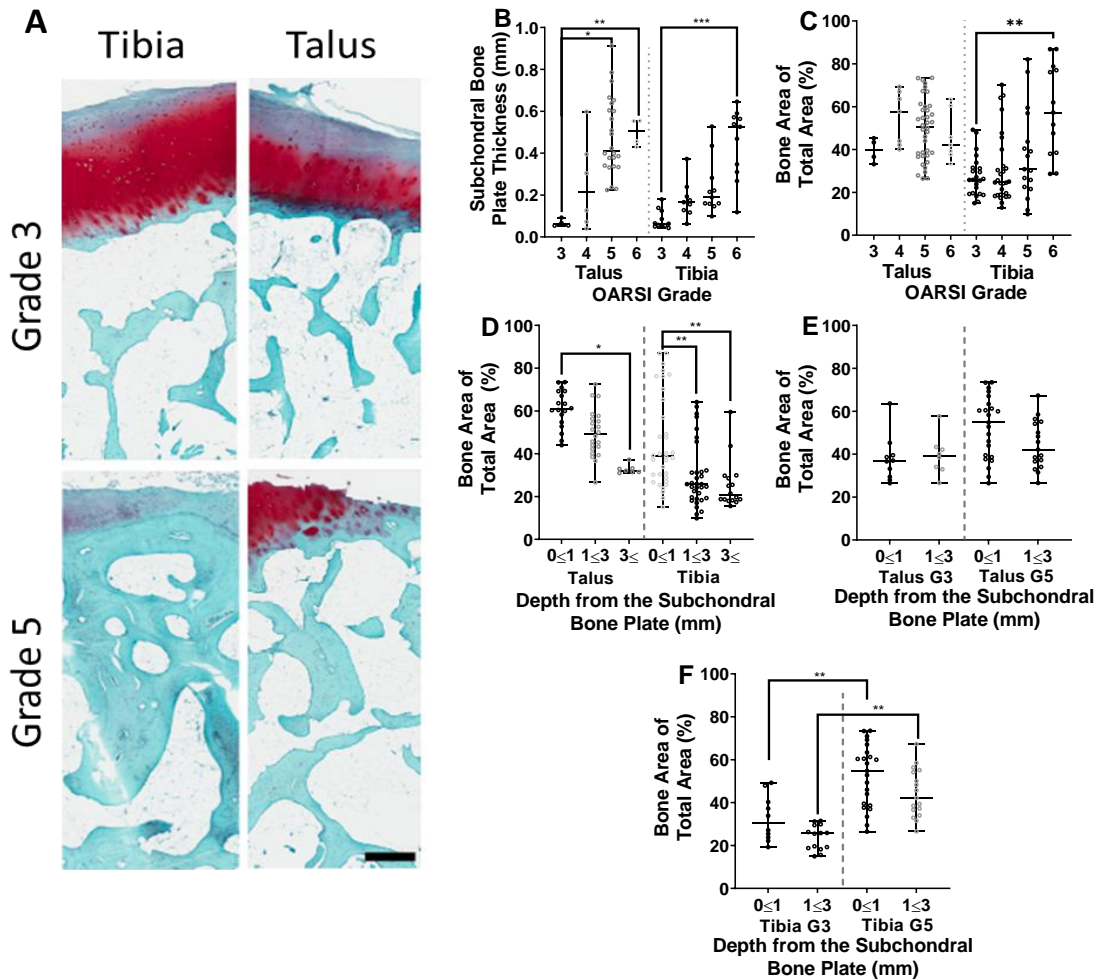


Figure 3.3.8 Relationships between Cartilage and Bone Changes Between High and Low Grade Damage Regions in OA Talus and Tibia (N=4). A Safranin O histology of talus or distal tibial osteochondral tissue Sections obtained from ankle fusion patients, denoting bone below cartilage damage grade of grade 3 (top) or grade 5 (below). B Comparison of Subchondral Bone Plate Thickness with overlying cartilage OARSI grade. C Comparison of Bone Area as a fraction of Total Area with overlying cartilage OARSI grade. D Comparison of Bone Area of Total Area with depth from the subchondral bone plate. E Relationship between bone area of total area with depth from subchondral bone plate in the talus between areas with grade 3 OARSI cartilage damage score and grade 5. F Relationship between bone area of total area with depth from the subchondral bone plate in tibia between areas with grade 3 OARSI cartilage damage score and grade 5. Scale bar represents 500 μ m. All statistics were performed using the Friedman test with Dunn's multiple comparison test, based on talus and tibial samples being paired. * = $p<0.05$, ** = $p<0.01$, *** = $p<0.001$

In combination with mCT work, this Section shows that OA of the ankle presents similar to that of other joints, with thickened subchondral bone plate and damage-related changes to bone area. Interestingly this additionally shows that underlying bone changes are directly correlated with overlying cartilage damage, with talus and tibia mostly responding similarly, however talar tissue being less resistant to SBP thickness changes but more resistant to BA/TA changes than tibia, likely linked to the tibia having a thicker SBP in non-diseased tissue and talus a higher BA/TA. To understand the driving forces of these tissue changes, cell behaviour was next investigated.

3.3.2. Investigating Relationships Between Bone Changes and Cellular activity

To investigate if subchondral bone MSCs could be responsible for forming new bone (and not cartilage) in ankle OA talus and distal tibia, immunohistochemistry for CD271+ cells was next performed. Whole image scans allowed entire bone segments to be compared, using the overlying cartilage grade as a disease progression reference. In the areas with minimal cartilage damage (grade 3. panel 1, i), CD271+ staining was found around cells lining trabeculae, as expected²¹⁹. Comparing less and more-damaged regions, CD271+ staining increased in worse-damaged (grade 5, ii) regions in line with areas of thickened trabeculae, with some evidence of CD271 in stromal tissue rather than just bone lining (Fig. 4.3.9). Non-specific staining was seen in cartilage due to its curvature and water absorptive properties.

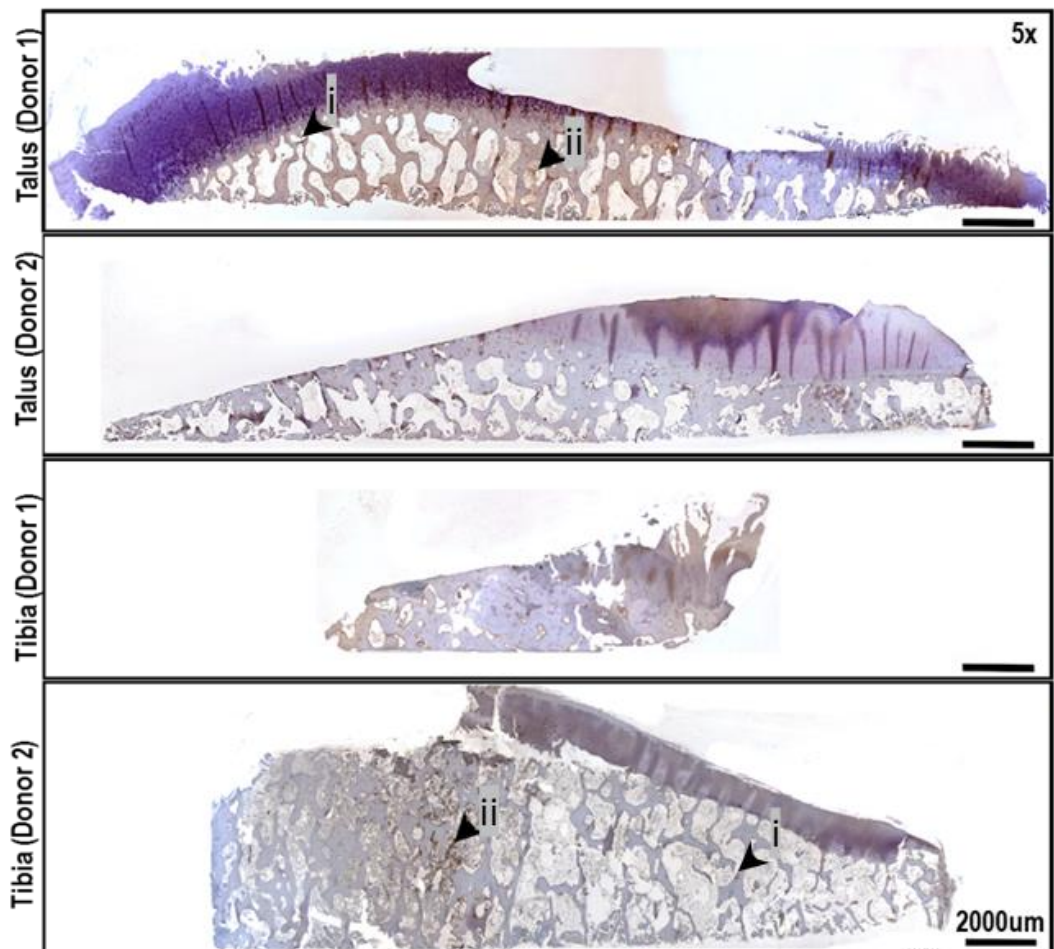


Figure 3.3.9 CD271 Antibody Positive Topography in the Distal Tibia and Talus. CD271+ cells are stained brown, and remaining tissue counterstained blue with haematoxylin. i – regions with undamaged cartilage showing CD271+ staining near trabeculae, ii – CD271+ increased in regions with damaged cartilage.

To further understand the role that MSCs played, the localisation of these cells relative to tissue damage was investigated under higher magnification (Fig. 3.3.10). In less damaged tissue (cartilage grade 3), CD271 associated with bone-lining cells of regions with higher mechanical pressure (apex of bone arches parallel to the bone surface (i)), and staining was not found in areas of lower mechanical pressure (ii). In higher grade (grade 5) regions, CD271+ and bone-lining cells were found lining the entirety of small trabecular spaces in highly sclerotic bone, as well as in almost entirely closed spaces (iii), suggesting the bone is no longer being formed against the direction of force, instead concentrically around gaps, with some form of CD271+ cell involvement. In stromal tissue, CD271 was found in both high and low grade damaged tissues (iv), however, higher grade tissues showed far more cellularity, alongside similarly increased CD271+ and in bone-lining cells. The cuboidal structure and bone-lining nature of these associating cells suggests they are developing into osteoblasts, as such the relationship between CD271+ cell abundance and bone and cartilage changes was next investigated.

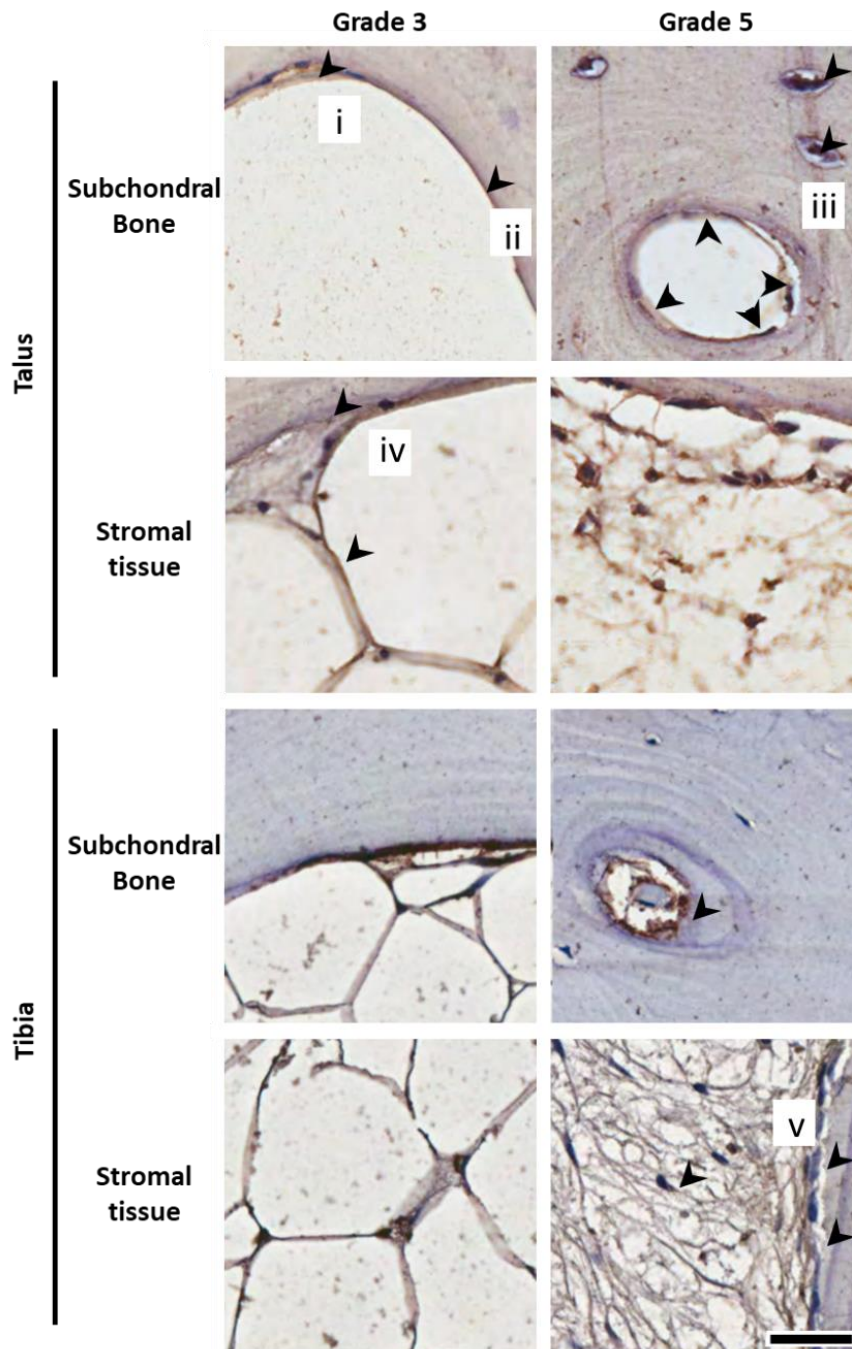


Figure 3.3.10 High Magnification Images of CD271 Immunohistochemistry of MSCs and Association with Cartilage and Bone Changes, comparing bone regions of grade 3 or grade 5 cartilage damage between talus and tibia. MSCs are stained brown, with an eosin counterstain leaving bone and nuclei blue. i – CD271 colocalising with bone-lining cells. ii- No CD271+ staining lining bone. iii- CD271 and bone-lining cells within remaining trabecular space of sclerotic bone. iv- stromal tissue with some CD271+ staining. V – highly cellularised stromal tissue with increased CD271+ staining and bone-lining cells.

To relate MSC abundance to bone and cartilage changes, stitched tile whole sample mosaics up to 3 mm depth were created to make plugs containing cartilage and underlying bone of grade 3 and grade 5 OARSI grade. These plugs further corroborated the link between bone and cartilage damage, with more CD271+ cells in grade 5 tissue plugs (Figure 3.3.11i). Additionally, there was evidence of CD271+ cells within subchondral bone plate thickening (ii), in trabecular spaces within cartilage adjacent to columnar chondrocytes (ii), suggesting CD271 involvement in bone progression into cartilage. Again, CD271 was found in regions of bone sclerosis, as well as surrounding blood vessels as typically seen elsewhere in the body. To investigate if there was correlation between bone changes and CD271+ cell association, these tiles were subsequently individually analysed for CD271+ area as a fraction of trabecular space area (Fig. 3.3.12).

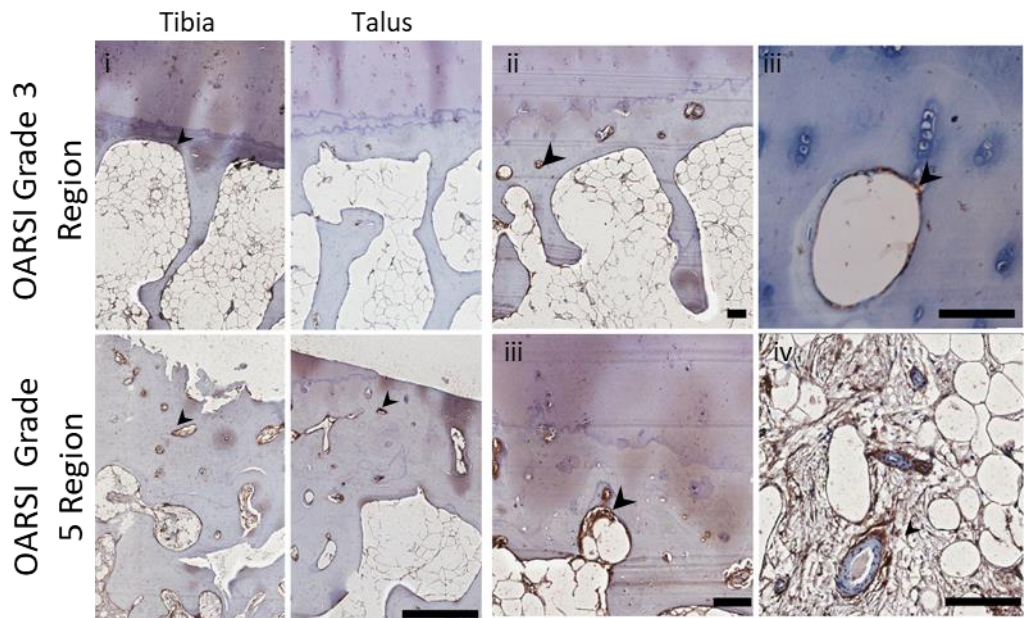


Figure 3.3.11 Relationships between CD271-Positive Cells and Bone Behaviour. A High magnification images of immunohistochemistry for CD271, a native marker of MSCs, showing staining: i) Overview of grade 3 and grade 5 regions from talus and tibia. ii/iii high staining in SB areas beneath the tidemark. iv areas of chondrocyte clustering. v bone marrow stroma around blood vessels.

In general, the talus and tibia showed similar abundance of CD271+ staining, if slightly higher in the talus (8.3% in talus vs 5.6% in tibia (Fig. 3.3.12A)). Subsequent comparisons of CD271 coverage with depth showed that CD271+ cells were most frequent near the SBP, with ~10% coverage in the first millimetre, falling significantly to 4% ($p=0.0031$) and 6% (0.0028) in the talus and tibia respectively at 1-3 mm depth compared to 0-1 mm depth (Fig. 3.3.12B). There was a clear association between the grade of cartilage damage and the amount of CD271 staining within trabecular spaces, with significant differences in the tibia between grade 3 and 6 ($p=0.008$), and 4 and 6 ($p=0.0197$) (Fig. 3.3.12C). This association is consistent with MSC behaviour primed for bone synthesis in the areas of cartilage damage and consequently, regions with abnormal biomechanics, particularly in the tibia.

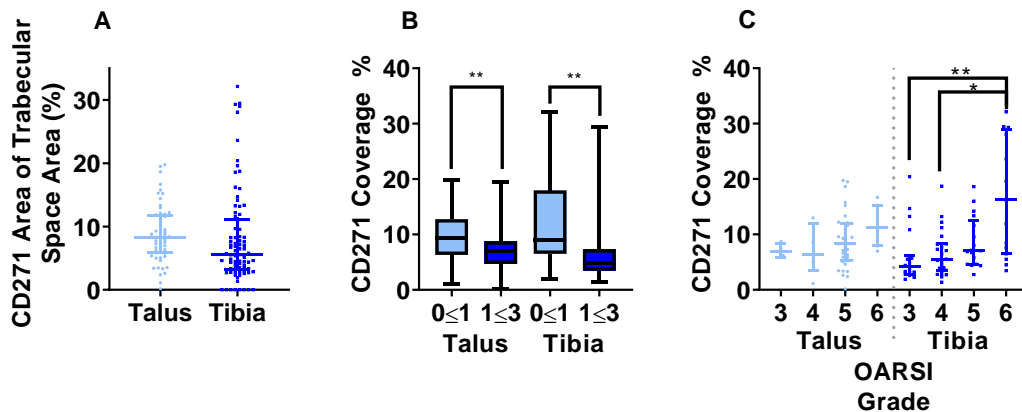


Figure 3.3.12 Quantified Analysis of CD271+ Staining for Endogenous Multipotential Stromal Cells with the Osteoarthritic Human Talus and Tibia. A Comparison of total CD271 coverage between talus and tibia. B Relative CD271 coverage comparing regions near the subchondral bone plate to that further away. Box plots represent medians and IQR from 3 donors measured from a minimum of 4 individual tiles. C The effect of overlying cartilage damage grade with CD271 coverage of trabecular space underneath. Symbols on A and C show individual measurements of each tile, lines and error bars represent medians and IQR. * $p < 0.05$, ** $p < 0.01$, Kruskal-Wallis test with Dunn's correction for multiple comparisons.

Previous work from our laboratory has shown previously in the knee that MSCs have also colocalised with osteoclasts, key cells for bone degradation and therefore essential to normal bone turnover²¹⁹. As it was visually apparent that CD271+ cells were associating with osteoblasts in OA talus and tibia, we sought to assess if CD271+ cells also associated with osteoclasts therefore a key role in bone turnover, particularly in the case of extreme bone sclerosis where bone turnover is more perturbed. To detect osteoclasts, Tartrate-Resistant Acid Phosphatase staining was performed. Staining

showed osteoclastic presence within sclerotic bone, suggesting that as often seen in OA, there is perturbed bone modelling, rather than just sclerosis, which will affect overall bone quality. These were mostly seen in the highly cellularised zones and sclerotic bone of the subchondral bone plate as was observed in CD271+ cells, which suggests osteoclasts are also correlating with MSCs within the tissue (Fig. 3.3.13). As this is similar as found in the knee for both osteoblasts and osteoclasts, this suggests MSCs have a key role in bone turnover, particularly in OA²¹⁹.

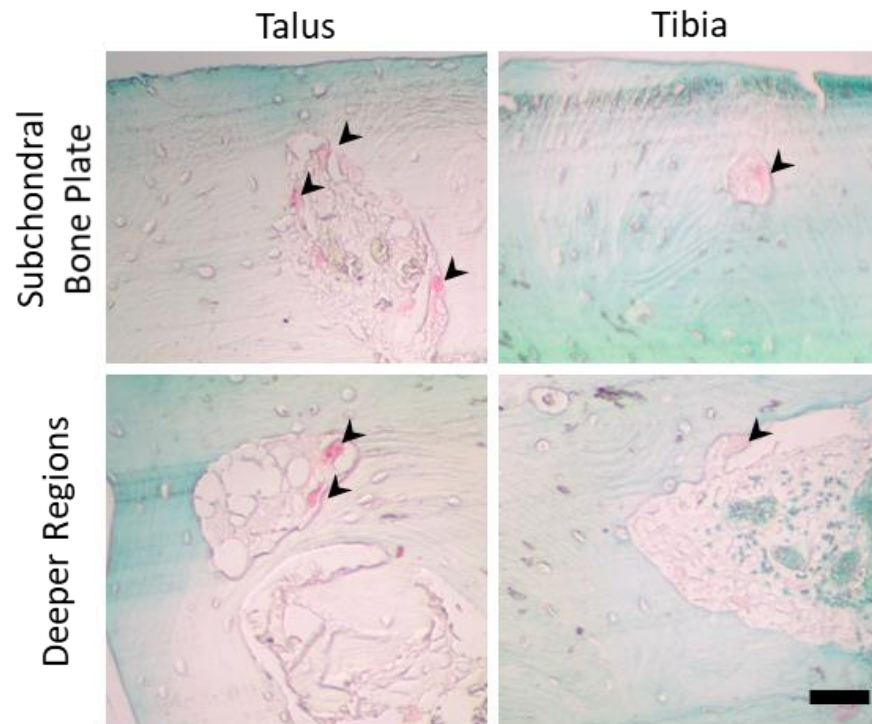


Figure 3.3.13 Osteoclast Behaviour in the Osteoarthritic Talus and Tibia by Tartrate Resistant Acid Phosphatase staining. TRAP-positive cells are stained in red, and bone is counterstained with fast-green. Arrows highlight regions of increased staining. Images taken at 200x magnification. Scale bar is 30µm

3.3.3. Uncovering the Driving Force of New Bone Formation in OA Talus and Tibia

As both bone synthesis and degradation showed topographic links with CD271+ cells, the quality of this bone synthesis was the next key property to investigate. Rapid sclerosis and bone formation is common in every joint of OA, however the orientation of bone proteins such as collagen is critical to healthy bone and has been less well investigated^{85,219,241}. Picrosirius red highlights collagen orientation and maturity based on its colour in biphasic light. In healthy bone, collagen is deposited and aligned against the direction of force, whereas in regions of rapid turnover this alignment does not occur²⁴². As such, in more rigid materials such as bone, red colouration is associated with

immature, unaligned collagen, and green is associated with more mature aligned structures²³³. Staining of the OA talus and tibia showed that in bone under healthier, grade 3 cartilage, collagen was aligned perpendicular to the direction of force, with mostly green biphasic colour (Fig. 3.3.14Ai). However, in bone from grade 5 cartilage damaged regions, this formation appeared fairly random, and parallel to trabecular spaces. Looking at biphasic light, the edges of trabecular spaces near the subchondral bone plate were bright red, suggesting new bone formation (Fig. 3.3.14Aii). These findings confirm that there is rapid bone formation within OA tibial and talar tissues which is unable to undergo full maturation and alignment, with strong links to CD271+ cells, or MSCs, in both degradation and synthesis. As such, these findings confirm the notion that biomechanical correction of MSC behaviour in OA may be key to successful management of the disease.

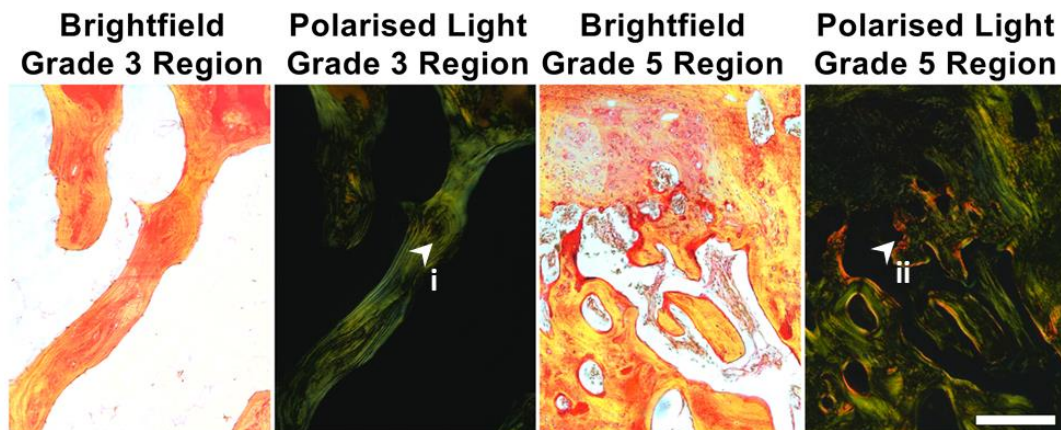


Figure 3.3.14 Representative Picrosirius Red Staining (A) and Analysis (B and C) of Proximal Talus of ankle OA. Brightfield and Polarised Light images of Proximal Talus comparing grade 3 (less cartilage damage) and grade 5 (more cartilage damage) regions. Picrosirius stains bone red/yellow, however under polarised light, red colouration reflects disorganised, immature collagen fibril alignment while green/yellow stains organised, mature collagen. i – organised, green coloured collagen in bone with fibres perpendicular to the direction of force, ii – disorganised, red coloured collagen. Scale bar is 200um.

These images were further quantified for red or green colouration of total area to identify the amount of mature or immature bone respectively. Quantification of this showed that in general, there was higher bone synthesis in the tibia than the talus (Fig. 3.3.15A). Comparing grade 3 to grade 5 tissue, both tissues showed an increase in red colouration in grade 5 tissue, suggesting more immature bone (Fig. 3.3.15B). Synthesis of bone seems to be focused at the edge of trabeculae and at the joint surface, again correlating with regions of MSC localisation, greatly supporting their involvement in the process. However, the effect of these changes on the mechanical competency of this new bone requires investigation.

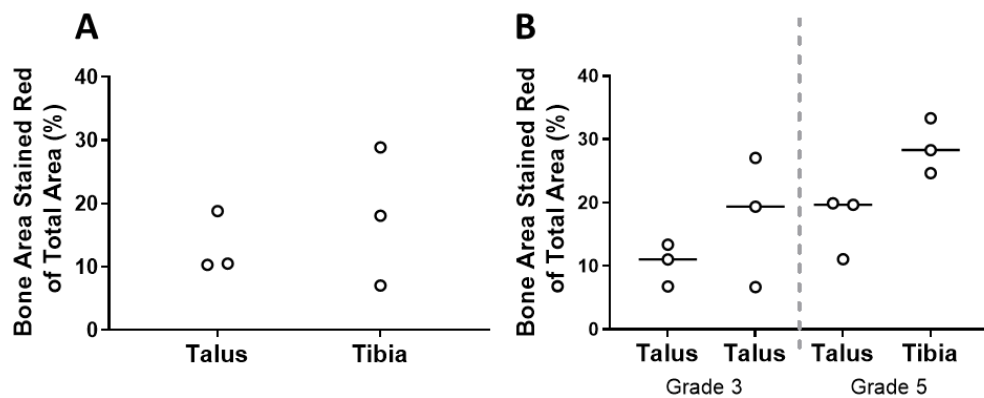


Figure 3.3.15 Picrosirius Red Analysis of Proximal Talus of ankle OA patients (N=3). A The percentage of red stained area (new collagen) of total area from polarised light images comparing of talus and tibia. B The percentage of red stained area (new collagen) of total area from polarised light images comparing less damaged grade 3 regions, to the more damaged grade 5 regions, in both talus and tibia. Bar graphs represent red area of total bone area of whole tali and tibia, once subchondral bone plate is subtracted. Data shows median and range with all datapoints

New bone formation in talocrural tissues was further investigated by immunohistochemical staining for CD56, a molecule present on bone-lining osteoblast progenitors, and E11, a marker of early embedding osteocytes, with both cell types present in the vicinity of cuboidal osteoblasts (Fig. 3.3.16)⁸⁵. This illustrates the three progressive stages of the bone formation process in vivo. Additionally, CD56 and E11 are also present in regions similar to where CD271, such as bone lining of highly sclerotic tissue (Fig. 3.3.16). This in combination with prior results in Figures 3.3.8-3.3.15, suggests the OA process drives bone sclerosis, however the effect of rapid bone formation on mechanical properties of the synthesised bone is still unknown. Additionally, as cartilage is degraded there is a more extreme effect on bone, with greater bone synthesis beneath denuded cartilage, suggesting a biomechanical relationship between the loss of cartilage and the bone response. CD271+ cells demonstrate key links with this process, and must play some level of involvement in bone sclerosis.

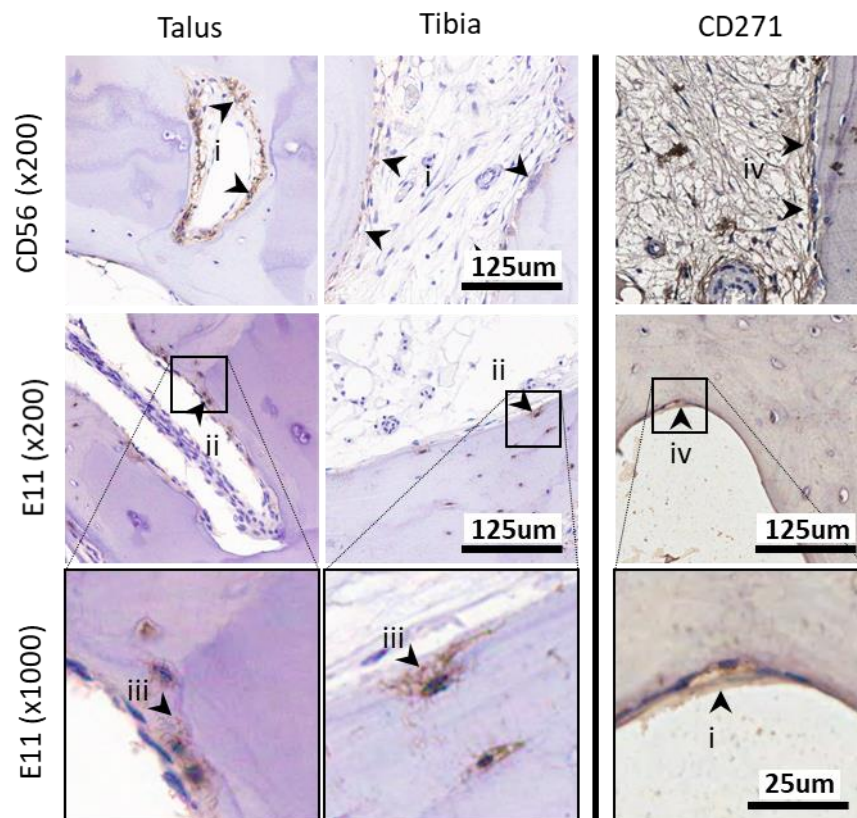


Figure 3.3.16 Investigation of Potential Cells Involved in New Bone Synthesis through CD56 and E11. Immunohistochemistry images of OA talar subchondral bone stained with CD56, a marker of osteoblast progenitors, and E11 a marker of early, embedding osteocytes⁹. i - CD56+ cells lining bone. ii - embedded E11+ cells. iii - Magnified images of E11 show immature, round morphology and disorganised processes of newly-formed osteocytes. iv - CD271+ cells lining bone as earlier shown (Fig. 3.3.10-11).

3.3.4. Developing Methods to Quantify Cartilage Quality in OA Talus and Distal Tibia

Work so far clearly demonstrated through a variety of methods that bone behaviour was significantly altered in OA, and that new bone formation and turnover was occurring more greatly in regions with damaged cartilage. Next, methods for investigating cartilage loss were developed to understand the changes in this tissue from a mechanical perspective. Due to the small size of OA samples, new methods were needed to be developed due to how thin the samples were. Custom-made Delrin plugs to bring overall depth up to around 8 mm, using porcine plugs to confirm that Delrin was a suitable material to compensate for this bone loss. It was additionally explored if indentation and needle indentation could both be performed on a single sample, to preserve rare tissues. As isolated tibial pins were too curved due to the structure of porcine tissue, only talar pins were used. Cartilage compression was performed first to test cartilage displacement over time. Uncut control samples showed the most variation in endpoint displacement, between 0.06 mm and 0.14 mm (Fig. 3.3.17A), which became less variable after samples were cut and indented again, being between 0.08 and 0.1, but not a large enough variance there would be any particular reason (Fig. 3.3.17B). There was up to a 40% difference in displacement between the first indentation, and the second indentation after trimming, but this was not significant (Fig. 3.3.17C).

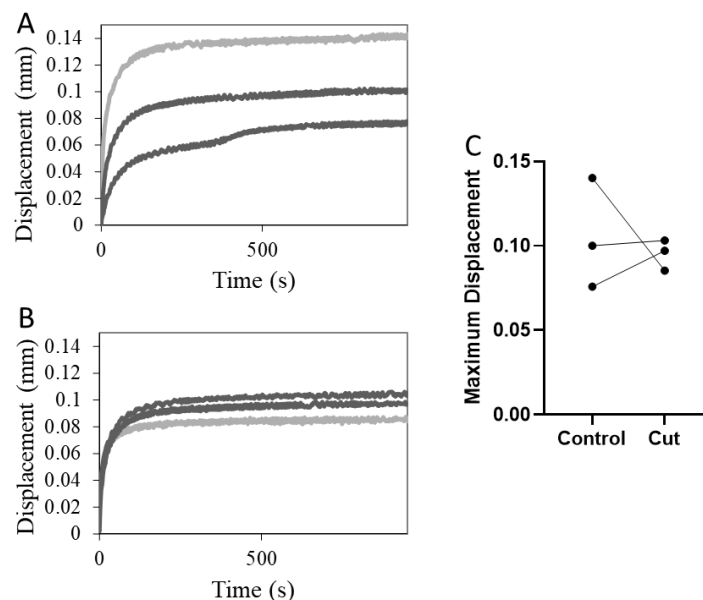


Figure 3.3.17 Assessment of Cartilage Displacement in Porcine Talar Samples with Minimal Bone. A Control sample displacement over time for N=3 samples. B Displacement over time for samples with bone under cartilage reduced to 2 mm. C Maximum Displacement, or cartilage resistance when all water has been pushed out, for bone samples with typical underlying bone (6cm) to those with minimal underlying bone (2 mm). In C, Lines represent paired samples.

Next, cartilage thickness was investigated. Samples from matched porcine tissue regions were tested after indentation (control), after cutting, addition of Delrin and indentation (cut), or just after 3-time freeze-thaw repeats. Whilst there was donor variation between samples, Delrin again seemed a suitable compensatory material for cartilage needle indentation with up to 30% variance between plugs, which is typical of neighbouring plugs in immature porcine tissue.

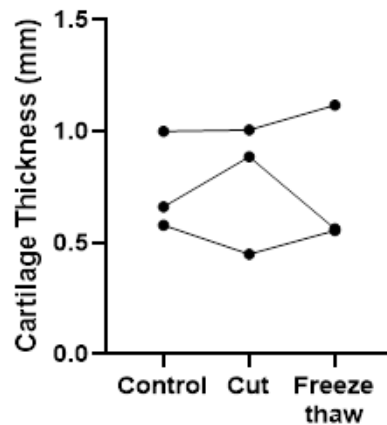


Figure 3.3.18 Assessment of Cartilage Thickness in Porcine Talar Samples with Minimal Bone. Control and freeze-thaw samples had a minimum of 5cm underlying bone, as typical in cartilage thickness studies (N=3). Cut samples were reduced to 2 mm bone using a scalpel before testing (N=3). Freeze-thaw samples underwent three rounds of freezing and thawing before testing. Samples were paired by using three plugs from neighbouring regions of the same talus as the method is destructive, represented by the lines.

3.4. Discussion

Many treatments of ankle OA, as well as osteochondral lesions of the talus, rely upon endogenous cells for repair, including microfracture and joint distraction, among others²⁴³. However, the quality and quantity of endogenous repair cells facilitating these treatments, including MSCs themselves, remains under-investigated.

In this chapter, it is shown for the first-time that MSCs identified by the CD271 marker concentrated in regions of cartilage damage and new bone formation, illustrating an aberrant repair attempt, as seen in other human joints or animal models of OA^{101,219,244}. This indicates that multipotential cells are present in OA, with potential to augment repair by enhancing cell homing, and somehow stimulating chondrogenesis for cartilage repair by resident cells, rather than injecting exogenous MSCs. By analysing both non-diseased and OA ankle tissues using 3D and 2D methods, this work confirms that bone changes in the ankle were similar to that in the inverted knee, with thickening of the SBP, and increased density of bone near the joint surface, with the talus matching changes to the femur, and distal tibia to the proximal tibia²²⁸.

mCT allowed an initial assessment of tissue structure, shape and size whilst also providing comparable data for both OA and health with other studies. Analysis of the mCT data for non-diseased specimens revealed that the SBP was thicker in tibia than the talus, and surprisingly the overall BV/TV trend was the opposite, with a higher talar BV/TV in non-diseased state than tibia. Depth-dependent BV/TV correlated inversely with distance from the SBP, with the highest BV/TV at the joint surface. Previous work has shown that cartilage in the talus and distal tibia have similar thickness and mechanical properties^{13,18}. Therefore, the main reason for this trend would appear to be the loading profile, with the convex talus directing force into the centre of the arch, whereas the concave tibia will have force over the whole SBP. In the knee, the convex femur has a thinner SBP, and the concave tibial plateau has a thicker SBP, showing the same trend²⁴⁵. As the shape of the bones converges force at the SBP or the centre of the arch, underlying bone mitigates less force, explaining this trend, and emphasising the role of biomechanical forces in normal bone structure of the ankle bones.

Comparing non-diseased to OA tissue, the SBP of the OA-affected talus was thicker than the tibia, opposite than in non-diseased specimens. SBP thickening is demonstrated in OA of both ankle and other joints, so the fact that the talus thickens more so than tibia is more likely to be due to local biomechanical differences, which may determine functional responses from endogenous cells including MSCs^{246,247}. Overall BV/TV did not change in OA, but depth-dependent analysis revealed higher BV/TV in the first 1 mm than non-diseased, and lower BV/TV

after 2 mm, more drastically in the talus than the tibia. Previous research shows BV/TV changes are both joint and depth specific. The hip demonstrates increases in overall BV/TV in OA, but like the present study the knee does not^{228,246}. Segmentation by depth showed BV/TV in the OA knee is always higher than non-diseased tissue, suggesting different biomechanical OA-mediated changes between knee and ankle^{228,248,249}. As explained earlier, this is likely due to the loading profile of the two talocrural bones relative to other joints⁵. Additionally, the talocrural joint is extremely congruent relative to other bones, which may also explain the differences in the ankle compared to the knee⁵. The present data demonstrates that ankle OA structural changes occur mostly at the joint surface. SBP thickness increased more-so in the talus, conversely BV/TV changes were greater in the tibia, suggesting different biomechanical adaptation to resist OA. It is possible that cartilage loss results in higher forces for the bone to mitigate, and so bone is synthesised at the naturally thinner SBP of the talus, whereas in the tibia as the plate is already thick, the relatively thinner bone just below will thicken. To address this hypothesis, this thesis presents initial optimisation work for identification of both cartilage thickness and biomechanical properties, which are discussed later in this Section.

Whilst 3D work showed overall bone changes, these did not allow direct comparison with cell behaviour, nor understanding of changes at the protein level. Histology is often undertaken in OA to link morphological changes with cell behaviour, as such informing future similar work of approximate decalcification time with this method would assist in research planning. This method avoids damage to cell surface markers utilised by immunohistochemistry, and use of X-ray was a non-destructive method to check for full decalcification without risking structural alteration. Decalcification rate relates to multiple properties of bone including bone mineralisation or density, however these results are mostly just advisory for future studies of the ankle requiring bone histology. As expected, as tibial samples were on average larger, they weighed more than talus. Interestingly decalcification of the talus was slower by mass, weight and size than tibia. Relating to mCT work, this may be due to the talar bone being more dense than tibial bones, as such it was more difficult for the calcium within the bone to be chelated by the EDTA. As whole bones took around 200 days to decalcify, future studies should either use bone plugs where possible to reduce size of samples, or alternatively to use methods without decalcification such as embedding in methyl methacrylate. This would additionally allow assessment of calcification through simple stains for new bone formation such as van Kossa or Movat's pentachrome²⁵⁰. Whilst this was attempted (Appendix 8.1), complications including length of methodology and scarcity of tissue meant that this could not be completed. For this work, whole bones were decalcified to allow comparison of areas of higher cartilage damage to areas of lower cartilage damage, to see how bone changes were related to overlying cartilage.

Whilst other, more rapid methods of decalcification exist, such as formic acid, increasing temperature or sample agitation, these are known to damage antigens such as CD271, which was critical to investigate resident MSCs for this work, as such were not considered^{202,251,252}.

The talus and tibia both had similar levels of typical OA damage, and presented typical hallmarks as found in the hip or knee, shown by both H&E staining and safranin O staining²²⁶. It appears there is minimal visible differences between ankle joint OA and that of other joints. The samples in this study were not reported for if they were post-traumatic or primary OA, so this could not be directly assessed. There is currently minimal work on the histology of talocrural tissues, with the majority of work completed by Li on cadaveric talar bone²⁰⁵. In this study, the worst damaged region of samples presented 46% minor osteoarthritic damage, and only 7% end stage damage. They identified a key damage marker termed a 'tram-track lesion', where osteophytes on the distal tibia created grooves on the cartilage surface. This was only found on 12 of 105 samples, so it is not unsurprising that they were not observed in our samples²⁰⁵. As such, whilst the present work suggests that ankle OA appears similar to that of other joints, a larger sample number or more complete sample analysis is needed to shed light on potential differences.

OARSI scores applied on Safranin O stains to investigate if the level of cartilage damage was similar, or were on one bone. Scores for cartilage damage between both the talus and tibia were similar, although slightly higher in the talus, akin to that of similar research⁷. As both bones interact during normal movement, it makes sense that if one side was damaged, this would increase shear forces on cartilage of the opposing bone and lead to both bones being similarly damaged. Curiously, BA/TA was significantly correlated with OARSI grade in tibia, but not in talus. As the talus had 2-fold higher BA/TA in grade 3 tissue than tibia (Fig. 4D), this may mean the talus resists increases due to a 'bone density limit', with bone density rarely going above 60%. In previous research of the OA knee, the highest medial condyle BA/TA was 60% higher than the OA lateral condyle, similar to the upper range of the talus in this study²¹⁹. As shown by mCT in the present study, SBP thickness was higher in OA tissue than non-diseased, and BA/TA increased most in the first millimetre from the SBP. The SBP appears to compensate for cartilage destruction, focusing forces at the joint surface. Micro-cracks in the SBP due to OA may also be enabling factors in synovial fluid and cartilage to reach bone. This cross-talk may be compounding thickening of the bone further at superficial regions, on top of biomechanical stimuli^{253,254}. Cartilage is mostly utilised to resist shear forces in the joint, as such when there is damage to one side, this will increase the shear force absorbed by the other side, particularly in the case of bone being exposed. Cartilage damage is likely to remain the same. However, as bone showed different damage responses, this is likely due to the differences in non-diseased

bone structure observed by mCT, and the difference direction forces are absorbed through as earlier discussed.

Bone turnover is largely performed by osteoblasts, which synthesise bone, osteocytes, which are embedded osteocytes which detect mechanosensory signals and allow signalling in bone through their projects, and osteoclasts, which break down mineralised bone. As MSCs are a major osteoblast cell progenitor, as well as having already been implicated in the OA process, these were chosen for investigation²⁵⁵. As a marker of bone-resident MSCs, CD271 has previously been used to look at changes in MSC localisation in OA^{256,257}. In this study, talus showed slightly higher overall CD271 staining than tibia, potentially correlating with the increased SBP thickening in talus. Similar to BV/TV changes, significantly more CD271+ MSCs were found within the first millimetre from the SBP compared to the next two millimetres in both bones. Additionally, CD271 area increased with OARSI damage grade particularly in the tibia consistent with greater BV/TV rise in response to cartilage damages in the tibia compared to talus. As such it appears MSCs are involved in bone synthesis, with picosirius red showing where new immature collagen synthesis was occurring in thickened bone, indicating new bone formation. Other methods such as PCR or undecalcified resin histology could have been used to prove this, however the lack of samples meant other experiments were prioritised. Progressive bone formation in talocrural subchondral bone was also evident by estimated co-localisation of CD56+ osteoblast progenitors, cuboid osteoblasts and early E11+ osteocytes which were observed in similar bone-lining regions^{220,234,258}. Additionally, TRAP staining also showed osteoclast localisation within sclerotic tissue. As such, *in vivo* it appears MSCs may be key drivers of OA bone sclerosis, and correcting their behaviour may slow or prevent OA progression. Gene expression profiling of uncultured talocrural MSCs, as performed using knee MSCs from more and less-damaged regions²¹⁹, would be necessary to confirm these observed differences such as increased expression of genes for osteogenesis and resorption as future work, as well as specific stains for osteoblasts such as ALP histology or osterix IHC²⁵⁹.

PCR can assess gene expression of isolated cells to detect upregulation of genes which would indicate new bone formation, such as ALPL, RUX2, SPARC or E11²²⁰. However, the process to perform this is complex and expensive, including fluorescent assisted cell sorting (FACS) of freshly digested bone, which would firstly be full of debris, and secondly require a large cell count which may not have been possible with the low cell count seen in ankle samples⁸⁵. Alternatively, using undecalcified resin histology would allow assessment of mineralisation and new bone formation as earlier discussed, through Movat's pentachrome stain. Again,

undecalcified histology could not be performed due to the complexity of reoptimizing the process and the time frame.

Lastly, experiments into the mechanical properties of cartilage in the ankle were attempted. This was originally planned to allow design of mechanical testing of the OA human samples, as the very small amount of bone retrieved from surgery was not comparable to that used for normal experiments. As such, the ability of Delrin to mitigate the small geometry, a material with similar mechanical properties to bone, was examined²⁶⁰. Briefly this work showed that Delrin appeared to act as a suitable compensatory material to allow accurate assessment of cartilage properties in porcine tissue, compared to porcine tibial and talar bone. The next stage was to run the values received through a MATLAB model to estimate an aggregate modulus and permeability at which matches the results for cartilage thickness and deformation seen, and then to repeat the experiment in non-diseased human tissue once porcine tissue had proven the method accurate. Overall this method could be used in future, as Delrin allowed suitable testing of tissue.

This chapter is also limited by small numbers of ankle OA patients and the amount of tissue that could be removed during surgery, which aimed to minimise harm to the patient. Ideally, samples would have been better age matched, however due to rarity of samples this was not possible. On a similar note, ideally there would be a similar gender split between techniques. Whilst it is known that bone changes are often different between men and women, again, the rarity of these samples made this not possible.

To logically design treatments to reverse or slow down OA progression, first we need to understand disease progression, and why natural repair processes are failing. This chapter identifies that CD271+ cells are indeed present in the talus and tibia, and increased abundance in OA. This highlights that while different biomechanical environments lead to different bone changes in OA between the talus and tibia, OA progression remains similar to that seen in other joints. As these native tissue changes have not yet been explored in ankle compared to other joints, the biomechanical differences, such as higher BV/TV increases in tibia, and strong CD271+ response to OA may be a driving force of different regenerative treatment outcomes in the talocrural talus and tibia compared to other joints such as the hip^{155,211,261}. However, the different bone responses in tibia compared to talus suggests that treatments will need to be tailored to each bone.

Overall, this chapter has shown by immunohistochemistry that in OA CD271+ cells associate near the SBP, and accumulate with tissue damage. As these MSCs localise predominantly to the joint surface, it is possible that the current technique of drilling until there is a release of fat from the

bone is too deep. This could inform other treatments such as nano-fracture, reducing the penetration depth but keeping the benefits of lessened tissue damage⁸⁴. Furthermore, focusing on new methods of MSC stimulation to form hyaline cartilage formation over bone synthesis are needed, which will be explored in the next chapter. This chapter also shows that future work should focus on the modulation of biomechanical environments in different bones in the ankle joint in order to create a growth environment facilitating repair specific to the changes in each joint. Some success in this area has been already achieved with ankle joint distraction, with up to 91% good outcomes in a study of 249 patients after 2 years^{84,161,262}. Between talus and tibia, it has been shown that joint distraction led to a greater reduction in bone density in the tibia compared to talus, with a 23% loss in density in tibia compared to 18% in talus at 1 year, matching the results from BA/TA measurements¹⁷¹. Combining both biological and mechanical stimulation to direct MSC repair behaviour towards cartilage formation, and predicting how cells respond to a variety of biological and mechanical environments, may lead to new joint-preserving treatments and avoid major surgical interventions. As such, the next Section of this work moves on to investigate the properties of these resident cells in standard MSC culture conditions, to see if this lineage commitment to bone affects their chondrogenic capability.

4. Chapter 4 In vitro Characterisation Talocrural Joint Mesenchymal Stem Cells

4.1. Introduction: The Need for an Endogenous Repair Source

Local, joint-resident MSCs are implicated in treatments (Section 1.3) of osteochondral lesions as the major regenerative cell within the joint, however their behaviour is poorly understood within the ankle compared to other joints like hip and knee ²¹². As MSCs are unlikely to be transported by blood^{213,214}, the subchondral bone, synovial fluid or synovium are considered to be the main MSC tissue sources within joints²¹⁵. In the previous chapter, it was shown that in ankle OA, CD271+ MSCs are located in the bone, and were associated with bone changes, which included subchondral bone plate thickening, increases in BA/TA near the joint surface with downstream effects resulting in thinner bone beneath, and CD271+ association with osteocytes and TRAP staining. Picrosirius red staining showed that collagen within the bone had yet to remodel and remained immature. The evidence suggests that despite MSCs correlating with

regions of cartilage damage, showing there is an attempted reparative response, they are creating sclerotic bone, perpetuating the OA pathology. To develop methods of repairing cartilage, MSC presence in ankle OA bone needed to be proven, and their differentiation properties investigated, to determine if intrinsic MSCs are able to repair cartilage, or if there is a bone-specific behaviour. Whilst MSCs have been isolated from the synovial fluid of ankle OA patients, MSC presence in talocrural subchondral bone, from which reparative cells released by microfracture would come from, remains unexplored⁹⁶. This study was the first to investigate resident subchondral bone MSC topography from OA distal tibia and talus and relationships to OA changes, and this chapter will investigate differences in differentiation capacity between talus and distal tibia in ankle OA patients, in comparison to non-diseased IC controls. A clear understanding of resident MSCs behaviour, and how tissue damage affects their function, from both biological and mechanical standpoints, is of major importance for the development of novel regenerative medicine strategies to treat ankle OA or osteochondral lesions²¹⁶.

Current regenerative therapies, as earlier described, include microfracture, osteochondral autologous transfer, joint distraction and juvenile cartilage allografts (Section 1.5). The literature cites that they recruit endogenous cells and factors to regenerate the surrounding tissue, only some directly cite cells such as MSCs and do not point out any specific targets, other than certain proteins such as fibrin^{155,156,243}. As aforementioned some papers do hypothesize MSC for repair, or utilise MSCs within scaffolds, as such it is well known they may exist within the tissue and hold the ability for chondral repair²¹⁵. However, even if exogenous MSCs are being injected, it is likely that any new scaffolds will interact with the endogenous cells²⁶³. This is particularly true as fibrin is typically used to cement the scaffolds in place, which has strong homing capabilities for resident MSCs^{186,264-266}. As such it is important to investigate the resident BONE MARROW MSC behaviour.

Isolation of MSCs requires first identification that isolated cells are indeed MSCs. Whilst CD271+ is regularly used to identify *in vivo* MSCs of bone and skeletal muscle, most of the literature utilises *in vitro* MSCs which lose surface expression of CD271 upon culture expansion^{72,85,101,215,267-269}. Therefore, there needs to be standardised *in vitro* testing to prove that these cells meet standardised criteria of MSCs. For this, the ISCT panel for *in vitro* MSCs is used⁹¹. This is a panel of cell-surface markers which identify and exclude any haematopoietic-lineage markers, but includes positive markers expressed on all MSCs. This includes CD14, CD19, CD45 and HLA-DR as negative markers, and CD73, CD90 and CD105 as positive markers⁹¹. This is run on passage 2 MSCs for expression of these markers, and consistency between research.⁹¹ CD14 marks for monocytes and macrophages, CD19 identifies B cells, CD45 is expressed on pan-leukocytes and HLA-DR is an immune response protein not expressed on MSCs unless stimulated

by immunomodulatory factors such as interferon- γ ⁹¹. CD73 identifies ecto 5' nucleotidase, which catalyses 5' mononucleotides into nucleosides, CD90 is Thy-1, a glycoprotein involved in cell adhesion and CD105 is endoglin, a transmembrane protein involved in the TGF- β receptor complex²⁷⁰⁻²⁷². Additional requirements of the ISCT definition for MSCs is plastic adherence, as well as successful differentiation into cartilage, bone and fat, termed chondrogenesis, osteogenesis and adipogenesis respectively. A confounding factor is some groups report successful MSC isolation with low or negative for expression of CD73, however this is usually only a proportion of cells²⁷³. Additionally, the level of differentiation is not always ubiquitous, as it is usually affected by donor age or tissue source²⁷⁴. As such it is essential that MSCs should be isolated and characterised from the specific tissue site being treated and to see if they are suitable for endogenous treatments, or if they will negatively impact exogenous cell injections. The ISCT panel for MSC identification is a standardised process simply for identification, and does not aim to qualify their behaviour in any way. As such further work into comparative behaviour should be used, such as comparison to iliac crest (IC) MSCs has become standard within our group^{219,220}.

MSCs have previously been isolated from the synovial fluid from patients with osteochondral lesions of the talus, but not full OA, by Kim *et al.*. Synovial MSCs are cited for their improved ability for chondrogenesis⁹⁵. These were all assessed by the ISCT panel, however were not assessed for differences in MSC differentiation capacity compared to other sources. The Authors showed plastic adherence, multi-lineage differentiation and typical surface protein expression of MSCs, proving their existence in synovial fluid of the talocrural joint with osteochondral lesions⁹⁶. However, there is no literature investigating MSC presence in talar or tibial subchondral bone.

At the time of writing, the only group to attempt ankle bone MSC isolation is Li *et al.*, who performed bone marrow aspiration from the calcaneus of healthy patients²⁷⁵. These isolated cells again presented typical MSC phenotype, however, were not compared to other sources. Firstly, the calcaneus is a different bone from talus and distal tibia, which are more frequently targeted by microfracture. Secondly, without quantification or qualification of differentiation, understanding their ability for endogenous repair is less understood, and cannot be linked to why microfracture appears more successful in the ankle than elsewhere. This still means there is critical need to better understand MSCs in the talus and tibia, as regular sites for microfracture and other MSC-reliant treatments.

In OA, the bone-resident environment is radically changed as shown in the previous chapter. In the hip, it has been shown that there is an increase in clonogenicity, matched with a reduction in capacity for differentiation into all three lineages, as well as other studies showing a pre-

disposition to bone formation^{85,101,220,267}. The first study also further described the loss of leptin receptor (LepR) and CD73, which may describe exhaustion of these MSCs, which may potentially be a reason for why regenerative therapies such as microfracture fail²⁶⁷. LepR is considered important for differentiation into fat and cartilage but mostly bone, and is associated with younger cells which are quiescent until injury induces their proliferation²⁷⁶. Comparatively, CD73 is thought to be associated with the immunomodulatory effect of MSCs, and in mouse was found that MSCs with lower CD73 were less able to repair tissue after myocardial infarction than those high in CD73²⁷⁷. As such, this rapid MSC growth as well as heightened osteogenic differentiation attempting to repair the wound may simply be exacerbating the disease, as concluded in the previous chapter. As ankle OA presents with younger donors than hip or knee, there is potential that resident MSCs will retain stronger differentiation properties leading to the improved outcomes seen in ankle OA regenerative treatments. As such, it is essential that the characteristics of resident MSCs is investigated. Knowing if resident MSCs present, and if they capable of chondrogenic repair as well as likely drivers of sclerosis is critical to being able to better develop treatments which target endogenous repair, which this chapter aims to investigate.

Specifically, this chapter will:

- Isolate plastic adherent, culture expandable cells from OA talus and distal tibia to compare with an IC control
- Identify if MSCs are present within these bones
- Investigate their differentiation properties relative to each other and a healthy IC control

Objectives:

- Enzymatically extract cells from talus, tibia and IC using collagenase for culture

- Test plastic adherence, cell surface marker expression and differentiation capacities in line with the ISCT minimal criteria for MSCs to prove MSC presence in the BM of talus and tibia
- Compare chondrogenic, osteogenic and adipogenic differentiation using standardised methods between talus, tibia and IC to investigate if different sites have different specific MSC capacities for repair

4.2. Methods

4.2.1. Relevant Sample Information (IC and ankle)

For these experiments, 3 ankle OA patients were used, and IC bone from 3 donors was obtained from patients undergoing orthopaedic surgery for metal removal following previous fracture, who were otherwise healthy (ages 32, 38 and 42, 2 male, 1 female). Samples were placed immediately into saline post-surgery and transferred to the laboratory. Ankle OA samples utilised in this chapter are listed in Table 4.2.1 and IC in Table 4.2.2.

Table 4.1 Distal Tibia and Talus Sample Characteristics Retrieved from Ankle Fusion

Sample ID	Experimental Use	Donor Age (Years)	Donor Sex
WJ011	MSC Isolation	58	F
WJ012	MSC Isolation	34	F
WJ013	MSC Isolation	66	M
<i>Averages</i>	<i>N/A</i>	<i>52.7</i>	<i>66% Female 33% Male</i>

Table 4.2 Fresh IC Sample Characteristics

Sample ID	Experimental Use	Donor Age	Donor Gender
ICC1	MSC Isolation	32	M
ICC2	MSC Isolation	42	F
ICC3	MSC Isolation	41	M
<i>Averages</i>	<i>N/A</i>	<i>38</i>	<i>66% Male, 33% Female</i>

4.2.2. MSC Isolation

Details on the MSC extraction process are given in Section 2.3.2. Non-diseased human ankles could not have cells extracted as freezing of tissue made them unsuitable for downstream analyses.

4.2.3. Measuring Egression of Cells from Digested Bone

In order to ensure that all cells were successfully being retrieved from digested bone, bone remnants after digestion were taken and placed into a round 300 mm tissue culture dish with DMEM with 10% FCS in order to see if MSCs would migrate from bone and adhere to the plastic dish. This method was developed for this work. Cultures were grown for 3 weeks with images taken every day to investigate cell movement.

4.2.4. Colony Forming Unit Fibroblast Assay

To estimate MSC number and cell fractions within isolated talar, distal tibia and IC, Colony Forming Units-Fibroblast Assay (CFU-F) was performed according to standard methods²⁷⁸. For talus and tibia, freshly isolated cells (Section 2.3.2) were seeded at densities of 2.5×10^3 , 5×10^3 or 1×10^4 per dish, in triplicate, in 60 mm culture dishes, in 2 ml StemMACS expansion media supplemented with 1% P/S. For IC due to no availability of 60 mm culture dishes, 100 mm dishes were used instead and cells seeded at 5×10^3 , 1×10^4 or 2×10^4 , and 3 ml of media or PBS used for subsequent steps. After two days to allow cells to adhere, media was removed and cells washed with two changes of 2 ml dPBS to remove remaining debris, and 2 ml StemMACS added. Cells were cultured for two weeks, with media half-changes twice a week. After 14 days, culture medium was removed, cells washed with two changes of with 2 ml dPBS, and then fixed with 2 ml 3.7% formaldehyde for 30 minutes. After this, formaldehyde was removed, and cells were washed again with 2 ml dPBS before staining with methylene blue for 45 minutes. The plate was then repeatedly washed with dH₂O until wash dH₂O was left clear, and then plates left to dry for 24 hours. Plates were then scanned using a plate reader at 1200 dpi. Colonies of approximately 50 cells (visible under microscope) or more were then counted manually within ImageJ from the scans, under the assumption that each colony would have been started by 1 MSC, thus can assess MSCs per seeded number of isolated cells. As such, MSC count per given cell number was calculated by seeded cells divided by colony count. Talus, tibia and IC results were manually

adjusted to account for size differences of plates on given graphs by multiplying talar and tibial results by 2.

4.2.5. Area and Density Analysis of CFU-F Colonies

To assess colony size and integrated density, which have been linked with changes in MSC behaviour, scans from the CFU-F assay (Section 4.2.3) were imported into ImageJ, according to standard practice²⁷⁹. To do so, scale was applied using the ImageJ function, and images were then converted to grayscale. A threshold was then applied, and the area of the dish was selected using the draw function to exclude anything outside of the dish. The 'analyse particles' function was then used to assess each individual colony for colony area and integrated density. The 'draw outlines' option was used to ensure only colonies of 50 cells or more were selected, and that the macro was effective on each image, which allowed manual adjustment if not.

4.2.6. Growth Rate Analysis

To assess differences in MSC growth rate between donors and bone origin, the date of seeding and trypsinization of cells was recorded, as well as cells seeded and cells retrieved after trypsinization, in order to calculate population doubling (PD) rate as according to previous work and standard practice²⁸⁰. First, PD was calculated for each passage as according to Equation 4.2.1, dividing the cell number counted at the end after trypsinization by the original cell number seeded. Next, for cumulative PD, the PD of the first passage was taken, and the next PD added on, and the next added on and so forth, to measure total PD over time. For the passage of fresh cells, the number of fresh cells seeded was multiplied by the MSC% of all isolated cells found by CFUF, to calculate MSCs seeded, and then final cell count divided by that. To calculate days per population doubling, PD was divided by the days that culture was grown for to reach confluency and be trypsinized (Equation 4.2.2).

$$PD = \log_2\left(\frac{\text{Final Trypsinised Cell Number}}{\text{Seeded Cell Number}}\right) \quad \text{Days per PD} = \frac{\text{Days in Culture}}{\text{Population Doublings}}$$

Equation 4.2.1 Population Doubling Calculation **Equation 4.2.2** Days per Population Doubling

4.2.7. Flow Cytometry for cultured MSCs

Human MSCs cultured *in vitro* are known to express a specific surface antigen combination that allows them to be differentiated from other cells, in accordance with the ISCT definition, the gold standard for MSC identification⁹¹. These surface antigens (or molecules or markers) can be identified by specific monoclonal antibodies with a fluorophore attached, and categorised

according to the colours emitted by the fluorophore after excitation by laser. Flow cytometry of cell cultures were performed once these cultures had reached confluence at passage 2 (Section 2.4.1).

4.2.7.1. Antibody Staining of MSCs

Cultured cells were trypsinized and counted (Sections 2.4.3, 2.4.2), then centrifuged at 500 g for 10 minutes. Cells pellets were next re-suspended in sterile PBS and 200,000 cells were each placed into FACS tubes. These were centrifuged again at 500 g for 5 minutes, the supernatant was discarded then the antibodies/isotype controls as described in Table 4.2.6.1 were added to the cell pellets.

Cells with antibody or isotype cocktails were left to stain for 15 minutes in a dark fridge at 4°C. Cells were then re-suspended within 400µl of FACS buffer before further centrifugation at 300 g for 5 minutes. The supernatant was discarded, and the pellet was again suspended in 300µl FACS buffer and placed on ice to be taken for data acquisition using flow cytometry.

Spectral compensation was performed using results from single antibody only tubes (2-5). This prevents fluorescence of other fluorescent channels from providing false-positive results, such as if FITC leached in the PE channel or vice versa. Isotype controls were used to confirm there was no false positive staining due to non-specific antibody binding, as well as to confirm correct region boundaries of cell gating. As antibodies bind non-specifically to Fc receptors, isotype controls confirm that binding was elevated in the sample due to specific binding of the target surface antigen. An isotype control is formed of the same antibody type, but cannot target the surface antigen. Laser voltage optimised using the non-stained tube (tube 1).

Table 4.3 Flow Cytometry Antibody Details

No.	Tube Contents	Antibody/Isotype Control	Fluorochrome	Volume
1	Non-Stained Control	None	Non-Stained	N/A
2	Single Antibody controls	CD73	PE Only	10 μ l
3		CD105	FITC Only	10 μ l
4		CD90	PerCP-Vio Only	2 μ l
5		CD34, CD14, HLA-DR, CD19, CD45 Cocktail	VioGreen Only	2 μ l each
		PE Ig Isotype	Isotype IgG1 PE	10 μ l
6	Isotype Controls	FITC Ig Isotype	Isotype IgG1 FITC	10 μ l
		VioGreen Ig Isotype	Isotype IgG1 VioGreen	2 μ l
		PerCP-Vio Ig Isotype	Isotype IgG1 PerCP-Vio	2 μ l
		CD14 (Negative)	Viogreen	2 μ l
	CD19 (Negative)	Viogreen	2 μ l	
	CD34 (Negative)	Viogreen	2 μ l	
	CD45 (Negative)	Viogreen	2 μ l	
7	ISCT Markers	HLA-DR (Negative)	Viogreen	2 μ l
		CD73 (Positive)	PE	10 μ l
		CD90 (Positive)	PerCP-Vio	10 μ l
		CD105 (Positive)	FITC	10 μ l

The non-stained and single antibody controls (1-5) tubes were only run for the first sample for adjusting flow cytometer laser settings and spectral compensation

4.2.7.2. Data Acquisition

Attune Cytometric Software v2.1.0 (Invitrogen) was used to collect and analyse the flow cytometry data. For each sample, flow cytometry was run until 10,000 events were captured, after debris was excluded. Gates were first set on Forward Scatter (FSC) and Side Scatter (SSC) dot plots to define the total cells without debris. FSC detects the size of events and SSC the granularity of events to be determined, allowing living cellular events to be differentiated from debris, and is typical for identifying living cells²⁸¹. The histograms were next drawn upon cellular events to determine the expression of a marker. Overlay histograms of each marker and its isotype control e.g. CD73 PE and isotype PE control were used to determine positive expression of a marker on cell populations. The gates were set on these histograms (based on isotype control) to determine the percentage of cells which were positive for CD73, CD90 and CD105, and negative for hematopoietic lineage markers CD14, CD19, CD34, CD45 and HLA-DR, which define cultured MSCs as according to the ISCT panel shown in table 4.2.6.1⁹¹. Quadrant gates were used upon dot plots to confirm co-expression of positive markers on single cell population according to the ISCT panel of cultured MSCs, to ensure events were not of single expression.

4.2.8. Osteogenic Differentiation

4.2.8.1. Osteogenic Induction

In order to osteogenically differentiate cells, 1×10^4 passage 3 cultured MSCs were trypsinized and seeded (Sections 2.5.1-2.5.3) per well in a 12 well plate in StemMACS™ OsteoDIFF media (medium with components which direct MSC to differentiate towards osteogenesis) or StemMACS™ MSC Expansion Media (Human) (encourages MSC proliferation whilst preventing MSC differentiation(SM)) as a negative (expansion) control, and cultured for either 14 days before testing for alkaline phosphatase, or 21 days for Alizarin red, Calcium Deposition and DNA measurements. These methods are standard practice for ISCT MSC identification^{101,182,203}. Each group was performed in triplicate. Media was half-changed twice a week, with images taken routinely during culture, including just before staining (Section 2.8.3). Any PBS used in this Section was calcium-free.

4.2.8.2. Alkaline Phosphatase Assay

Alkaline Phosphatase (ALP) is an enzyme thought to be found in osteogenic cell progenitors, but has also been suggested as a marker of differentiation capability^{282,283}. ALP hydrolyses the naphthol, which couples to the diazonium salt to stain the ALP-expressing cells blue²⁸⁴. Following 14 days, media was removed and samples were washed twice with 5 ml dPBS, and then fixed using 2 ml of 2:3 citrate:acetone for 30 seconds. Samples were then washed twice more with 5 ml dPBS. Fast blue mix was then added to the plate, and the plate covered in foil and left to stain

for 1 hour at room temperature in the dark. Wells were then washed twice with 5 ml dPBS. Images were taken under EVOS microscope (Section 2.7.3) and also scanned at 1400 dpi (Section 2.7.3).

4.2.8.3. Alizarin Red Staining

Alizarin red binds calcium to form a lake pigment, staining deposited calcium red, proving that MSCs have undergone functional osteogenic differentiation²⁸⁴. At 21 days, wells had media removed and were washed twice with PBS. Cells were fixed using 70% ethanol (cooled to -20°C) for 1 hour. Once fixed, cells were washed once with PBS. These were then stained with pH 4 Alizarin red for 10 minutes at room temperature, and then rinsed three times in PBS. Images were then taken under EVOS microscope as well as plates scanned at 1400 dpi (Section 2.7.3).

4.2.8.4. Calcium Deposition Quantification

Calcium quantification allows direct comparison between MSCs and their propensity for osteogenic differentiation, but only in terms of calcium deposition. After 21 days, plates were removed from culture, media removed and washed twice with PBS. To each well, 300 µl of 0.5 M hydrochloric acid was added for 5 minutes at room temperature to extract calcium deposited by cells. A cell scraper was then used to detach remaining cells from the plate, and then the solution collected and transferred to a 1.5 ml tube and mixed at 4°C on a shaker for 4 hours. This solution was centrifuged for 250 g for 5 minutes to remove debris. Supernatant was then transferred to a fresh Eppendorf and stored at -20°C.

Calcium was then measured using a Calcium Colorimetric Assay Kit according to manufacturers' instructions. From 500mM Calcium Standard Solution, a 5 mM calcium standard solution was prepared by diluting with calcium-free PBS. Standard concentrations of 0, 0.4, 0.8, 1.2, 1.6 and 2.0 µg calcium per well were prepared from this standard solution and calcium-free PBS. Sample test wells were prepared in duplicate per sample, with 50 µL of sample solution per well. To every well, 90 µl of chromogenic agent, 0-cresolphtalein, was added and gently mixed, and then 60 µl of calcium assay buffer was also added. Calcium binds the 0-cresolphtalein, creating a complex which absorbs at a wavelength of 575nm²⁸⁵. This was protected from light by wrapping in tin foil, and then left for 10 minutes at room temperature. The well-plate was then taken to the plate reader, and absorbance measured at 575nm. All wells had the background subtracted by removing the result from the blank well, and a standard curve was created from the standard concentration wells. To calculate calcium concentration for each sample, the calcium concentration was divided by 50 to get calcium per microlitre.

4.2.8.5. Isolation and Measurements

As a rough estimate of cell number per well for each donor, DNA was isolated to allow comparison of osteogenesis relative to cell number. For this, media was removed and samples were washed twice with PBS. To each well 500 μ L of triton buffer was added, and then a pipette was used to detach cells and debris from the well. The solution was then pipetted into a 1.5 ml tube, and then freeze thawed at -20°C and then room temperature three times, for 5 minutes per freeze. Once thawed again, the sample was centrifuged at 300 g for 5 minutes, and the supernatant taken to be measured. DNA was then measured by using the Nanodrop, to detect double-stranded DNA, using triton buffer as the blank (Section 2.5.1).

4.2.9. Chondrogenic Differentiation

4.2.9.1. Chondrogenic Induction

For chondrogenic cultures, with 6 repeats per donor, passage 3 cells were trypsinized, neutralised with DMEM with 10% FCS and counted (Sections 2.5.1-2.5.3). Cells were pelleted by centrifuging for 300 g for 10 minutes, and then resuspended in 0.5 ml DMEM. In quadruplicate, 2.5×10^5 MSCs were added to sterile screw-top tubes. These were then centrifuged at 500 g for 5 minutes to re-pellet the cells, the supernatant removed, and then cells resuspended in either 0.5 ml StemMACS™ ChondroDIFF media (to encourage MSC differentiation into chondrogenic cell lineages), or SM as a negative (expansion) control. Cells were again pelleted by centrifuging at 500 g for 5 minutes. Leaving the cells in a pellet, the screw tops of tubes were loosened by a half-turn to allow gas-exchange, then placed into incubation at the same conditions as cell culture (Section 2.4.6). Media was half-changed twice per week being careful not to disturb pellets. After 21 days, pellets were removed from culture, and then washed twice in PBS and images of each pellet taken alongside a ruler, before being used for either toluidine blue staining or GAG assay. These methods are standard practice for ISCT MSC identification⁷².

4.2.9.2. Measuring Pellet Diameter

From images captured, pellet diameter was calculated to determine pellet growth, which is an indirect measure of chondrogenesis. Images were loaded into ImageJ, and the ruler in pellet images used to apply a scale within the program using the 'set scale' function. Next, the line tool was used to draw the pellet diameter, in the thinnest region of the pellet as they are not truly spherical. This distance was then measured⁹⁴.

4.2.9.3. Glycosaminoglycan Assay

To quantify differences in chondrogenesis, sGAG created per pellet was measured. To each pellet, 100 μ l papain buffer was added and lids were securely tightened. This was left for 24

hours at 65°C in order to digest proteins. Contents were then thoroughly mixed, and then centrifuged at 2500 g for 5 minutes and frozen at -20°C including the supernatant.

GAG assay was then performed using the Blyscan sulphated glycosaminoglycan assay kit. This kit utilises the dye 1,9-dimethyl-methylene blue, which has an innate dark blue colour. This cationic dye specifically binds sulphated GAGs (sGAGs), and in the process of this stain, samples are placed in excess dye for maximal binding, excess dye removed, and then a dissociation reagent used to release any dye bound. This dye can be measured by absorbance between 625-675nm to measure how much dye was released in comparisons to standards²⁸⁶. In tubes, standards of 0, 2, 3, 4 and 5 µg were created from the reference standard of 100 µg/ml of bovine tracheal chondroitin-4-sulphate, diluted in dH₂O. For test wells, 10 µl of test sample was used, and made up to 100 µl using dH₂O. Both samples and standards were run in duplicates. To each tube, 1 ml of Blyscan reagent was added, and then tubes were left on a mechanical shaker at room temperature for 30 minutes. After this, samples were centrifuged at 14000 g for 10 minutes. Excess dye was removed by tapping open tubes upside down onto tissue paper, in order to avoid the pellet being disturbed. Then, 0.5 ml of dissociation reagent was added to each tube to release dye into solution, and roughly vortexed until dissolved. These were then centrifuged for 5 minutes at 14000 g to remove bubbles. To a 96 well plate, 200 µl of standards or test samples were added per well. The plate was then run through a plate reader to test for absorbance at 656nm. To calculate GAG content, a standard curve was calculated, and the equation of the line used to establish GAG content per well. To estimate GAG produced per pellet, this was multiplied by the dilution factor to attain GAG per 100 µl, the same of buffer the pellet was dissolved in.

4.2.10. Adipogenic Differentiation

4.2.10.1. Adipogenesis Induction

For adipogenic differentiation, passage 3 cells were trypsinized, neutralised with DMEM with 10% FCS and counted before being centrifuged at 300 g for 10 minutes. Supernatant was removed, and MSCs were resuspended in 0.5 ml of DMEM 10% FCS. In triplicate per experiment, cultures to be tested for Nile Red/DAPI staining were plated at 4×10^4 MSCs per well in a 48-well plate, and made up to 0.5 ml with StemMACS™ AdipoDIFF media (to encourage MSC differentiation into adipogenic lineages), or StemMACS for expansion (negative) controls. For Oil Red cultures, 5×10^4 MSCs were added per well to a 24-well plate, and made up to 1 ml with AdipoDIFF media, or StemMACS for expansion (negative) controls. For both Nile Red and Oil Red experiments, cells were cultured for 21 days, with a half media change twice per week. Media was then removed from wells and carefully washed twice in PBS. Prior to staining, images were

captured under EVOS microscope(Section 2.7.3) and then samples stained as described below (Section 4.2.9.2-4.9.3). These methods are standard practice for ISCT MSC identification.

4.2.10.2. Nile Red/DAPI Staining

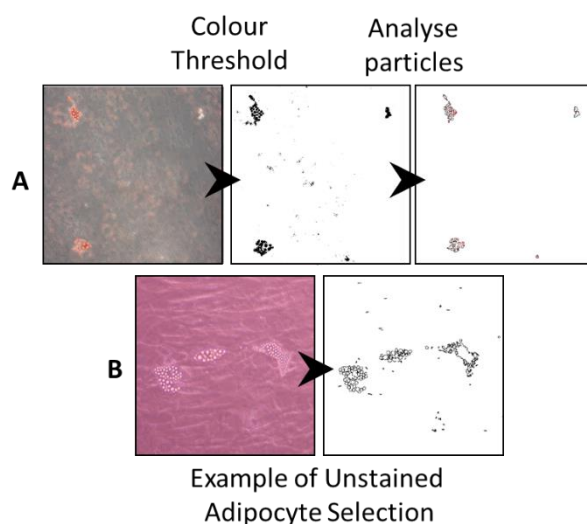
PBS was removed from wells, and 10% formalin added to each well for 30 minutes to fix cells. A 0.2% solution of Saponin was created, and then Nile Red and DAPI added to a working concentration of 1µg/ml. Formalin was removed from the wells, and then the wells were washed twice in PBS. A background read was performed by adding 200 µl of PBS and then reading on the plate reader at 335nm for DAPI and 485nm for Nile Red. PBS was removed and 200 µl of 0.2% saponin 1µg/ml DAPI/Nile Red was added per well for 15 minutes in the dark under foil, after which the solution was removed and the wells washed with PBS. This was again taken to the plate reader, and read at the same wavelengths as before. Following this, fluorescent images were taken under EVOS microscope.

4.2.10.3. Oil Red Staining

PBS was removed from wells, and cells were fixed in 10% formalin for 10 minutes. Oil red dye (0.5% W/V in propan-2-ol diluted 2:3 in PBS) was heated to 30°C for 30 minutes, and then filtered through a 0.8µm filter. Formalin was removed from wells and washed twice with PBS. To each well, 1 ml Oil Red solution was added, and left to stain for 10 minutes. Stained cells were then washed twice with PBS. Once dried, images were again taken under EVOS microscope.

4.2.10.4. Quantifying Oil Red O and Unstained Adipocyte Area of Total Area

Similar to BA/TA measurements, ImageJ was used to quantify adipocyte area of both Oil Red O and unstained adipocytes, to investigate relative capacity of MSCs to form adipocytes. This method was developed for this work considering Nile Red O did not provide reliable results. Firstly, for Oil Red O, images were loaded into ImageJ. To this, a colour threshold was applied



using the Image>Adjust>Colour Threshold tool. Manually, the red region was selected and brightness chosen that best covered all adipocytes. The intrinsic black and white threshold was then applied to colour

Figure 4.2.1 ImageJ Selection of Adipocytes. A Oil Red O colour thresholding for adipocytes. B Example of selection of unstained adipocyte from other cell types. Both examples are taken from talar samples.

adipocytes black, and everything else white. Analyse>Analyse particles tool was then used to measure percentage of total area, giving the output. For unstained adipocyte area of total area measurements, again, ImageJ was used. Images were converted into 8-bit, and then a threshold manually applied to select adipocytes, which were brighter than normal cells due to their less flat structure. To normalise these results to DAPI, the percentage area covered was divided by DAPI staining for matched cultures used in Nile Red/DAPI staining (Section 4.2.10.2). Images of the process are given in Fig. 4.2.1. This was repeated for 5 images each from each donor for both Oil red O and unstained images.

4.2.11. Measuring Correlations between Differentiation Lineage Propensity

To allow relative comparison between propensities for MSCs to go down different lineages, for example to see if increased adipogenesis correlates with reduced osteogenic capacity, quantitative measures of adipogenesis (Oil red area of total area normalised to matched well DNA content), chondrogenesis (total sGAG per pellet) and osteogenesis (calcium concentration normalised to DNA) were calculated as a percentage of the highest donor value for all other donors in the same bone. For example, the donor in talus with the highest GAG deposition was used to measure the percentage of itself (100%) and the other two donors by (Donor 1/Donor 2*100). This was performed for all lineages for each bone, and then compared against each other. Linear regression was then run to visualise correlations.

4.2.12. Statistics

Statistics were performed as described in Section 2.9.2, and Table 4.2.4 demonstrates specific tests in this chapter.

Table 4.4 Choice of Statistical Test for Each Dataset

Figure	Test Chosen	Groups
4.3.5	Linear Regression	3
4.3.6-8	Kruskal-Wallis with Dunn's multiple comparisons	3
4.3.13	Kruskal-Wallis with Dunn's multiple comparisons	3-6
4.3.16	Kruskal-Wallis with Dunn's multiple comparisons	3-6
4.3.18,19	Kruskal-Wallis with Dunn's multiple comparisons	6

4.3. Results

4.3.1. Growth and Morphology of Tibial and Talar Plastic-Adherent Cells in 2D Culture

Cells isolated from bone were first seeded on tissue culture flasks and passaged to generate sufficient cell numbers for experiments to identify MSCs presence. During culture, cell behaviour was monitored. As shown in Figure 4.3.1, talus and tibia both had plastic-adherent cells with a fibroblast-like shape (Figure 4.3.1i), which MSCs usually present in culture. Interestingly, whilst MSC behaviour was relatively similar between talus and tibia, there were some small differences between cellular behaviour. At day zero, cells were still attaching as such were difficult to identify, as well as small bone fragments were remaining despite filtration (Figure 4.3.1i). Once cells had adhered, these bone pieces were removed by washes and cells were easier to identify. At day 2, these cells showed a stellar shape with small extensions. By day 8, the talar cells remained more rounded and separated, whereas tibia cells seemed to have adopted a more fibroblastic morphology with longer projections. By day 10, cultures approached confluency on the plate. Talar cells again seemed to stay more rounded, but started to show some alignment and were congregating together. Tibial cells became flattened, and formed aligned colonies or sheets. These changes in behaviour were then further monitored over the first three passages to check for further changes over time.

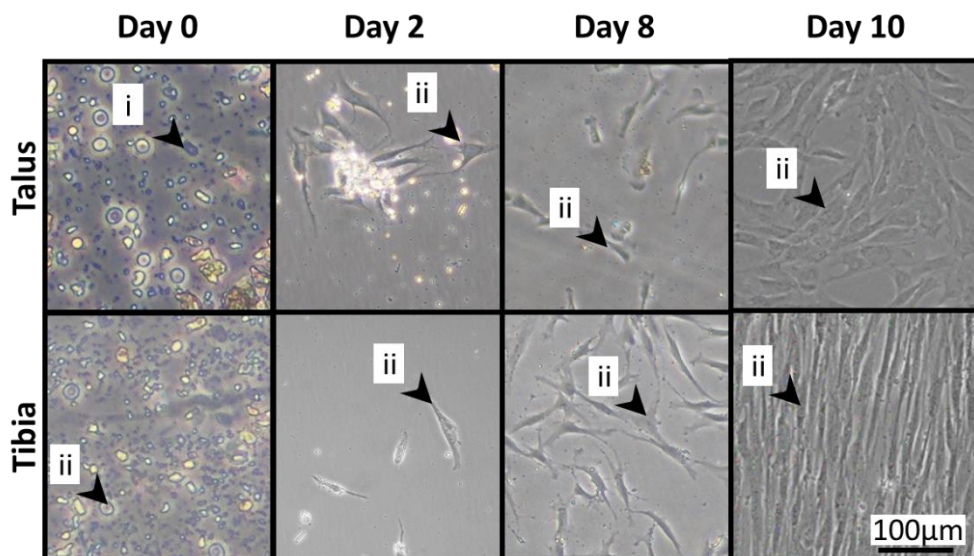


Figure 4.3.1 MSCs 2D in culture following isolation from bone. Cells isolated from talus and tibia were cultured on plastic in StemMACS media. Images were captured at 200x. i – bone fragments left over from digestion. ii – Examples of plastic-adherent MSCs.

Once confluent, cells were split and passaged to generate larger numbers as well as reach a passage which is comparable to existing research. MSCs are usually identified by flow cytometry at passage 2, and passage 3 for differentiation capacity⁹¹. During culture, images were again taken to assess changes to cells throughout culture, with day 2 of each passage chosen to see individual cell effects rather than colony effects. Again, overall, talar and tibial cells did not show particularly different behaviour (Fig. 4.3.2). However, talar cells showed slightly more spreading out, and less spindle-shaped cells. Over time, cells from both bones produced created larger projections and thinner morphologies.

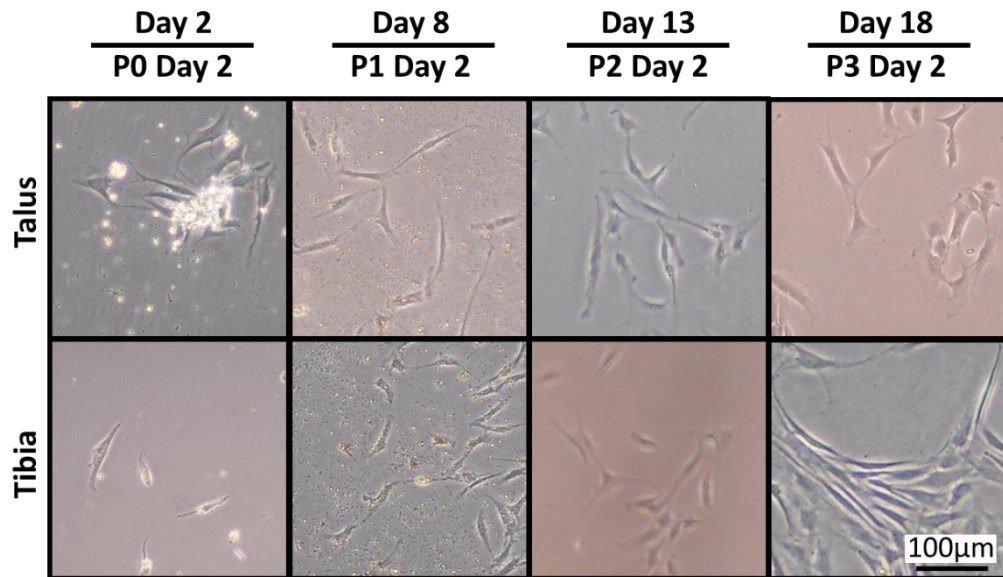


Figure 4.3.2 Changes to Talar and Tibial Plastic-Adherent Cell Morphology During P0-P3 Culture. Images were taken at 200x magnification. P denotes passage number of cells. P0 denotes cells which were cultured straight after isolation.

The main benefit of enzymatically extracting cells is supposed to be the larger cell populations retrieved than processes such as bone marrow washes, it was pertinent to see if all cells were being retrieved⁷². To test if this is true, bone pieces from one donor after enzymatic extraction of cells was cultured to see if cells would migrate onto the plastic. Digested bone from both talus and tibia showed adherent cells at 7 days (Fig. 4.3.3), entirely focused near the bone fragments. After 24 days cells reached around 40% confluence, suggesting that whilst some cells remain (i), there were only few. More cells were visible in tibia compared to talus, suggesting that more cells remained within the bone, with some macrophages (ii) and visible bone fragments (iii/iv). This provided sufficient evidence that only a minority of cells remained in bone, and therefore the next work was completed on extracted cells. Next, the potential for MSC identity of these cells was investigated.

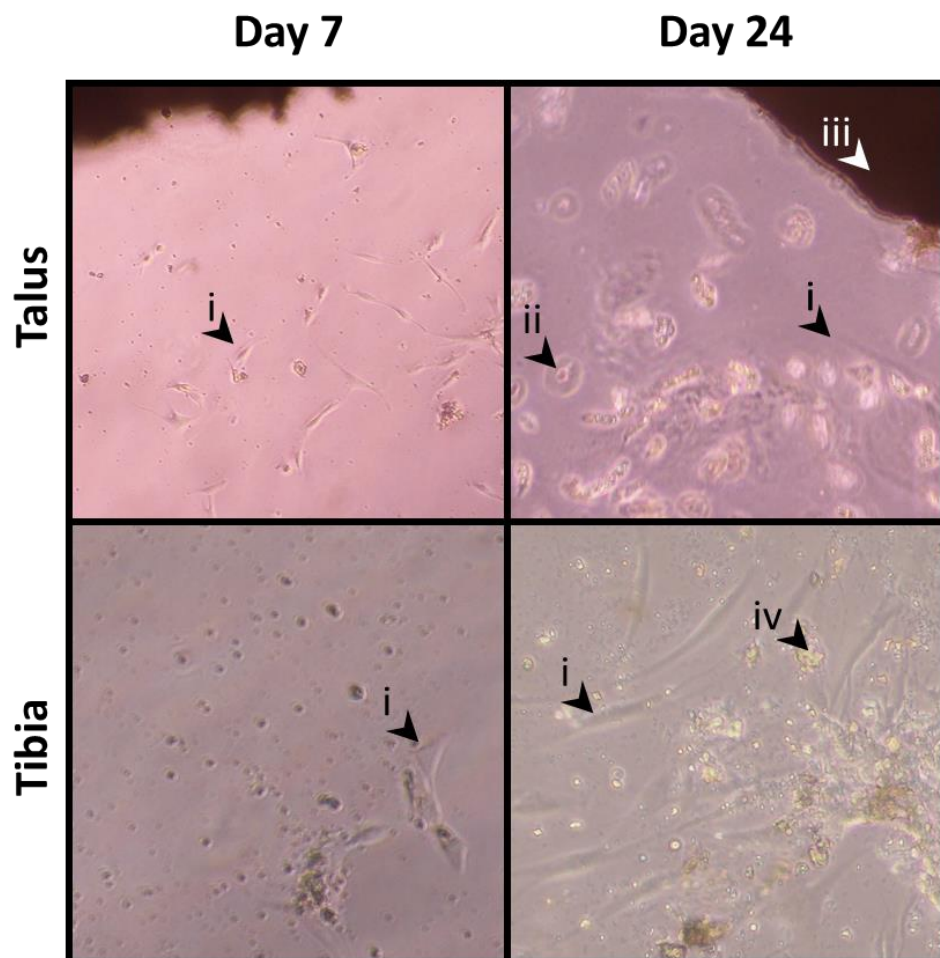


Figure 4.3.3 Cell Egression from Enzymatically Treated Bone. Images were taken at 200x magnification. i – MSC on plastic, ii – macrophage, iii – large bone fragment iv – small bone fragments

4.3.2. Measuring Putative MSC Frequency, Colony Behaviour and Growth Characteristics

To better understand the nature of these extracted cells, these were investigated for their relative number found in IC, talus and distal tibia, as well as their surface phenotype investigated, to start identifying if these were indeed MSCs, and if there was a potential for increased numbers in talocrural OA as found in hip¹⁰¹.

To investigate relative potential MSC presence, a CFU-F assay was performed on 3 donors with 3 replicates. By seeding freshly isolated cells by estimated cell number in multiple concentrations, total MSC frequency by cell number can be predicted (Section 4.2.4). This is shown in Figure 3.4.3. Talus, tibia and IC all presented positive methylene blue staining, showing that plastic-adherent, self-replicating cells were present, and demonstrated higher colony counts with increased cell seeding density (Fig. 4.3.4A). Total colony numbers showed strong positive correlation with seeding number ((Fig. 4.3.4B) $r = 0.99, 0.96$ and 0.78 respectively (2 significant figures). Linear regression showed talus and tibia were not significantly different, however they were both significantly different from IC ($p < 0.0001$). As described in Section 4.2.4, IC CFU-F assays were performed on larger tissue culture plates with higher initial densities, as such colonies appear smaller and more frequent in Fig. 4.2.4A. This was compensated for in Fig. 4.2.4B. These colonies were next used to estimate how many plastic-adherent cells were being isolated per sample.

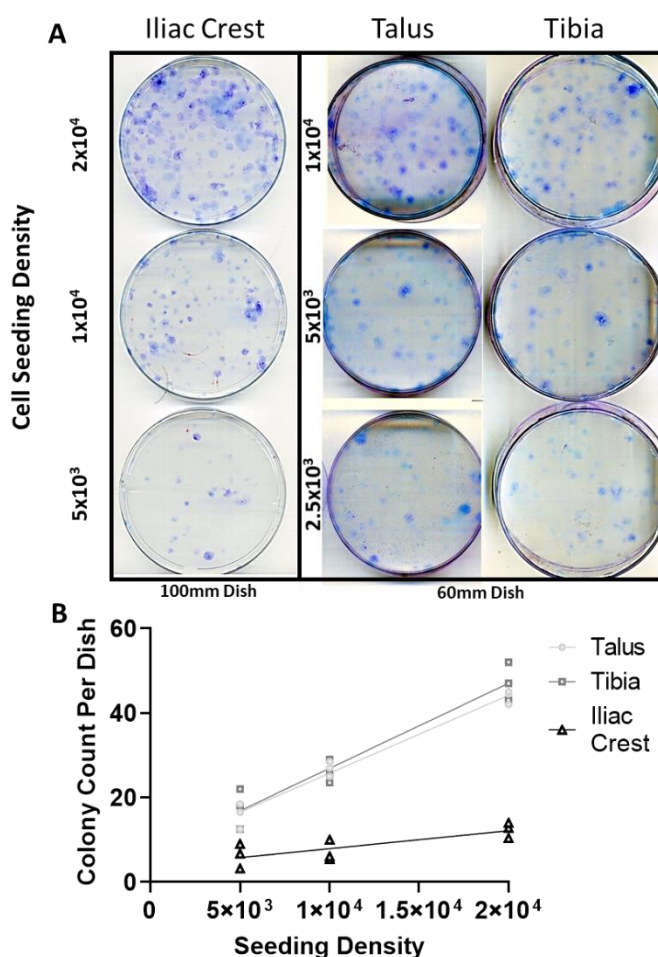


Figure 4.3.4 Colony Forming Unit Fibroblast Assay of Plastic-Adherent Putative MSCs from Talus, Tibia and IC Enzymatic Digests. A – Methylene blue staining of plastic-adherent cells at different seeding densities. B – Colony counts in relationship to seeded cell number. All data points are shown with line of best fit.

The frequency of putative MSCs of total extracted cells can be calculated from CFU-F assay, as the colonies produced per seeded cell number estimates the percentage of MSCs in the sample. This can then also be used to demonstrate other characteristics (Fig. 4.3.5). Putative MSC frequency was taken from the 1×10^4 cell seeding density group due to there being some overlap of colonies in the 2×10^4 seeded cell density group. Firstly, it was found there was a similar frequency of colony-forming cells of total cells in talus and tibia, at just under 0.3%. This was a significant 30-fold increase on MSCs isolated from the IC, with around 0.03% ($p=0.0048$ and 0.013 respectively) (Fig. 4.3.5A). As now putative MSC frequency was known, this was used to calculate MSCs isolated per bone weight (Fig. 4.3.5B) and by per sample (Fig. 4.3.5C). Conversely, there was a significant, 4-fold higher putative MSC content per gram in the IC relative to talus and tibia ($p=0.0015$, 0.0016 respectively) likely due to the comparably lower weight and higher cellularity of the IC (Fig. 4.3.5B). The overall effect of this was that there were 2-fold more putative MSCs overall per talus and tibial sample compared to IC (Fig. 4.3.5C). This showed key differences in MSC availability between talar, tibial and IC samples, which has not been investigated previously. Next, colony behaviour was investigated to see if there were different growth behaviours between MSC source or between OA and non-diseased tissue.

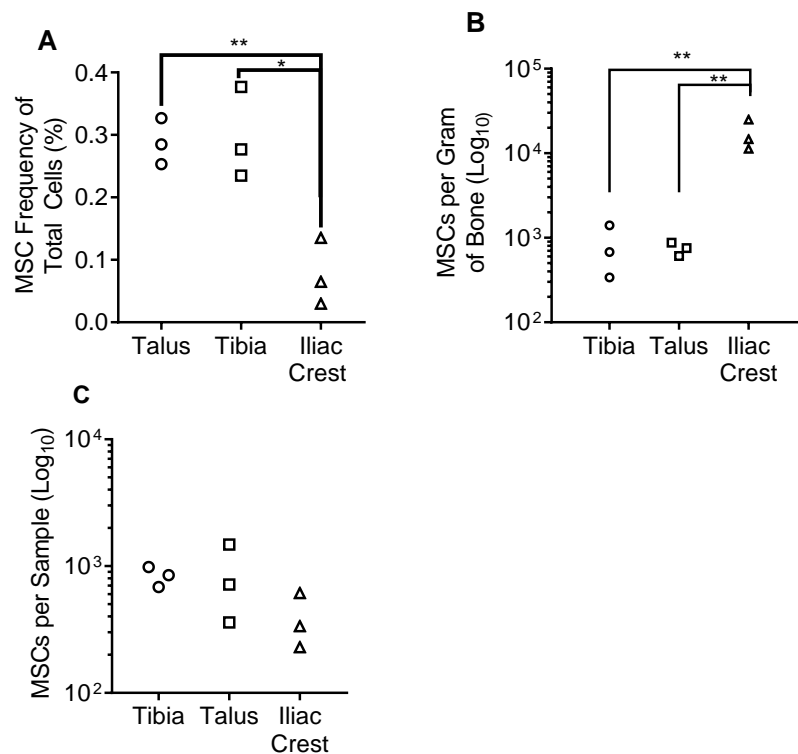


Figure 4.3.5 Estimation of Plastic-Adherent Putative MSC Content in Surgically-Retrieved Bone Samples of Talus, Tibia and IC by CFU-F Assay (N=3). A MSC frequency per total cell number (%). B MSCs per gram of bone. C Total MSC frequency isolated per tissue sample. Graphs show median and range with all data points. Significance was tested with Kruskal-Wallis with Dunn's multiple comparisons test. Significance was set at * = $p < 0.05$, ** = $p < 0.01$

Whilst understanding MSC content per donor sample informs research, it is also essential to investigate proliferation and migration to understand the potential function of these cells²⁸⁷. This was investigated by measuring colony area as well as integrated density (Fig. 4.3.6). There were slight differences, such as IC having slightly higher colony area (Fig. 4.3.6A) and integrated density (Fig. 4.3.6B), suggesting these cells prefer forming more dense colonies compared to talar or tibial cells (Fig. 4.3.6A-B). To further understand cell behaviour, growth characteristics of these cells was next investigated.

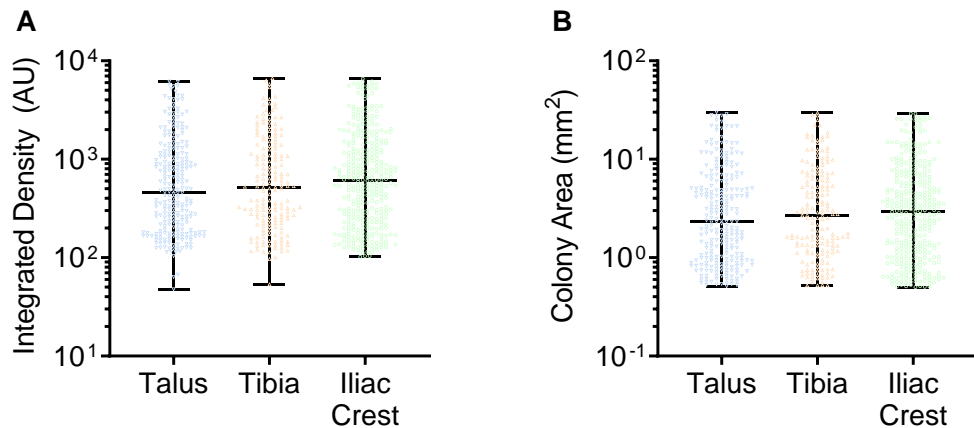


Figure 4.3.6 Colony Characteristics of Plastic-Adherent Putative MSCs Isolated from Distal Tibia, Talus and IC (N=3, 252, 179, 348 colonies per bone respectively). A Histogram of colony number and area size comparing distal tibia, talus and IC. B Integrated density comparisons between Talus, Tibia and IC. Data shows median and range with all data points. Data was tested by Kruskal-Wallis and found no significance.

Growth characteristics of MSCs informs upon their potency, particularly when comparing them from different tissues. By measuring the number of seeded cells, time taken to confluency and total MSCs isolated after trypsinization at each passage, the rate of the population doubling (i.e., their speed of growth) can be estimated (Fig. 4.3.7). Overall, there were no apparent or significant differences between talar, tibial and IC MSCs, with relatively steady growth speed from passage 0 to passage 3 (Fig. 4.3.7A). IC showed significantly faster growth at P0 ($p=0.0429$) but there were no significant differences at other passages. Whilst growth was relatively linear, both talus and IC showed a trend for reduced doubling time at P1 compared to P0 (Fig. 4.3.7B), and subsequent increase in doubling time with subsequent passages, except for talus in P3 (Fig. 4.3.7C-E). This is consistent with previous data from our research group^{72,219}. Overall, these cells showed plastic adherence and colony formation, as would be expected of MSCs, and whilst there was a significantly higher MSC frequency in talus and tibia, there was not key differences in growth or colony behaviour. Next, further steps to show MSC identity were required.

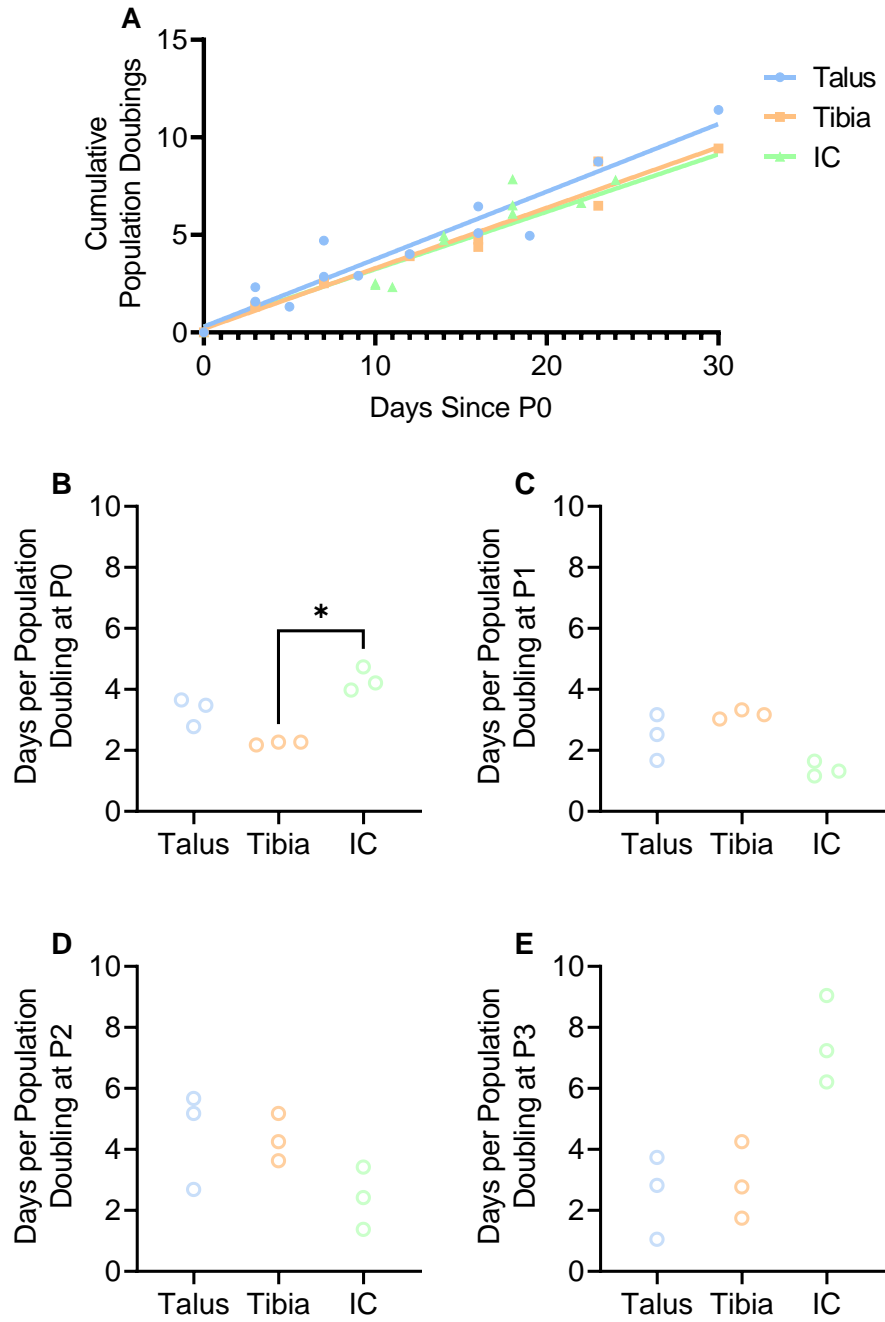


Figure 4.3.7 Population Doubling Times of Plastic-Adherent Putative MSCs from Passage 0 to Passage 3 from Distal Tibia, Talus and IC (N=3). A Growth rate of MSCs over several passages. B Doubling time at Passage 0, based on MSC frequency from CFU-F Assay. C Doubling time at P1. D Doubling time at P2. E Doubling time at P3. Data shows median and range with all data points. Friedmann test with Dunn's correction was used to test significance on B. Significance was set at * $P < 0.05$.

4.3.3. Proving MSC Identity by Surface Protein Expression

As these cells had shown plastic-adherence, and the ability to form colonies, two of the requirements for MSC identity had been met. To fully confirm these were MSCs, analysis of their surface protein expression was undertaken through flow cytometry.

Firstly, flow cytometry was performed to collect 1×10^4 events from each sample, and gates applied to identify living cells, as well as positive events. These are demonstrated in Figure 4.3.8. Firstly, live cells were identified by FFC and SSC (Fig. 4.3.8A). Events for CD73, CD90 and CD73 (red) were distinct from isotype controls (purple), showing their presence (Fig. 4.3.8B-D). Negative markers overlapped with isotype controls, showing no expression (Fig. 4.3.8E). An example of double-positive expression is shown for CD73 and CD90 (Fig. 4.3.8F).

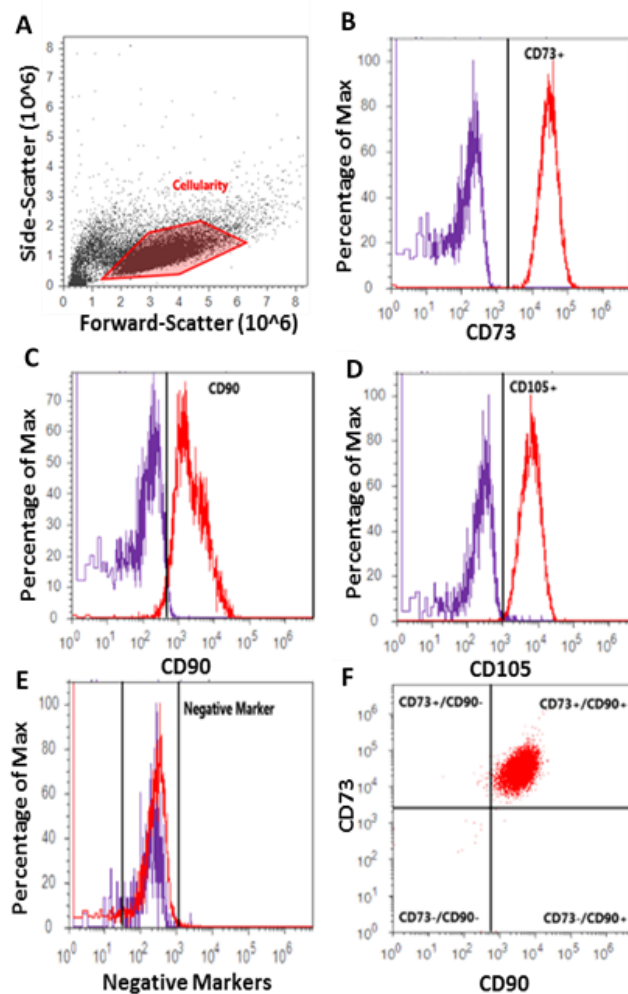


Figure 4.3.8 Gating Strategy for Characterisation of Surface Phenotype of Cultured Cells Isolated by Enzymatic Extraction from Talar, Tibial and IC Bone. Red events denote cellular events, and purple the isotype control events. A Gating for live cells based on FSC and SSC. B Gating for CD73 positive events. C Gating for CD90 positive events. D Gating for CD105 positive events. E Gating to exclude negative markers F Example of double-positive expression of CD73 and CD90.

Once grown to passage 2, flow cytometry was undertaken to ensure that these isolated plastic-adherent cells were indeed MSCs. During culture, the expression profile of MSCs can change based on their stage, and passage 2 cells are required for the ISCT standardised definition of an MSC, as earlier explained (Section 4.1.2). Isolated, plastic-adherent cells showed positive expression for each positive marker of at least 95%, and below 5% for negative markers (Fig. 4.3.9A). Additionally, 95% percentages or higher of MSCs were double positive for each possible combination of CD73, CD90 and CD105, showing that the majority of cultured cells expressed all three surface markers (Fig. 4.3.9B-D).

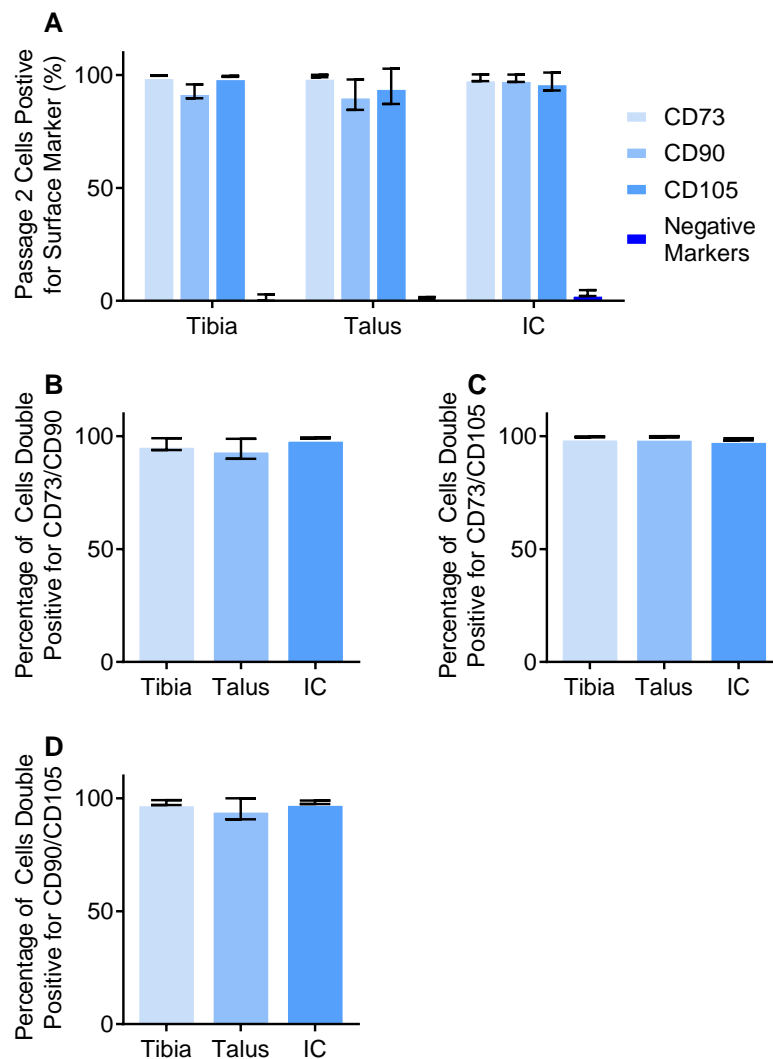


Figure 4.3.9 Surface phenotype of isolated cells from talus, tibia and IC after culture to passage 2 by flow cytometry (N=3). Negative markers reflect absence of haemopoietic lineage cells. Bar graphs represent means and standard deviations (SDs). A Overall surface marker expression. B Proportion of MSCs which showed dual-positive expression of CD73 and CD90. C Proportion of MSCs which showed dual-positive expression of CD73 and CD105. D Proportion of MSCs which showed dual-positive expression of CD90 and CD105. Data shows mean and standard error.

4.3.4. Multi-Lineage Capacity of Talocrural MSCs in Comparison to IC MSCs

Isolated, plastic-adherent cells had now shown the majority of requirements for being identified as an MSC, however their differentiation capacity still needed to be shown, which was explored next. Additional to proving MSC identity, differences in adipogenic, osteogenic and chondrogenic differentiation capacity between talus and tibia was also investigated to see if endogenous MSCs were a suitable target for repair strategies, in comparison to IC MSCs as a positive control.

MSCs are thought to naturally be capable of osteogenic, chondrogenic, and adipogenic differentiation. MSCs were induced into each of these differentiation pathways by use of medias which provide the required conditions for differentiation. Adipogenic and osteogenic cultures were grown in 2D culture, so the effect of the media on cells was investigated under microscopy. Images were captured at day 21, to demonstrate the cells post-differentiation (Fig. 4.3.10). Osteogenesis results in calcium deposition, leaving significant amount of acellular material which covered cells. Where MSCs were visible, they showed the polygonal morphology associated with osteogenic commitment (Fig. 4.3.10i), which were visible underneath acellular material (Fig. 4.3.10ii). Adipogenesis demonstrated the most striking differences between different tissues. The talus presented more rounded highly confluent cells, but only small amounts of bright, circular fat deposits associated with adipocytes (Fig. 4.3.10iii). However, in both tibia and IC cultures, there was an abundance of circular, fully formed adipocytes, showing successful adipogenic differentiation (Fig. 4.3.9iv,v). To confirm successful differentiation, histochemical staining of wells was performed to prove calcium and adipogenic activity.

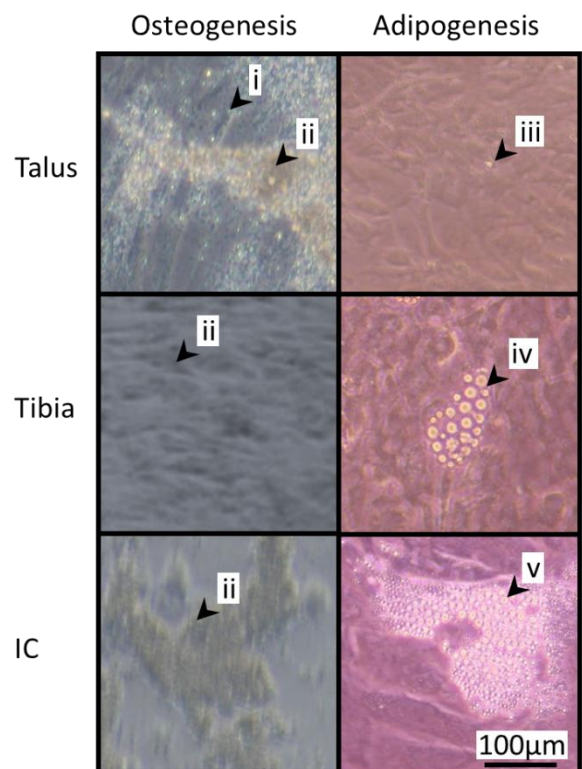


Figure 4.3.10 Morphology of Adipogenic and Osteogenic Differentiation Cultures at 21 Days of Culture in Osteogenic and Adipogenic Media of Distal Tibia, Talus and IC MSC cultures. Images were taken at 200x magnification. i – Polygonal cells under acellular material, ii – acellular material deposited during osteogenic differentiation, iii – small fat deposit within cells of talar cultures, iv – adipocyte within tibial culture, v – large adipocyte within IC culture.

Osteogenically induced putative MSC cultures were stained at 14 days for ALP, an early marker of osteogenic differentiation. At this point, donors WJ11-13 and IC1-3 were included to see donor variances (Fig. 4.3.11). Cultures from distal tibia, talus and IC all presented blue staining (Fig. 4.3.11i), showing ALP activity, however in both osteogenic media, as well as the negative expansion controls. Overall most cultures showed similar levels of ALP expression, however there were some donors that had more cells with low activity (Fig. 4.3.11ii), however this seemed to be donor related rather than tissue source related, for example donor 13 compared to donor 11. Early deposition of debris was also visible in some cultures (Fig. 4.3.11iii). Markers of later stages of osteogenic differentiation were next investigated to confirm successful bone differentiation.

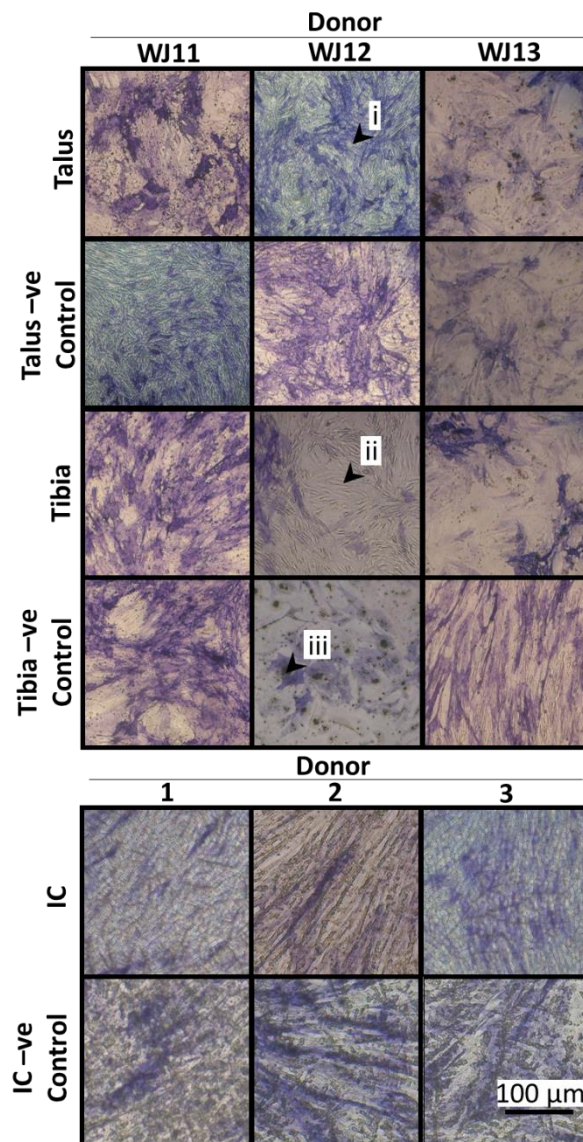


Figure 4.3.11 Alkaline Phosphatase (ALP) Activity in Talar, Tibial and IC Cultures Initiated by Passage 3 Putative MSCs Grown in either Osteogenic or Expansion Media after 14 Days Culture (N=3 for each). i – Positive ALP activity of MSCs. ii – MSCs without ALP expression. iii – Acellular debris deposited by MSCs during culture. Negative control is StemMACS as an expansion control.

After 21 days culture, MSCs were stained with 2% alizarin red to detect calcium deposition. Talus, tibia and IC MSCs in osteogenic media all showed positive staining, with expansion controls showing a small amount of background staining, however no large deposits of calcium. Large deposits of calcium stained a deep red (Fig. 4.3.12i), with controls showing some staining in the background, but cells were clearly visible (Fig. 4.3.12ii). However, this did not quantify the level of osteogenesis per cell to compare MSCs from different sources.

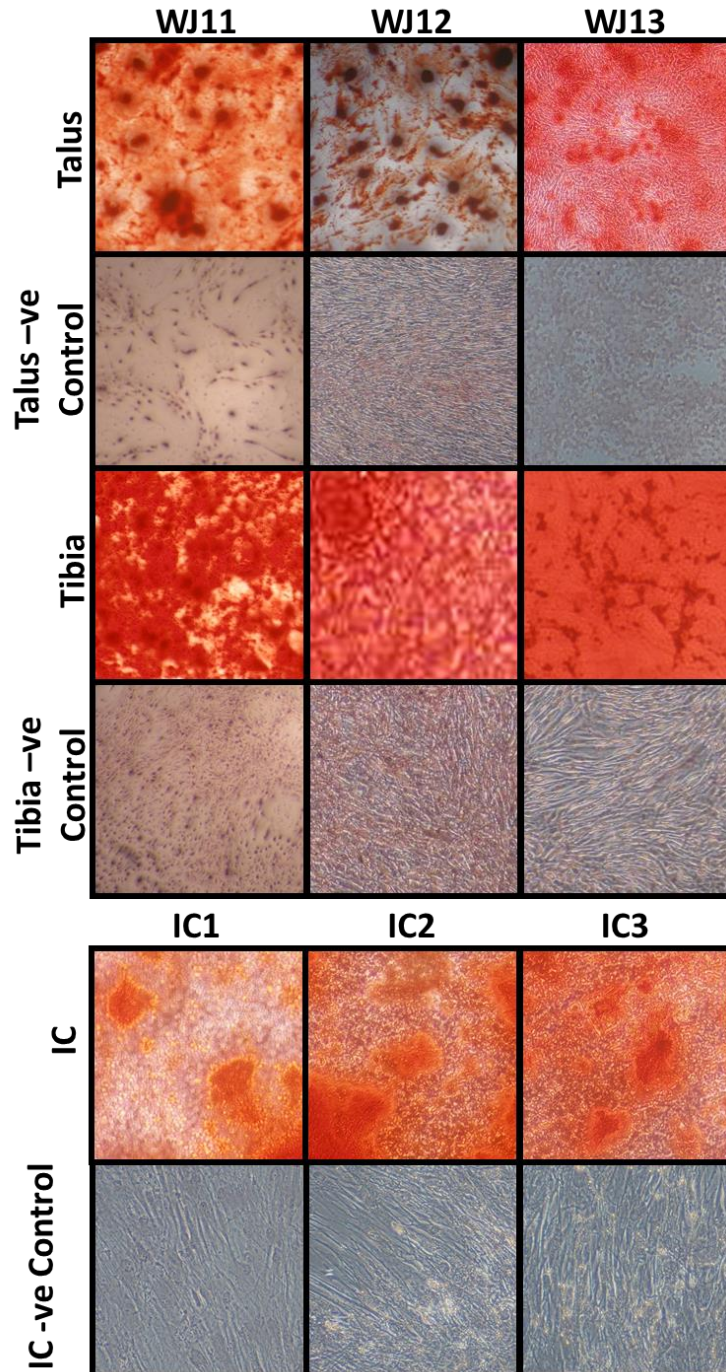


Figure 4.3.12 Alizarin Red Staining of Cultures from Distal Tibia, Talus and IC from Putative MSCs after 21 Days Growth in Osteogenic or Expansion (negative control) Media (N=3 for each). i – Calcium deposition stained with alizarin red. ii – Cells with minor background staining.

The amount of calcium deposited was next quantified, using total DNA content to proportion results to relative cell number. In all cases, osteogenically differentiated MSCs produced more calcium than their expansion counterparts overall, with the talus producing more calcium than tibia or IC, although there was no significant differences (Fig. 4.3.13A). When just looking at DNA content, this was highest by 1.1-1.5 fold in each case in the negative expansion control relative to the differentiation media for each bone, but more or less similar between each tissue, matching results of growth rates (Fig. 4.3.13B). When calcium content was normalised to DNA, talar cultures produced near 2-fold that of both tibia and IC cultures, whereas IC and tibia cultures were similar (Fig. 4.3.13C). These results show that MSC cultures of talus, tibia and IC all successfully underwent osteogenesis, being slightly higher in talus and tibia, and 2 more lineages were required to prove MSC identity.

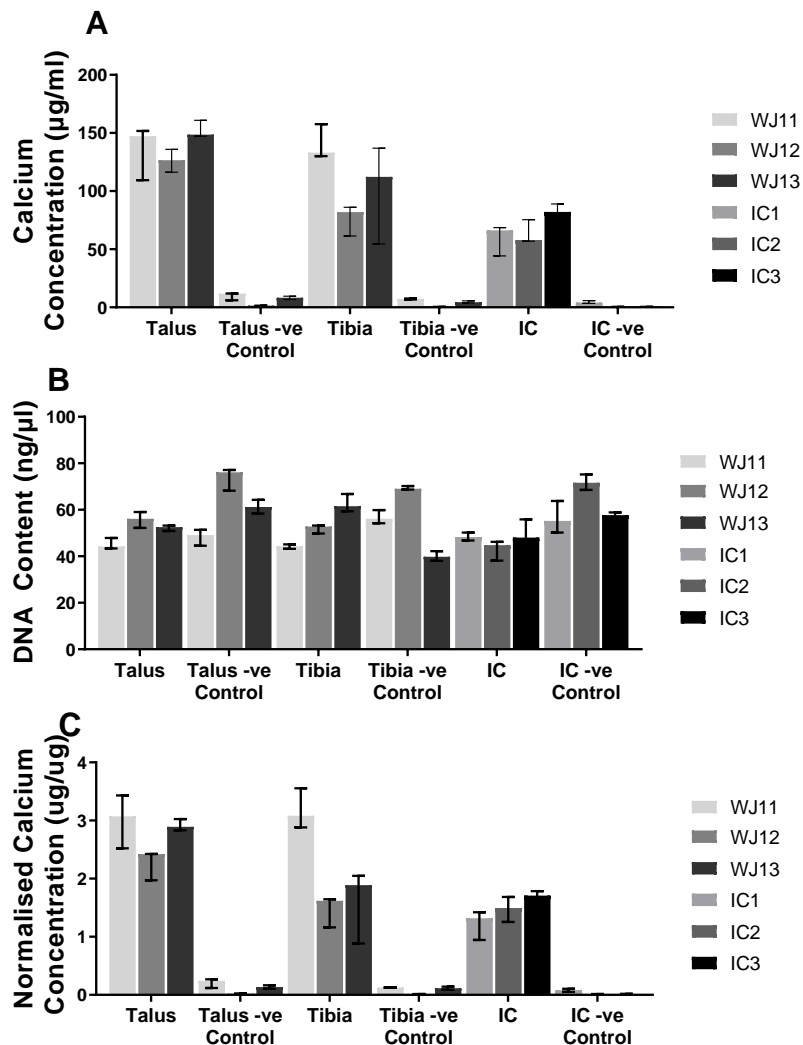


Figure 4.3.13 Quantitative Assessment of Calcium Deposition of MSCs from Distal Tibia, Talus and IC Cultures after 21 Days Culture of Putative MSCs in Osteogenic or Expansion (negative control) Media (N=3 for each with 3 technical replicates). A Total calcium concentration of osteogenically cultured MSCs. B DNA Content of cultured MSCs. C Calcium concentration normalised to DNA content of matched cultures. Data shows median and range.

Adipogenesis of MSCs was investigated after 21 days in culture, firstly by staining for Oil Red O. Treated tibial, talar and IC cultures successfully produced mature adipocytes, however this was far less in the talus with a few small adipocytes being visible (Fig. 4.3.14). Under 200x magnification, talar cells presented 'horseshoe' morphology (Fig. 4.3.14i), with small amounts of fat globules within the cells at the periphery, suggesting early stages of differentiation. Tibia and IC cultures both showed full adipocyte formation, with similar amounts in the two (Fig. 4.3.14ii). None of the negative expansion controls showed any positive staining. To further understand the level of fat synthesis, particularly within the talus where incomplete differentiation was occurring, Nile Red normalised to DAPI staining was performed²⁸⁸.

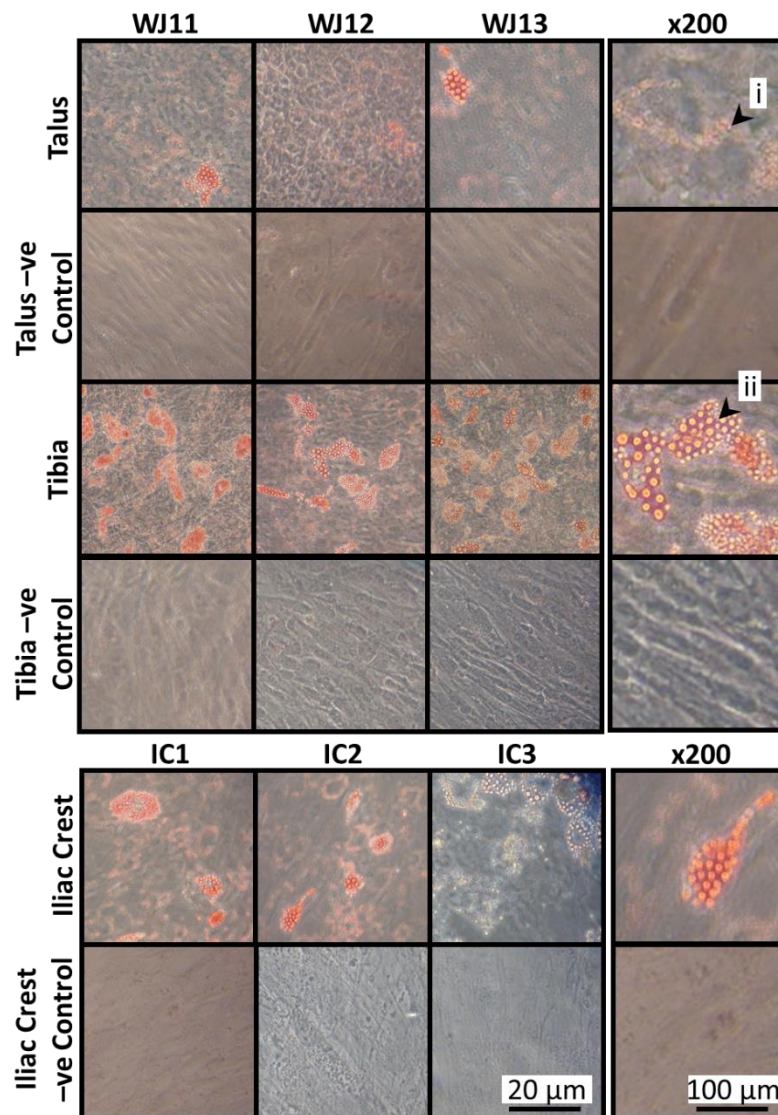


Figure 4.3.14 Oil Red O Staining of Talar, Tibial and IC Cultures After 21 Days Culture in Adipogenic Medium or Negative Expansion Control of Putative MSCs (N=3 for each). i – 'Horseshoe', incompletely differentiated cell showing some fatty deposits. ii – Mature adipocyte. First 3 columns are taken at 40x magnification, fourth column taken at 200x magnification (Representative images of each donor).

Nile Red fluorescently stains intracellular lipids yellow, allowing specific staining of cells with fat globules within them. Again, talus, tibia and IC MSCs all showed positive staining, with no staining in the negative controls. Talar MSCs retained these 'horseshoe' fat presentation, with few fully formed adipocytes (Fig. 4.3.15i), which retained similar morphology to cells from the negative expansion control (Fig. 4.3.15ii). Tibial and IC MSCs presented similar amounts of fully formed adipocytes, but also had evidence of partially early-stage adipocytes, suggesting the talar MSCs are somehow slower at adipocyte formation (Fig. 4.3.15iii). Whilst this proves that these isolated plastic-adherent putative MSCs can undergo adipogenesis, quantification was needed to investigate differences between tissues.

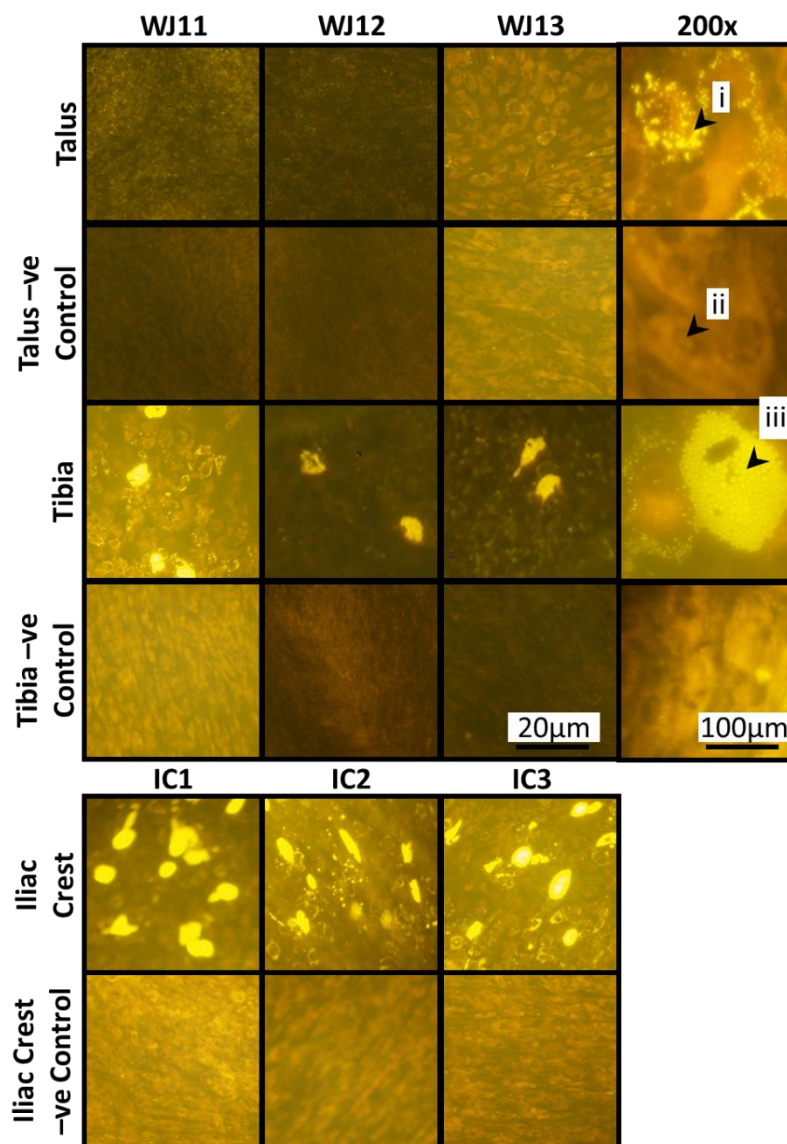


Figure 4.3.15 Nile Red Staining of Talar, Tibial and IC Cultures After 21 Days Culture in Adipogenic Medium or Negative Expansion Control of Putative MSCs. i – 'Horseshoe', incompletely differentiated cell showing some fatty deposits. ii – Cell from negative control. iii – Fully formed adipocyte. First 3 columns are taken at 40x magnification, fourth column taken at 200x magnification (images taken from best representative images).

To quantify the level of adipogenesis, adipocyte content in relationship to DAPI staining was next performed (Fig. 4.3.16). In accordance with standard practice, absorbance of Nile Red in proportion to DAPI was performed. DAPI absorbance showed similar increase in absorbance in each condition, with WJ13 in most cases showing the least increase in absorbance. Overall, talar cultures grown in adipogenic media had the least growth (Fig. 4.3.16A). Nile Red increase on absorbance normalised to DAPI absorbance increase did not produce results representative of what was seen by staining (Fig. 4.3.16B in comparison to Fig. 4.3.14-15). This may have reflected technical issues such as poor dye quality, or excessive background staining. As such, quantification of Oil Red area was performed, which demonstrated the low staining found in negative controls. Importantly, this showed that talar cultures had far less staining than tibia or IC (Fig. 4.3.14C). This method was additionally performed on unstained adipocytes to ensure reproducibility, which showed similar results, although area was around 0.5-fold that of Oil Red O image analyses, likely due to the specificity of a red colour filter over selecting for adipocytes by greyscale thresholding (Fig. 4.3.14D). To match this to relative cell content, these results were then normalised to the matched cultures stained with DAPI in Fig 4.3.14A. Firstly, normalised Oil red O staining showed a significant 10-fold reduction in area, relative to tibia and IC ($p=0.0075$, $p=0.0415$ respectively), with no difference between tibia and IC (Fig. 4.3.14E). This was again repeated on unstained adipocyte area, which were normalised to DAPI, and showed the same significant differences, although again each value was 0.5-fold that received by Oil red O area analysis. This was a 5-fold reduction and 6-fold reduction in talus compared to tibia and IC respectively (Fig 4.3.14F $p= 0.0255$, 0.0082). In summary, adipogenesis and osteogenesis are occurring in putative MSCs from the three bones, with key differences in trilineage potential behaviour between each source. To prove these cells as MSCs however, chondrogenic capability still needed to be tested.

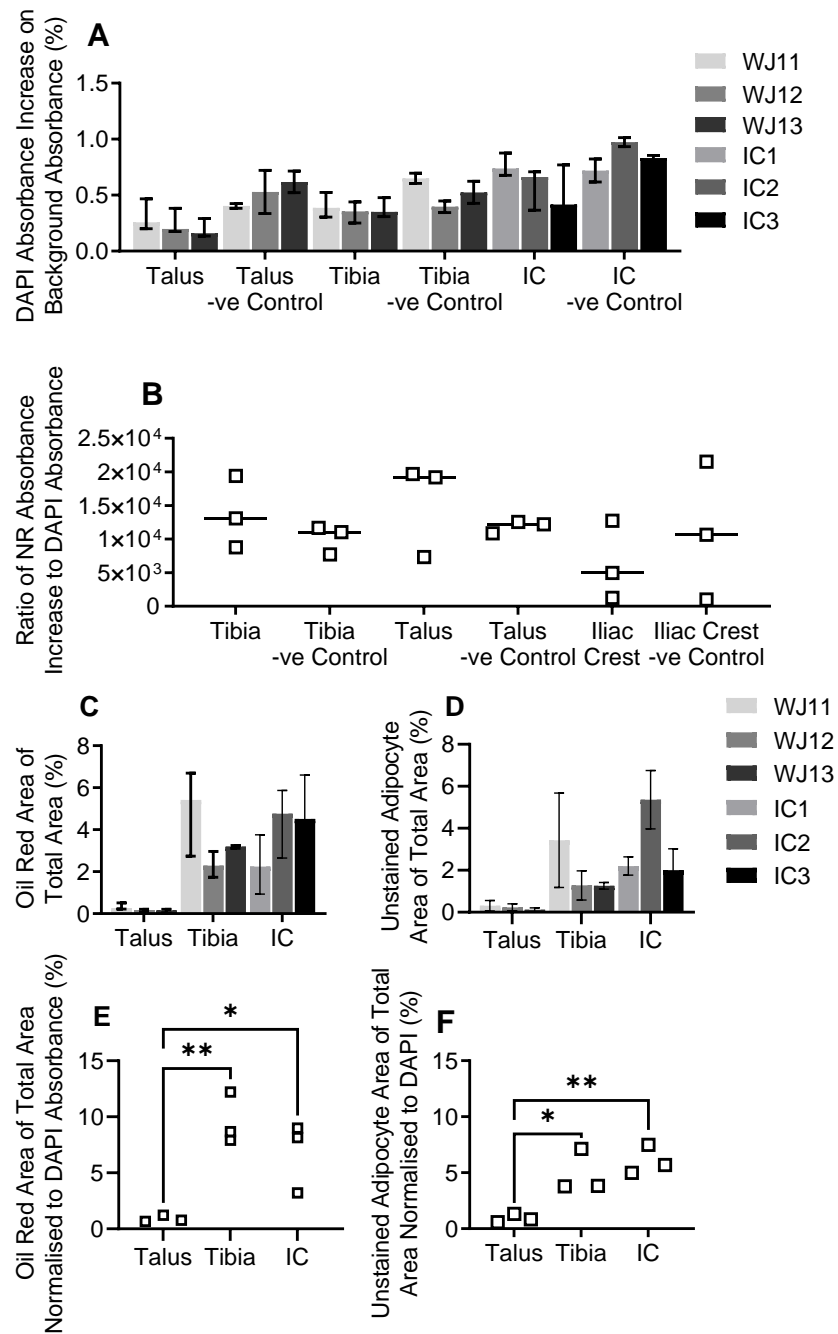


Figure 4.3.16 Quantification of Adipogenesis by Putative MSCs from Distal Tibia, Talus and IC after 21 Days Culture in Adipogenic Medium or Expansion Media as Negative Control (N=3). A – DAPI Absorbance Increase Against Background (% increase). B – Nile Red absorbance increase against background normalised to DAPI of donor-matched cultures. C - Oil red O area of total area. D – Unstained adipocyte area of total area. E – Oil red O area of total area normalised to DAPI of donor-matched cultures. F – Unstained adipocyte area of total area normalised to DAPI staining of donor-matched cultures. C-F do not show expansion controls due there being no fat detected. Normalisation of B, E and F was performed by dividing the original value by the donor-matched DAPI increase on background value. For C-F, 5 images at x10 magnification were analysed from each technical replicate. Data shows median and range with all data points A Kruskal-Wallis test with Dunn's multiple comparisons test was used to test for significance. * = $p < 0.05$, ** = $p < 0.01$.

For chondrogenesis, putative MSCs were pelleted using centrifugal force to create a 3D physical environment, required for cartilage formation. Chondrogenic pellets formed over 21 days should slowly expand as ECM, including GAGs, is deposited. Pellets formed showed a white sheen (Fig. 4.3.17) similar to that of fresh cartilage, such as that seen in cartilage of the non-diseased human control tissue (Fig. 3.4.1). Pellets from treated MSCs showed far larger pellets in talus and tibia than negative expansion controls, as well all as also being larger than IC pellets.

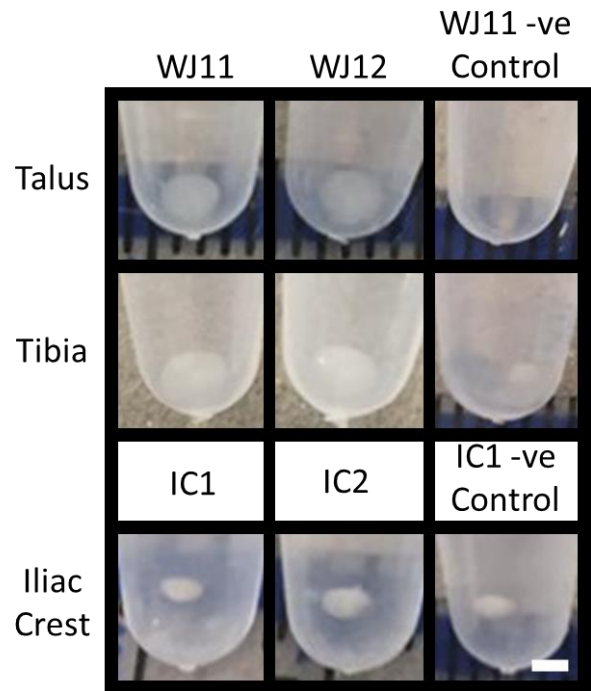


Figure 4.3.17 Chondrogenic Pellets After 21 Days of Talar, Tibial or IC Putative MSC Culture in Chondrogenic Media or Negative Control in Expansion Media. Images were taken without magnification. Scale bar is 2 mm.

The size of the pellets was next investigated on the assumption that pellets which produced more GAGs would be larger. Talar and tibial cultures were approximately the same size, varying from 1.1 mm to 2.4 mm, with strong correlation between the donor and pellet size from both bones. IC pellets were around 2-fold smaller, and had strong correlation between the tested MSCs and control MSCs by donor. Tibia and talar negative control cultures were the smallest, and were of approximately the same size. To ensure that these cultures contained chondrogenic cells, GAG content was tested for by quantitative assay.

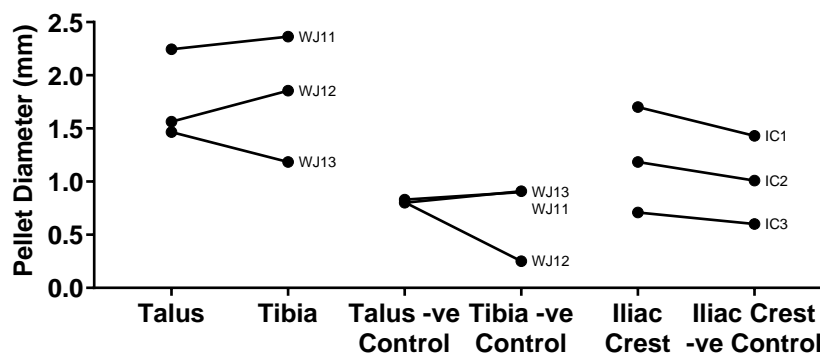


Figure 4.3.18 Diameter of Putative MSC pellets from Talus, Tibia and IC After 21 Day Culture in Chondrogenic Medium or Negative Control Expansion Media (N=3, average of technical replicates). The shortest edge-edge diameter per pellet was taken. Lines represent paired donor samples.

Pellets were enzymatically degraded using papain, which cleaves peptide bonds, releasing GAGs from the matrix. The resulting mix was used for a colorimetric assay to prove GAG synthesis and quantify differences between the origin tissues (Fig. 4.3.19). Negative controls showed negligible levels of GAG synthesis. Talar and tibial cultures both showed around 2-fold higher GAG synthesis than IC, however this was only significant in the talus ($p=0.012$). GAG was identified in talus, tibia and IC, meaning that the ISCT criteria for MSCs had been met, proving that MSCs are present in both talar and tibial bone, for the first time. Additionally, MSCs had shown key differences between capacity for different lineages, such as the IC being more adipogenic and less chondrogenic, as such correlations between different lineages were investigated.

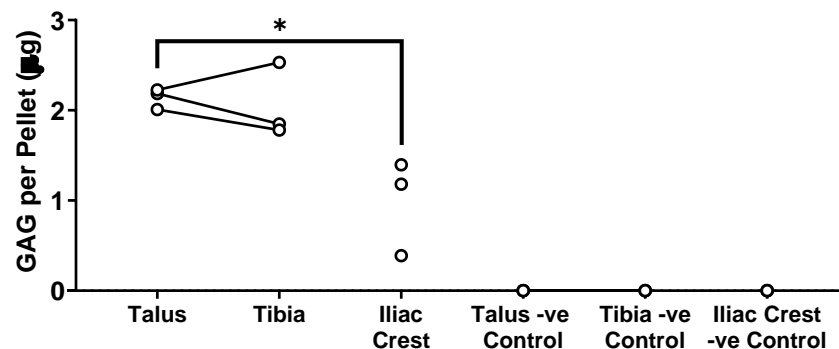


Figure 4.3.19 GAG Concentration of Talar, Tibial and IC Cultures After 21 Day Growth in Chondrogenic Medium or Negative Control Expansion Media (N=3 with 3 technical replicates). Lines show donor sample pairs. A Kruskal-Wallis test with Dunn's Multiple comparisons test was used. Technical replicates were averaged to only represent biological replicates. Significance was set at * $p<0.05$

To investigate if higher differentiation capacity in each lineage was related to other lineages, relative differentiation capacity was compared. To measure this, for each lineage, the average of technical replicates for each donor was calculated, and then converted to percentage of the highest mean donor value (therefore, each graph has one donor at 100% for each lineage capacity)(Fig. 4.2.20). This was performed using GAG per pellet for chondrogenesis, calcium deposition per DNA for osteogenesis, and normalised Oil red O area for adipogenesis. The percentages were then used to identify patterns in differentiation capacity (Fig. 4.3.20). Dotted lines show lines of best fit. Generally, donor values are similar, as such it is hard to draw any trends. Osteogenesis and chondrogenesis showed little correlation, with relative osteogenesis always being high (Fig. 4.3.20A-C). Osteogenesis and adipogenesis showed a negative relationship for talus and IC, but not tibia, potentially affected by the one donor who had the highest differentiation capacity for both in tibia (Fig. 4.3.20D-F). This matches existing data showing osteogenesis and adipogenesis have a negative relationship for IC and talus^{289,290}. Lastly, chondrogenesis and adipogenesis seemed to show little trends, and appeared to be more affected by donor quality.

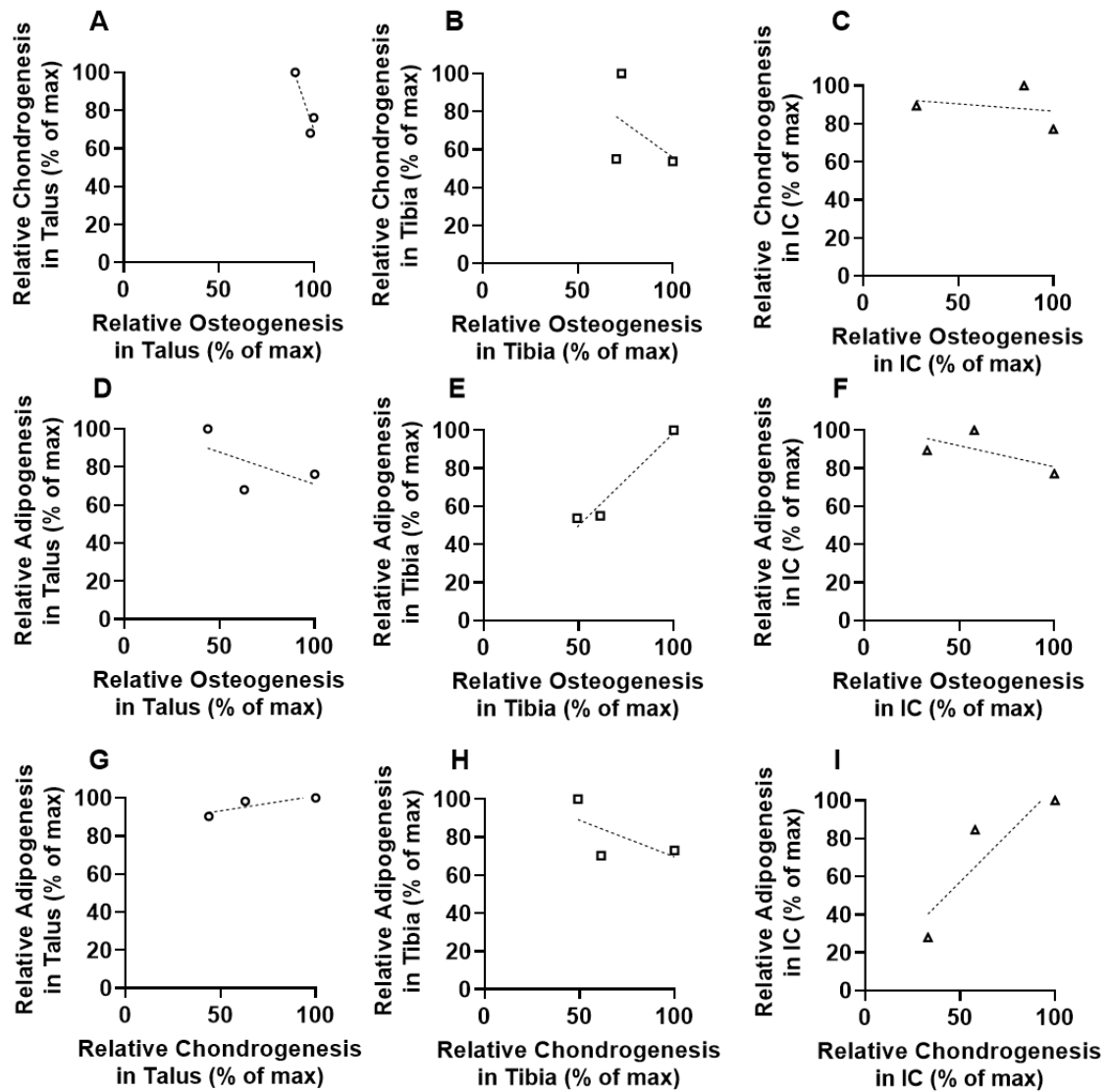


Figure 4.3.20 Relationships of Relative Differentiation Capacity for Adipogenesis, Chondrogenesis and Osteogenesis in Tibia, Talus and IC. The highest donor value of each quantitative measure of differentiation capacity was used to calculate relative differentiation capacity of maximum (highest). For chondrogenesis, GAG per pellet was used, for osteogenesis, calcium concentration per DNA was used. For adipogenesis, Oil red O area of total area normalised to DAPI was used. A-C compare osteogenesis to chondrogenesis in Talus, Tibia and IC respectively.. D-F compare osteogenesis to adipogenesis in Talus, Tibia and IC respectively. G-I compare chondrogenesis to adipogenesis in Talus, Tibia and IC respectively. Trend lines were calculated by linear regression.

Talus, tibia and IC resident MSCs seem to have specific differentiation, with the talus showing the least adipogenesis, and both OA tibia and talus showing highest osteogenesis and slightly higher chondrogenesis to IC. This matches with results of chapter 3, where CD271+ MSCs associated with bone-forming cells, and may be an effect of OA. These results suit the relative roles in the body, and suggests that talocrural MSCs are suitable for regenerative therapies for cartilage, however there needs to be inhibition of osteogenesis in the case of cartilage repair.

4.4. Discussion

Regenerative therapies of ankle OA, and in particular osteochondral lesions of the talus, such as microfracture, rely upon endogenous cells for repair²⁴³. However, the quality, quantity, and identity of these endogenous cells, such as MSCs, is still poorly understood. In microfracture, this is thought to mostly be from MSCs from subchondral bone, whereas other treatments such as joint-distraction more likely rely upon synovial fluid MSCs, as there would be limited access for bone MSCs to enter the cartilage repair site²⁹¹. As such, it is critical the actual regenerative cells required for the specific treatment are understood.

In this chapter, it has been proven for the first time that subchondral bone MSCs are indeed present in both OA talus and tibia. Isolated OA talar and tibial cells presented typical MSC surface phenotype, trilineage differentiation capacity, and plastic adherence, the main criteria forth set by the ISCT⁹¹. Similar to MSCs from hip or knee, MSCs in the talus and tibia were found in higher frequency than the IC^{219,220}. These MSCs showed similar growth, colony characteristics and surface marker expression to well-characterised IC MSCs. Both distal tibial and talar MSCs showed enhanced chondrogenesis compared to the IC, suggesting greater ability to form cartilage. Talar cells showed increased osteogenesis and significantly reduced adipogenesis to the IC, whereas the tibia did not. As found in previous work in MSCs from rat, osteogenesis and adipogenesis showed a negative relationship in talus and IC^{289,290}. These resident MSCs show strong capability for chondrogenic differentiation, and may be a good target for regenerative therapies for cartilage repair, but there needs to be direction away from osteogenesis and towards chondrogenesis.

During basic culture, MSCs from talus and tibia were investigated for changes over the first few days of culture, and the effect of change from bone to plastic, to investigate if the different cells sources had different responses to change in environment and more or less resistance to forming a fibroblastic structure. This would inform on their relative differentiation capacity based on shape. Isolated cells showed typical MSC morphology, with only very minor differences in cell structure, such as talar cells being more rounded, and slightly less dense, however still keeping the associated spindle shape²⁹². Highly dense colonies of MSCs are thought to have reduced differentiation capacity, as well as MSCs cultured in 3D are shown to have a 3D shape, suggesting talar cells seem to slightly resist these structural changes, which may potentially link with their slightly increased osteogenic and chondrogenic capability as found in this study^{87,180,273,293}. Whilst there is still relatively little literature on the effect of cell shape on their characteristics, McCorry *et al.* showed in 3D culture that when initiating MSCs were of a rounder morphology and less densely packed, there was enhanced GAG synthesis and retention within the cartilage matrix²⁷³. However, our own group has shown these rounded cells are associated

with osteogenic differentiation, which is particularly relevant considering the study also utilised OA bone MSCs but from this hip, and showed that in uncultured CD271+ CD56+ MSCs, there was 100-fold increased expression in osteopontin, osteocalcin and chondroadherin, all three related to osteogenesis and the last also involved in chondrogenesis. This morphological difference of talar MSCs presenting a rounder morphology during early culture may be related to their *in vivo* role in OA, for osteogenic and chondrogenic differentiation, matched by the increased osteogenic and chondrogenic capability in comparison to IC cultures. However, these are visual observations and need to be qualified by further methods, such as holographic imaging. The importance of MSC cell shape changes has been highlighted in other fields from differentiation, with cell structure offering insight in MSC aging and tumorigenesis, highlighting the need for further understanding of MSC morphology relationship to behaviour^{273,293-295}.

Over several passages, MSCs from both tibia and talus showed similar behaviour, gradually showing more dense colonies and a more spindle-like morphology. This is expected of MSCs grown on plastic and is the typical morphology associated with MSC 2D culture, and may affect their differentiation capacity²⁹⁶. Another possibility is the reversion from an early stage of differentiation, as MSCs structure has been linked to differentiation, however as mentioned before, these rounded cells are linked to osteogenesis in freshly isolated cells⁸⁵. Current work into MSC morphology mostly characterises MSCs as three types; spindle-shaped, star shaped, and large flattened cells, with none of these specifically describing the rounded morphology found in early culture of talar or tibial MSC²⁹⁷. The latter two morphologies have been associated with reduced differentiation capacity, or MSCs of early osteogenic lineage^{292,298}. This rounded MSC has however been seen in OA, and was part of a CD56+ subset associated strongly with osteogenesis and mildly with chondrogenesis, as such is not unique to talar MSCs. Whilst not shown, some cells did present with these other structures, however they did not persist past the first passage, which is consistent with existing work²⁹². Talar and tibial cells retain the more trilineage-capable cell morphologies, as such should retain high levels of differentiation capacity as was found in this work considering the elevated chondrogenic and osteogenic capabilities.

When assessing if the entirety of MSCs were being enzymatically extracted using collagenase, an egression assay was used, finding that some MSCs were retained, however as these took at least 24 days to reach 40% confluency, the MSCs remaining in bone was likely incredibly low. Enhancements of this method such as using an additional trypsin step on the remnant bone pieces could be used to increase the amount of MSCs released, allowing more MSCs to be obtained following enzymatic degradation of collagen. More cells egressed from the tibia compared to the talus in the two donors tested, likely relating to the samples being larger (Table 3.3.1) and that the BV/TV was lower in tibia than talus. Bone was macerated and collagenase

was applied based on sample total weight, and whilst this may be affected by mineralisation or other factors, the overall weight is less likely to affect MSC release. Therefore, it is more likely to relate to bone structure. Tibial bone was found to have a lower BV/TV and BA/TA (Fig 3.3.3/3.3.4) than talar bone, resulting in a higher surface area. As CD271+ MSCs were located mostly at the bone-lining *in vivo* (Fig. 3.3.10), this higher surface area may have made enzymatic extraction less able to release all MSCs.

The egression assay technique itself present a method to collect more MSCs from digested bone fragments, which is particularly valuable in rare samples, which can be used as P0 cells for later experiments and can be used synergistically with enzymatic extraction.

Colony counts of MSCs demonstrated similar MSC colony numbers in talus and tibia, and far less in IC, showing both that MSCs were isolated, and at higher frequencies than IC. It has been shown previously, particularly in OA, that this is expected. Campbell *et al.* presented a 4.3-fold increase in MSCs in areas of bone marrow lesions compared to healthier regions of tissue¹⁰¹. This 30 to 300-fold higher MSCs per cell number in talus or tibia compared to IC. This is mostly due to IC being a key region of bone marrow for blood cell formation, as such there is very high cellularity with densely packed cells. In bone there is no haematopoiesis, and therefore this explains this increased MSC number found. Whilst there may be an additional affect of OA increasing MSC number, evidenced by CD271+ cells being associated with regions of tissue damage (Fig. 3.3.15), the lack of healthy control means this cannot be directly tested, but has been shown by other studies¹⁰¹. Their high presence in talar and tibia does however indicate that targeting these endogenous, tripotential MSCs for regenerative therapies is viable. Relating this to total MSCs released from the sample, there were significantly more MSCs per gram of IC bone than talus or tibia. This is likely due to the high cellularity of the IC compared to load-bearing joints such as the talus or tibia, shown to be around 5-fold higher by bone-marrow aspiration²⁹⁹. However, per sample, it was shown that MSCs isolated were similar, which relates to how small IC samples are.

Colony characteristics may shed light on the function of resident MSCs, such as lower growth speed being associated with older donors which in turn is linked with reduced differentiation capacity²⁸⁷. MSCs from all three sources showed extremely similar colony area and integrated density, both by median and overall spread. Area simply refers to the size of the colony, whereas integrated density accounts for the number of cells in the colony, by measuring the colour intensity²⁸⁷. The OA state does not seem to alter MSC proliferation or colony structure. Aging is known to affect colony structure and density, and as donors are of similar ages, this is not a confounding factor in this results²⁸⁷. In the previous chapter, OA talar and tibial 271+ MSCs were associated with osteogenic cells, and so likely play a tissue-resident osteogenic role, whereas IC

MSCs are not involved in differentiation or much proliferation. As such it is interesting that there is so little difference in colony structure, as CD271+ MSC localisation would suggest a key focus on bone formation, compared to the IC role as a 'stem cell niche'. Previous work has shown up to 'four' main groups of colony structure, however the majority has just shown colony structure reflects MSCs aging, and therefore it may simply be that colony area and integrated density do not reflect differentiation capacity^{279,287}.

Growth characteristics of cells both inform future experiments but also provide insight into their potential roles within the tissue. Talar and tibial cells showed similar population doubling speed to IC MSCs. The fact that doubling time reduced in the second passage (P1) compared to the first (P0) makes sense, as MSCs need to attach to plastic and the large amounts of bone debris or non-adherent hematopoietic cells remaining will inhibit growth during P0. As these are then removed from P1 onwards, as shown by flow cytometry, doubling rate then for the most part being lowest in passage 2 and then slowing by passage 3, particularly in the IC, matches existing work. As culture continues into later passages, PD time increase due to the accumulation of senescent cells³⁰⁰. However the fact that this was not consistent nor significant also matches up with work into short culture periods^{296,301}.

To confirm MSC presence by surface phenotype, flow cytometry was completed. According to the ISCT criteria, MSCs were successfully isolated, cultured and presented the MSC surface phenotype in both the talus and tibia, with a frequency of over 90% by passage 2. In general, it is accepted that over 95% of all MSCs express CD73, CD90 and CD105, and less than 2% express CD14, CD34 or CD45, however it has been shown that some CD34+/CD45+ MSCs can arise during culture, which explains the remaining negative marker expression³⁰². Additionally, expression of CD73 is linked to the reparative function of MSCs, it has been shown some MSCs which lack CD73 are early-stage progenitors with the flattened morphology MSCs which have already entered early stages of differentiation, which may have been present in the sample, and why CD73 was sometimes the least expressed^{277,292}. Over 95% of MSCs were double positive for each marker, making it highly likely the majority of cells were triple-positive for positive markers.

For osteogenic differentiation, ALP was positively stained for in all samples at 14 days, including expansion controls. Positive ALP staining in unstimulated controls has been reported numerous times, and so is typical^{303,304}. ALP has been linked with differentiation capacity of multi-lineage capable MSCs, so its expression in control cultures may suggest a level of differentiation capacity²⁸². To further investigate osteogenic changes, alizarin red staining was performed as well. Talus tibia and IC all showed positive alizarin red staining, with no clear difference between the three tissue sources. Lastly, calcium quantification demonstrated calcium deposition in all tissue, proving capacity for osteogenic differentiation of talar, tibial and IC MSCs. This was

highest in the talus, slightly lower in the tibia, but both being 1-1.5 fold higher than IC⁵. This is, to my knowledge at the time of writing, a novel finding. The higher osteogenic potential may be related to the joint structure, as the bone undergoes much higher forces than the IC as earlier mentioned, as such needs to be more responsive for bone formation when repeated stress⁵. This may also related to the OA state of the tissue, with the association of MSCs with newly-embedded osteocytes and new bone formation (Fig. 3.3.14-16), however the lack of healthy controls means this cannot be directly tested. Additionally, this behaviour likely relates to the higher adipogenicity seen in tibia and IC than talus, due to the differences in load, bone structure and size of the bones. This is firstly demonstrated by the higher BV/TV seen in talus, but further described in the next Section to better describe the link between adipogenesis and osteogenesis.

For adipogenic lineage, first Oil Red O staining was performed to prove adipocyte formation. As in culture images, talar MSCs showed limited adipocyte formation compared to tibia or IC, again suggesting this limited ability for fat formation. Nile red staining showed the same trend, with visibility of 'horseshoe' cells, suggesting talar MSCs were beginning differentiation and undergoing some of the loading of fat around the nucleus, but not completing it, which has been described previously²⁸⁸. Both Nile red and Oil red O stains showed similar trends, cementing the fact that tibia and IC are more able to undergo adipogenesis. Attempts to quantify Nile red staining were unsuccessful, as despite the clear differences between bones showed by images, Nile red data showed similar levels of staining in every sample, even controls. Whilst data was not shown, serial dilutions of Nile red was performed and background staining was still visible. Subtraction of the background staining also did not show improvements, and performing a scan of absorbance over a series of relevant wavelengths of light did not identify a better target than the one previously chosen from the literature. Other options to improve this staining would have included attempting different staining time, however as Oil red O area of total area showed results consistent with what was visible from histology, time was not invested in optimising the Nile Red stain. Analysis by Oil red O area and unstained adipocyte area of total area both obtained similar results, which reflected the data seen in the images, as such were chosen for adipogenesis quantification. The slightly lower results in unstained adipocytes reflects the difficulty of selecting adipocytes within ImageJ by thresholding, and so parts of the cell were excluded. From Oil red O normalised to DAPI staining for cell number estimation, it was seen that the talus had around 5-fold lower adipocyte area of total area. This stark difference is likely related again to the structure of the bone. As the talus generally undergoes higher loads throughout the whole bone than tibia, and fat deposits are linked with worse impact-loading properties, this makes it likely resident MSCs of the talus will be more primed towards bone synthesis than adipogenesis, as seen in the osteogenesis work^{5,305}. This is also shown by the

higher BV/TV found in talus than tibia (Fig. 3.4.2), as well as the fact that higher cyclic loads direct MSCs towards osteogenesis³⁰⁶.

The last differentiation method required to prove MSC behaviour was the ability to synthesise cartilage. Talar and tibial pellets were far larger than IC or negative controls, either suggesting higher GAG synthesis, protein deposition such as collagen 2, or increased cell proliferation. Proliferation is unlikely, based on the expansion controls being smaller than pellets treated with chondrogenic media, as StemMACS would have encouraged far more than ChondroDIFF. However to prove this, DNA quantification would've been required, which was not performed due to requiring extra pellets, which means more cells, which would require expansion past P3. Quantification of diameter confirmed this, with the slightly higher size of expansion control IC pellets to talar and tibial control pellets possibly being due to higher cell counts, based on later GAG quantification showing no GAG content, which is consistent with the IC having the highest growth rate at P3 compared to talus or tibia (Fig. 4.3.7). Whilst overall there were no significant differences, quantification of pellet GAG showed that the talar and tibial cultures produced slightly higher GAGs than IC cultures, and the expansion controls had minimal GAG synthesis. If there is a difference, talar and tibial MSCs would be more chondrogenic again due to the environment, as there is some evidence of cartilage repair with the extended tidemark in some samples (Fig. 3.3.6viii). As talar, tibial and IC were not precisely age-matched, the fact that talar and tibial MSCs show increased osteogenic and chondrogenic differentiation capability relative to the younger donors' IC MSCs furthers the argument that talocrural MSCs have a greater ability to initiate osteochondral joint repair, considering that aging of MSCs has been shown to reduce chondrogenic potential²³⁴. As such, talar and tibial MSCs provide a suitable target for endogenous repair with increased differentiation properties, confirming that chondrogenesis may be induced using appropriate differentiation conditions.

Lastly the relationships between different differentiation pathways were investigated to see if MSC differentiation capacity could be predicted based of specific lineages. As found in previous work, this study showed a negative relationship between adipogenesis and osteogenesis, which has been explained by some key proteins, such as BMP-2, having specific effects (adipogenesis at low concentrations, osteogenesis at high concentrations) based on their concentration. This was also explained by the fact that fat deposition reduces impact properties of bone, and so an inverse relationship is beneficial^{289,290,307,308}. However, as there were only 3 donors, strong trends were not observed and it hard to truly draw any conclusions from these results as there is not consistent variance in differentiation capacity. Chondrogenicity and osteogenicity, as well as adipogenicity and chondrogenicity pairings seemed to be unrelated, and no relationship between these pairs has previously been reported in the literature, and so is expected.

Overall this chapter confirms that MSCs are indeed present within subchondral bone of OA talus and tibia with joint-specific differentiation behaviour, but similar growth and colony characteristics. Confirming positive CD271+ staining in the third chapter could be marking MSCs, MSCs were successfully isolated from OA bone. MSCs showed the standard characteristics expected of MSCs, as set by forth by the ISCT. Linking in with accelerated bone formation in the third chapter, talus and tibia both expressed osteogenic differentiation capacity, however this was only higher in the talus, and not the distal tibia, compared to the IC control. Elevated chondrogenic potential was found in both distal tibia and talus compared to the IC, highlighting their potential as an endogenous repair source for cartilage regeneration in OA, supporting the basis of microfracture to restore cartilage by releasing MSCs. Interestingly the talus displayed extremely diminished adipogenic potential compared to tibia and IC, which may also be of benefit to repair strategies and has been indicated as an issue in treatments other degenerative changes, particularly in bone marrow during aging³⁰⁷. Bone marrow ankle MSCs have only previously been isolated by Li *et al.* through bone marrow aspiration²⁷⁵. This chapter provides many novel results to the field of regenerative therapies for the ankle and will hopefully inform further treatment development. In line with this, the next step of investigation was to develop methods of enhancing endogenous repair to identify strategies which enhance ankle MSC chondrogenesis at the expense of osteogenesis, using clinically approved biological stimulants.

5. Chapter 5 – Biological Enhancement of MSCs of the Talocrural Joint

5.1. Introduction

Barriers to successful regenerative therapies of cartilage remain, in that despite being able to synthesise cartilage simply by releasing MSCs from bone by microfracture, the tissue formed often fails and forms fibrocartilage¹⁵⁵. The reasons why this occurs and methods for correcting or avoiding this are still being developed. Chapter 3 of this work showed a sclerotic response in bone, associating with cartilage defects. MSCs were shown to localise to these regions, however localising with early osteocytes and other cells involved in bone turnover, suggesting a sclerotic response rather than the cartilage reparative response for which they are utilised for in regenerative therapies. Chapter 4 showed MSCs isolated from OA talocrural tissue were shown to be capable of chondrogenesis as well as osteogenesis and adipogenesis, with a potential favouring of osteogenesis based on their morphology. This evidence suggests that whilst there is an intrinsic signal within the body that's promoting sclerotic bone growth, bone resident MSCs are capable of cartilage repair given the correct signals. Existing research has shown that many factors are responsible for cartilage repair, including biological signals (or growth factors), biomechanics, material and cell source, but also other interacting cells. This presents an extremely complex barrier to directing MSC differentiation, and any of which may explain why microfracture does not always provide a long-term solution. Improving treatments using scaffolds or biological stimulants has shown great potential, but also limitations, and there is likely a need for a multifaceted process. This chapter will explore the ability of biological stimulants to modify MSC differentiation by preconditioning in 2D with biomechanics and materials being investigated in the next chapter.

One of the four key parts of cellular differentiation and tissue repair mentioned is biological signals. There are many different signalling pathways and thousands of molecules involved, as such this work will focus on that relevant to cartilage, bone and fat differentiation. As mentioned at the beginning of this Section, one of the apparent facts is that *in vivo*, these MSCs are undergoing bone differentiation and present a sclerotic phenotype in OA bone. Managing these different factors will be critical for directing differentiation *in vivo* away from bone and towards chondrogenesis, to enable sustained cartilage repair.

In OA, MSCs are exposed to an altered mechanical environment, which as seen in chapter 3, seem to be driving MSCs towards bone synthesis. To mitigate this, a method of directing MSCs towards cartilage formation and away from bone is needed. Ideally, this should occur prior to sclerotic bone being formed which provides an altered mechanical environment and many new osteogenic cells being present which would provide further osteogenic signals^{85,220}. Chondrogenesis presents a particular challenge as it requires an extended period to occur, with some chondrogenic genes such as collagen type 2 not being expressed until at least at 7 days,

and only high expression after 14 days of differentiation³⁰⁹. The introduction of biological stimulants such as platelet rich plasma into the body will only last until they are degraded or absorbed, which will likely not be long enough to maintain signals for the 14 days required, however would give recruited endogenous MSCs a head-start towards chondrogenic induction. Potential intervention can be modelled through MSC preconditioning, a short period of specialised culture before movement of MSCs into the repair environment, to prime MSCs for chondrogenic differentiation. This requires a significant understanding of biological signalling to ensure that MSCs are pre-disposed to the required differentiation lineage, and not other lineages.

Great amounts of work into biological signalling of MSCs and their differentiation has already been undertaken, and relevant pathways involved for differentiation are well understood, but not yet fully characterised. Quantitative Polymerase Chain Reaction (qPCR) provides a particularly useful tool for understanding the pathways being activated, by enabling the researcher to measure the expression of different proteins, described in Section 2.6.1.

To direct differentiation of MSCs, understanding the biological signalling pathways specific to each lineage and the proteins they induce are critical. Of key note for osteogenic pathways in MSC differentiation are the Runt-Related Transcription Factor 2 (RUNX2) pathway and the alkaline phosphatase (ALP) pathway³⁰⁸. RUNX2 has been shown to be critical to osteoblast differentiation of MSCs³¹⁰. The RUNX pathway works through the formation of a heterodimer of one of the RUNX proteins forming a heterodimer with the core binding factor β , after which the dimeric transcription factor will translocate to the nucleus, and bind the Runt sequence, beginning transcription of relevant proteins. Of this pathway, RUNX1 is important for chondrogenic cartilage matrix synthesis and haemopoietic stem cell differentiation^{311,312}, RUNX2 is key in differentiation into osteoblasts and chondrogenic cells³¹³, and RUNX3 is needed for epithelial, neural and chondrogenic differentiation³¹³⁻³¹⁵. The ALP pathway is critical for differentiation of BONE MARROW MSCs into osteoblasts, and are an essential part of bone mineralisation, with MSC-specific knockouts showing hypophosphatasia, showing the criticality in MSCs specifically. ALP is involved in the phosphorylation of GSK3 β by binding LRP6, altering the WNT/ β -Catenin pathway and enabling lineage switching into osteoblasts. Therefore, these are critical genes for examining osteogenic differentiation of MSCs, and potential of treatments for directing differentiation from this sclerotic phenotype noticed. As additional gene involved in osteogenesis is VEGF, which indirectly mediates ossification by angiogenesis, or blood vessel formation, as such is also commonly expressed in MSCs³¹⁶.

Whilst critical for osteogenesis, ALP has also been cited as a marker for general differentiation, with aged cells showing low expression not being able to differentiate^{282,283,317}. Increased expression of ALP suggests a greater capacity and inclination for MSCs to differentiate, and so whilst foremost marks osteogenesis, may also describe differentiation capacity, as seen in Chapter 4, with ALP expressing cells still undergoing chondrogenesis.

For chondrogenesis, critical pathways include the Transforming Growth Factor Beta (TGF β) and SRY-Box Transcription Factor 9 (SOX9) pathways, as well as expression of Collagen 2 (COL2A), Aggrecan (ACAN) and Cartilage Oligomeric Protein (COMP), all of which being driven by the SOX9 pathway³¹⁸⁻³²⁰. The SOX9 pathway is considered the master pathway for chondrogenesis, being the primary regulator of chondrogenic differentiation and maintaining cartilage and preventing transition to bone. TGF- β is also critical in this process, but is closer linked to maintaining cartilage over initiating chondrogenesis³¹⁹. This is also critically involved in many other processes such as the cell cycle and apoptosis³²¹. In terms of articular cartilage in MSCs TGF β 3 prevents terminal differentiation of chondrocytes from MSCs to prevent movement towards bone³¹⁹. This could potentially provide reasons for why microfracture eventually leads to fibrocartilage formation, as terminal differentiation was occurring.

The last pathway, adipogenesis, was determined by the previous chapter to be less important in the talus, considering the reduced level of adipocyte differentiation, but is still important in terms of the tibia, as fat formation within a region where cartilage regeneration is being attempted would disrupt any growth. For MSCs, the key signalling pathway is the Peroxisome Proliferator Activator receptor gamma (PPAR γ) pathway, which allows formation of adipocytes from pre-adipocytes. A knockout of PPAR γ prevents any adipocyte formation, whereas knockout of other pathways does not prevent adipogenic differentiation by PPAR γ ³²². Secondly is FABP4, which allows the maturation of these adipocytes. As such, both of these are excellent gene targets for identifying fat formation.

When testing gene expression of MSCs, there is still need for additional markers outside for key differentiation pathways. Firstly, a "housekeeping" gene is required. This is defined as a gene which is expressed at the same level despite the conditions it is placed in. As such for this work, it was important that the different conditions wouldn't have an effect, as such HPRT-1 was chosen, as it is used in the majority of similar studies^{219,291,323}. Additionally, to ensure there was remaining MSCs, CD90 was measured (as in Flow cytometry work, Figures 4.1.9-10) as a surface marker of MSCs which had already shown CD90 expression and lack of negative markers which would indicate other cells present. Lastly, as uncultured MSCs were used, CD45 was also assessed, as a key surface marker of immune cells.

Overall, there is strong literature upon the general process of MSC differentiation, if not to a point where it can be directly controlled. The previous paragraphs show key genes required for MSC differentiation, and potential targets to investigate the lineages being induced by different stimuli. Next was to determine how best to direct MSCs away from this apparent bone-directed differentiation as seen in the previous chapter, towards a chondrogenic, reparative phenotype. As there is potential for these MSCs to already be directed towards bone synthesis, preconditioning was chosen to shift this to a chondrogenic phenotype. This has recently become a common technique in MSC treatment, with extensive literature^{320,323-325}. Key strategies have included hypoxia, pharmacological agents and mechanical conditions. Hypoxia is used as resident MSCs inside niches are kept at 1-5% O₂ before being exposed to higher conditions in the general culture environment (20% O₂)³²⁶. Preconditioning of MSCs in hypoxia has shown increases in both proliferation, motility and differentiation capacity, however the latter only when in their micro-environment of umbilical cord MSCs^{323,325}. Pharmacological agents for chondrogenic preconditioning employed most recently include both Platelet Rich Plasma (PRP) (or its derivative, platelet lysate (PL) and Kartogenin (K))^{134,141,142,194,324}. To isolate PRP, blood is taken from the patient with an anti-coagulation agent added to prevent clotting. This is then centrifuged once to separate the blood into three layers, the upper (lightest) layer with mostly platelets and white blood cells, a second layer called the buffy coat, that is rich in white blood cells, and a bottom layer (heaviest) which is mostly red blood cells. Either the first or first and second layers are transferred to a new tube, and then this mix is centrifuged again to concentrate platelets and white blood cells, with any remaining plasma above (termed platelet-poor plasma) removed. Pellets are then homogenized in ~ 5 ml of plasma to create PRP. This is demonstrated in Figure 5.1.1. For use in the lab, this undergoes 3 rounds of freeze-thawing to lyse the platelets, and release any growth factors within. This enables long term storage as well as potentially increased growth factor content, however this was only shown for VEGF, TGFβ1, PGDF-AB and bFGF¹³⁶. Preparation of both PRP and PL is not always consistent, as some preparations use different centrifugation steps or different amounts of plasma to mix the pellet in, and for PL there is different freeze-thawing temperatures. As such it is essential that when using PRP or PL that the composition that shows the best benefits for the researchers aim is chosen, and that there is sufficient volume for the entirety of the

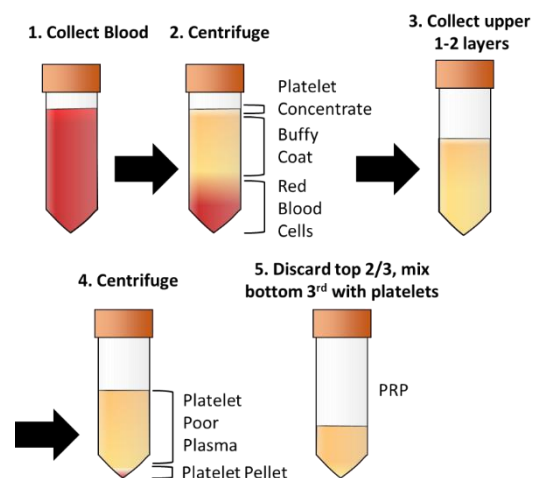


Figure 5.1.1 Extraction of PRP from human blood. An anti-clotting agent including EDTA is added to blood to prevent clotting.

experiment¹³⁶. PL preconditioning of MSCs has previously shown enhanced chondrogenesis of synovial fluid MSCs from the hip in pellet culture, as well as, as well as significantly enhancing chondrogenic potential of MSCs by 1-3-fold during 3D treatment after preconditioning^{138,140,327,328}.

The second stimulant mentioned was K. This is a small heterocyclic molecule shown to increase chondrogenesis by binding Filamin A, a protein which usually binds to actin. This displaces CBF β from its cytoplasmic binding site, allowing it to move to the nucleus and begin the RUNX1 pathway, which as earlier mentioned directs MSCs towards chondrogenesis. As this is specific, there is potential for RUNX2, which has been implicated as a driving factor of OA, being downregulated, leading to reduced osteogenic differentiation^{141,329}. As such this drug shows potential for both inhibiting osteogenesis and promoting chondrogenesis, the exact aim of this research. K preconditioning has shown significantly reduced expression of osteogenic-related genes (Collagen X and MMP13), as well as increased SOX9, aggrecan and collagen 2 compared to TGF β treated cells³²⁴. Additionally, a second study found that 10 μ M K also increased proliferation 2-fold relative to standard 10% FBS MEM medium whilst also increasing chondrogenic potential by collagen 2 and aggrecan deposition in an osteochondral explant relative to human bone marrow MSCs without K³³⁰.

Additional to stimulants used, it was also important to conduct experiments in media devoid of any xenogeneic materials, including FBS, to mimic cell environments and be closer to *in vivo* conditions. Typical *in vitro* growth serum includes FBS, which is derived from its namesake, bovine foetuses. Research has already shown that the use of human serum (HS) instead of FBS increases proliferation, although evidence suggests it does not affect surface marker expression or differentiation capacity^{331,332}. Stimulants PL and K were added to media containing HS, and media with HS alone was used as a control. ChondroDIFF® (C) was used as a positive control to study MSC chondrogenic progression.

This chapter aims to develop a method of preconditioning MSCs for chondrogenic differentiation in 2D, and investigate the effects, if any, of K, PL and hypoxia upon MSC behaviour. Osteogenic and adipogenic gene expression were additionally measured to observe and reciprocal relationships to chondrogenesis. It was expected that MSCs would have elevated expression of chondrogenic genes and reduced expression of osteogenic genes under hypoxia, K and ChondroDIFF (C) pre-treatment, whilst PL-treated MSCs would show less specific increases that may be further enhanced by 3D treatment.

Specifically, this chapter will:

- Develop a novel methodology for 2D preconditioning of MSCs towards chondrogenesis and test if histological methods show reliable results compared to gene expression
- Investigate changes to MSCs behaviour during culture after 2D treatment with stimulants including K, PL and Hypoxia

Objectives:

- Develop methods to stimulate MSCs in 2D for preconditioning and investigate changes to morphology, ALP-expression and gene expression levels
- Test the effectiveness of controls, using 10% HS in DMEM as an unstimulated control, C as a positive chondrogenic control, and SM as a negative control for chondrogenic preconditioning in 2D
- Elucidate the effects of 10 μ M K, 50 μ M K, 10% PL, and hypoxia upon MSC differentiation capacity by ALP staining
- Investigate the changes to the expression of osteogenic, adipogenic and chondrogenic critical genes after preconditioning using qPCR

5.2. Methods

5.2.1. Sample Information

For method development, uncultured IC MSCs from patients undergoing orthopaedic surgery for metal removal following previous fracture were used, who were otherwise healthy with informed consent and ethical approval. Samples used in this chapter are in Table 5.2.1. These samples were from prior work as such were revived from frozen as explained in 2.5.6.

Table 5.1 Donor Information for MSCs used in Preconditioning Experiments

Donor	Donor Age	Sex
GCBM011	28	M
BM140207	19	M
TRBM010	44	F
BM213	50	F
BM313	42	M
RC071	35	F
Average	28	1:1

5.2.2. Choice and Development of Biological Stimulants

5.2.2.1. Pooled Human Serum

HS was collected and pooled to create a large volume of serum with identical properties, as performed elsewhere³³². Blood was collected from patients undergoing orthopaedic surgery for metal removal following prior fracture who were otherwise healthy, with informed consent and ethical approval. Blood was allowed to clot for 30 minutes, and then centrifuged at 15 minutes at 400 G to separate the serum from blood cells, and then serum collected. Table 5.2.2 shows donor information.

Table 5.2 Donor Information for Pooled Human Serum

Donor	Donor Age	Sex
HCOA1	46	M
HCOA2	49	M
HCOA3	27	F
HCOA5	23	F
HCOA7	40	M
HCOA8	35	F
HCOA9	42	F
Average	37	3M:4F

5.2.3. Design of Culture Process

To assess if preconditioning of MSCs with chosen conditions was beneficial for chondrogenesis, IC MSCs were treated with chosen biological stimulants and tested. This was performed in a 6-well plate due to the ease of imaging and for performing replicates, as well as allowing sufficient cell growth for 14-day experiments and follow up assays. Basal media chosen was low glucose DMEM to mimic the environment of native chondrocytes, with 10% human serum (HS). ChondroDIFF® (C) was chosen as a positive control as used in chapter 4 for chondrogenesis. SM was used as a negative control, as it is used to ensure MSCs do not spontaneously differentiate during culture. K and PL were used as test biological stimulants as discussed in the introduction, for their reported ability to increase chondrogenesis, and K's ability to suppress osteogenesis^{141,143,327} (Section 5.1). PL and K were both prepared in DMEM with 10% HS. Lastly, hypoxia was considered as resident chondrocytes are in low oxygen conditions, at around 2% oxygen concentration, compared to the 5% oxygen concentration used in the laboratory³²⁵.

These MSCs were fed with basal media. Each media also contained 1% P/S to prevent infection.

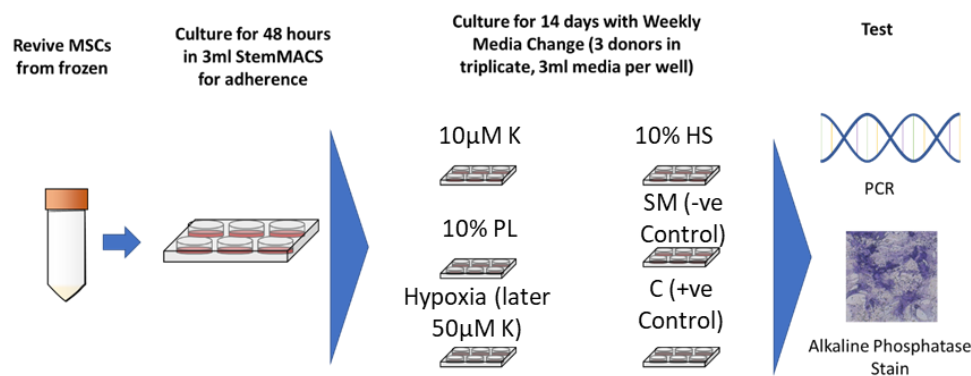


Figure 5.2.1 Preconditioning methodology including revival, adherence, culture and testing steps.

Media are given in Table 5.3, and the general experimental process is outlined in Figure 5.2.1.

Table 5.3 Culture Condition Shorthand and Media Composition

Media	Shorthand	Control
Low Glucose DMEM with 1% P/S	Basal Media	Test
10% PL in basal media with 10% HS	PL	Test
10 µM K in basal media with 10% HS	10 µM K	Test
50 µM K in basal media with 10% HS	50 µM K	Test
10% HS in basal media (1% P/S)	10% HS	Basal media control
ChondroDIFF (1% P/S)	C	Positive Control
StemMACS(1% P/S)	SM	Negative Control

Frozen, uncultured MSCs extracted from human IC samples were revived (as in Section 2.4.8) into 1.5 ml of pre-warmed DMEM with 10% FBS. MSCs were seeded in triplicate wells for each condition, with 5×10^5 cells per well. This was counted as in Section 2.5.2. To each well, 2 ml of StemMACS media was added before thawed cell suspension was added, and left for 48 hours for MSCs to adhere. Media was then removed, wells washed with PBS, and respective media added (Given in Table 5.3). Wells were cultured for 14 days in 3 ml of respective media, with a half change twice a week. Subsequently, 1 well was used for qPCR to investigate changes in gene expression (Sections 5.2.9-5.2.116), and the other two wells were stained with alkaline phosphatase followed by toluidine blue to investigate changes in ALP expression and estimate differentiation potential (Sections 5.2.6-5.2.8). Hypoxia culture is explained Section 5.2.4.

5.2.4. Culture in Hypoxia

Hypoxia was used to mimic *in vivo* conditions in cartilage. Hypoxia creates a key challenge to maintain the low oxygen environment throughout the whole experiment. Whilst key technology exists, access to a full hypoxic station was not possible for this project. Hypoxic culture was performed using an incubator which maintained oxygen concentration at 2% and other conditions the same as normal (37°C, 5% CO₂), as used in similar work³³³. Cultures were briefly removed from hypoxia for media changes (twice per week) and images captured (once per week). Media was prepared prior to media changes to minimise the time spent. The hypoxic incubator was not opened outside of media changes and imaging as this would briefly change internal conditions. Ideally, use of a hypoxic tissue culture hood would have been available to maintain hypoxia during media changes to maintain a constant hypoxia environment, but this was unavailable. Following 14 days in culture, cultures were tested, with cultures fixed or lysed before normoxia of cultures.

5.2.5. Imaging

Live cells imaging and well-plate scans were performed as described earlier (Section 2.7.3).

5.2.6. Alkaline Phosphatase Staining

Alkaline phosphatase staining was performed as earlier described (Section 4.2.7.2). This was chosen as ALP is routinely used for assessing osteogenic differentiation capacity of MSCs (Fig. 4.3.11). High basal level ALP staining has also however been associated with MSCs with higher differentiation capacity, without addition of differentiation medium (Section 2.3.2). This is a method designed by another group that was tested here to develop a method of investigating differentiation early on, whereas this group used it to investigate general differentiation capacity²⁸². This was additionally followed up with colony analyses to understand differences between conditions, and toluidine blue analysis to examine whole colony structure, where feasible. ALP staining of hypoxic treated cells detached from the plate, as such images are not shown. As hypoxia did not show benefit by qPCR, it was not repeated.

5.2.7. Toluidine Blue

Toluidine blue was used to stain whole colonies, as it stains the background of all cells blue. This was used over methylene blue due to the fixation method. Toluidine blue is used as a standard method for cell colony area analyses³³⁴. MSCs were stained with toluidine blue after ALP, by adding 1 ml of 0.1% toluidine blue in dH₂O for one hour. This was then washed 3 times in dH₂O, until washes were clear.

5.2.8. Cell Size Analysis

Analysis of cell size was investigated based on previous chapter work showing key changes in MSC morphology, potentially relating to osteogenic precommitment⁸⁵. A rudimentary analysis of cell size and shape was performed, as elsewhere³³⁵. From each culture, 3 images were captured at random and analysed. Scale was set using the set scale function from the scale bar on each image. In each image, 5 cells were chosen to be measured, for 15 replicates per donor. Manually, the line function was used to draw a line between the longest edge-to-edge distance of the cell, and this was defined as cell length. Another line was drawn perpendicular to this between the edges of the cells, and defined as the cell width.

5.2.9. Colony Analysis

Colony area analysis and integrated density was performed as earlier (Section 4.2.4-4.2.5), for both ALP and for toluidine blue stains. Area and integrated density were measured, however as seeded cell number was unknown, and PL colonies merged, colony number was not recorded. To further investigate ALP activity as a proportion of total cell number, toluidine blue area as well as integrated density was divided by the respective ALP value for each donor and multiplied by 100 to calculate ALP positive area of total area (or integrated density).

Table 5.4 Genes Measured by qPCR of Preconditioned Samples

Gene	Full Name	Function
ALP	Alkaline Phosphatase	Osteogenesis
RUNX2	Runt-Related Transcription Factor 2	Osteogenesis
FABP4	Fatty Acid Binding Protein 4	Adipogenesis
PPARG	Peroxisome Proliferator Activator Receptor γ	Adipogenesis
SOX9	SRY Box 9	Chondrogenesis
HPRT	Hypoxanthine Phosphoribosyltransferase-1	Housekeeping Gene
COL2A1	Collagen 2 α 1	Chondrogenesis

ACAN	Aggrecan	Chondrogenesis
COMP	Cartilage Oligomatrix Protein	Chondrogenesis
VEGFA	Vascular Endothelial Growth Factor α	Angiogenesis
PTPRC (CD45)	Protein Tyrosine Phosphatase, Receptor Type C	Immune Cell Marker (Regulates cell growth and differentiation)
THY-1 (CD90)	Cluster of Differentiation 90	Marks some stem cells

5.2.1. Real-Time Reverse Transcribed Polymerase Chain Reaction

Methods are given in Sections 2.6.1-2.6.5. Genes assayed in this chapter are given in Table 5.4.

5.3. Results

5.3.1. The Effects of Short-Term Stimulant Effect Upon IC MSC Behaviour

Chapter 4 showed that talar and tibial MSCs have elevated chondrogenic potential to IC MSCs, however chapter 3 results suggested that MSCs were directed within the body to differentiate towards osteogenesis. In this chapter, experiments were undertaken to develop a method of investigating MSC differentiation to see if talocrural bone marrow MSCs could be directed into chondrogenesis instead, and the possibility of reducing osteogenesis, using IC cells as a model for experimental design. IC MSCs are often chosen for expansion *ex-vivo* and transplantation, and this chapter will also inform on the effects of PL, K, hypoxia, and HS in 2D culture.

MSCs were imaged through culture to study growth behaviour, with Fig.5.3.1 showing MSCs at day 7. Whilst originally thought 2D culture method of the same MSCs would not present changes, there were some visibly clear differences. Controls 10% HS and SM both showed dense colony formation with typical fibroblast-like MSC shape (i), with the same seen in 10 μ M K, PL and hypoxic cultures, whereas 50 μ M K cultures showed loose colonies and poor growth (ii).

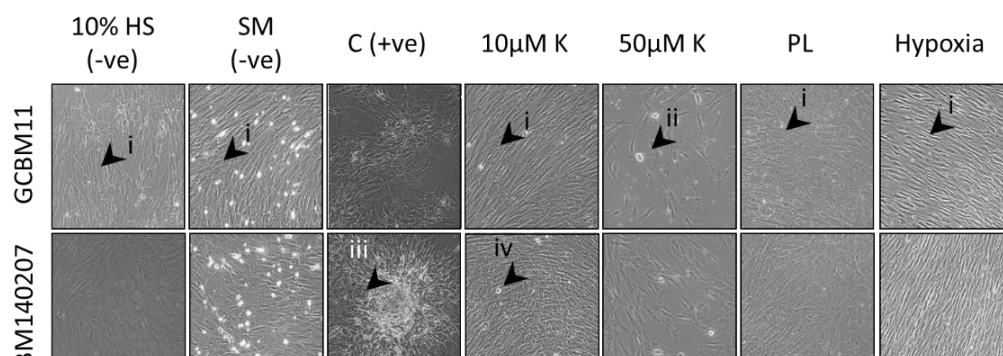


Figure 5.3.1 Effects of Different Biological Stimulants upon Cellular Morphology After 7 Days Preconditioning. i Dense MSC colony, ii Sparse colony structure, iii multi-layer MSC nodule-like formation, iv MSC pre-nodule formation v- Loose colony-edge. vi – tight colony-edge. Images captured at 10x magnification, colony edge is GCBM011. Scale bar is 200 μ M

MSCs treated with C showed rounded cells, and rare colonies with nodule-like formation, forming a round multi-cell layer structure (iii). 10 μ M K preconditioned MSC cultures additionally showed early evidence of nodule formation with multi-cell layer regions, seen in other work of chondrogenesis (iv)³³⁶. Colony boundaries were loose in 10% HS, SM and 50 μ M K cultures (v), but tight in C, 10 μ M K, PL and hypoxic cultures(vi). These results support 10 μ M K for preconditioning, showing MSCs most closely mimicking C-preconditioned cultures. To further understand potential differences biological stimulants, MSC cell size was next quantified.

MSC shape varies depending on the length of culture, as well as culture medium and the serum chosen. MSC shape shows links with differentiation precommitment, as such quantifying changes can provide some information on the effects of different biological stimulants and media. Firstly, images were captured under higher resolution to investigate the cells themselves (Fig. 5.3.2A). Of controls, SM showed elongated fibroblast-like structure and were relatively thin (i) compared to C treated MSCs which were far rounder (ii). Other treatments were somewhere between the two, however MSCs treated with 50 μ M K were much flatter with multiple projections (iii). Quantification MSC circularity (Fig. 5.3.2B) showed C-treated MSCs were the most round, being significantly more so than each other condition ($p < 0.02$). Controls SM and 10% HS showed the least round MSCs, representing the fibroblast-like shape seen. Of treatments, 10 μ M K and PL preconditioned MSCs were around 2-fold more round than than 50 μ M K or hypoxic cultures, significantly more so for PL MSCs ($p = 0.0152$ for both). Hypoxic and 50 μ M K treated MSCs mimicked the negative control, SM (Fig. 5.3.2B). Overall, MSCs preconditioned with PL or 10 μ M K retained the most similar morphology to C. After culture had finished, differentiation capacity was analysed.

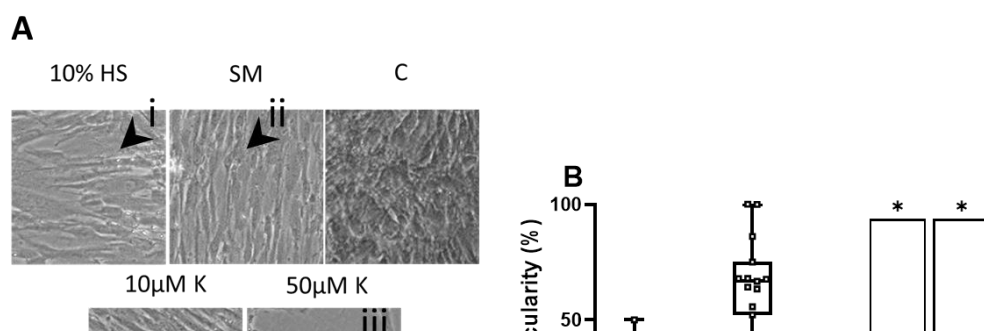


Figure 5.3.2 The Effect of Different Biological Stimulants Upon MSC Circularity after 7-day culture. A MSC morphology under higher magnification. i Thinner, more fibroblast-like morphology –. ii –rounded MSC morphology B MSC circularity. Circularity was calculated from height and length measurements 5 MSCs of 5 images for 15 replicates, of 3 donors. Technical replicates are shown. Median and interquartile range with all data points is presented. A Friedmann test of biological replicates identified no significant differences. Significance was set at * $p < 0.05$. C was significantly greater than each other condition ($p < 0.02$).

After 14 days, samples were removed from preconditioning culture and investigated for differentiation capacity. Firstly, MSCs were stained for ALP, as a rough estimate of differentiation potential, based on findings of similar literature showing ALP is critical to differentiation of MSCs (Fig. 5.3.3)²⁸². Hypoxic-treated colonies lifted off the plate during staining, and so are not included. All cultures stained positively for alkaline phosphatase. C-treated MSCs presented many small colonies, whereas other treatments showed high ALP expression and many colonies, with almost full confluency in PL-treated cells. All conditions expressed ALP, showing they retained the osteogenic marker. However, comparison to the colony as a whole is required to understand how many cells are or are not expressing ALP. As such, plates were next examined under a microscope to better see the proportion of cells producing ALP.

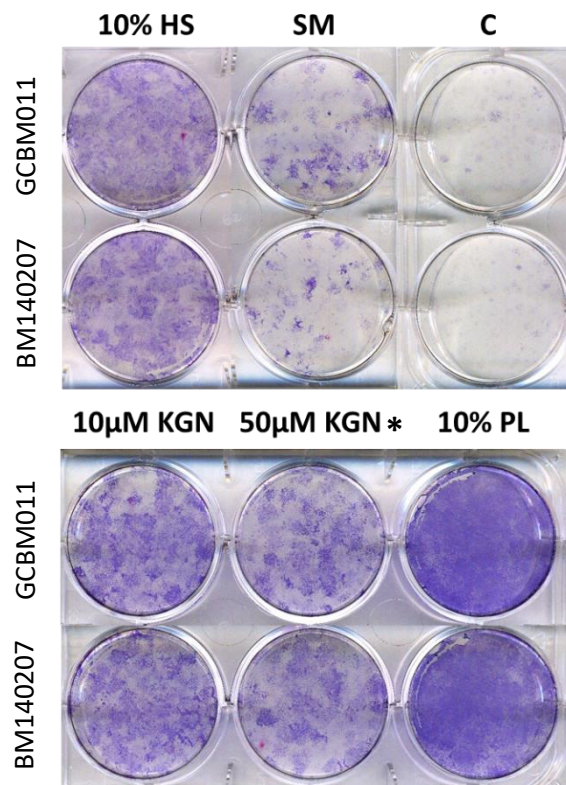


Figure 5.3.3 Changes in ALP Expression by IC MSC Colonies after 14 Day Preconditioning with Different Stimulants as a Comparator for Differentiation Capacity. Representative images from 2 donors are shown. * - 50µM K shows donors are BM213, BM313 respectively.

Microscopy images of ALP staining mostly showed similar cell structures to what was seen at day 7 (Fig. 5.3.2), with 10% HS, SM and hypoxia treated colonies being dense with thin, long cells, and C or 10 μ M K treated MSCs showing slightly rounder cells (Fig. 5.3.4). PL-treated cells showed more rounded cells at this stage, and 50 μ M K treated MSCs again showed the flattened, spread out structure. Of the treatments, C, 10 μ M K and PL treated MSCs showed the darkest staining visible in most cells, suggesting higher ALP expression. SM-treated cells and hypoxic treated cells had the least staining, potentially suggesting these treatments are inhibiting ALP expression. The next step was to quantify overall colony structure and integrated density to investigate relative ALP expression per colony.

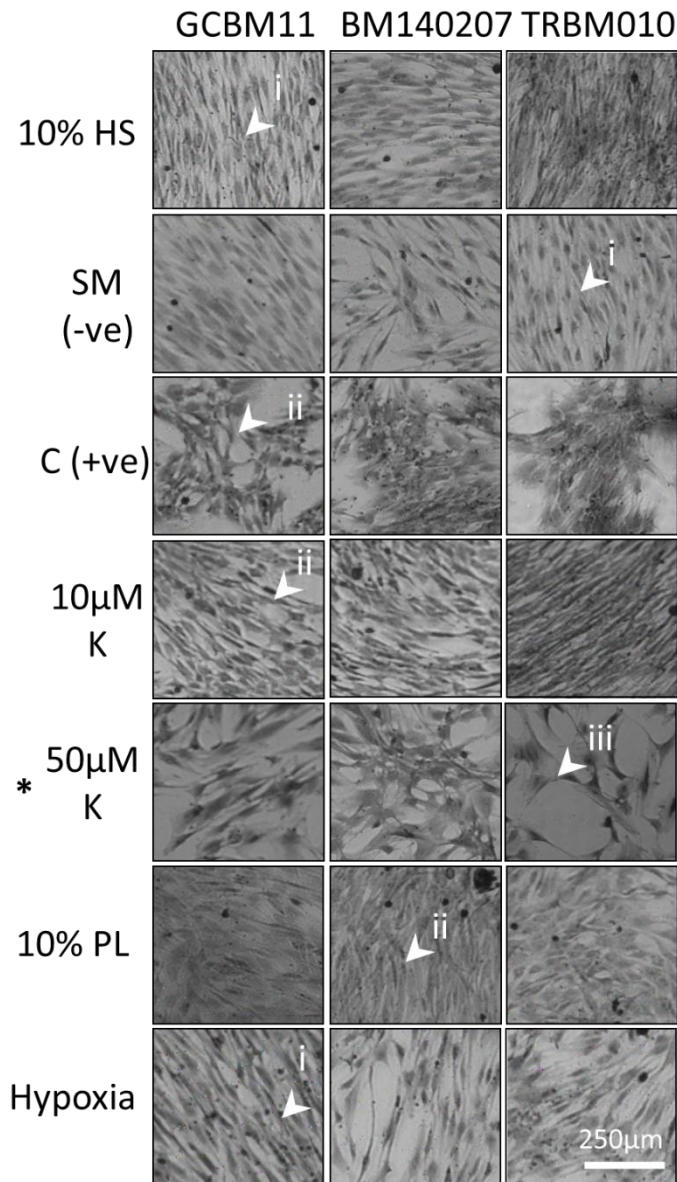


Figure 5.3.4 ALP Staining of MSCs after Preconditioning in Various Biological Stimulants Under Microscope (N=3). i – fibroblastic MSC morphology. ii – rounded morphology MSCs. iii – Flattened, spread out MSC morphology. Images were taken at x100 magnification. * For 50 μ M K the three donors are BM213, BM313 and RC071 respectively.

Integrated density was utilised earlier in this work to investigate MSC colonies stained by methylene blue (Fig. 4.3.7). In this case, relative ALP-positive density should reflect the intensity of ALP staining in each colony. This was performed on scans of the 6-well plates (Fig. 5.3.3). Of controls, SM showed the lowest integrated density, reflecting its typical role to prevent spontaneous MSC differentiation in culture. MSCs treated with 10% HS had the highest integrated density, around 50-fold higher on average than SM treated MSCs and was significantly greater than C colonies ($p=0.04$). Treatments 10 μ M and 50 μ M K treated MSCs had around 10-fold higher integrated density than C-treated MSCs. PL-treated colonies were of similar integrated density to C. These results suggest that 10% HS and K treated MSCs greatly express ALP, and may be slightly more osteogenic than PL. To detect differences in all MSCs and not just ALP positive cells, MSCs were subsequently stained with Toluidine Blue to see the effect on colonies overall.

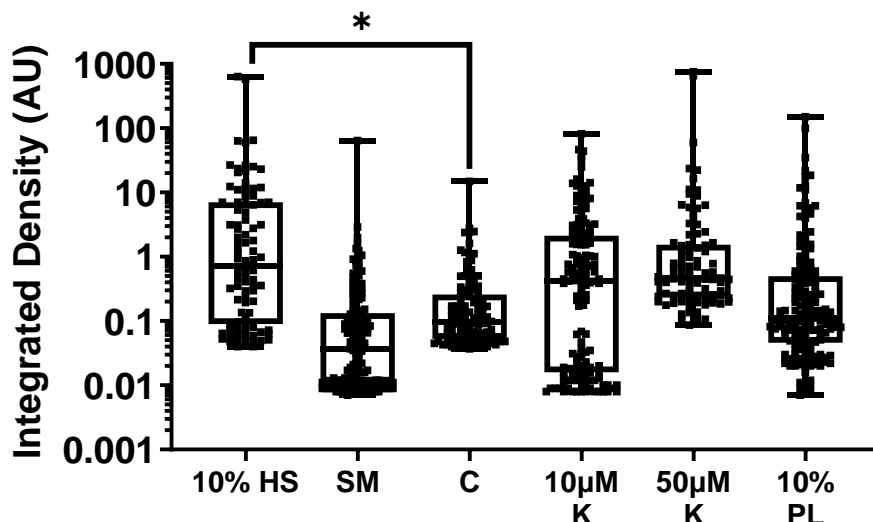


Figure 5.3.5 Comparison of ALP-Positive MSC Integrated Density Between IC MSCs Treated with Different Stimuli. Median, interquartile range and range is shown with all datapoints. Data shows each individual colony measured from 3 donors, with median and interquartile range. Data was compared using the non-parametric unpaired Kruskal-Wallis test with Dunn's multiple comparisons test on biological replicates. * $p < 0.05$.

To fully visualise colonies, toluidine blue was used to stain ALP-stained colonies (Fig. 5.3.6). Colonies were now more visible, and showed that other than C treated cultures, most conditions were fully confluent, with overlapping colonies. Again, C-treated MSC colonies were smaller with many spread out colonies. Colonies treated with 50 μ M K and SM were slightly more spread out and less confluent than other conditions, suggesting slower growth rates. PL and 10% HS treated colonies were the most confluent, suggesting the highest growth rates. The far higher SM staining compared to ALP suggests a reduced tendency for differentiation. Overall colony area and density was next quantified to investigate the effects of different treatments on MSC colony structure.

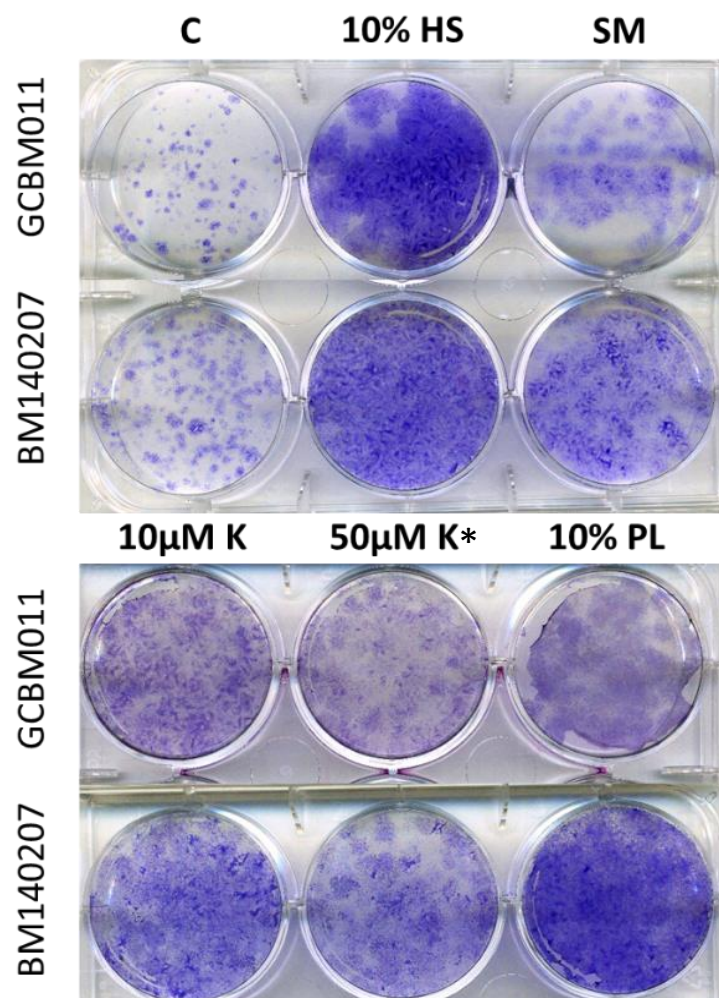


Figure 5.3.6 Toluidine Blue Staining of ALP-Stained IC MSC Colonies after 14 Day Stimulation with Various Biological Stimulants. For each condition 2 donors are shown. * - 50 μ M K images are from donors are BM213, BM313.

Changes in colony structure demonstrate the effect on MSCs of utilised conditions. Larger colonies suggest high proliferation, whereas dense colonies suggest reduced motility, both of which will affect the quality of tissue formed. Results will have been affected by the extent of merged colonies, but integrated density will still reveal, to an extent, relative differences in MSC number between colonies. Generally, colony area was similar in 10% HS and C controls, and remained similar in PL-treated MSCs also. SM colony area was higher, but 10 μ M K and 10% PL colonies were the largest by 50-fold of 10% HS controls (Fig. 5.3.7A). This will likely have been affected by colony overlapping however, and so the true increase is likely less. Integrated density was similar in each control, as well as 50 μ M K-treated MSCs. Similar to colony area, integrated density was higher in 10 μ M K treated samples, but highest again in PL-treated cultures, being 8-fold higher than controls (Fig. 5.3.7B). To directly compare ALP expressing MSCs as a portion of total and colony size between each treatment, ALP area as a proportion of Toluidine Blue area was measured as a final comparison.

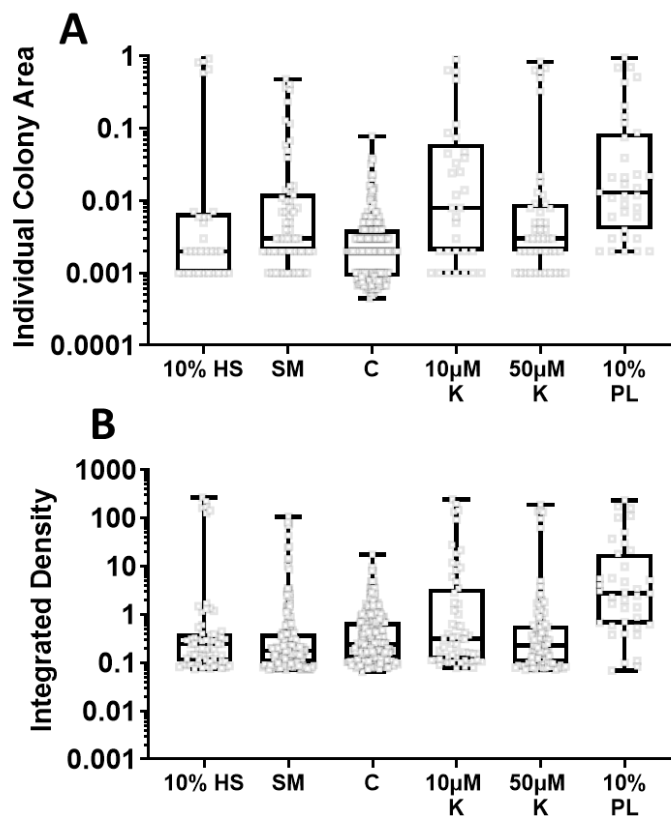


Figure 5.3.7 Quantification of Toluidine Blue Stained MSC Colonies Between IC MSCs Treated with Different Stimuli. A MSC Colony Area of after 14-day culture with different treatments. B Integrated density of MSCs after 14-day culture with different treatments. Median and interquartile range is shown with all datapoints. Data shows each individual colony measured from 3 donors.

By measuring ALP area as a proportion of total colony area by toluidine blue staining, a more accurate measure of relative differentiation capacity estimation could be established, by directly comparing ALP+ MSCs of total MSCs. As in ALP-only integrated density (Fig. 5.3.5), SM treated colonies had the lowest ALP+ proportion, being significantly lower than all other treatments except 50 μ M K (Fig. 5.3.8). Most treatments had around 60% ALP area of total colony area, including DM, 50 μ M and 10% PL treated cultures. The highest average ALP expression was by 10 μ M K treated MSCs at around 75.6%, followed by C-treated MSCs at 64.6%. This method appeared to show the results expected, as well as positive results for the biological stimulants of interest by cell structure, colony area and ALP expression. However, as this is a new method, further validation was required to see if these results were accurate. As such, the relative changes in gene expression was next investigated.

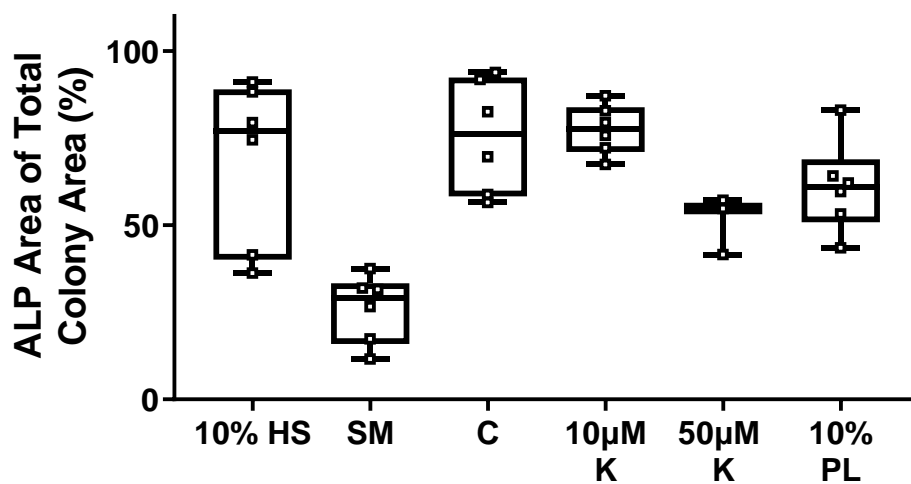


Figure 5.3.8 Assessment of ALP Colony Area of Toluidine Blue Area to Estimate Relative Differentiation Potential of MSCs after Preconditioning in Different Media. Data points show whole well results for each donor and interquartile range. As 50 μ M K was only performed on 3 donors there is only 3 results. Data shows median and interquartile range with all data points.

5.3.2. The Effect of Biological Stimulants Upon MSC Gene Expression

By investigating relative gene expression, the effects of the different treatments upon MSCs grown in 2D culture could be quantified down to the signalling level for genes specific to MSC lineage-switching. As such, this is the only method of testing if chondrogenesis can be upregulated and osteogenesis downregulated in 2D cultures. As a first step, RNA needs to be isolated from cultures to be converted into cDNA for analysis. Relative RNA yield shows that MSCs remained transcriptionally active, and so is demonstrated first.

As a reminder, this experiment was run twice, with hypoxia being removed in the second run as using the hypoxic incubator was impractical and cells lifted in ALP stains. Instead, 50 μ M K was added as a condition. This means there are 3 cultures from 50 μ M K and Hypoxia, and 6 for the remaining conditions. The total amount of RNA isolated is shown in Figure 5.3.9. Cultures from all stimulants remained transcriptionally active, with similar RNA being retrieved from each culture. The 50 μ M K sample had 1.3-1.5-fold RNA of other conditions. This RNA was next taken to be investigated for differences in gene expression, starting with chondrogenesis, as the main target of this work is to develop potential candidates for cartilage repair therapies.

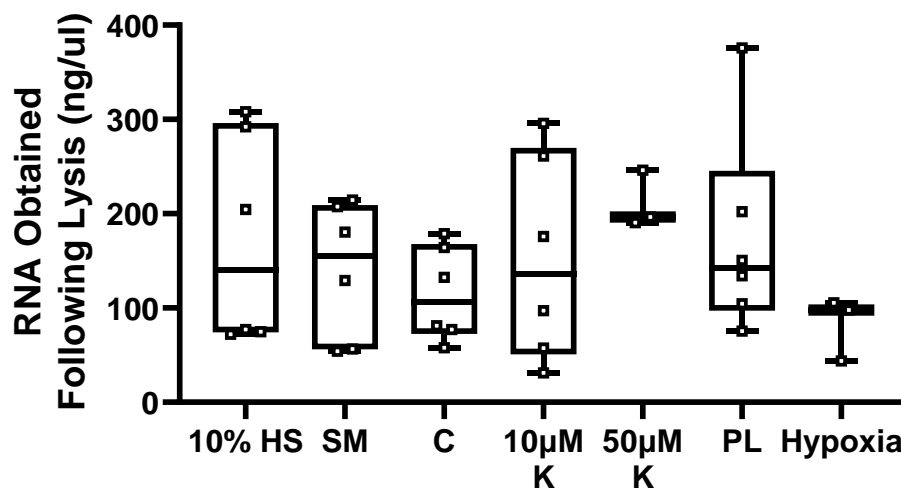


Figure 5.3.9 Estimation of Isolated RNA Concentration Following Preconditioning in Various Biological Stimuli (N=3). Box plots show median and interquartile range.

First, qPCR was used to investigate chondrogenic gene expression (Fig. 5.4.10). Overall, no single condition created the highest increase in chondrogenic expression for every transcript chosen (Fig. 5.4.10A). As expected, C showed the highest expression of COMP, SOX9 and COL2A1, by 4-fold, 2.2-fold, and 0.5-fold increases respectively of SM, the negative control, with 10% HS between the two. However, C showed no apparent increase in ACAN expression, whereas 10 μ M K showed a 2.5-fold increase, and was the only treatment to increase compared to SM. COMP, COL2A1 and SOX9 expression was similar in 10% HS, and all three treatment groups. Neither hypoxia nor 10% PL showed increased expression in any gene on the negative control. Hypoxia also showed an 8-fold decrease in COMP compared to the negative control.

For donor specific trends in COMP, C-treated MSCs showed a stable increase in COMP, of 4.5-fold the housekeeping gene for all donors (Fig. 5.4.10B). Donor GCBM11 showed increased in COMP expression by each biological stimulant, likely due to the 28-year old donor having highly chondrogenic MSCs. For the other 5 donors, there was a consistently lower expression in all test conditions of around 5-fold, other than the 8-fold reduction seen in hypoxic treated MSCs.

For the most part, ACAN expression was identical in all treatment medias with stable behaviour between each donor, suggesting that all controls did not affect its expression (Fig. 5.4.10). However, in all 6 donors there was an increase in 10 μ M K compared to the positive control with a 2.5-fold increase on the negative control.

Expression differences in COL2A1 were again stable between each donor, with expression increasing in 5 of 6 donors in C-treated MSCs relative to SM-treated MSCs, averaging a 4-fold increase (Fig. 5.4.10D). MSCs treated with 10 μ M K showed only a 1.1-fold increase on SM-treated cells.

Lastly, SOX9 expression showed increased expression in the highly chondrogenic donor in 10 μ M K. However, there was no clear trends in other conditions or donors for SOX9 expression. As such it seems apparent that SOX9 was not greatly altered in 2D conditioning (Fig. 5.4.10E).

Overall results confirm that C is the most effective at enhancing chondrogenic gene expression in 2D, however 10 μ M K does increase ACAN, a major component of cartilage, where C did not show an increase. Additionally, PL showed similar chondrogenic response to the positive control in 3 of 4 genes, as such does show efficacy. As it was hoped these biological stimulants could also suppress sclerosis seen in the OA environment, osteogenic gene expression was next investigated.

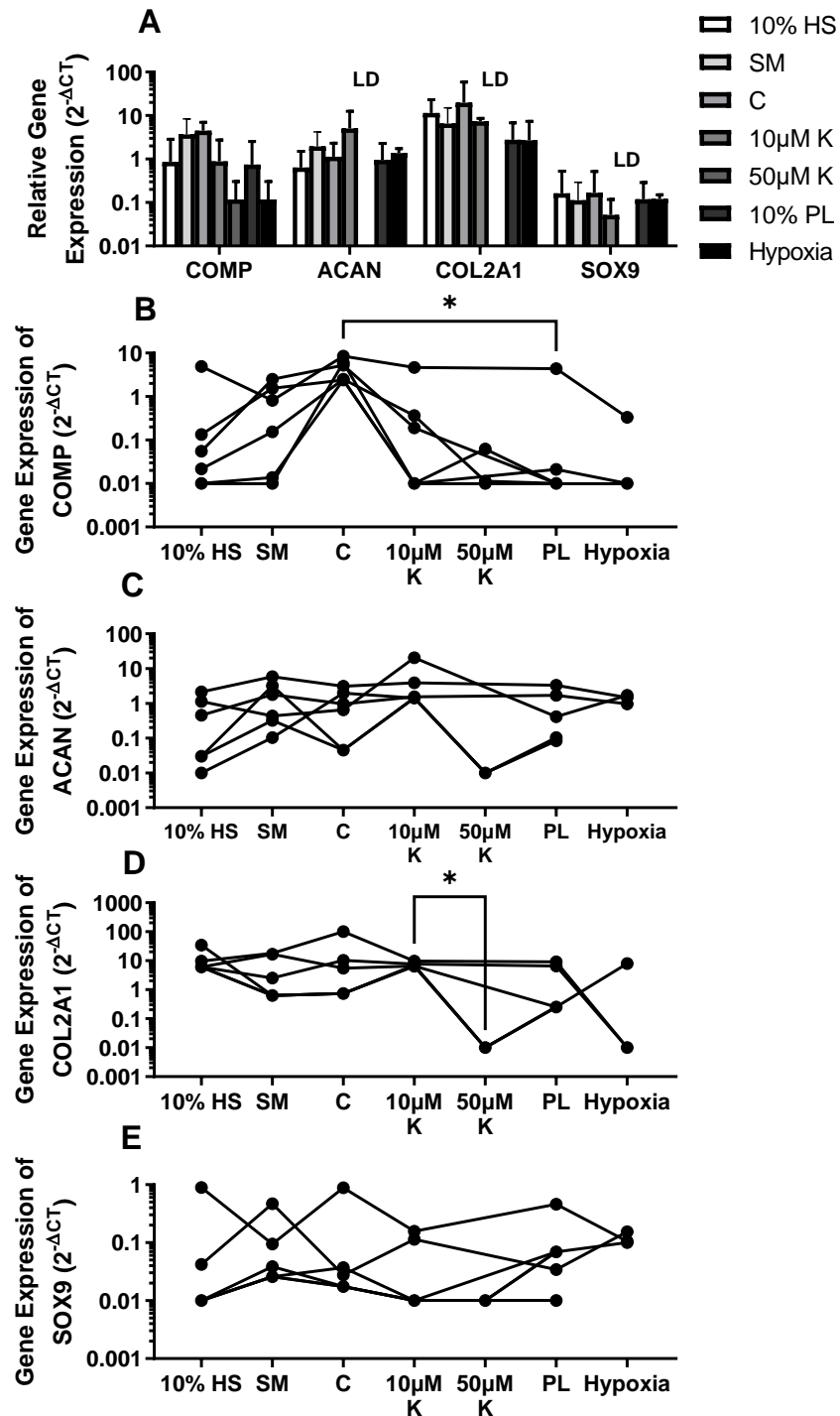


Figure 5.3.10 Expression of Genes Related to Chondrogenesis in IC MSCs after 14 Day Preconditioning in Various Stimulants (N=6, 50µM K and Hypoxia N=3). A Comparison of overall expression of COMP, ACAN, COL2A1 and SOX9. B Paired donor gene expression response of COMP by different biological stimulants. C Paired donor gene expression response of ACAN by different Biological Stimulants. D Paired donor gene expression response of COL2A1 by different biological stimulants. E Paired donor gene expression response of SOX9 by different biological stimulants. LD on A means Low detection, in that less than 3 donors had recordable levels of expression. Error bars on A are mean \pm standard error. On B-E, lines connect individual donor results between each condition. Data was analysed by the non-parametric Kruskal-Wallis test with Dunn's multiple comparisons test. * $p < 0.05$.

The potential for suppression of osteogenic gene expression was investigated next. ALP, RUNX2 and VEGFA have all shown to be key links in osteogenesis and so were measured by qPCR. (Fig. 5.3.11). Again, there were no significant differences of assessed transcripts. Of controls, as expected, SM cultures most greatly suppressed ALP, RUNX2, and VEGF, as it is designed to reduce differentiation. The most expression of ALP, RUNX2 and VEGF in the controls was in 10% HS cultures, with C-treated cultures being slightly below 10% HS, both around 2-fold of SM-treated cultures for each. Interestingly, 10 μ M K preconditioned MSCs had the highest ALP, RUNX2 and VEGFA expression, by 2-fold or more of C, meaning RUNX2 or other osteogenic genes were not suppressed, at least in 2D conditions, at this concentration. However, 50 μ M K successfully suppressed RUNX2 relative to other cultures, and so may be more effective at this concentration. However, VEGFA and ALP were at similar levels to 10% HS. PL cultures showed similar ALP and RUNX2 behaviour to 10% HS, which considering their similar components makes sense, although VEGFA expression was lower. Lastly, hypoxia showed higher expression of RUNX2 and ALP relative to 10% HS, and similar VEGFA, suggesting an osteogenic response (Fig. 5.3.11A).

Generally, donor trends were clear for all 3 genes, with SM suppressing expression of all 3 genes relative to C, 10 μ M K cultures showing higher expression of RUNX2 relative to C cultures, whereas 50 μ M K cultures had lower expression than C (Fig. 5.3.11A-C). Overall, it seems that 10 μ M K is unable to suppress RUNX2 in 2D, and no treatment suppressed RUNX2 as much as SM, and so further work in 3D is required to see if RUNX2 can be suppressed. Whilst 50 μ M could suppress RUNX2, it also suppressed chondrogenic gene expression. As another key lineage of MSCs, changes to adipogenic gene expression was next investigated.

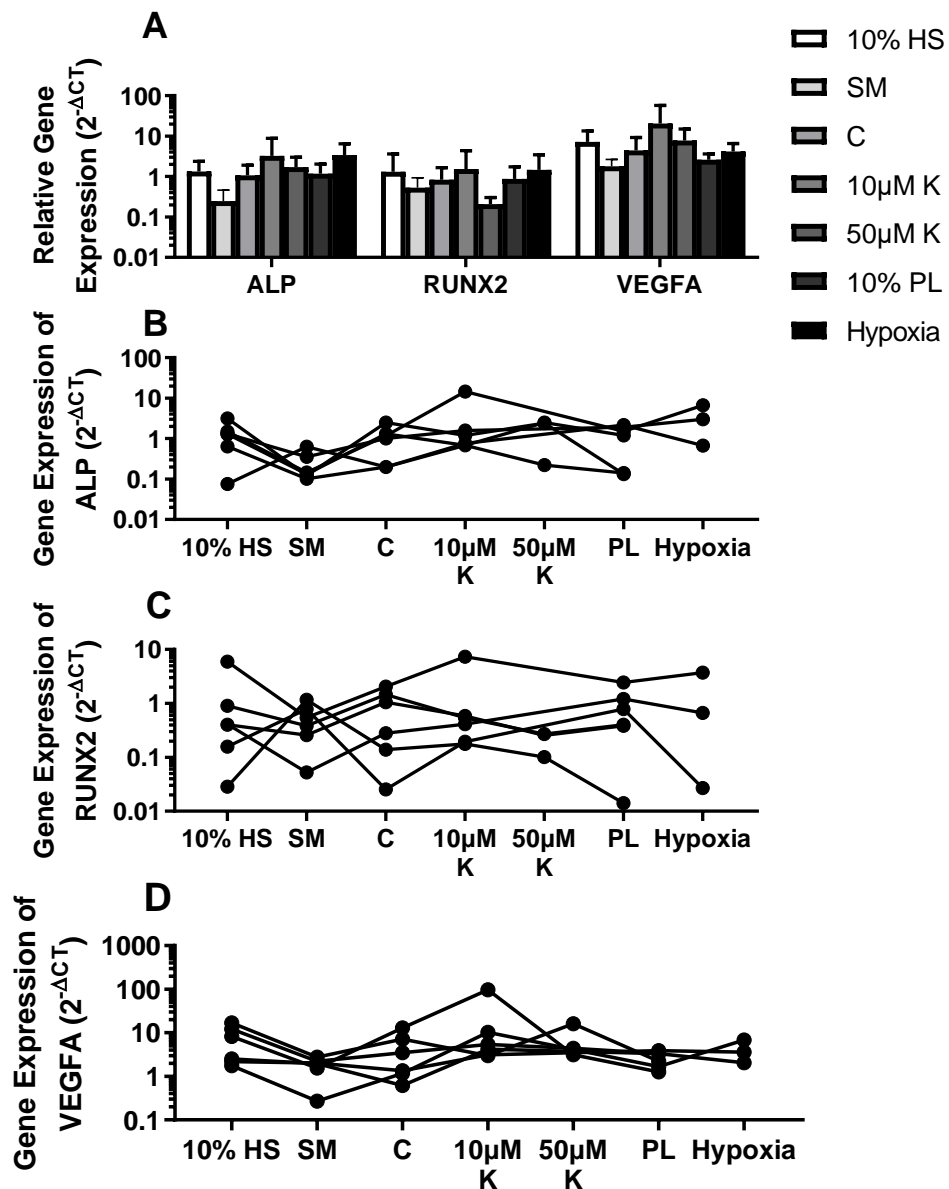


Figure 5.3.11 Expression of Genes Related to Osteogenesis in IC MSCs after 14 Day Preconditioning in Various Stimulants (N=6, 50 μ M K and Hypoxia N=3). A Comparison of overall expression of ALP and RUNX2. B Paired donor gene expression response of ALP by different biological stimulants. C Paired donor gene expression response of RUNX2 by different biological stimulants. D Paired donor gene expression response of VEGFA by different biological stimulants. Mean \pm standard error is shown for A. On B-D, lines connect individual donor results between each condition.

Whilst increased adipogenesis was not seen in the histology of resident talocrural BM MSCs, elevated adipogenic protein synthesis would inhibit healthy repair of both bone and cartilage, as such understanding if different biological stimulants affect these was important. As such, FABP4 and PPARG were measured (Fig. 5.3.12) Of controls, 10% HS, SM and C all had similar FABP4 expression, and only SM suppressed PPARG relative to C and 10% HS. 10 μ M KGN increased FABP4 expression but not PPARG relative to 10% HS and C, but kept similar PPARG expression. 10% PL and Hypoxia both showed the lowest FABP4 and PPARG expression (Fig.

5.3.12A). Donor trends were similar for both FABP4 and PPARG, with only one exception being one donor treated with C showed FABP4 suppression, not matched in other cultures (Fig. 5.3.12B). For PPARG, the general trend per donor was very consistent, with a sustained reduction in expression in SM compared to 10% HS and C, with 10% HS and C treated cells showing similar levels of expression per donor. PL showed significant reduction of PPARG expression compared to 10% HS control and 10 μ M K cultures, and SM had significantly reduced expression to 10% HS as well, suggesting both can reduce expression of PPARG (Fig. 5.3.12C). It seems no stimulant had a major effect on adipogenic gene expression, other than PL suppressing PPARG.

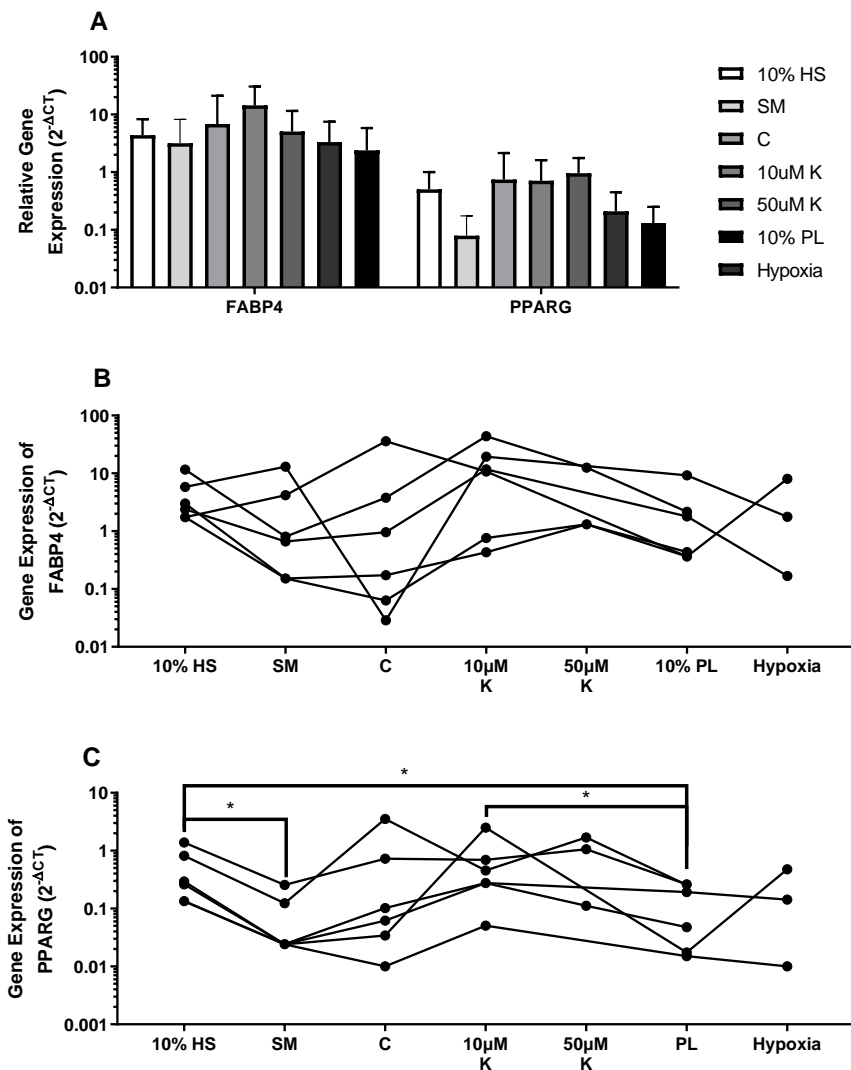


Figure 5.3.12 Expression of Genes Related to Osteogenesis in IC MSCs after 14 Day Preconditioning in Various Stimulants (N=6, 50 μ M K and Hypoxia N=3). A Comparison of overall expression of ALP and RUNX2. B Paired donor gene expression response of ALP by different biological stimulants. C Paired donor gene expression response of RUNX2 by different biological stimulants. Mean \pm standard error is shown for A. On B-C, lines connect individual donor results between each condition.

All three biological stimulants caused growth in cultures with active transcriptional activity, and therefore support cellular activity. To summarise, controls showed expected behaviour, with SM-preconditioned cultures showing suppression of most genes measured relative to other controls, and C-preconditioned cultures induced higher expression of chondrogenic genes COMP, COL2A1 and SOX9. Basal media 10% HS presented a middle ground of expression of each gene without major biological stimulants. Of treatment conditions, only 10 μ M K elucidated any increase in chondrogenic gene expression, and only for K, however it did not suppress RUNX2 in preconditioning. Whilst 50 μ M K suppressed RUNX2, there was also suppression of chondrogenic genes and poor growth rates as seen earlier in the chapter. Both 10 μ M K and PL supported IC MSC growth with larger and more dense colonies, and either had similar chondrogenic gene expression or increase relative to C, and so were taken further into 3D conditions to see any effects that may be elucidated in 3D. Hypoxia mostly suppressed chondrogenic gene expression and elevated osteogenic genes, which is not beneficial to cartilage repair, and therefore was not taken further.

5.4. Discussion

This chapter aimed to develop a method of preconditioning MSCs, and to see the effects upon MSCs proliferation, cell shape, and differentiation marker ALP, to test if it was effective. The previous chapter showed that talar and tibial MSCs are more capable of chondrogenesis than IC MSCs, however also show increased calcium deposition. This follows on from results of Chapter 3, which showed CD271+ resident MSCs were correlated with more damaged regions of cartilage bone, as well as with bone sclerosis and newly embedded osteocytes. This suggests resident MSCs are focusing on bone synthesis instead of cartilage repair, leading to large changes in tissue biomechanics. This chapter has developed methods of preconditioning MSCs towards a chondrogenic phenotype, using xeno-free, clinically applicable biological stimulants, K and PL.

This chapter has shown that both K and PL show evidence of being able to enhance chondrogenic capability by preconditioning, being compared with a positive control for the first time, C. Both 10 μ M K and P induced rounder MSC phenotype associated with chondrogenesis, but not to the same extent as C. Unexpectedly, 10 μ M K did not suppress ALP activity after 14 day 2D culture, as a stimulant cited for its ability to suppressing osteogenesis, which has not been shown before¹⁴¹. However, neither C nor 10% PL suppressed ALP area of total colony area relative to SM either. Both 10 μ M K and PL were shown to support MSC proliferation to a far greater extent than the control C, but also SM. All conditions retained transcriptional activity of MSCs, however C showed the greatest increase in chondrogenic gene expression for COMP, COL2 and SOX9, which as media for *in vitro* chondrogenesis is expected. ACAN expression was only increased in the 10 μ M K preconditioning MSCs. However, other markers of chondrogenesis did not increase in this condition relative to the negative control, SM. Osteogenic genes were only suppressed by 50 μ M K preconditioning, and adipogenic gene expression was elevated in each condition relative to the basal media, which has not been shown before. K showed the most effect in preconditioning as a xeno-free medium to enhance chondrogenesis, with strong proliferation not seen in C, however, did not suppress osteogenesis. PL showed rapid proliferation without loss of chondrogenic gene expression, which is also of benefit to preconditioning. In general, there were no significant differences between treatments, however K and PL both showed benefits by preconditioning and so were taken forward for 3D treatments.

The effect of colony structure upon differentiation capacity is not well explored in the literature, and so the importance of different colony boundaries is unknown. However, the chondrogenic nodule formation has been visualised previously, and has been positively stained for Alcian blue, which stains sulphated GAGs¹⁸⁰. This process starts by MSCs moving from a single-layer structure to a multi-layer cell structure, which was seen in both C and 10 μ M K treated samples. This demonstrates that MSCs were beginning early chondrogenic differentiation *in vitro* on a 2D

surface, in both C-treated and 10 μ M K treated samples. This supports preconditioning for initiating the differentiation process. This greatly supports 10 μ M K preconditioning for MSC chondrogenesis, and that C is an effective positive control.

MSC structure has been tightly linked with their differentiation capacity in the literature as already discussed in previous chapters^{273,337}. MSC shape effects differentiation through the cytoskeleton, activating intracellular signalling¹⁸⁰. Freshly isolated cells present a circular morphology when first seeded, but typically become fibroblast-like, as demonstrated in Chapter 4 (Fig. 4.4.2). This structure however has been associated with all 3 lineages, osteogenesis, chondrogenesis and adipogenesis, but was observed in the positive control, C, PL and 10 μ M K treated MSCs in this work (Fig. 5.4.1-2)²⁷³. Therefore, in this example, it seems more likely to be related to chondrogenesis. Remaining conditions demonstrated a more fibroblastic shape, confirmed by MSC circularity measurements, typical of cultured MSCs.

Whilst ALP staining is used as an early marker of osteogenic differentiation in MSC classification, as performed in Chapter 4 (Fig. 4.3.11), this does not demonstrate osteogenic commitment and is also associated with general differentiation capacity as well²⁸². As earlier mentioned, non-tissue specific ALP production has been linked in multiple studies with increased differentiation capacity of MSCs, into bone, fat, and cartilage^{282,283}. As ALP was expressed in each treatment, MSCs remained capable of differentiation. SM showed the most suppression by ALP of total colony area, showing that the media suppresses differentiation as it is intended to. 10% HS and C treatment showed similar ALP of total area to total area as each treatment condition, with 10% PL being slightly lower. This suggests that in each condition MSCs remains capable of differentiation, but without major reduction in the osteogenic marker ALP. This has been shown previously, with HS showing increased differentiation potential and proliferation in 2D culture^{331,332}. K has been shown to enhance chondrogenesis in both 2D and 3D culture, whereas PL has been shown to contribute to all three lineages in 2D and 3D^{136,141,328}.

Looking at colony structure after toluidine blue staining, PL and 10 μ M K showed the largest colony areas. However, these cultures were highly proliferative, and so there was merging of colonies, and so is it likely individual colonies were smaller. C showed the smallest colonies, showing there was low amounts of proliferation. As PL has both growth factors from HS and PL, this would likely account for the rapid proliferation and large colony size. As both 10 μ M K and PL showed high proliferation, and similar MSC morphology to C-treated MSCs, preconditioning in these conditions may enhance chondrogenic ability whilst also allowing the rapid MSC proliferation required. Integrated density was similar in every condition except from PL-treated MSCs, suggesting that not only is the colony area larger as just mentioned, it is also more dense. This however may be related to containing both PL and HS, and therefore many growth factors.

Gene expression of cartilage genes was investigated to see if preconditioning could induce a prechondrogenic state in MSCs. As this was a 2D methodology, there was not expectation that these markers would be elevated as chondrogenesis usually requiring a 3D environment. Previous work has shown COMP and ACAN being increased in 2D MSC culture however²¹⁹. Gene expression results confirmed that positive control C was the most chondrogenic, with elevated COMP, COL2A1 and SOX9 expression. For the most part there were little differences between the negative controls and the test conditions, with no significant differences. Interestingly, 10 μ M K did lead to a marked increase in ACAN, not seen in C-treated MSCs. This may be through a specific pathway K is able to act through, which C does not. Another study of K-preconditioning in 2D has been completed, and also found increased ACAN activity, but also increased COL2A1 or SOX9 expression. However, these genes were measured after additional 3D culture, which shows hope for K-treatment in 3D³²⁴.

Osteogenic gene expression was used to see if the osteogenic traits seen in OA MSCs from talus and tibia could be suppressed by preconditioning, to revert the behaviour seen in Chapter 4. ALP gene expression results were very similar to what was seen in ALP area of total area, validating this method at least in terms of estimating ALP expression. Interestingly, RUNX2 was elevated in 10 μ M K treated samples relative to controls. Whilst the literature states that RUNX2 should be suppressed by 10 μ M K, this is from treatment in 3D, as such K may not be able to suppress RUNX2 in 2D at this concentration¹⁴¹. Whilst 50 μ M K was able to suppress RUNX2, it also induced a morphology suggestive of senescence, as well as poor proliferation, and appeared to suppress chondrogenic gene expression. As such this suppression comes at a cost to the target of cartilage repair. MSCs were also investigated for VEGFa expression, as it has been shown to be related to osteogenic activity of MSCs. This was unchanged in all conditions bar one donor after 10 μ M K treatment which showed a marked increase. This appears to be a donor specific response, or an anomaly. To understand this further, analysis in 3D work was required to see if this continued. Overall, it was unclear if any drug was able to suppress bone formation whilst retaining chondrogenesis by commonly assessed markers of osteogenic differentiation^{303,313,318,329}.

Adipogenic gene expression was again lowest in SM and hypoxia. This is as expected, as SM inhibits differentiation, and hypoxia has previously been shown to downregulated adipogenesis, specifically in MSCs³³³. Interestingly, 10 μ M K and C increased PPARG expression relative to the other controls. This is potentially related to cytoskeletal differences as mentioned earlier, as the cytoskeletal arrangement may also be preferable for adipogenesis. As such, seeing if this persists in 3D culture is important to see if this may be a complication³³⁷. PL-treated MSCs did not increase adipogenic gene expression relative to negative controls, and so may be more suitable in the case that adipogenesis does initiate in 10 μ M K treated samples.

MSCs from some donors showed more specific responses to different treatment conditions. Older donors (RC071) seemed to have high adipogenic and angiogenic expression, whereas younger donors, in particular GCBM, showed a stronger chondrogenic gene response. This matches existing literature that younger MSCs are more able to form cartilage, however also advocates attempting regenerative treatment either at early stages or prior to when OA is thought to be onset, such as to small cartilage lesions from sports injuries³¹⁷. However, as shown in chapter 4, MSCs from donors of all ages were able to synthesise cartilage, and as talocrural MSCs had an apparent higher chondrogenicity, this may not be as true in MSCs from this site. Additionally, the extent of OA progression will have likely played a role, particularly based on the early-osteogenic behaviour seen in freshly seeded MSCs in Chapter 4. As these talocrural samples were so rare however, this chapter was only performed on IC cells, with ankle MSCs only being used once the preconditioning and 3D culture method was optimised.

In conclusion, controls C, SM and 10% HS all performed as anticipated, with C showing increased chondrogenic marker expression, SM showing suppression of both ALP activity and gene expression from each lineage, and 10% HS a middle ground as the basal media. ALP staining of total colony area showed similar results to ALP gene expression, therefore is a valid, cheaper method for investigating relative number of MSCs capable of osteogenic differentiation. Preconditioning showed elevated chondrogenic markers and therefore appears beneficial for initiating chondrogenesis whilst expanding low numbers of MSCs, however osteogenicity was not suppressed by any condition. Treatment 10 μ M K showed increased ACAN expression, whilst both PL and 10 μ M K conditions did not suppress remaining chondrogenic markers relative to basal media whilst greatly increasing proliferation, and so are suitable xeno-free biological stimulants for attempting to drive chondrogenesis. Whilst C did enhance chondrogenesis, the lack of proliferation made it unsuitable for treatments. The next step was to investigate the ability of these biological stimulants in 3D conditions, to see if chondrogenesis was increased further and if osteogenesis could be suppressed, and then the model applied on talocrural cells to see if K or PL could enhance chondrogenesis in OA samples. Based on results of this chapter, PL and K were chosen for preconditioning for their ability to rapidly generate large numbers of MSCs, which C could not. For 3D treatments, both PL and K were attempted based on results of this chapter and the literature suggesting their benefit, and C was used as a positive control after preconditioning.

6. Chapter 6 – The Ability of PL and KGN to Act as Chondrogenic Inducers in a 3D Model in Combination with Preconditioning

6.1. Introduction

In this work so far, MSCs with chondrogenic potential were for the first time successfully isolated from bone of the human talus and tibia isolated from end-stage OA patients. Histology of the osteochondral tissue in talus and distal tibia showed *in vivo* CD271+ MSC presence, however this associated with new bone formation and in regions where new bone formation was identified including osteoblasts, new osteocytes, and immature collagen, suggesting a link between MSCs and bone formation. Compared to IC controls from non-OA patients, these MSCs showed increased chondrogenic capacity, and in the talus reduced adipogenic capacity. Despite this increased chondrogenicity, there was a favouring of bone formation within the tissue, suggesting that MSCs may be pre-disposed towards bone formation in the body, but still retain a strong chondrogenic ability with the right stimuli.

The previous chapter investigated the effectiveness of preconditioning for enabling chondrogenic expression of IC MSCs in a 2D environment, comparing K and PL to C, 10% HS DMEM and SM. Compared to SM, the expansion control, all conditions increased ALP expression and expression of various differentiation markers. Importantly, there was increased colony growth seen in 10% HS-treated and PL-treated IC MSC cultures compared to SM without loss of expression markers. The positive control, C, was the most effective for the upregulation of SOX9, COL2A1 and COMP genes, however ACAN expression was upregulated most greatly in K-treated cultures. However, none of these increased significantly compared to other groups. As chondrogenesis cannot occur without 3D conditions, this was expected. As chondrogenic gene expression was similar between 10% PL, 10 μ M K and the positive control treated, without any significant changes compared to C. PL and K were selected as suitable conditions for chondrogenic treatment of MSCs. The next step was to move these preconditioned cells into a 3D environment, to develop a method using IC MSCs that could also be applied to talar and tibial MSCs, and allow assessment of actual chondrogenic behaviour such as GAG production.

As mentioned in previous chapter, MSC differentiation depends on biological signalling, biomechanics, material and cell source, as well as interacting cells. As such, the choice of 3D environment needs to match both material and mechanical requirements, as well as allowing cell adhesion, interactions and biological signalling. Hundreds of different materials for chondrogenic differentiation of MSCs have been investigated, with simple methods of chondrogenic inducement, or materials with additional functions such as inhibition of matrix degrading enzymes. The most common and successful methods include simple pellet culture as used in chapter 4 (Section 4.2.8), as well as specific materials including agarose, alginates, chitosan, collagen, fibrin, hyaluronic acid, polyglycolic acid and polycaprolactone, or combinations of these. Of these, collagen-based scaffolds are the one most often made to the

clinic, such as in the form of Chondro-Gide. Comparatively, alginate, agarose and PCL find far less use clinically. This is in part due to the difficulty of getting medical approval, with devices that already have medical approval setting a precedent, allowing more rapid approval of devices and materials with the same approach. As such, collagen has become a common material, on top of its suitable properties and ability for functionalisation. The benefits and examples of these are listed in Table 6.1.1.

Table 6.1 Common Biomaterials Used for Cartilage Synthesis

Name	Key Benefit	Key Pitfall	Clinical Example
Agarose	Tuneable mechanical properties Simple to use Suitable for mechanical loading, inert	Doesn't interact directly with cells which can make them abnormal	Cartipatch®
Alginate	Easily gelled, cheap, tuneable mechanical properties, can encapsulate cells	Relatively fast degradation Does not directly interact with MSCs alone	Cartipatch®
Chitosan	Similar structure to GAGs Enhances collagen type II and aggrecan synthesis Broken down by intrinsic human enzymes. Produces good quality neocartilage, may inhibit adipogenesis	Unstable and low porosity, and can be difficult to develop scaffolds	None found for cartilage repair, used in wound healing (Chitoseal (Abbot Vascular Inc.))
Collagen	Cells adhere and interact with collagen, maintaining their phenotype	Quality varies between batches including degradability and mechanical properties	MeRG® Chondro-Gide® NeoCart® MaioRegen® CaReS® CartiMaix®

Table 6.1 Common Biomaterials Used for Cartilage Synthesis

Fibrin	Low toxicity and cost, promotes adhesion and cell migration, regularly used in surgery	Can be broken down by cellular enzymes, poor biomechanical properties	BioCartTMII® (ProChon Biotech) Used to glue most other scaffolds into the repair site
Hyaluronic Acid	Maintains hydration, firmness, plasticity and viscosity. Low toxicity, supports MSC migration	Poor biomechanical strength, some evidence its as effective as PBS	Hyalofast® (Anika) Chondrotissue® (Biotissue) BioCartTMII® (ProChon Biotech)
Polyglycolic Acid	Tuneable mechanical properties, high modulus, Can be combined with other materials Easy to direct structure	Rapid degradation, degradative products (glycolic acid) can cause acidosis	Chondrotissue® (Biotissue)
Polycaprolactone	Good for drug release, biodegradable, biocompatible, resistant to hydrolysis, good mechanical strength	Amorphous so difficult to use	None found for cartilage repair

Data adapted and combined from ³³⁸⁻³⁴¹

Material design has become an extremely complex process, and more recently the addition of specific proteins has become the forefront. This may aid cell recruitment, motility or differentiation, such as addition of RGD peptides or entrapment of chondrogenic factors like TGF- β , making a field which requires an understanding of chemistry, biology, engineering and medicine.

This work was designed to identify if endogenous MSCs have the capacity to be recruited to the defect from the bone, and then if these MSCs could be directed towards chondrogenesis and away from their previous osteogenic behaviour, with the use of stimulants which could be used within the human body. Based on this, as well as the above, the following criteria were chosen. The scaffold needed to enable diffusion of nutrients into the scaffold. The scaffold needed to match the mechanical properties of cartilage to direct a chondrogenic MSC response. The

scaffold should be able to work synergistically with existing techniques such as microfracture. Lastly, the scaffold should be able to last long enough to initiate repair, but be biodegradable within the body when it is no longer required.

The biomechanical properties of cartilage differ by both joint and by location. Studies are not always comparable, as the mechanical properties tested vary by the aim of the project, and the available tissue, resulting in different experimental methodology and different units, making comparison more difficult. As mentioned, methods for investigating cartilage properties of OA talocrural tissue were optimised and attempted in this work (Section 3.2.13-15), however the results are not available yet. One study investigating compressive modulus in non-diseased tissue found that cartilage of the ankle has the highest compressive modulus of all joints, varying between 10.3-20.4 MN/m² in talus and 8.0-16.1 MN/m² in distal tibia, compared to 4.2-11.6 MN/m² at the femoral head³⁴². This is linked to the composition of human ankle cartilage as discussed in Chapter 1, such as the increased superficial cartilage depth¹³. To use a more comparable value, the elastic modulus of articular cartilage is generally cited to be 0.25-0.7 MPa, again being slightly higher in the non-diseased human talus and tibia, at 1.06 MPa and 1.19 MPa¹⁵. However, on the nano-scale, this value is much lower, of around 30-60 kPa³⁴³. As this project aimed to develop a material which drives MSC chondrogenic differentiation, this lower value was aimed for, firstly based off the mechanical properties of cartilage and secondly off the existing literature that shows MSCs are more driven towards chondrogenic differentiation in softer materials. Xue *et al.* showed that chondrogenic markers were upregulated on a material with an elastic modulus of 1.6 kPa compared to 40 kPa, including SOX9, ACAN and COL2A1³⁴⁴. The composite material Fibrin alginate (FA) can provide these properties. Previous literature for FA at this concentration and bead size has shown an elastic modulus value matching between cartilage properties and the soft material, of around 20 kPa with a 30 mg/ml fibrin to 16 mg/ml alginate ratio¹⁸¹. Additionally, the material is simple to sterilise, synthesise, as well as simple to break down for follow-up experiments. Lastly, the material is well tolerated biologically and breaks down over time without external influence³⁴⁵. FA-based scaffolds however also have additional benefits – fibrin has been shown to encourage MSC homing, as well as increasing chondrogenic gene expression as well as vasculogenic, myogenic and neurogenic lineages^{181,187,346-348}. Calcium alginate can be instantly broken down using EDTA, beneficial for experiments that require isolation of cells, as well as have been shown to maintain rounded chondrocyte structure and chondrocyte phenotype, which would aid MSCs once differentiated³⁴⁹. Additionally, mechanical properties of alginates are controlled by temperature, G-content of alginate used, and rate of gelation. Slower gelation means a more rigid structure, as such room temperature, alginate and calcium as a the gelling agent were chosen for rapid gelation to attain a lower elastic modulus³⁵⁰.

This chapter aims to develop methods for investigating the ability of 3D culture to drive MSC differentiation towards chondrogenesis, including in FA and by pellet culture. This was performed following 2D preconditioned MSCs detailed in the previous chapter, and compares pellet culture to a FA biomaterial. Additionally, the ability of biological stimulants with potential for clinical use, PL and K were further investigated for their ability to drive chondrogenesis whilst downregulating osteogenesis. The method was developed on IC MSCs before testing distal tibial and talar MSCs.

Specifically, this chapter will:

- Develop a 3D biomaterial and conditions for 3D culture of MSCs for chondrogenic differentiation which mimics the clinical scenario
- Investigate effects of different 3D culture methodologies in combination with K, PL or C treatment upon MSC morphology and gene expression in IC, distal tibia and proximal talus after preconditioning.

Objectives:

- Design methods of 3D culture and analyse the effect upon MSC chondrogenic capability through imaging and biochemical assessment of GAG content
- Measure changes to MSC behaviour through histology including toluidine blue and immunohistochemistry, and gene expression
- Test the effectiveness of 10% PL, or 10 μ M K/10%HS preconditioning upon MSCs after additional 3D culture
- Test the effectiveness of 50% PL or 50% PL with 10 μ M K as a treatment in 3D compared to C-treated MSCs after 2D preconditioning
- See if the innate differences in MSC differentiation capacity demonstrated in Chapters 4 and 5 effects the chondrogenic capability of distal tibia and talar MSCs compared to IC MSCs
- Investigate if K sufficiently reduces osteogenic gene expression through qPCR

6.2. Methods

6.2.1. Sample Information

In this Section, samples from both IC, and OA talus and distal tibia were used. These are listed in Tables 6.2.1 and 6.2.2. All MSCs used were from frozen, previously isolated from donor IC, distal tibia or talar bone (Section 2.4.2), which were thawed (Section 2.5.7) and then underwent minimal manipulation during preconditioning (Section 5.2.3), and then 3D culture.

Table 6.2 Distal Tibia and Talus Sample Characteristics Retrieved from Ankle Fusion

Sample ID	Donor Age (Years)	Donor Sex
WJ011	58	F
WJ012	34	F
WJ013	66	M
<i>Average</i>	<i>53</i>	<i>33% male 66% Female</i>

Table 6.3 IC Sample Characteristics Used for Preconditioning with 3D Treatment

Sample ID	Donor Age (Years)	Donor Sex
TRBM10	44	F
GCBM11	28	M
BM140207	19	M
RC071	36	F
GCBM11	28	M
BM313	42	M
<i>Average</i>	<i>41.5</i>	<i>33% male 66% Female</i>

6.2.2. Minimal Cell Culture and Processing before Alginate Embedding or Pellet Culture

The conditions used in Chapter 5 (Section 5.2.2) were utilised to precondition cells before they were placed into alginate or pellets for culture in a 3-dimensional environment, to generate sufficient cells for 3D cultures. For each donor, uncultured cells were defrosted according to Section 2.5.8, and then seeded in four 75cm² flasks in 7 ml StemMACS. IC, talar and tibial cells were seeded at a concentration that would contain 600 MSCs. This was estimated from CFU-Fs run for each donor (Fig. 4.3.5). This number of MSCs was chosen such that a total of 3x10⁶ MSCs per flask would be generated by the end of preconditioning to provide sufficient cells for subsequent assays (Table 6.2.3). Based on results from preconditioning in Chapter 5, 600 MSCs per flask were chosen. After 48 hours, StemMACS was removed, cells washed with PBS, and test medium added. This was 7 ml of 10µM K in 10% HS DMEM added to two flasks, and 7 ml 10% PL in DMEM added to the other two flasks. Media was half-changed every three days for 14 days, with images taken every week. At this point, the media was removed, cells were washed with PBS and then trypsinized (Section 2.5.3). Cells were then prepared for either 3D culture in pellet form, or alginate encapsulation. Pellet culture was performed to generate pellets as before (Section 4.2.8.1).

6.2.3. Alginate Synthesis

Alginate synthesis methods were adapted from prior studies which had shown success in cartilage repair both *in vivo* and *in vitro* when combined with stimuli by growth factor or select biological stimulants^{181,351,352}. The key focus for this study was creating alginates with comparable mechanical qualities to healthy cartilage, and to see what effect this had on the quality of repair, leading to the concentrations of reagents chosen. As discussed in the introduction, MSC differentiation changes based on the mechanical properties of the material, with hard materials prioritising bone and softer materials chondrogenesis³⁵³. Therefore, 1.2% Calcium alginate was combined with 15 mg/ml fibrin to create a tensile modulus mimicking micro-level cartilage properties, of around 30 kPa based on work with similar concentrations, in addition to other beneficial properties discussed earlier (Section 6.1)^{181,343,354}.

Firstly, sodium alginate powder was dissolved in sterile calcium-free PBS, using a magnetic stir bar for agitation, and then adjusted to pH 7.4 once dissolved. To sterilise the mix, the solution was pasteurised by heating to 70°C for 20 minutes, then cooled to room temperature (RT, 20°C), and the process repeated 3 times. This mixture was then stored at 4°C until use. Fibrinogen solution was then prepared at a concentration of 30mg/ml using bovine type I-S fibrin in sterile, calcium-free PBS, which was then sterilised using a 0.22µm filter, and then stored at -20°C until use. A 102 mM solution of calcium chloride was prepared in ddH₂O, which was stored at RT, and

a separate solution of 50U/ml of thrombin (from bovine plasma) was also prepared in ddH₂O, stored at -20°C.

Prior to synthesis, solutions were warmed to 37°C. Alginate was mixed at a 1:1 ratio with fibrinogen to create a 1.2% alginate, 15 mg/ml fibrinogen solution, termed fibrinogen alginate (FA). Thrombin solution was mixed with calcium chloride to produce a 5U/ml, 2 mM CaCl₂ solution. In a 6-well well-plate, 2 ml CaCl₂ thrombin solution was added to every well. Four droplets of FA solution were added dropwise using a 19 gauge, 1.5 inch needle from a height of 5 mm above the solution. This was enough to prevent water tension from holding droplets at the surface, but not so much the bead was deformed. This method delivers spherical FA beads of same size, and therefore approximately identical mechanical properties³⁵⁰. Care was taken to keep beads apart so there was not gelation between two separate beads during gelation and crosslinking. Beads were left to gelate and crosslink for 10 minutes. Beads were then washed in sterile dPBS 3 times to prevent further gelling.

6.2.4. Image Capture of Preconditioning and Alginate Beads

Whole alginate beads were imaged using an iPhone 7 camera (12 megapixel camera). For higher magnifications, such as during cell culture, the EVOS microscope (Section 2.8.3) was used.

6.2.5. Bead Diameter

Bead diameter was the first method used to start analysing bead properties. Beads were synthesised as described (Section 6.3.3), and then left in PBS for 30 minutes before imaging. Images of beads were taken alongside a ruler using an iPhone 7 camera, and then loaded into ImageJ. The 'set-scale' process was used to tell the program pixel width, and then the 'measure' process used to measure bead diameter 'x'. Bead diameter was then measured again at a 90° angle to the first measurement to take a second, 'y' measurement of each bead.

6.2.6. Sphericity

To ensure that spheroids were of similar sphericity in order to have near-identical mechanical properties, sphericity was measured, according to standard methods³⁵⁵. To do this, the earlier measurements of bead diameter (Section 6.2.8) were taken, and the x diameter was divided by y diameter in order to roughly estimate sphericity. The closer to 1, the closer to a true sphere.

6.2.7. Swelling Ratio

Swelling ratio denotes the degree to which the scaffold is able to absorb water, from a completely dry state, and forms a standard method of hydrogel analysis³⁵⁶. To do this, the scaffolds were synthesised in a 6-well plate (Section 6.2.3) without cells, with one bead per well. Once washed, beads were removed from solution, and excess water removed carefully using a tissue. Samples were then frozen at -20°C for 2 hours before using a Christ Alpha 1-2 LDplus freeze-dryer to remove any remaining water. This was performed at -65°C under 0.013 mbar pressure for 24 hours. Beads were then weighed individually using a balance. Following this, beads were placed back into the well plate, and PBS was added. Bead weight was measured every 30 minutes, until the weight became constant.

6.2.8. Degradation Rate

Degradation rate reflects how quickly a bead will break down, which is important for biocompatibility. As such, this was measured according standard practice¹⁸⁴. Beads were again synthesised in a 6-well plate (Section 6.2.3) without cells, with one bead per well. Once washed, beads were immersed in DMEM and left in the incubator to mimic culture conditions. Beads were weighed at the initial point, and every day subsequently over 14 days.

6.2.9. Encapsulating IC and Talocrural MSCs within FA, and Pellet Culture

Following MSC preconditioning (Section 6.2.2), alginate reagents were prepared as described in Section 6.2.3, and both the fibrinogen alginate and calcium chloride were warmed to 37°C in a water bath. In sterile conditions, MSCs were trypsinized from their T75cm² flasks (Section 2.5.3) and 10 µl of solution was taken to count cells (Section 2.5.2). MSCs were resuspended in 0.5 ml DMEM, and the relevant amount of volume was used to split MSCs for FA embedding or for pellet culture. MSCs for FA culture were spun down and then resuspended in the fibrinogen alginate mix. In a 24-well plate, 2 ml of warmed CaCl₂ with 5U/ml thrombin was added per well, and then fibrinogen alginate cell mix added dropwise from a 5 ml syringe through a 19 gauge, 1.5 inch needle to the CaCl₂ thrombin. For each well, 4 FA beads were synthesised. These were allowed to gel for 10 minutes, and then pellets were washed in sterile PBS. Following this, the relevant treatment media was given. Due to the complexity of this experiment, sample groups and shorthand are listed in Table 6.2.2. Henceforth, preconditioning media will be referred to as preconditioning, and the media MSCs in 3D were cultured in is defined as differentiation medium.

Table 6.4 Preconditioning and Differentiation Media for IC, Talar and Tibial MSCs

Preconditioning Media (3 weeks)	Differentiation Media (2 Weeks)	Shorthand
10 μ M K in 10% HS DMEM	ChondroDIFF	K-C
	10 μ M K in 50% PL DMEM	K-K
	50% PL in DMEM	K-PL
10% PL in DMEM	ChondroDIFF	PL-C
	10 μ M K in 50% PL DMEM	PL-K
	50% PL in DMEM	PL-PL

From each preconditioning method and donor (10% PL, low glucose DMEM and 10 μ M K, low glucose DMEM), 4 pellets and 4 alginate spheroids replicates were made for each differentiation culture medium, which included ChondroDIFF (C) as a gold-standard control, as well as 50% PL in high glucose DMEM and 50% PL, 10 μ M K in high glucose DMEM as test media. The reason why 50% PL was chosen was that promising results were seen in pellet culture by a related study performed by a colleague, which showed 10% more GAG production and 45% less calcium deposition using 50% PL DMEM in non-diseased synovial fluid MSCs compared to FCS treated pellets¹⁴⁰. For each treatment condition, FA beads were grown together in one well of a 24-well plate per donor, with 3 ml media per well, whereas pellets had an individual Eppendorf for each technical replicate with 1 ml media per pellet, due to pellets being formed in the tube, and would bear unnecessary risk moving them into one well.

Media was half-changed twice per week to minimise disturbance of scaffolds. A pipette was inserted away from the scaffold or bead, and 1.5 ml of 0.5 ml aspirated respectively, and fresh media added.

After three weeks, pellets/FA beads were removed from culture and taken for testing. Images were taken of all pellets using an iPhone 7 Camera. All culture media was retrieved and frozen at -20°C, as some solutions appeared to have released a gelatinous substance which could have been extracellular GAG. One pellet/bead per donor was taken for PCR (Section 6.2.12), two were taken for GAG estimation (Section 6.2.14), and one was taken for histology (Section 6.2.15-6.2.18).

6.2.10. XTT Assay

The XTT assay is a tool used for measuring both cell viability and proliferation used as standard practice to investigate cell proliferation or toxicity³⁵⁷. The process works by use of the soluble dye sodium-3'-[1-(phenyl carbonyl)-3,4-tetrazolium]-bis (4-methoxy6-nitro) benzene sulfonic acid hydrate (XTT). Increased cell number means increased activity of mitochondrial dehydrogenases in the sample, which can break down XTT to an orange formazan dye, which can be directly quantified by multi-well spectrophotometer. This method was used according to manufacturers' instructions to investigate indirect cytotoxicity of FA on MSCs. Firstly, a FA-media was produced by synthesising beads as before (Section 6.2.3), and leaving them in DMEM for 48 hours in the incubator. At the same time, in quadruple replicates, uncultured IC MSCs from 3 donors were seeded at 250, 500 and 1000 cells per well in microplates, and cultured in 1 ml FA media, negative control 10% DMSO in DMEM or positive control SM. These were then cultured for 72 hours. XTT mix was then produced by mixing 5 ml of XTT and 0.1 ml of electron coupling agent. Cultures were placed in the spectrophotometer and absorbance read at 550nm prior to measure baseline absorbance. Next, 50 µl of XTT mix was added and cultures were incubated for 4 hours. Cultures were then again placed into the spectrophotometer to measure absorbance at 550nm. Readings were then normalised to the background as an increase on background ratio (Final reading / baseline - baseline).

6.2.11. Measuring Effects of Pellet Culture on MSC Expression by qPCR

To measure RNA content as before (Section 2.6), as well as prepare cDNA for qPCR, RNA had to be extracted from the pellet. To do this, the pellet was compressed between two sterile glass slides to mechanically degrade the pellet, and then the pellet was covered with lysis solution. This was additionally thoroughly pipetted to further degrade the pellet, and vortexed until the pellet was visibly fully broken down. This lysis-cell mix was then purified as described earlier (Section 2.6.3) to retrieve the RNA. For RNA content measurement, 5µl of solution was taken from each sample condition and measured as before (Section 2.5.2).

RNA was then reverse transcribed (2.6.4) and pre-amplified as earlier described (Section 2.6.5). The retrieved cDNA was frozen at -20°C until use. The Fluidigm chip was loaded with cDNA and TaqMan's as before (Section 5.2.6), using the genes given in Table 6.2.4.

Table 6.5 Genes used for qPCR of 3D Treatments

Gene	Full Name	Gene	Full Name
<i>MMP1</i>	Matrix Metalloproteinase 1	<i>PPARd</i>	Peroxisome Proliferator Activated Receptor Delta
<i>COL10A1</i>	Collagen Type 10 α 1	<i>CCR5</i>	C-C Chemokine Motif Receptor 5
<i>GDF6</i>	Growth Differentiation Factor 6	<i>CCR1</i>	C-C Chemokine Motif Receptor 1
<i>IGFBP3</i>	Insulin-Like Growth Factor Binding Protein 3	<i>CTGF</i>	Connexin Tissue Growth Factor
<i>TNFRSF11B</i>	Tumour Necrosis Factor Receptor Super Family Member 11B	<i>MMP3</i>	Matrix Metalloproteinase 3
<i>VEGFA</i>	Vascular Endothelial Growth Factor Alpha	<i>PSIP1</i>	Lens epithelium derived growth factor
<i>CCL5</i>	C-C Motif Chemokine Ligand 5	<i>DIO2</i>	Iodothyronine Deiodinase
<i>LCN2</i>	Lipocalin-2	<i>Grem1</i>	Gremlin-1
<i>GDF5</i>	Growth Differentiation Factor 5	<i>MMP2</i>	Matrix Metalloproteinase 2
<i>TNFa</i>	Tumour Necrosis Factor alpha	<i>STMN2</i>	Stathmin 2
<i>NGFR</i>	Nerve Growth Factor Receptor	<i>IL6</i>	Interleukin 6
<i>VEGFC</i>	Vascular Endothelial Growth Factor C	<i>TIMP1</i>	Tissue Inhibitor of Metalloproteinase 3
<i>IGF1</i>	Insulin-like Growth Factor 1	<i>TGFBR2</i>	Transforming Growth Factor Beta Receptor 2
<i>PTH1R</i>	Parathyroid Hormone 1 Receptor	<i>TGFb2</i>	Transforming Growth Factor Beta 2
<i>SOX9</i>	SRY-Box Transcription Factor 9	<i>TGFb3</i>	Transforming Growth Factor Beta 3
<i>IL10</i>	Interleukin-10	<i>SFRP4</i>	Secreted Frizzled-Related Protein 4
<i>MMP14</i>	Matrix Metalloproteinase 14	<i>CYR61</i>	Cysteine-Rich Angiogenic Inducer 61
<i>S1PR1</i>	Sphingosine-1-Phosphate Receptor 1	<i>IBSP</i>	Bone Sialoprotein
<i>PTGS2</i>	Prostaglandin-Endoperoxide Synthase 2	<i>POSTN</i>	Periostin
<i>SPHK1</i>	Sphingosine Kinase 1	<i>IGF1R</i>	Insulin-like Growth Factor 1 Receptor
<i>COL2A1</i>	Collagen Type 2 α 1	<i>PTH1H</i>	Parathyroid Hormone Like Hormone
<i>CCL19</i>	C-C Motif Chemokine Ligand 19	<i>THBS4</i>	Thrombospondin 4
<i>TGFB1</i>	Transforming Growth Factor β 1	<i>BCL2</i>	B-Cell Lymphoma 2
<i>CXCL12</i>	C-X-C Motif Chemokine 12	<i>TIMP2</i>	Tissue Inhibitor of Metalloproteinase 2
<i>ROR2</i>	Tyrosine-Protein Kinase Transmembrane Receptor 2	<i>ANKH</i>	Progressive Ankylosis Protein homologue
<i>TIMP3</i>	Tissue Inhibitor of Metalloproteinase 3	<i>ADAMTS4</i>	A Disintegrin and Metalloproteinase with Thrombospondin Motifs 4
<i>ACAN</i>	Aggrecan	<i>MMP13</i>	Matrix Metalloproteinase 13
<i>CCL20</i>	C-C Motif Chemokine Ligand 20	<i>CCL2</i>	C-C motif ligand 2
<i>ALPL</i>	Alkaline Phosphatase	<i>COMP</i>	Cartilage Oligomatrix Protein
<i>Wnt10b</i>	Wingless-related integration site 10 beta	<i>ASPN</i>	Asporin
<i>CCR7</i>	C-C Chemokine Receptor 7	<i>IL1B</i>	Interleukin-1B
<i>ADAMTS5</i>	A Disintegrin and Metalloproteinase with Thrombospondin Motifs 5	<i>HGF</i>	Hepatocyte Growth Factor
<i>SPP1</i>	Osteopontin	<i>MMP9</i>	Matrix Metalloproteinase 9
<i>CCR6</i>	C-C Motif Chemokine Receptor 6	<i>DDR2</i>	Discoidin domain-containing receptor 2
<i>TGFBR3</i>	Transforming Growth Factor β receptor 3	<i>DIRAS2</i>	GTP-binding Ras-like Protein 2
<i>COL1A2</i>	Collagen Type 1 α 2	<i>Notch1</i>	Notch Homolog 1
<i>FABP4</i>	Fatty Acid binding Protein 4	<i>TNFSF11</i>	Tumour Necrosis Factor Ligand Superfamily 11
<i>PPARG</i>	Peroxisome Proliferator Activated Receptor Gamma	<i>BMPR1B</i>	Bone Morphogenic Protein Receptor 1 beta
<i>RUNX2</i>	Runt-Related Transcription Factor 2	<i>NOS2</i>	Nitric Oxide Synthase 2
<i>CXCR1</i>	C-X-C Motif Chemokine Receptor 1	<i>Leptin R</i>	Leptin Receptor
<i>IGF2</i>	Insulin-like Growth Factor 2	<i>SFRP1</i>	Secreted Frizzled-Related Protein 1
<i>COL1A1</i>	Collagen type 1 alpha 1	<i>SPARC</i>	Osteonectin
<i>ARNTL</i>	Aryl Hydrocarbon Receptor Nuclear Translocator-like Protein 1	<i>WISP1</i>	Wnt-1 Inducible Signalling Pathway 1
<i>Bmal1</i>	Bone Gamma-Carboxyglutamate Protein	<i>NGF</i>	Nerve Growth Factor
<i>BGLAP</i>	Bone Gamma-Carboxyglutamate Protein	<i>SERP</i>	Plasminogen Activator Inhibitor 1
<i>SP7</i>	Osterix	<i>PAI-1</i>	Plasminogen Activator Inhibitor 1
<i>CXCR4</i>	C-X-C Motif Receptor 4	<i>GAPDH</i>	Glyceraldehyde 3-phosphate dehydrogenase
<i>GAPDH</i>	Glyceraldehyde 3-phosphate dehydrogenase	<i>HPRT1</i>	Hypoxanthine Phosphoribosyltransferase-1
<i>HPRT1</i>	Hypoxanthine Phosphoribosyltransferase-1		

6.2.12. Glycosaminoglycan Content

For GAG content, the Blyscan kit was again used for analysis (Section 4.2.8.4).

6.2.13. Snap-freezing of Pellets

Pellets were snap-frozen prior to storage and cryo-sectioning. Liquid nitrogen was collected in a chamber using appropriate PPE. Tinfoil boats were prepared by creating small buckets of appropriate size to hold the pellets with long wings to enable them to be lowered into liquid nitrogen without risk to the user. Boats were then filled with Optimal Cutting Temperature Medium (OCT) with care to prevent bubbles forming. Pellets for snap freezing were washed in 500 μ l PBS, PBS removed, and pellets placed into the OCT. Tinfoil boats were slowly lowered by the wings towards but not submerged in the liquid nitrogen until frozen, and then fully submerged. These were stored at -80°C .

6.2.14. Cryo-sectioning of Pellets

Snap frozen pellets were sectioned by microtome. The apparatus was cooled to -20°C , and then OCT was used to adhere snap-frozen pellets to a cork plate before being attached to the block. OCT blocks were trimmed until parallel to the blade with the pellet visible, and $10\mu\text{m}$ sections were taken, and then adhered to a glass slide. These were then stored at -20°C until staining.

6.2.15. Toluidine Blue Staining of Pellets

Toluidine Blue is an acidophilic dye which stains GAGs blue, due cartilage being strongly acidic, and forms a standard method for investigating GAG synthesis³³⁴. Toluidine blue was prepared 0.1% in 50% isopropanol. Sections were fixed in methanol at -20°C for 2 minutes, and then stained for 30 minutes using filtered toluidine blue at 37°C . Isopropanol was then added by wash bottle to decolourise the sample, and then slides dehydrated in 3 cycles of xylene, and then a coverslip attached using Acrytol. This is outlined in Table 6.2.5.

Table 6.6 Toluidine Staining Protocol

Process	Step	Step	Time (minutes:seconds)
Fixation	1	Fix in -20°C Methanol	2:00
Toluidine Blue	2	Stain with filtered 37°C Toluidine Blue	30:00
Decolourise	3	Wash with isopropanol by wash bottle	0:05
Clearing	4-6	Xylene	3:00 (x3)
Coverslip	7	Acrytol	N/A

6.3. Results

6.3.1. Mechanical Properties of FA Bead Hydrogels

Biomaterials need to be tested to ensure they are reproducible, as well as can support cell growth as in the intended purpose. As such the mechanical properties of the FA beads were first assessed to ensure they could provide the mechanical structure as required, that they can survive culture for an extended period.

Firstly, in order for FA structure to maintain similar mechanical properties, each scaffold needs to have similar bead size and sphericity. Images were taken after bead synthesis to firstly show their similar structure, as well as for subsequent image analysis (Fig. 6.3.1). External to PBS, beads were translucent and maintained a rounded, spherical morphology (Fig. 6.3.1A). Within PBS, beads were white and spherical and of similar size between each replicate (Fig. 6.3.1.B/C). Under high microscopy, beads had smooth curvature and stayed clearly separated without crosslinking (Fig. 6.3.1D). The beads were next analysed to see the level of similarity between each bead.

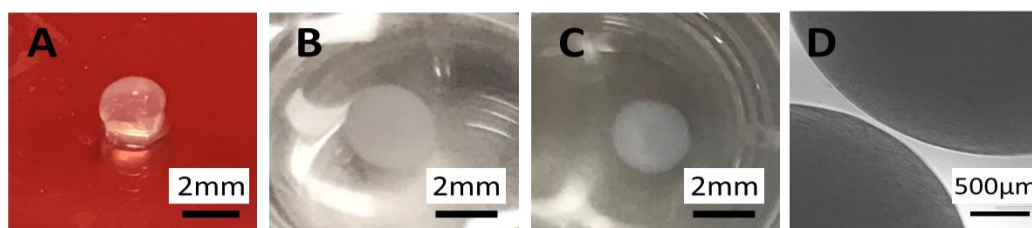


Figure 6.3.1 Fibrin Alginate Bead Structure After Synthesis. A Bead outside of PBS. B Alginate bead submerged in PBS. C Fibrin alginate bead imaged at 40x microscopy. Beads largely showed a smooth, spherical structure.

Images were analysed for differences in bead diameter (Fig. 6.3.2A) as well as sphericity (Fig. 6.3.2B) to investigate reproducibility of beads synthesised. All beads were between 2.0-2.7 mm in diameter at the widest point. Average diameter was 2.31 mm \pm 0.16 (Mean \pm SD), with a maximum 20% variance from the mean. To assess sphericity of beads, a rough estimate of bead roundness was performed by dividing one measurement of diameter to the perpendicular diameter. Multiple beads were measured, and the consistency of beads being spherical was assessed by the gradient of the line of best fit for all beads. If beads were true spheres, this would show a gradient of 1. FA beads showed a gradient of 0.75 and r^2 value of 0.74. Whilst not a true sphere, the high r^2 value and a gradient approaching 1 suggests the beads were near spherical and of similar size. This means the beads have similar size and shape, and therefore mechanical properties. Next, the ability of the scaffold to absorb and retain water was assessed by measuring the swelling ratio.

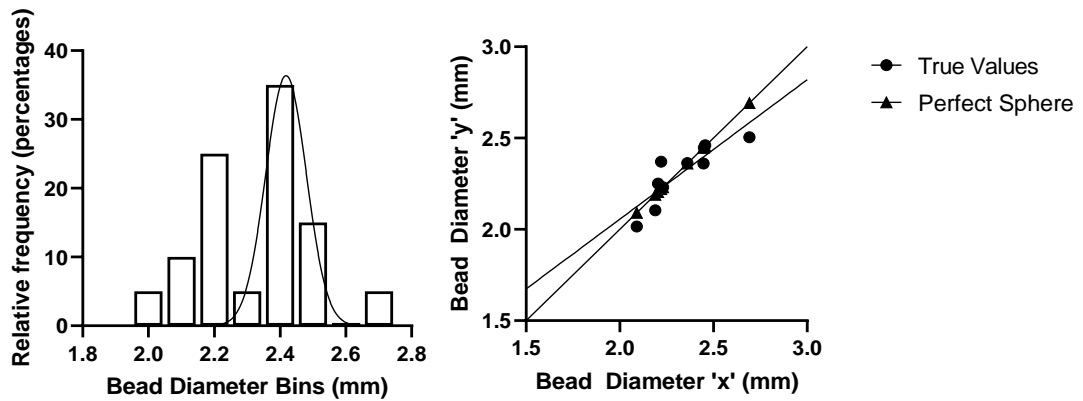


Figure 6.3.2 FA Bead Diameter and Sphericity (N=20). A Bins of 0.2 mm were selected to best represent the data. A gaussian distribution using the least squares fit method is applied. B Fibrin Alginate Sphericity. A perfect circle would have equal X and Y diameter. Linear regression was used to create the line of best fit for both true values and perfect sphere values. Bead diameter had an R2 value of 0.74.

Swelling ratio assesses the difference in weight of a scaffold from being completely absent of water to its size when fully hydrated. This measures both the porosity of the scaffold, and the mechanical strength of the scaffolds (Fig. 6.3.3). This can therefore investigate if fibrin cross-linking is similar between different beads. FA swelling ratio by mass was a mean $1058\% \pm 253.7$ increase on dry weight, with a range of 757-1450. With a standard deviation of around 25% of the mean, crosslinking was unlikely to be identical between each bead, however, is within the range seen in other studies³⁵⁸. The longevity of beads during culture without cells was next investigated to ensure they could provide a vehicle for cell growth over time.

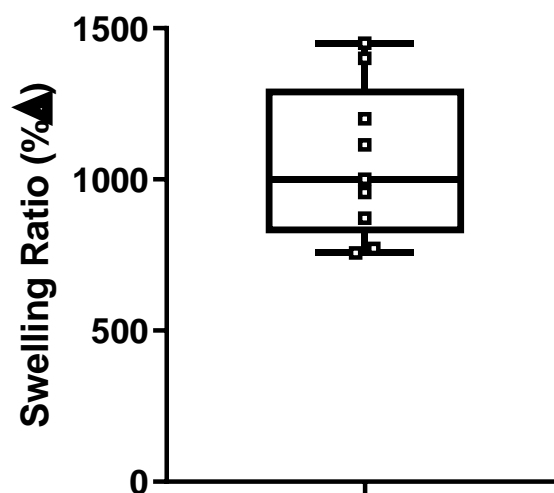


Figure 6.3.3 Characterising the Swelling Ratio of Fibrin Alginate by Weight After Freeze-Drying in PBS (N=10). Shows the percentage change between dry weight and final wet weight. Data shows mean \pm standard deviation.

Images of beads were taken consistently during culture without cells to be able to visually assess changes to cells (Fig. 6.3.4). Whilst mostly spherical from the start of culture, by day 14 in some beads there was a small amount of deformation, however beads mostly maintained their spherical structure. To further clarify changes to the beads, weight was analysed during culture to investigate changes over time.

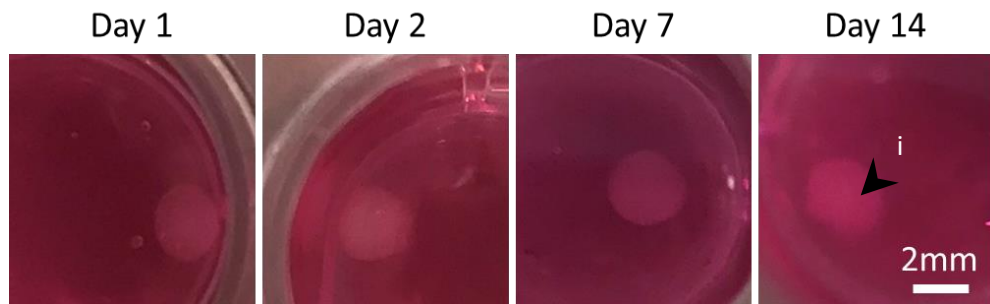


Figure 6.3.4 Fibrin Alginate Structure During Culture Over 14 Days in DMEM. Fibrin alginate was cultured in DMEM without FBS over 2 weeks. i – slight loss in sphericity at day 14.

FA bead weight over time was measured during culture to see if there were changes, which would signify any degradation (Fig. 6.3.5). Initially, there was a large increase in weight that then fell back down to the same level. Some beads were damaged and broke down, thought to be due to mechanical degradation by repeated bead removal and drying before weighing. However, some made it to 15 days, maintaining a similar weight over the period. As the scaffolds had the potential to allow diffusions of material as seen by swelling assay, as well as the ability to maintain structure for prolonged culture, the next step was to investigate if the scaffold had any effect on MSC proliferation or cytotoxicity.

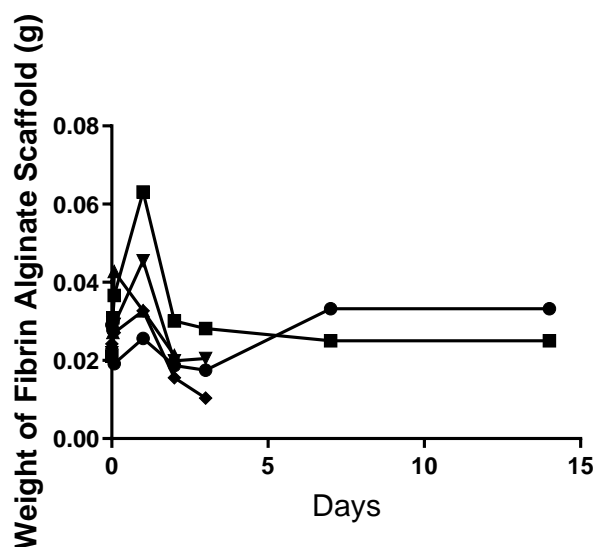


Figure 6.3.5 Figure 6.3.1 Change in FA Weight Over Culture (N=5). FA beads were Cultured for 2 Weeks in DMEM without FBS.

The XTT assay measures cellular metabolism, by adding the XTT compound, which is broken down by cells to produce a yellow colour measurable by absorbance spectra. The visible changes as well as changes in absorbance are shown in Figure 6.3.6. A negative control of 10% DMSO in DMEM, a positive control of StemMACS and a test media of DMEM which FA was cultured in for 48 hours and then filtered, was used. Negative control showed no change in colour from the basal media as expected (Fig. 6.3.6A,-). Positive control showed a dose-dependent visible increase in colouration with increased cell seeding density (Fig. 6.3.6A, +). FA extract showed a strong increase in colouration at all cell concentrations, suggesting a positive effect of FA on MSC metabolism (Fig. 6.3.6A, FA). Absorbance showed that both controls were effective, and that at 3 donors, the fold change in absorbance was significant between positive and negative controls, but only at the highest cell concentration ($p=0.003$). There was a cell concentration dependent absorbance, with the negative control showing no change, whereas the positive control doubled as the number of cells seeded did. Comparatively, FA extract treated cells did not show a cell concentration dependent response, instead all 3 cell concentrations showed around 1.5-fold increase in absorbance after XTT culture, similar to that of the 1000-seeded cell concentration of the positive control. This shows that FA has a positive effect upon cell metabolism, which would be beneficial for a reparative structure. Now that the scaffold had been established as mechanically competent and non-toxic, next was to investigate its ability to direct MSCs towards chondrogenesis.

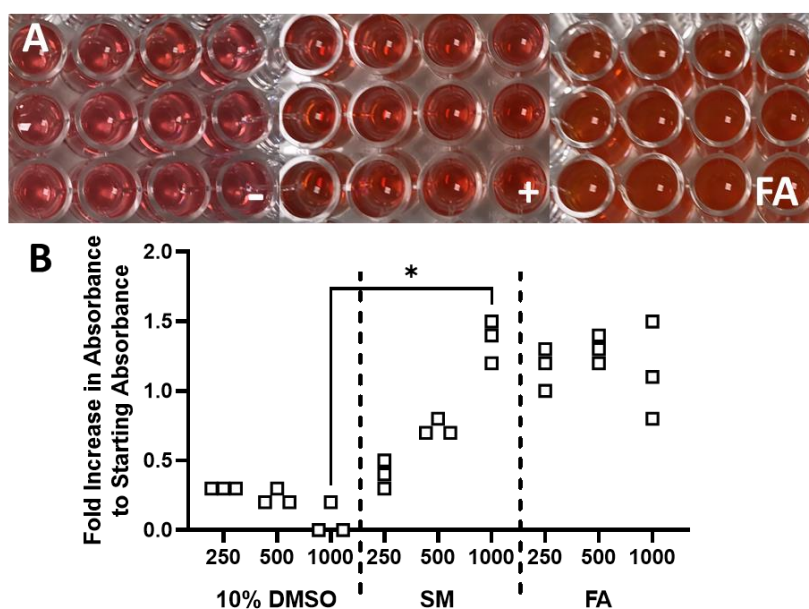


Figure 6.3.6 Effect of Fibrin Alginate on MSC Viability by Indirect Toxicity Assay (N=3). A Photo of XTT wells following 72 hours in culture with FA extract (FA extract in DMEM with FBS), StemMACS (+), or 10% DMSO in DMEM as a negative control (-). First row is 250 cells seeded, second row is 500, and third row is 1000. B XTT assay results demonstrating relative increase in absorbance of Fibrin Alginate culture by a measure of cellular metabolic activity. Data shows median and range with all data points.

6.3.2. IC MSC Behaviour in in 3D FA or Pellet Culture after PL or K Preconditioning

With two working 3D culture methods – FA and pellet culture, the preconditioning method developed in chapter 5 could now be applied and followed by a 3D culture period as planned. MSCs were first loaded into the FA beads and images taken to show encapsulation (Fig. 6.3.7). Beads retained their spherical structure (Fig. 6.3.7A). Under magnification, the edge of the bead remained spherical, and MSCs were visible dispersed throughout the scaffold (Fig. 6.3.7B). At high magnification, MSCs were clearly seen dispersed in the scaffold (Fig. 6.3.7Ci). Some MSCs were clustered but not in groups larger than three (Fig. 6.3.7Cii). MSCs were rounded in shape, expected of MSCs on a material that would suit chondrogenesis, and dispersed, showing successful encapsulation. As culture was continued, cultures were monitored to investigate changes in MSC morphology in response to conditions used.

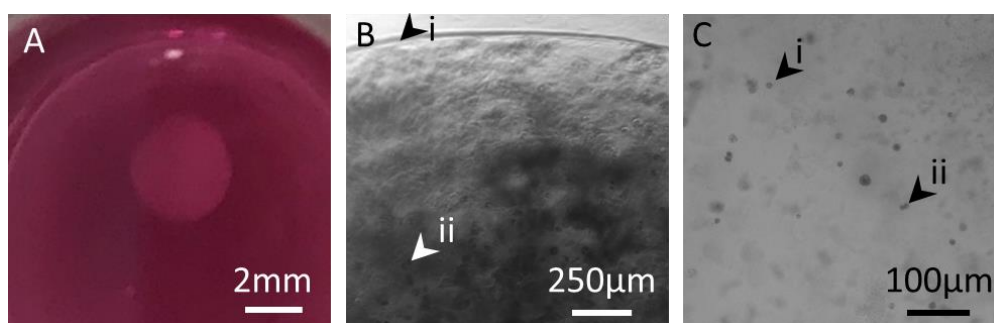


Figure 6.3.7 FA Bead and MSC Behaviour after 48 Hour Culture in StemMACS (N=1). A – FA retaining spherical structure during culture. B – MSCs in Fibrin Alginate showing cell encapsulation, clustering and dispersion. i – Rounded edge of bead. ii – MSCs encapsulated within FA. Taken at 40x magnification. C – High magnification of Encapsulated MSCs in Fibrin Alginate, showing round MSC morphology. i – Single rounded MSC. ii – Two clustered, rounded MSCs. Taken at 250x magnification.

After 7 days, images of MSCs were taken under high microscopy to investigate changes to MSC morphology based on the culture medium. At this time-point, all beads remained and were spherical, so more pictures of the bead were not taken. MSCs remained dispersed and maintained a rounded morphology in all conditions (Fig. 6.3.8). PL-preconditioned cultures showed higher clustering, suggesting increased growth rate relative to MSCs preconditioned in K. Of the 3D culture mediums, there were no outright clear differences, however compared to prior images there were more MSCs per scaffold. As all MSCs were still growing within the culture and maintaining a spherical structure, the scaffold was effectively encouraging both growth and expected beneficial phenotypes. Culture was continued until day 14 at which the experiment was due to be completed and samples analysed.

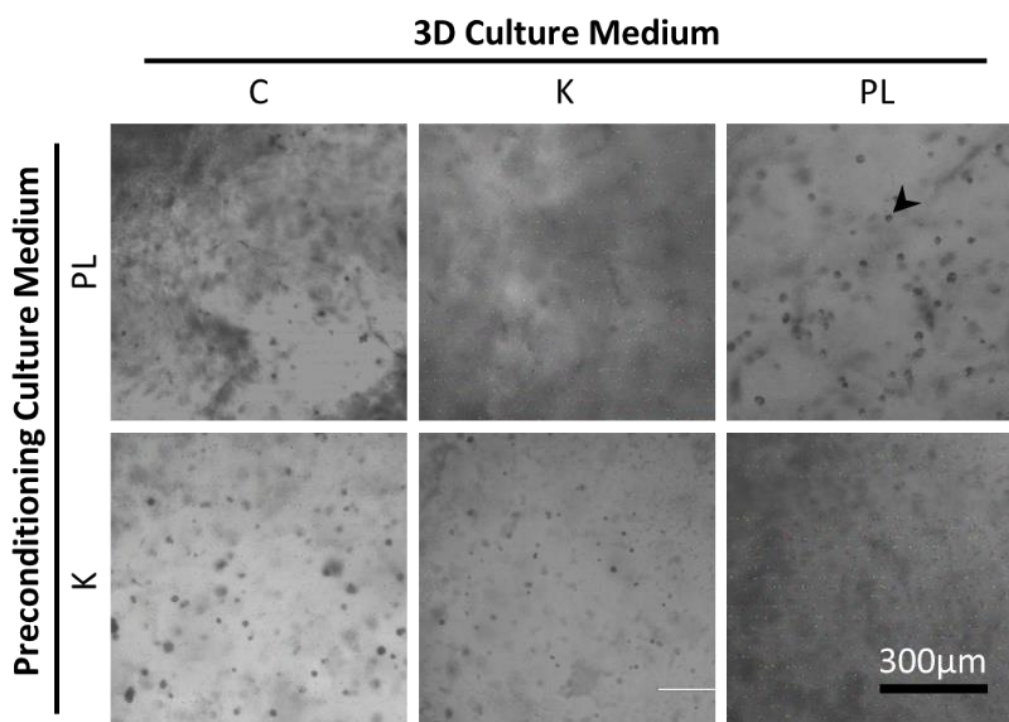


Figure 6.3.8 MSC Appearance in Fibrin Alginate Beads Grown in C, PL or K at 7 Days after 14 Day Preconditioning in C, PL, or K (N=3). All images were taken at 100x magnification. Conditions are further explained in Table 6.2.2.

After 14 days, many of the scaffolds started to burst, or show MSCs external to the scaffold, in all conditions (Fig. 6.3.9). In beads which remained, MSCs could be observed adhered to plastic, which was not seen before this timepoint (Fig. 6.3.9Ai). However, MSCs remained within the scaffold with a rounded phenotype (Fig. 6.3.9Aii). MSCs were visibly adhered around and directly underneath the scaffold (Fig. 6.3.9Bi). MSCs within the scaffold were circular, larger than adherent MSCs and clustered together. Some scaffolds had burst and left remnant pieces (Fig. 6.3.9C,D). In these, MSCs had escaped in larger numbers with visible surrounding debris (Fig. 6.3.9C,D i). Some MSCs remained within these fragments, as such the fragments were collected for analysis (Fig. 6.3.9C,D ii). It was additionally clear that the beads had lost their spherical shape by often concave edges (Fig. 6.3.9C, Diii). Beads were subsequently stained for methylene blue to investigate cell remnants, and what remained of the beads.

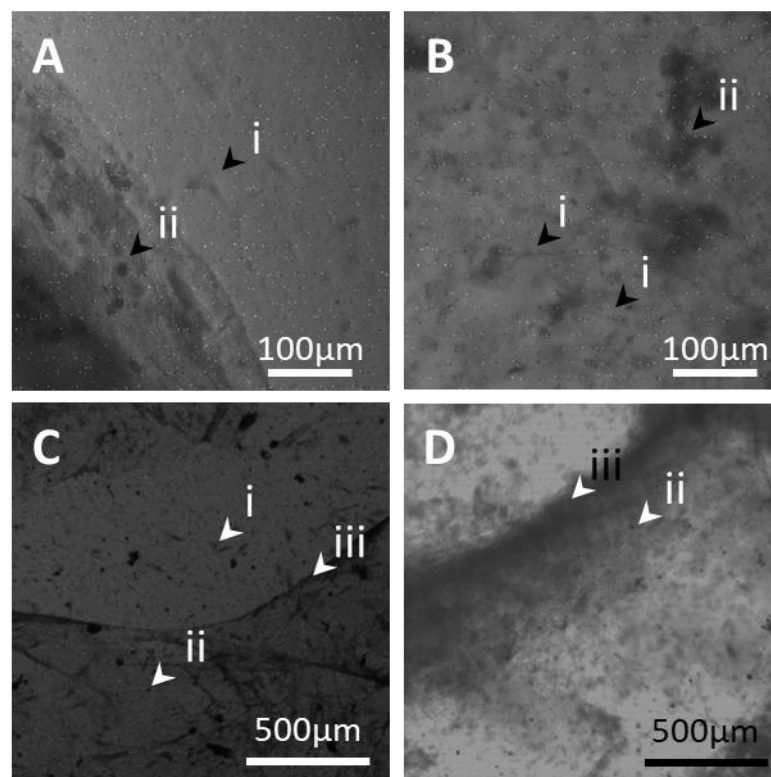


Figure 6.3.9 Analysis of Burst FA Cultures (N=3). A/B MSC escape from FA beads. i – Plastic-adhering MSC outside of bead. ii – Retained MSC with rounded phenotype within FA. Images taken at 20x magnification. C/D Burst FA bead structure. i – Plastic-adhering MSC outside of FA. ii – Retained MSC with rounded phenotype with FA. iii – border of burst bead.

Methylene blue successfully stained remaining FA beads, which most often attached to the side of the wells (Fig. 6.3.10). In wells where there is no stained material, this is due to beads or fragments all being removed for analysis as other experiments were prioritised. Interestingly, MSCs preconditioned in K and treated in C showed the most adherent cells over the plate, suggesting either an unexpectedly high growth rate or higher enzymatic activity. MSCs treated in PL in 3D showed the most alginate remnants, suggesting the highest protection of the beads. To attempt to understand these changes, and if there was any GAG synthesis, histological analysis was undertaken.

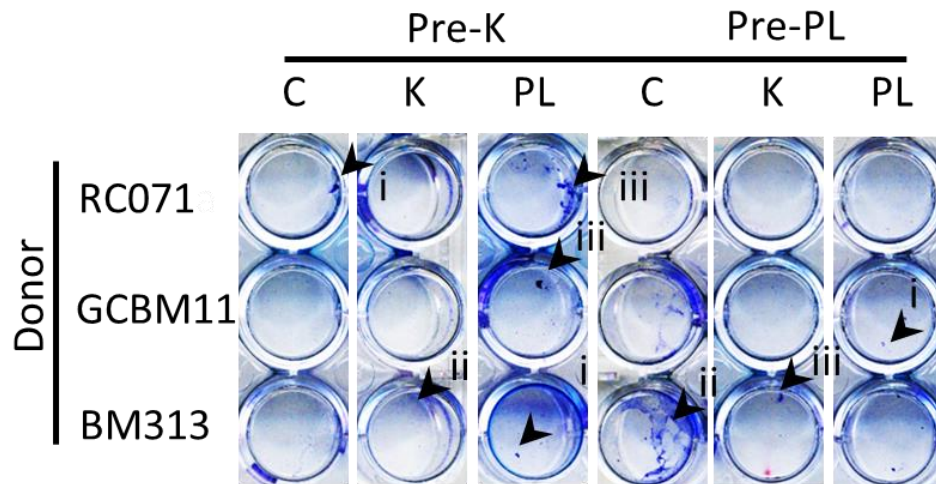


Figure 6.3.10 Methylene Blue Staining of FA Beads After 14 Days Culture (N=3). Pre-PL – Preconditioning PL treatment. Pre-K – Preconditioning K treatment. i – Segmented or reduced-size FA beads. ii – Fully burst spheres with MSC growth over the well. iii – Larger, mostly whole FA spheres.

Histology of FA beads by toluidine blue was performed to investigate cells presence and if there was any GAG deposition (Fig. 6.3.11). Toluidine blue, as a cationic dye, stains proteoglycans in a metachromatic manner dependent on the amount. As such, GAG deposition is typically purple, and cells and background light blue. Beads were largely degraded, however there were some that retained morphology (Fig. 6.3.11A). Under higher magnification, FA beads stained a dark blue as expected (Fig. 6.3.11Bi), with large amounts of visible GAG deposition (Fig. 6.3.11B/Cii). This was more-so within regions where there was some erosion (Fig. 6.3.11B/Ciii). This may have been driven by MSCs, or considering the vast amounts of GAG, lacunae produced by chondrocytes consisting of pericellular matrix such as Collagen VI or IX³⁵⁹. In more degraded beads (Fig. 6.3.11D), large amounts of erosion were visible, however there were still also significant amounts of GAG deposition (Fig. 6.3.11Bii) within the bead remnants. This shows that FA successfully supported chondrogenesis to a strong degree, however the rapid degradation of beads needs to be further optimised. As this 3D culture method needed further optimisation, pellet culture was next investigated to see differences between treatment conditions in another 3D model.

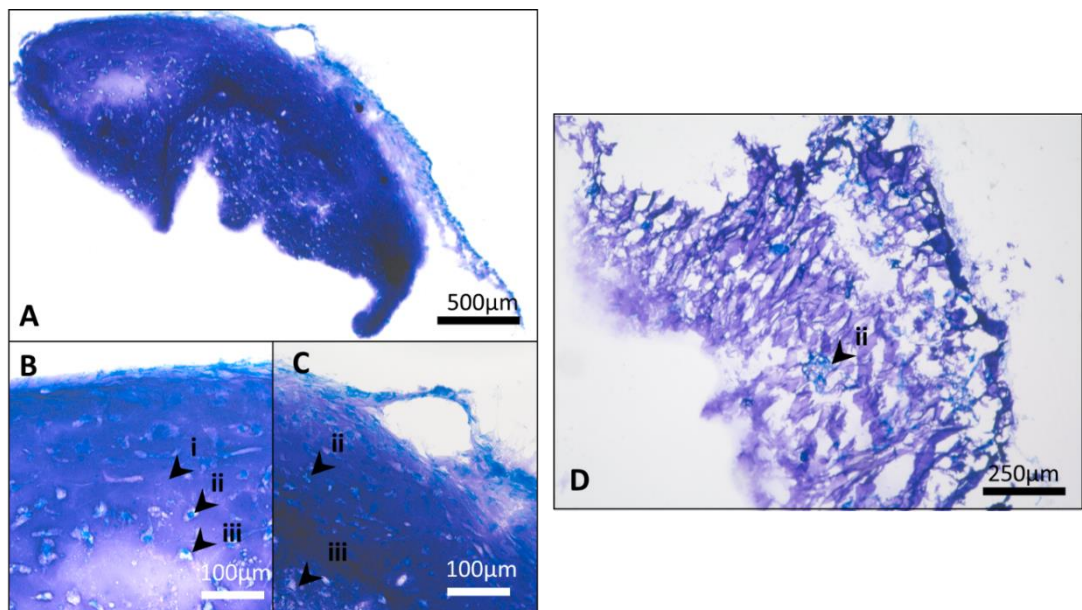


Figure 6.3.11 Toluidine Blue Staining of FA Beads (N=3). A Mildly degraded bead. B Magnified region of A to show GAG deposition. C Magnified region of A showing a more degraded region with higher cell density. D Largely degraded bead. i – FA, ii – GAG deposition, iii – Spaces within FA. A was taken at 50x magnification, B & C were taken at 200x magnification, D was taken at 100x magnification.

Pellet culture is commonly used to study MSC chondrogenesis in terms of general differentiation capacity, but also for other conditions, due to its simplicity and low cost. At day 14 in IC treated MSCs, all culture mediums showed successful pellet formation (Fig. 6.3.12). Interestingly, for all conditions differentiated in K, pellets had instead formed a gelatinous 'pool' at the bottom of the Eppendorf in place of the pellet, which was potentially either a collapsed pellet, or GAG being released into solution. As such when media was removed care was taken not to disturb this pool. Of the different preconditioning medias, K-preconditioned MSCs generally produced larger pellets, but not by a large margin. Of 3D treatments, C-treated MSCs produced noticeably larger pellets compared to PL but were not comparable to K-treated pellets due to the pools formed. This was expected with C being the positive control, but to investigate if this size increase was related to MSC proliferation or chondrogenic potential, measurement of GAG in the pellet was needed. Media was also retrieved for each condition as visible on the right of Fig. 6.2.12A. Visibly, media from pellets treated with K in 3D conditions was less translucent than other conditions, suggesting that GAG was released into the media. Media from C-treated conditions were the most translucent compared to PL or K treated conditions, meaning C may increase the amount of GAG being retained in the pellet. When K-treated pools were dislodged to attempt flash-freezing for histology, small beads were noticeable within the fluid, as seen in Fig. 6.2.12B. This either means there was a more solid core, or that the viscous white fluid was something moved externally from the pellet. To try and understand if what was being generated was cartilage, pellets were snap frozen, cryo-sectioned and stained for toluidine blue.

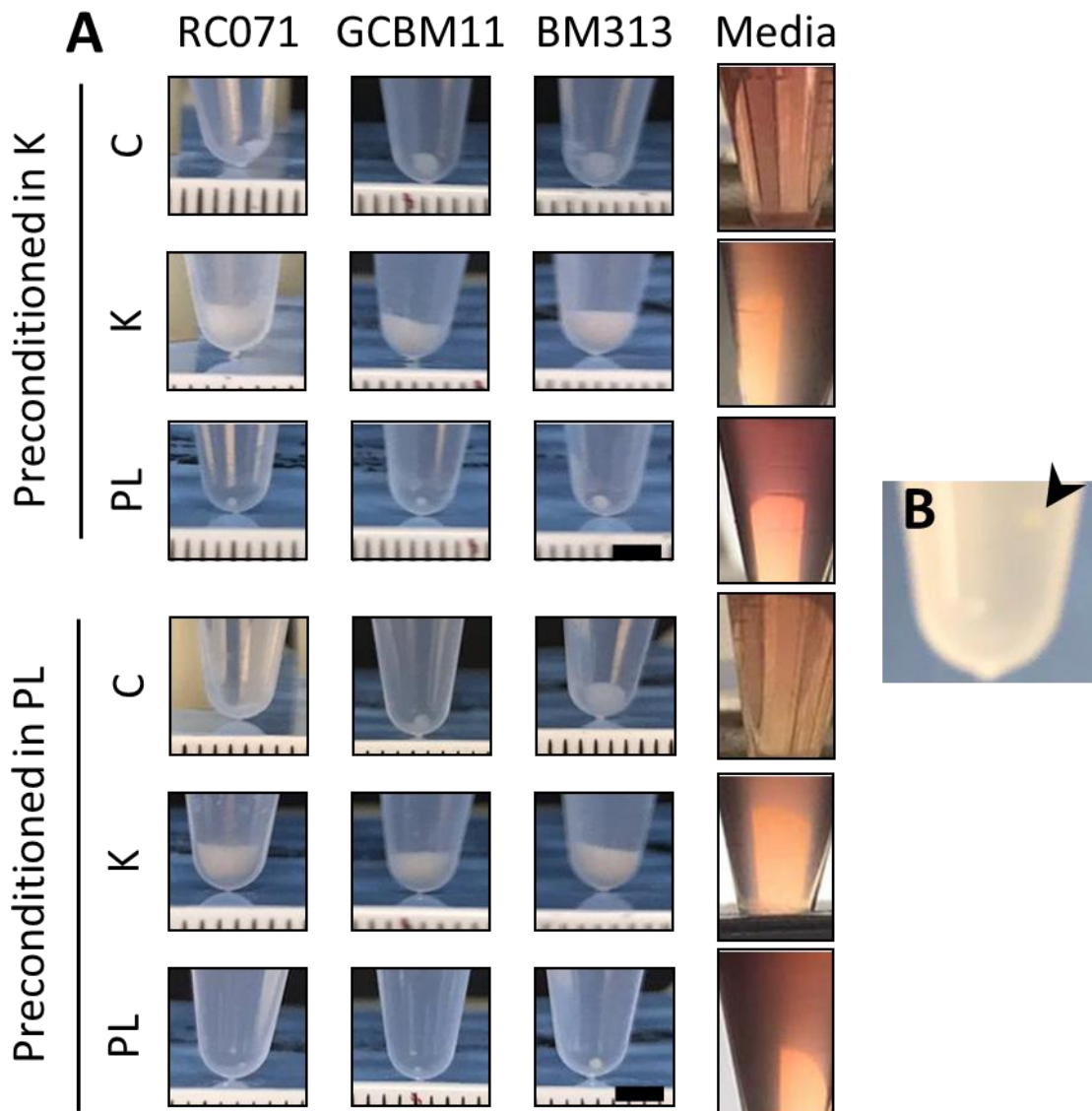


Figure 6.3.12 Pellet and Media from IC MSCs Preconditioned in K or PL for 14 Days Before 3D Culture in Pellets in K, PL or C. A Pellets and Media in respective conditions. Each image of the media is from donor BM313 as repeats looked similar. B Pellet visible from K cultures after sample disruption. Arrow shows a pellet after mixing of samples treated with K in 3D. Scale bars are 3 mm.

Toluidine blue, as mentioned earlier, shows GAG deposition within extracellular matrix, based on the cationic dye binding proteoglycans. Pellets demonstrated GAG deposition, showing both that pellet culture supports chondrogenesis and that this preconditioning method and 3D culture treatment system was effective (Fig. 6.3.13). Both examples presented a mostly rounded pellet (Fig. 6.3.13A/B), with the background being stained a light blue (i), cells dark blue (ii), and GAG deposition purple (iii). This shows the method is suitable for testing GAG production, however the small size of the pellets limited how many successful stains could be obtained.

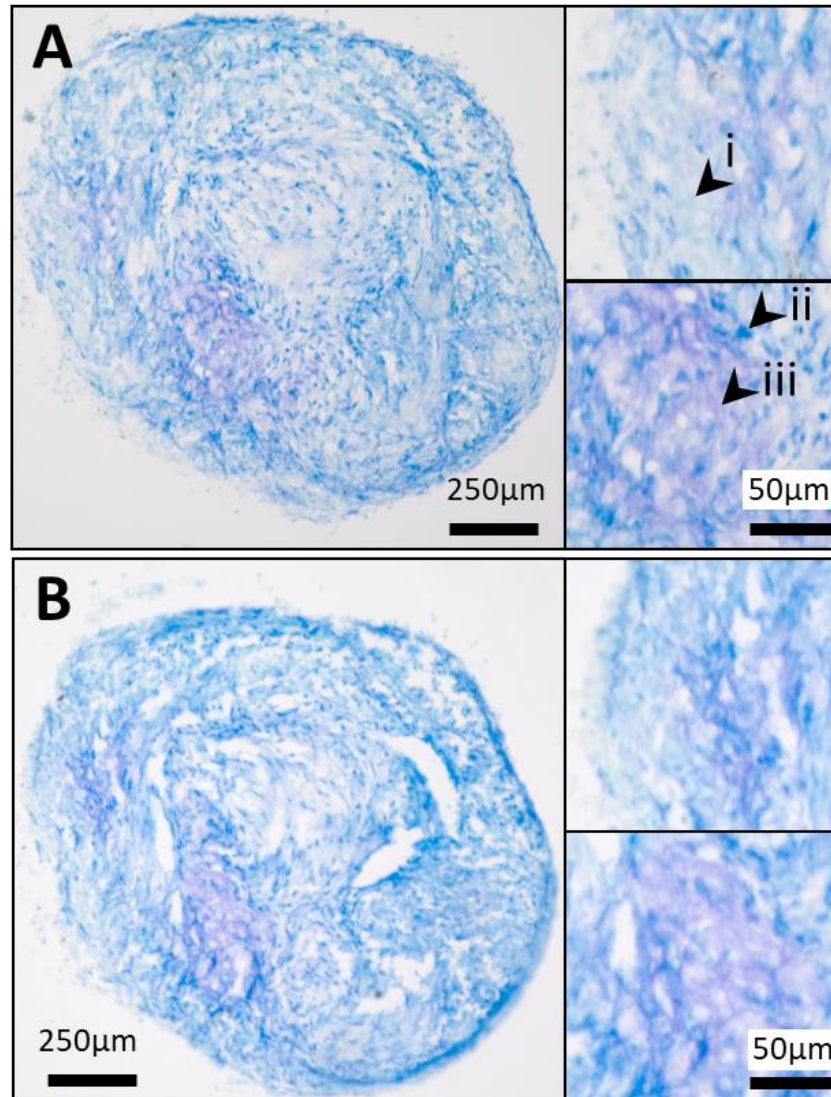


Figure 6.3.13 Toluidine Blue Staining of Chondrogenic Pellets Demonstrating GAG Deposition (N=1). A Pellet from IC MSCs preconditioned with K and treated with C. B Second pellet Section to demonstrate GAG deposition. i – Background staining, ii – cell, iii – GAG deposition. Larger photos are 100x magnification with 250µm scale bar (left) and small paired photos (right) are 600x with 50µm scale bar.

As in differentiation experiments (Section 4.2.17), pellet diameter was measured, as pellet size is associated with GAG production as the same number of starting MSCs is used, although can also relate to collagen production or cell proliferation (Fig. 6.3.14). Due to pools formed by samples treated with K in 3D, height of the pool was measured instead for these samples, as such were not be directly compared to pellets. Preconditioning with K or PL did not have large effect upon pellet size, although the largest pellets of K-preconditioned pellets was higher than PL preconditioned pellets (Fig. 6.3.14A). Differentiation in C produced 1.8-fold larger pellets than those differentiated in PL. These two groups of 3 suggest preconditioning plays a key role (Fig. 6.3.14B). In 2 of 3 donors, K-differentiated pools were taller after K-preconditioning than PL. Of combinations, K-C and PL-C showed up to 3-fold larger pellets than K-PL or PL-PL, although donors had specific responses. RC071 showed small pellets in all conditions. GCBM11 responded to K-C, being 2-fold larger than all other conditions. Donor BM313 presented large pellets after both K-C and PL-C treatment, but not K-PL or PL-PL. This suggests differentiation in PL does not greatly increase pellet diameter. To further understand changes to chondrogenic capacity after treatment, GAG content of both pellet and media was performed.

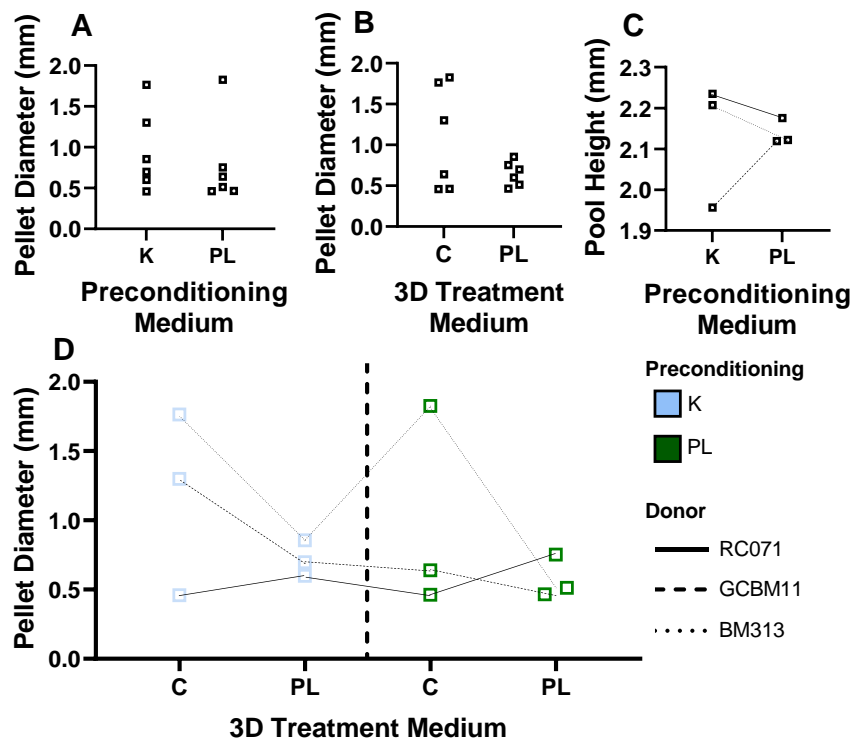


Figure 6.3.14 Diameter of IC Pellets after 2 Week Preconditioning with K or PL, and 3 Week 3D Culture with K, PL or C (N=3). Diameter was defined as the largest edge-to-edge distance (N=3). A Effect of preconditioning media upon pellet diameter after both preconditioning and 3D culture with C or PL. There are 6 data points due to 3 donors 2 differentiation media B Effect of 3D culture medium on final pellet diameter. There are 6 data points as there are 3 donors and 2 preconditioning media. C The effect of preconditioning media on pool depth of samples treated with K in 3D (3 donors) D Combined effect of preconditioning and 3d culture mediums upon pellet diameter. Data shows median with all data points. Lines connect same donor.

Pellet GAG content reflects the total amount of GAG produced by MSCs, a critical part of new cartilage synthesis as shown earlier in differentiation assays (Section 4.2.19), again reported here (Fig. 6.3.15). Pellet sGAG was similar after both K and PL preconditioning (Fig. 6.3.15A). Differentiation treatments showed 1.4-fold higher GAG content in K-treated pellets than PL or C treated cultures (Fig. 6.3.15B). However, this was not significant ($p=0.252$). PL and C-differentiated cultures had similar GAG content within the pellet. K-C and PL-C showed similar levels of pellet GAG, with a small 1.1-fold increase in K-K and a large 2-fold increase in PL-K but this was not significant ($p=0.1324$) (Fig. 6.3.15C). As GAG concentration did not match the pellet diameter results, collagen production or MSC proliferation may be affected. Overall, K seems to be the most effective 3D treatment for GAG within the pellet. As GAG was also seen in media, sGAG content of the media was next investigated.

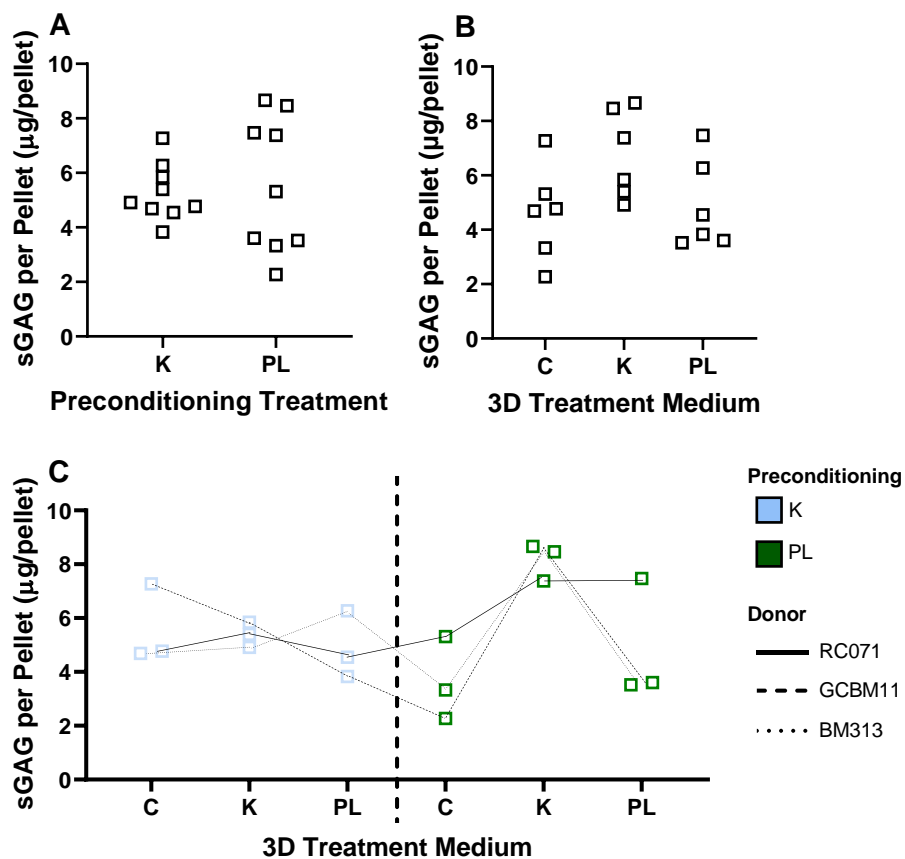


Figure 6.3.15 GAG Content of IC MSC Pellets after K or PL Preconditioning for 2 Weeks and Differentiation in C, K or PL in Pellets for 3 Weeks (N=3). A Effect of preconditioning medium on pellet GAG content after 3D treatment (Differentiation medium results are pooled). B Effect of K, PL or C as a 3D treatment medium on pellet GAG content (Preconditioning results are pooled). C The effect of preconditioning with K or PL and 3D culture medium upon GAGs produced and retained in the pellet. For all graphs, technical replicates were averaged to show biological replicates. Graphs shown median \pm range with all data points. Lines connect same donor.

As media of the pellets was visibly different between different cultures, as well as the unusual pool shape seen after K-differentiation, GAG in media was additionally measured (Fig. 6.3.16). K-preconditioned cultures showed higher GAG content than PL, but not by a clear margin (Fig. 6.3.16A). C-differentiated cultures had the lowest GAG in media. K and PL-differentiated cultures were similar GAG in the media, 1.5-fold-higher than C (Fig. 6.3.16B). Donors presented similar overall trends, with K-C and PL-C having 10%-50% less GAG in the media compared to other differentiation treatments. To clarify this, GAG retained in the pellet was compared to the GAG within the media to see if there were correlations between how much was retained.

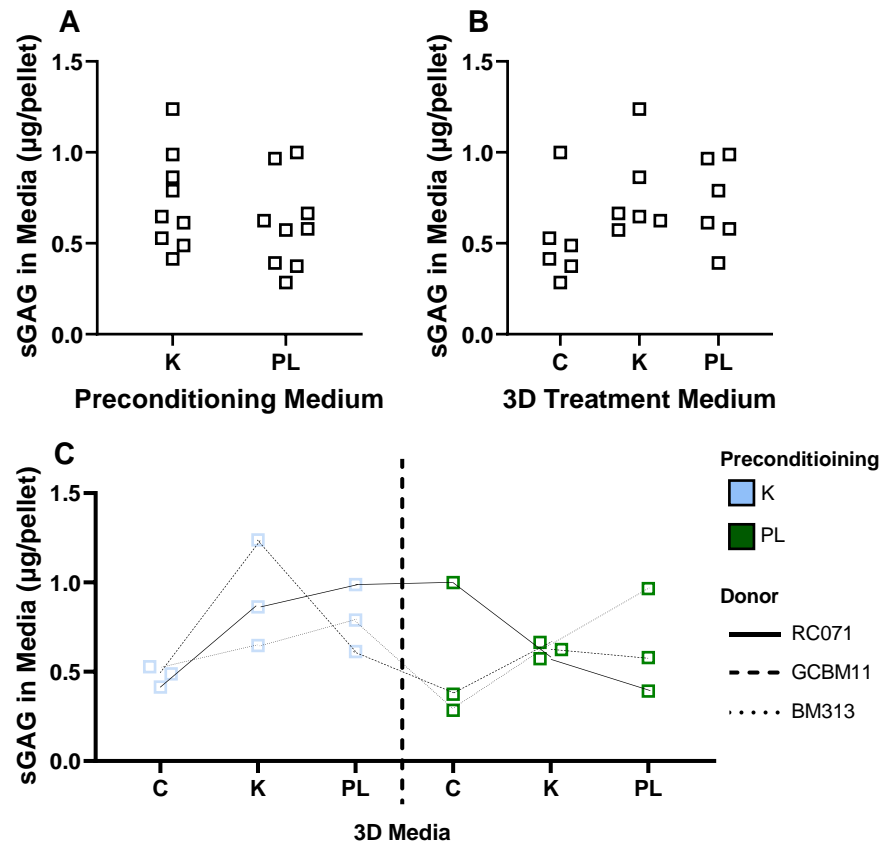


Figure 6.3.16 GAG Content of Media from IC MSC Cultures after K or PL Preconditioning for 2 Weeks and Differentiation in C, K or PL in Pellets for 3 Weeks (N=3). A Effect of preconditioning medium on GAG in media after 3D treatment (Differentiation medium results are pooled). B Effect of K, PL or C as a 3D treatment medium on GAGs released into medium (Preconditioning results are pooled). C The effect of preconditioning with K or PL and 3D culture medium upon GAGs released into media. For all graphs, technical replicates were. Data shows median and range with all data points. Lines connect individual donor results.

As GAGs were in both the media and pellets, GAG retention in the pellet of total GAG was assessed for each condition. GAGs remain in the local extracellular region by adhering to cells, which may affect cartilage regeneration (Fig. 6.3.17)³⁶⁰. Preconditioning media did not greatly affect GAG retention, but was on average higher in PL (Fig. 6.3.17A). Differentiation with K or C led to similar levels of GAG retention in

the pellet, falling 5% points in PL differentiated cultures (Fig. 6.3.17B). In combination, K-K and PL-C led to the highest amount of GAG retained, consistently around 93% of GAGs, 10-15% higher of remaining treatments including control K-C (Fig. 6.3.17C). Choice of both preconditioning and differentiation stimulant affect GAG retention in the pellet, but the impact of this depends on how critical it is that GAGs remain in the local ECM. Using K with 50% PL appears to be able to revert PLs effect on GAG retention, but only after K preconditioning. As K-K produced similar GAG to C, released more GAG into media and consistently retained the most sGAG of total sGAG, it would seem K-K is the most effective biological stimulant for non-diseased IC MSCs, but it remains to see if the same is true in OA MSCs.

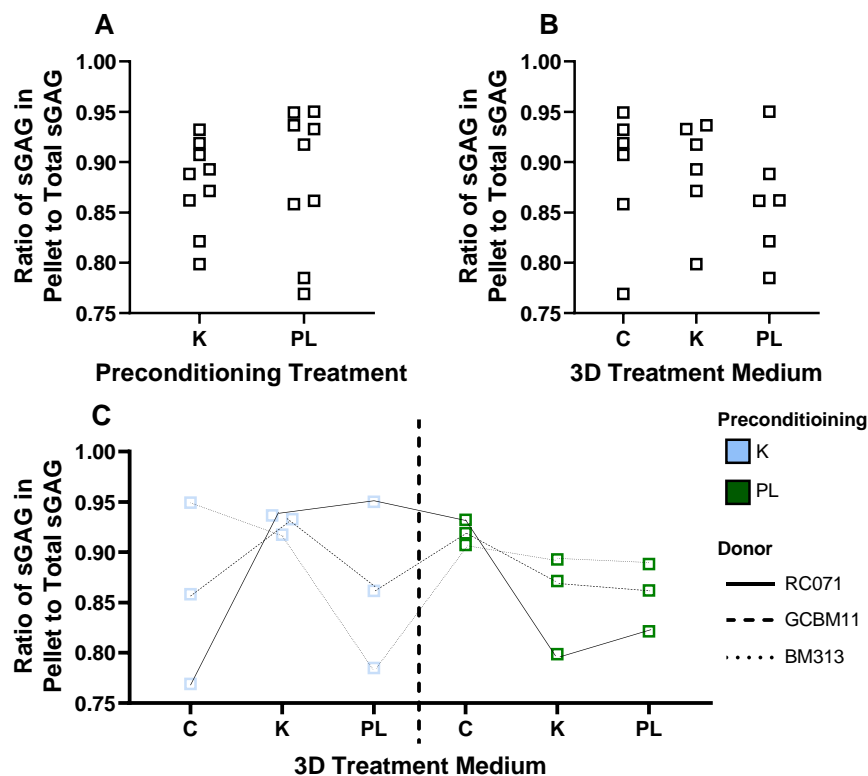


Figure 6.3.17 Ratio of GAGs Retained in the Pellet to Total GAG in IC MSC Cultures, after K or PL Preconditioning for 2 Weeks and Differentiation in C, K or PL in Pellets for 3 Weeks (N=3). A Effect preconditioning on GAG retention after 3D culture (differentiation medium results are pooled). B Effect of differentiation medium on GAG retention (preconditioning medium results are pooled). C Effect on GAG retention of IC MSCs. Technical repeats were averaged to show biological replicates. Graphs shown median \pm range with all data points. Lines connect individual donor results.

This work has shown that each condition can produce GAGs, however a critical part of this investigation was to see if biological stimulants could drive chondrogenesis without osteogenesis, as such gene expression was next investigated.

Gene expression was investigated through qPCR. However, the nature of the pellets and the GAGs within them made extraction difficult, and many genes were below detection. Unfortunately, the treatment combination which seemed most beneficial, K-K, was not available. Pellets treated with PL-PL and PL-C showed the mostly complete dataset and is shown first (Fig. 6.3.18). After PL preconditioning, PL differentiated samples compared to C differentiated samples showed 6-100-fold reduced expression of all chondrogenic genes (TGF β 1, TGF β 3, SOX9, ROR2, IGF1 and SPHK1) (Fig. 6.3.18A), increased expression of each osteogenic gene (RUNX2, ALPL and SPP1) other than BGLAP (Fig. 6.3.18B). Additionally, there was reduced expression of genes related to other lineages (PPARG, CCL12, CCL20 and VEGFC), showing reduced adipogenic and angiogenic activity (Fig. 6.3.18C). PL-differentiated samples also showed reduced expression of ECM remodelling factors MMP14, TIMP3, and ADAMTS, but not MMP1 (Fig. 6.3.18D). PL showed reduced expression of immunomodulatory related gene, S1PR1, compared to C. Remaining genes were inconsistent with no clear trend (Fig. 6.3.18E). Overall, C treatment showed elevated chondrogenic genes but increased ECM and remodelling proteins. PL-PL showed increased expression of MMPs and other lineages, but reduced chondrogenic expression compared to PL-C, suggesting PL is not suitable for differentiation.

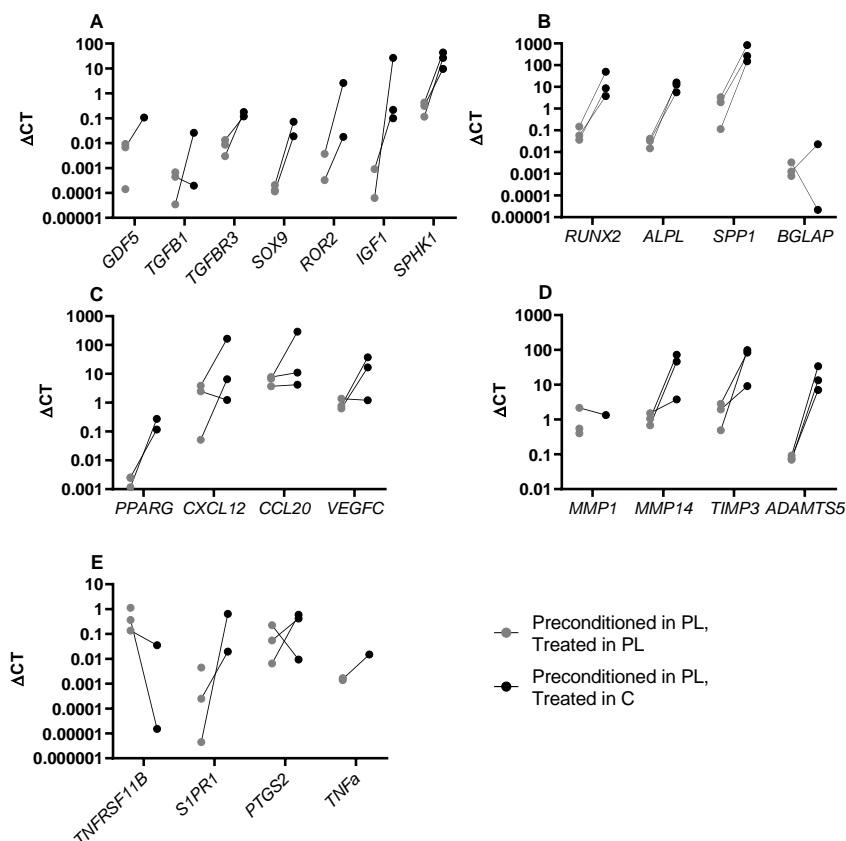


Figure 6.3.18 Gene Expression of IC MSCs Preconditioned for 2 Weeks PL and Differentiated in PL or C (N=3). A Chondrogenesis-related gene expression changes. B Osteogenesis-related gene expression changes. C Stromal-related gene expression changes. D ECM-remodelling related gene expression. E Immunomodulatory gene expression change. N=3, where 3 donors are not presented, one or more was below detection. Lines demonstrate paired cultures.

Next, available comparisons for preconditioning with either K or PL, followed by differentiation in C, were investigated (Fig. 6.3.19). Firstly, osteogenic gene expression was successfully suppressed by K-preconditioning in 2 of 3 donors for RUNX2, ALPL and SPP1, as the medium is intended to do so (Fig. 6.3.19A). Of genes related to other factors, K-preconditioning again reduced expression in 2 of 3 donors for CXCL12, CCL20 and VEGFC, and the only paired donor for PPARG (Fig. 6.3.19B). Whilst results were not obtained for key chondrogenic genes, K did successfully show suppression of osteogenic genes, as well as reduced expression of genes relating to other differentiation pathways, suggesting preconditioning may have potential to focus differentiation away from other lineages. Lastly, a complete dataset for 1 donor on 4 genes in 4 conditions was obtained and investigated.

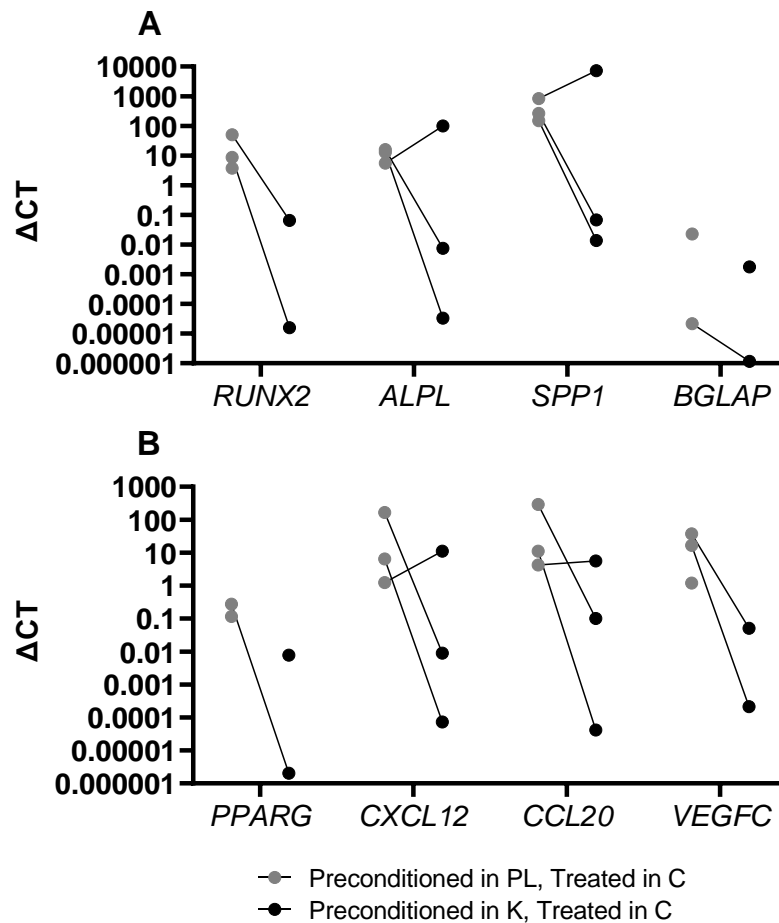


Figure 6.3.19 The Effect on Gene Expression of IC MSCs after PL or K Preconditioning followed by Pellet Culture in C. A Changes in osteogenic-related protein gene expression. B Changes in adipogenic and stromal-related protein expression. N=3, where 3 donors are not presented, one or two was below detection. Lines demonstrate paired cultures. Pre denotes the preconditioning media, and post denotes the 3D treatment medium.

In a single donor, gene expression results were obtained for RUNX2, CXCL12, CCL20 and VEGF after preconditioning in PL or K and 3D treatment in PL or C. As the most complete dataset, this was investigated for differences (Fig. 6.3.20). Positive control K-C suppressed all 4 genes 1×10^4 - 1×10^5 -fold compared to PL-C, showing that K-preconditioning suppresses expression of these genes. K-PL compared to K-C showed a 1×10^3 - 1×10^4 -fold increase in all 4 genes, suggesting PL induces their expression. PL-PL had slightly suppressed expression of all 4 genes compared to PL-C, of around 100-fold, suggesting PL and C together somehow elevate these genes, as the opposite was seen in K-PL and K-C. As PL-PL and K-PL results were similar, it seems PL in 3D reverts the suppression of expression seen in K-C. Overall, K-preconditioning showed reduced RUNX2 compared to the other treatment groups, suggesting reduced osteogenic differentiation. This was also accompanied by other markers of non-chondrogenic differentiation, which would be a boon for the ideal treatment. As the experimental design worked, with some difficulty with qPCR, next it was investigated if the same trends were observed in talar or tibial samples using the same conditions.

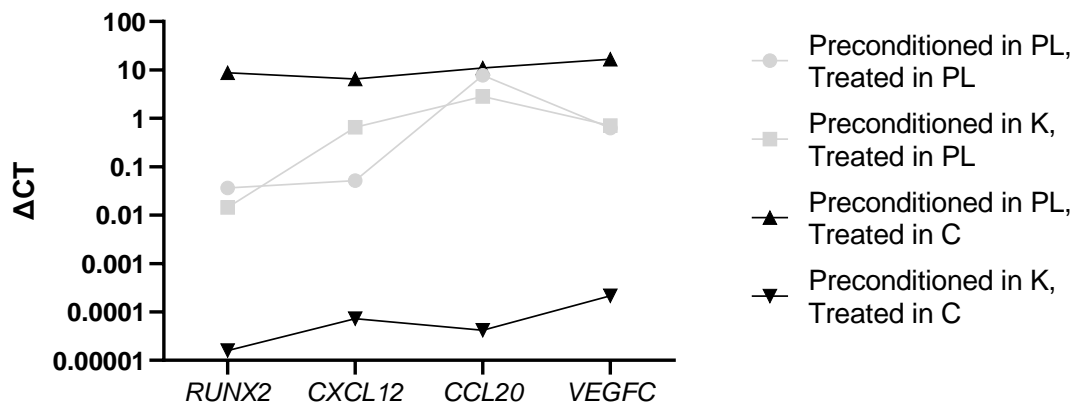


Figure 6.3.20 The Effect on Gene Expression of Preconditioning in PL or K followed by Pellet Culture in PL or C for Donor RC071 (N=1). Osteogenic (RUNX2), stromal (CXCL12, CCL12) and angiogenic genes (VEGFC) where expression was detectable in all 4 conditions are shown. Lines connect paired individual donor results.

6.3.3. Preconditioning and 3D Culture Effect on Talar and Tibial MSC Chondrogenesis

Earlier chapters had showed key differences in differentiation capacity between talar and tibial MSCs compared to IC MSCs, with tibial and talar MSCs showing increased chondrogenic potential, and talar MSCs showing significantly less adipogenesis. However, the OA bone they were taken from was extremely sclerotic, and so may be naturally predisposed to osteogenic differentiation without prolonged *in vitro* culture used in Chapter 4, which would not suit a treatment. This chapter has shown so far that IC MSCs preconditioned in K-K showed the most GAG production both in pellet and media, as well as the highest GAG retention, and seems the most suitable treatment for non-diseased IC MSCs (Fig. 6.3.15-6.3.17). Additionally, K-preconditioning also showed reduced markers for other differentiation pathways, which was also seen to a lesser extent in PL-PL treated MSCs in comparison to PL-C treated cultures (Fig. 6.3.18, 6.3.19). Next, these conditions were tested on talar and tibial MSCs using the pellet method to see if the same effects were seen in this tissue and could be used for development of a treatment. Since FA sphere broke down, potentially due to enzymes produced by cells, it was decided that due to time constraints and the rarity of OA talocrural samples, the FA method should not be used for talar or tibial MSCs. Following culture, images of pellets were captured to visualise of the effect of the conditions on talocrural BONE MARROW MSC chondrogenic ability.

During culture, pellets increase in size, due to either ECM production and therefore pushing cells apart, or cell division. As before, final pellet size was captured for comparison (Fig. 6.3.21). Overall, there were no clear differences between preconditioning treatments, as expected from earlier results. Of 3D treatments, the positive control, C-treated pellets, were the largest in most cases, with little to no visible difference between K or PL treated pellets. WJ11 typically produced the largest pellets, with WJ13 typically showing the smallest, suggesting a difference in innate chondrogenic capability. Some pellets showed white fragments (i) and deformed pellets (ii), which may be related to ECM-degrading proteins being produced. This was more common in PL-preconditioned and PL treated cultures. Compared to IC, there were none of the pools seen in K-treated pellets. This may have been due to the osteogenic precommitment of these minimally-cultured talocrural cells as seen in the results of Chapter 3 and 4, and so less GAG was produced, or these MSCs were able to produce pellets which were mechanically stronger. To test this GAG produced by pellets was required. Firstly, to identify if there were any clear differences between different treatments, individual pellet sizes for each treatment were investigated.

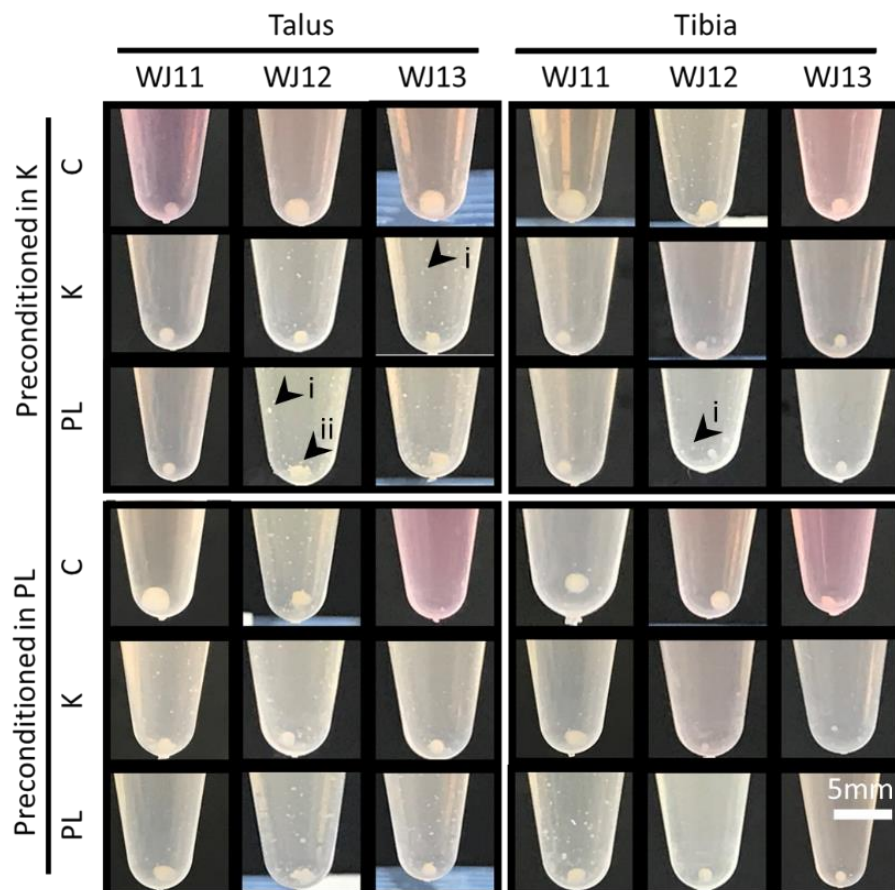


Figure 6.3.21 Talar and Tibial MSC Chondrogenic Pellets After Preconditioning in K or PL, and 3D treatment in C, K or PL (N=3). Scale bar is 5mm. Arrows show i – white fragments, ii – deformed pellets.

To quantify visible changes in diameter and detect any trends, pellet diameter was measured as before (Fig. 6.3.14) for talar and tibial cultures (Fig. 6.3.22). Pellets were mostly the same size after both K or PL preconditioning in talus and tibia for each condition, again as expected. Tibial pellets were slightly larger than talar pellets, but again only by 0.05 mm (SFig. 8.2.1A). Differentiation in C produced the largest pellets in both talus and tibia, being 1.2-1.6 that of K or PL treatments (SFig. 8.2.1B). Talar MSC pellets differentiated in K were smaller than PL differentiated pellets, but the opposite was true in tibia, with K-differentiated pellets being larger. For both preconditioning and differentiation together K-C and PL-C produced the largest pellets in both talar and tibial cultures, being 1.4-2-fold larger than K or PL differentiated cultures (Fig. 6.3.22A/B). Remaining cultures did not vary between each other, and donor response was consistent. Overall, C differentiation was the most effective at increase pellet diameter, however large pellets were still formed in every instance (compared to Chapter 4) showing successful chondrogenesis. However, unlike non-diseased IC MSCs, K-K treated unexpectedly did not produce the pools of GAG. Next, the amount of GAG produced within each pellet was assessed to quantify chondrogenic capacity.

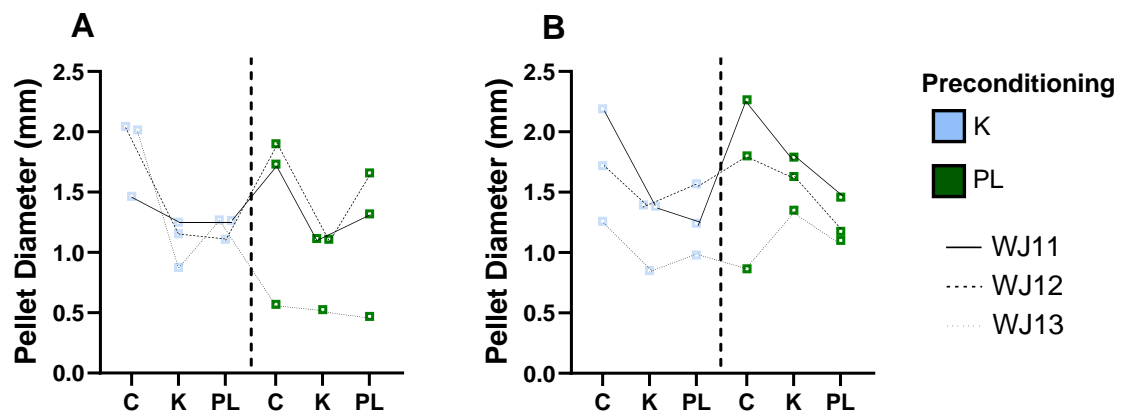


Figure 6.3.22 Pellet Diameter of Distal Tibial and Talar MSC Cultures, after K or PL Preconditioning for 2 Weeks and Differentiation in C, K or PL for 3 Weeks (N=3). A The effect upon talar MSC pellet diameter. B The effect upon tibial MSC pellet diameter. For all graphs, technical replicates were averaged and therefore only biological replicates are shown. Graphs shown median± range with all data points. Lines connect individual donor results.

As before (Fig. 6.3.15), pellet sGAG was measured both within the pellet and in the media to investigate the level of GAG MSCs were producing, with pellet GAG being shown first (Fig. 6.3.23). Due to the variation seen, a logarithmic Y axis was used. Preconditioning in K produced more GAG in the pellet than PL in both talar and tibial pellets, but more so in talus, consistent with earlier results. Talar and tibial pellets contained similar levels of GAG (SFig. 8.2.2A). As in IC, pellets differentiated in C contained more GAG, being around 1-5-fold higher than other conditions, and similar between talus and tibia (SFig. 8.2.2B). When comparing both preconditioning and differentiation media together in the talus, K-C produced more GAG in each donor than K-K, whereas K-PL was higher in the least chondrogenic donor than K-C, and similar in the other two. PL-preconditioned groups were similar between PL-C/K/PL, except in the most chondrogenic donor (WJ011) where PL-C produced around 2-fold GAG (Fig. 6.3.23A). This behaviour was similar in the tibia, with K-C producing the most GAG for each condition, however K-PL again produced the most GAG for donor WJ011 (Fig. 6.3.23B). Consistent with IC MSCs data, K is the more effecting preconditioning treatment compared to PL; however, unlike in IC MSCs, the positive control C is generally most effective for differentiation, with little difference between K and PL. As GAGs were found in the media of IC cultures, GAG were next measured again in talocrural cultures.

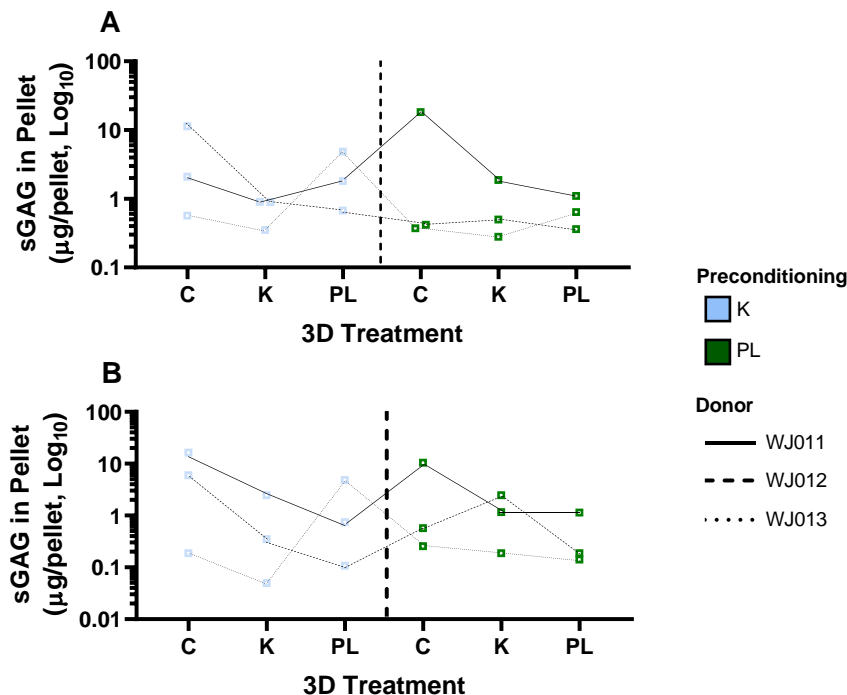


Figure 6.3.23 GAG Content of Pellets from Distal Tibial and Talar MSC Cultures, after K or PL Preconditioning for 2 Weeks and Differentiation in C, K or PL for 3 Weeks (N=3). A The effect upon GAGs produced and within talar MSC pellets. B The effect upon GAGs produced within tibial MSC pellets. For all graphs, technical replicates were averaged and therefore only biological replicates are shown. Graphs shown median \pm range with all data points. Lines connect individual donor results.

GAGs were measured again in media in line with IC work. Potentially, if talocrural MSCs were predisposed to osteogenesis, they may be less capable of retaining GAG, either through loss of adhesion molecule expression, or the production of ECM degrading enzymes (Fig. 6.3.24). K preconditioning showed 2-fold more GAG was release into media than PL (SFig. 8.2.3A). More GAG was released in tibia (Fig. 6.3.24B) than talus (Fig. 6.3.24A), unlike GAG production in the pellet (Fig. 6.3.23). Consistent with IC MSCs, Pellets differentiated in C released the least GAG into media, whereas K and PL differentiated pellets released similar levels of GAG compared to eachother in both talus and tibia (SFig. 8.2.3B). Donor trends between talus and tibia were consistent for each stimulant. K-C-treated cultures released the least GAG into media overall, and PL-C showed the most retention in PL-preconditioned groups, similar to IC cultures (Fig. 6.3.16C, Fig. 6.3.24C). Donor WJ011 however showed large amounts of GAG in the media in every condition suggesting this donor was less able to retain GAGs (Fig. 6.3.24B). Overall, it appears K-preconditioning increases GAG retention, however only C reduced GAG release into media in differentiation. Additionally, some donors may have intrinsically lower GAG retention which may need additional consideration.

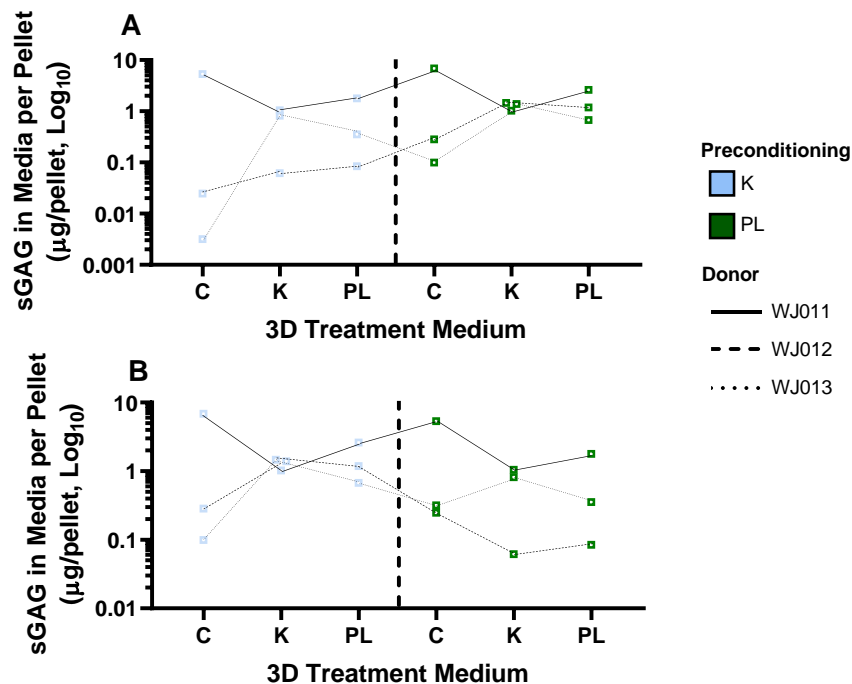


Figure 6.3.24 GAG Content of Media from Distal Tibial and Talar MSC Cultures, after K or PL Preconditioning for 2 Weeks and Differentiation in C, K or PL in Pellets for 3 Weeks (N=3). A The effect upon GAGs produced and released into media by talar MSC pellets. B The effect upon GAGs produced and released into media by tibial MSC pellets. Technical replicates were averaged to only show biological replicates. Graphs shown median± range with all data points. Lines connect individual donor results.

Lastly, GAGs retained in the pellet of a ratio of total GAG produced was investigated to (Fig. 6.3.25), as shown with IC data (Fig. 6.3.17). K preconditioned cultures retained 1.2-fold more GAG of total GAG than PL. Talar MSC cultures retained more GAG than tibia, particularly in PL-preconditioned cultures (SFig. 8.2.4A). Again, C-differentiated pellets retained the most GAG, but K-K treatment in talus showed greater retention. By differentiation stimulants, generally the talus again retained more GAG than tibia, other than the K-C condition. PL-differentiation showed the least retention of GAG (Fig. (SFig. 8.2.4B). In talus, K-K treatment showed consistently high GAG retention, followed by K-C and PL-C. PL-C showed near full GAG retention in 2 of donors. As in IC pellets, K-PL and PL-PL cultures showed the least GAG retention (Fig. 6.3.25A/B). In tibia, K-C and PL-C cultures both showed the highest GAG retention, K-K again showed the next highest retention. The talar pellet from donor WJ013 showed little to no GAG retention after K-K treatment, potentially due to a more osteogenic phenotype. Overall, K-preconditioned cultures retained more GAG than PL preconditioned cultures, and differentiation in K and C retain the more GAG, as seen in IC, however with more variation by donor in talus and tibia. IC showed medians of 85% GAG retention, higher than talus or tibia which appeared to be closer to 70%. This likely relates to the OA state.

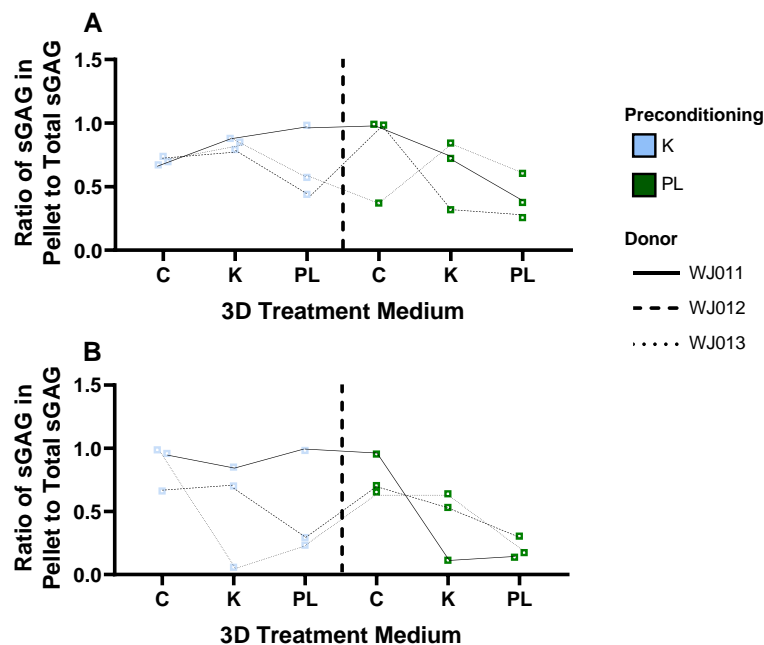


Figure 6.3.25 Ratio of GAGs Retained in the Pellet to Total GAG in Distal Tibial and Talar MSC Cultures, after K or PL Preconditioning for 2 Weeks and Differentiation in C, K or PL in Pellets for 3 Weeks (N=3). A Effect on GAG retention of Talar MSCs. B Effect on GAG retention of Tibial MSC cultures. Technical repeats were averaged and only biological replicates are shown. Graphs shown median \pm range with all data points. Lines connect individual donor results.

6.4. Discussion

This chapter investigated the potential of minimally manipulated OA talar and tibial MSCs for chondrogenesis, to determine if there is potential for encouraging endogenous repair through biological stimulation by both preconditioning and 3D differentiation, without the use of any xenogeneic materials or growth factors. This follows on from the previous chapter, which showed that whilst the non-clinically applicable C encouraged the most chondrogenic gene expression and morphology in 2D, there was not enough proliferation of MSCs to generate sufficient numbers to treat cartilage damage. On the other hand, xeno-free PL and K preconditioning of IC MSCs had shown similar chondrogenic gene expression, and good ALP staining, as well as higher proliferation. In this chapter, 3D differentiation was added as an additional step to see the effect on chondrogenesis, and if different biological stimulants in preconditioning and differentiation would synergistically enhance chondrogenic differentiation.

Firstly, FA beads were explored due to their potential for enhancing chondrogenesis seen in the literature, and ease of use. Beads showed the capacity to encourage chondrogenesis, with large amounts of GAG deposition by histology but required further work to prevent their degradation. However, they did successfully allow MSC proliferation and large amounts of GAG staining, and cell morphologies associated with chondrogenic growth. In the pellet model, the addition of 3D treatments, in this chapter has shown that both PL and K are competent chondrogenic inducers of GAG synthesis in 3D conditions. K-C and K-K treatments both showed the highest GAG synthesis, largest pellets and mostly the highest GAG retention in talus, tibia and IC. However, as K-C contains xenogeneic materials that cannot be used clinically, the next best results were from K-K conditioning of MSCs, which showed the highest GAG production in both pellet and media, and highest GAG retention in the pellet in IC, even compared to C. Additionally, K preconditioning showed the ability to suppress the osteogenic gene RUNX2, as well as other stromal and angiogenic genes. In talus and tibia, K-C produced higher GAGs and had similar or better retention than K-K, however K-K was the next best option. PL differentiation showed reduced chondrogenic gene expression in comparison to C, as well as the highest expression of RUNX2 in IC cultures, and so would still enable osteogenic MSC activity. As K differentiation also contained PL, it seems that K can prevent RUNX2 expression when combined with PL, but not just in preconditioning (K-PL). In talus and tibia, whilst PL differentiation led to higher GAG production in the pellet, there was very poor GAG retention, of around 30%, which would negatively impact treatment. Some donors did show specific responses to biological stimulants, for example poorly chondrogenic IC donor RC071 showed far better GAG retention in K-K than K-C, however the opposite was true in talar and tibia cultures for the least chondrogenic donor WJ013. This suggests there is a degree of donor-specific response to each treatment, but a higher number of donors would be required to understand this.

Some studies have performed similar work. PL injection has been used for osteochondral lesions of the talus, and showed that despite naturally containing TGF- β , a key component which is known to be strongly chondrogenic, PL did not enhanced chondrogenic repair³⁶¹. K and PL have both previously been used in preconditioning and pellet culture of MSCs from other sources. K has shown commitment of human umbilical cord MSCs towards a pre-cartilaginous stage, showing increased expression of FGFR3, however there was not increased expression of chondrogenic genes such as collagen 2 as found in the previous chapter³²⁴. Micro-pellet culture of human IC MSCs has shown K synergistically enhanced chondrogenesis with TGF- β , but not with K alone, which may potentially relate to the small pellets they used being less responsive to K, or other differences in methods¹⁴⁴. PL has been shown to enhance chondrogenesis, however with conflicting results, potentially due to PL composition, or timing of application which has been shown to direct towards cartilage when used early on but not later, which may have affected existing results^{140,328}. This study is novel in that it is the first to directly investigate MSCs from OA for preconditioning and 3D culture, showing that OA MSCs seem to be less able to retain GAGs than non OA, healthy IC MSCs. Additionally, enhancement of chondrogenesis in talocrural MSCs has not been directly investigated, however PL has been added surgically, with this study showing PL was inferior to K or C treatment. This is one of only a few studies to use preconditioning and pellet culture synergistically, and confirms the same results in that PL maintains chondrogenic differentiation capacity and differentiation potential in preconditioning, however in pellet culture PL can reduce chondrogenic capability³²⁸.

Firstly, FA was attempted as a 3D hydrogel to encourage chondrogenesis. This is a scaffold which has been used successfully in other literature, particularly for treatment with PL^{181,183}. Beads were successfully produced and showed rounded morphologies as expected, and whilst there was some variation in size and sphericity, this was not so large that beads would be significantly different in mechanical properties. The homogeneity of beads would be further improved by using a more autonomous method to produce beads rather than by hand, considering the possible extent for human error³⁵⁵. However, there will always be some variation in bead structure. Swelling ratio is unfortunately not performed the same way in all studies, as such can be hard to compare, with one study showing an 8-fold different between the two³⁶². For example, the gel may be freeze-dried first, as performed here, to remove all water, as more commonly performed³⁶². Otherwise, a swelling ratio may be investigated from air drying the bead and then placing in PBS and measuring weight over time³⁶². As such, there was no available direct comparisons for swelling ratio. In a similar study by Montalbano *et al*, where they instead used a collagen-fibrin-alginate bead, a swelling ratio of 3300-3800 was found compared to the value of around 1000 found in this study. The variability in that study was similar to that identified in this study, as such should be an acceptable level.

To identify if beads could support long term culture of MSCs, a degradation assay was performed. As cultures were planned for 14 days, this was the target length. After initial placement of beads into DMEM, there was a large increase in bead mass after 24 hours. The reason for this is unknown, but mostly likely due to beads absorbing DMEM after being washed in PBS. As this equilibrated over time it fell back to the starting mass weight, as the pure PBS retained in the bead may have encouraged diffusion of some components of DMEM but not others. As beads were placed back into culture after weighing, there may have been some mechanical damage to beads which would also affect weight, which may explain why some beads broke down. This was why as time went on, the bead weight was measured less often. For future experiments, it may be worth making multiple beads for measurement at the initial timepoint after DMEM has had time to diffuse in, and then using individual beads for reading at a second timepoint spread over 14 days, to prevent mechanical degradation from being removed from wells for multiple weighs. Normalising to well and media weight would not be viable, as any degraded bead material would still be in the media.

When assessing the effect of FA on MSC viability, interestingly there was a substantial increase in metabolism, suggesting that not only is FA tolerated by MSCs, but it also encourages their proliferation. Whilst alginate themselves do not directly support cell growth due to having no bioactive molecules, their combination with other materials, such as fibrin in this study, has been shown to increase proliferation³⁶³. Additionally, as alginate is a polysaccharide, and there may have been some breakdown of the scaffold, this may have had its own effect upon proliferation, as alginate is a source of carbon and energy in nature, being broken down into mannuronic acid and guluronic acid³⁶⁴. Fibrin hydrogels have been shown to increase MSC survival under stress, as well as increases expression of some immunosuppressive and proliferative markers such as VEGF, TGF β and prostaglandin E2, whilst allowing robust MSC attachment and also limiting the amount of migration out of fibrin^{265,266,347}. This may be beneficial in the case of MSCs being retained in the scaffold, and potentially reduce their apoptosis as often seen in treatments where MSCs are injected, whilst improving expression of proliferative factors²⁶⁶. However, the extent of this exhibited in this study could have been further elucidated using a lower initial cell starting concentration, considering that ratios were the same for all densities in FA extract, which may have masked any significant differences in proliferation.

MSCs successfully grew and survived in FA beads, without altering the spherical structure in the first 48 hours, with no MSC migration out of the beads. As these MSCs showed a spherical structure associated with MSCs primed towards chondrogenic differentiation, rather than the polygonal or elongated structures sought for in pre-osteogenic MSC studies, this suggests FA would successfully support chondrogenic differentiation^{180,337}. As this structure was maintained

over time, up to at least 7 days, with a visible increase in cell number, this suggests the scaffold was allowing cell proliferation whilst encouraging chondrogenic differentiation similar to that seen in work by Ichinose *et al.*⁸⁷. As there were few differences between different treatments, each individual treatment was not directing differentiation away from this rounded morphology and towards other lineages.

However, after 14 days, MSCs were observed external to the beads and many of them were starting to burst, which was not previously observed. Whilst MSCs within the scaffold maintained the rounded structure, those that escaped had rapidly moved towards the fibroblastic phenotype typical of 2D culture. The bead may have burst for several reasons, such as MSC proliferation creating a load that the beads couldn't sustain, or MSC excretion of ECM enzymes which broke down the scaffold. MSCs have been shown to express genes of the fibrinolytic cascade, including plasminogen activator, and have been reported to have strong fibrinolytic capacity¹⁸⁷. Some literature uses inhibitors such as 3000U of aprotinin per ml to prevent beads breaking down, by preventing release of fibrin-degrading enzymes which may have prevented the bead breaking down³⁴⁷. With more time, this would have been possible, however the effect on long-term longevity of the bead would be required to identify if it would still be remodelled into native tissue *in vivo*. Additionally, within the body there would be far more ECM degrading enzymes, particularly in OA, and so a scaffold with its own innate ability to prevent degradation may also be required, yet whilst still being bioresorbable, presenting a particular challenge³⁶⁵. As these scaffolds are currently being designed, this may be viable in future, with the scaffold from Gao *et al.* showing the ability to inhibit MMPs in a model of OA human synovial fluid³⁶⁶.

Methylene blue staining showed that the majority of beads were broken down, and those that were still there had vastly decreased in size. It was interesting that PL-treated cultures showed the most remaining material, opposite to what was expected, since PL-treatment showed increased MSC growth rate in other cultures. As K-treated cultures also had the same concentration of PL in 3D, the difference between the two cultures is more striking, but could be entirely random. Toluidine blue of these pellets showed large break down of even the least degraded beads, with high amounts of GAG deposition within the beads. Additionally, visible cells had small regions of space around them, similar to lacunae seen in native cartilage, which are associated with production of collagen II, VI, IX and XI, as well as GAGs³⁵⁹. This shows that MSCs are being directed towards chondrocyte differentiation in these conditions. Even in heavily degraded FA beads, there was still a large amount of visible GAG within the bead, and so hopefully *in vivo*, this bead degradation would be remodelled into the native cartilage. K, PL and FA beads have all been successfully used to produce GAGs in the past, with Ma *et al.* showing

increased chondrogenic gene expression including SOX9, aggrecan and type 2 collagen relative to pure fibrin, and high GAG content per DNA relative to pure alginate. Lower fibrin content to GAG ratio showed generally higher chondrogenic gene expression, which combined with the changes in mechanical properties lends itself to the choice of equal fibrin and alginate content, which is a lower fibrin content than the work by Ma *et al.*, but this may have contributed to the bead breaking down from the weaker mechanical properties¹⁸¹.

Overall, the FA bead showed a strong ability to support chondrogenesis through MSCs attaining a rounded shape and large amounts of GAG deposition, however, did not last long enough for the experiment therefore making it impossible to retrieve DNA or quantify GAG deposition. Optimising the bead through the addition of enzyme inhibitors may increase the longevity of the bead to better allow support of chondrogenesis. Whilst the time required to initiate a reparative chondrogenic response in the OA ankle is unknown, considering that some key chondrogenic proteins are not expressed until 3 weeks, the bead is likely to need to survive longer than 3 weeks to enable ECM being produced within the bead to integrate with OA cartilage or osteochondral lesions. Immunohistochemistry was attempted on retrieved beads to investigate production of chondrogenic proteins; however the beads being damaged already meant that the embedding process degraded a large majority of them down prior to staining.

Chondrogenic pellets were used as another method of 3D culture for chondrogenesis, based off standard assays^{95,101,328}. The pellet method also allows for simple mechanical testing for the longer term by simply placing the pellet-containing Eppendorf's in a shaker or rocker, which was a consideration for this work, which in theory could have been applied to FA beads as well³⁶⁷. During culture of IC MSCs, it was noted that K led to a gelatinous pool rather than a pellet. To the author's knowledge this has not been observed previously, however K has not been used for treatment of human MSCs in pellet culture. GAG release into media after K treatment has been reported before, but in a micro-pellet model with human bone marrow MSCs. This showed minimal GAGs in media, but also did not show GAG produced in the pellet either. This may be due to differences in model, or K source¹⁴⁴. Due to the semi-liquid nature, histology of the pool was attempted by flash-freezing and cryo-sectioning but was not successful. As a small pellet was observed within the fluid, it may be that the weight of ECM produced could not be borne by the pellet, and as such the pellet broke down, or again cells are remodelling the tissue which separated the cells from the pellet. This seems less likely however, considering the size of the pellets talocrural MSCs reached in Chapter 4. Interestingly, pellets in this chapter had higher GAG content than in chapter 4 (Fig. 4.2.19), with the median of talar and tibial pellets being 2-3-fold that of standard cultured MSC pellets, even with the same 3D treatment, C. As the same talar and tibial donors were used, this shows preconditioning is effective, as seen in the

literature^{197,323,324}. Existing work has shown culture of MSCs, as done in Chapter 4, to P3 may impair chondrogenic ability by endoplasmic reticulum stress, which may have affected these results however³⁶⁸. As typical of biological tissue, there was a consistent but large variation between individual donors, with BM313 always showing the largest pellet, and RC071 the smallest. Chondrogenic capability varying between donors is well established, being reduced in older donors or patients who smoke. However, as patients in this study were between 28 and 44 in IC, and 34-66 in talus and tibia, this is less likely to have played a role, as differences are cited to occur in patients over 70 years old³⁶⁹. Variation due to other lifestyle choices however would be expected and may affect the response to different biological stimulants downstream^{234,370}. A key concept here is if a biological stimulant was more effective on a certain patient group than another. In general, K-preconditioned cultures had larger pellets than PL-preconditioned pellets, as well as higher pools. This aligns with K being thought to be a key chondrogenic inducer, however there is some debate as to TGF- β being more effective, particularly with Music *et al.* finding BONE MARROW MSCs presenting low GAG synthesis^{144,324}. In differentiation treatments, RC071 was unresponsive to each biological stimulants, as such it is likely MSCs from this donor were more senescent than other donors, whereas C produced larger pellets in the other two donors, which would be expected of the positive control.

For pellet culture, there were many analysis of similar concepts, and so Table 6.4.1 summarises results for IC cultures.

Table 6.7 Summary of IC Pellet Chondrogenic Results After Preconditioning and Differentiation

	GAG				Gene Expression			
	Pellet Diameter	Pellet	Media	Retention	Chondrogenic	Osteogenic	ECM Remodelling	Stromal
K-C	++	+	-	-	N/A	--	N/A	--
K-K	N/A	+	++	+++	N/A	N/A	N/A	N/A
K-PL	-	+	++	-	N/A	-	N/A	N/A
PL-C	-	-	-	++	+	++	++	-
PL-K	N/A	++	+	-	N/A	N/A	N/A	N/A
PL-PL	--	-	+	-	-	-	-	+

Simplification of GAG results. – denotes minimal difference. Compared to the middle value, + means increase, -- means decrease. Larger increases are denoted by ++ or +++, relative to other differences seen.

Whilst pellet diameter varied greatly, it did not correlate well with GAG content, GAG in the pellet or GAG retention, as such may not be worth repeating again for work on minimally manipulated MSCs. However, as it did correlate with GAG content in Chapter 4, there is some validity in its measure in the case of studying general differentiation capacity in standard conditions, as some stimulant conditions lead to far more GAG in the media than C. GAG in the pellet was similarly increased in all K-preconditioned cultures, however was most increased in PL-K, which was not matched by later results in talus and tibia. This may relate to PL maintaining overall expression, and so in IC was beneficial, but in talus and tibia MSC coming from an osteogenic environment, this may have meant chondrogenesis was not enhanced¹³⁹. As this is not matched in other PL cultures however, there may be interplay with factors in other medias. Since K and C suppresses RUNX2, perhaps cell signalling feedback meant chondrogenesis was not enhanced. Generally, GAG in the pellet correlated with increased GAG in the media in conditions without C, where K-K and K-PL had the most GAG released into media, followed by PL-K and PL-PL. The most GAG of total GAG was retained in K-K and PL-C, suggesting that K has the best ability to produce and retain GAGs in non-OA IC cultures. As this is coupled with the highest GAG in media however, this also represents a larger amount of GAG overall, suggesting for non-OA tissue, K-K is an effective chondro-inducer, even more so than K-C. A keynote is that for K pools, media was removed up until the pool, and the pool considered part of the pellet. As such, this may alter the accuracy for GAG retention of K-treated pellets. However, as the beads collapsed, it is a point of discussion whether these should be considered 'media' or 'pellet' GAGs. As PL-K did not show the same level of retention however, this suggests K-K can increase retention of GAGs.

Lastly, qPCR was run on the pellets. Due to the nature of chondrogenic pellets being filled with ECM and GAG, retrieving RNA is notoriously hard. Some work does this by agitation with pipette, as in this study, freeze thawing, or the addition of enzymes such as papain or collagenase^{371,372-374}. However, despite the method, there is still debate on the accuracy of isolating RNA from these pellets³⁷². Of available results, it was seen that PL-C best increased chondrogenic gene expression. This matches preconditioning results in that C showed the most upregulation of chondrogenic genes COL2 and COMP, whereas K showed the most upregulation of ACAN. As such, it is unfortunate K results were not obtained, especially considering the positive results in GAG production and retention. Bone gene expression was most greatly reduced by K-C, whereas it was higher in K-PL and PL-PL, and highest in PL-C, suggesting K has the ability to suppress RUNX2 as well reported, but also repress other osteogenic genes^{143,324,330}. ECM degrading enzymes including MMPs were more expressed in PL-C than PL-PL, meaning PL in differentiation may be able to reduce cartilage degradation. ECM degrading proteins like MMPs are often cited as a driver of the OA process, but also some stromal components such as VEGF^{375,376}. PL has a

chondroprotective effect, reducing apoptosis, and so this result shows this would benefit cartilage reparative treatments³⁶¹. Lastly, stromal gene expression was highest in PL-PL, suggesting that it can maintain differentiation potential, as previously reported¹³⁹. K-C most greatly suppressed stromal gene expression, which suggests K preconditioning can direct MSCs towards a mostly chondrogenic lineage which is beneficial for cartilage repair treatments, matching similar literature, which more reliably showed chondroprogenitor cells through expression of surface marker FGFR3³²⁴.

As GAG release from the cell mass is less reported, there is little discussion on the importance of its retention. GAG is mostly retained within cartilage by connecting to hyaluronan through link proteins, enabling the cartilage as a whole to retain large amounts of water. However, expression of cell-surface proteins such as CD44 and RHAMM are thought to be important in this too^{360,377}. As the main idea of adding a scaffold to aid microfracture would be eventual remodelling of the scaffold into the local tissue, GAG retention would be important in this.

Overall, in treatment of chondrogenic pellets of healthy IC MSCs, both PL and K showed benefits by preconditioning, as well as treatment in PL or K during 3D culture similar results to the positive control, if not better, as such both are useful to the field of tissue engineering of cartilage. K showed the greatest chondroprotective activity, as well as highest amount of GAG expression, similar to previous research. PL also produced large amounts of GAG and was better than K in some select biological stimulant combinations, however also had poor GAG retention and expression of genes of other lineages, as such may have both positive and negative repair behaviours. As both stimulants showed good outcomes, in particular K-K and K-PL combinations, both were utilised for talocrural cultures.

Once designed, the experiment was performed again on talocrural MSCs. Learning from previous lessons, FA beads were not attempted again due to rarity of samples and the required optimisation, and the same was true of real-time PCR. Ideally, this would be repeated in future with optimised methods to better understand protein changes by these biological stimulants to OA MSCs. As such, pellet culture was utilised again with a focus on pellet GAG content. Summary data is again presented in Table 6.4.2 to simplify comparisons.

Table 6.8 Summary of Talocrural Pellet Chondrogenic Results

	Talar MSC Cultures					Tibial MSC Culture			
	Pellet Diameter	GAG in Pellet	GAG in Media	GAG Retention		Pellet Diameter	GAG in Pellet	GAG in Media	GAG Retention
K-C	+++	++	---	+	K-C	++	+++	--	++
K-K	-	-	+	++	K-K	-	--	+	+
K-PL	-	+	-	--	K-PL	--	-	+	---
PL-C	++	--	-	+++	PL-C	++	-	--	+
PL-K	--	--	+	-	PL-K	+	+	-	-
PL-PL	-	-	+	---	PL-PL	--	---	--	---

Simplification of GAG results. – denotes minimal difference. Compared to the middle value, + means increase, -- means decrease. Larger increases are denoted by ++ or +++, relative to other differences seen.

Pellet diameter was largest in pellets differentiated in C, as seen before. This was more-so after K-preconditioning in the talus. Pellets in other conditions remained smaller, as seen in the IC. There was visible debris in the media in some cultures, again suggesting GAGs in the media and perhaps some pellet degradation. After prior results from Chapter 4 on the differentiation of cultured MSCs taken from the ankle (Fig. 4.2.17-4.2.19), it was anticipated that talocrural MSCs would have larger pellets than MSCs from the IC. Talus and tibial-treated pellets were of similar size to that in Chapter 4 (Fig. 6.3.17), K-treated and PL-treated pellets however were a median 0.5-fold the size of C-treated pellets. This suggests that again C is more effective on pellet diameter for talus and tibia as seen in IC.

Pellet GAG content was highest in K-C treatments in MSCs from both talus and tibia, and most other conditions had similar GAG content, being slightly higher in K-PL in talus and PL-K in tibia, again showing C produces the most GAG in the pellet, and that K-preconditioning is more effective. GAG in media was elevated in K-K in both talus and tibia, and lowest in K-C and PL-C conditions, showing again C encourages the most GAG to be retained. K-C and PL-C generally led to the most GAG of total GAG being retained in the pellet, as seen with PL-C in the IC. However, again, K-K treatment showed the highest GAG retention. K-PL and PL-K showed the least GAG retention. As mentioned before, this may relate to the proteins which retain GAGs, whether that's cell-surface or mediated through hyaluronan link proteins. PL may either not induce synthesis of GAG-binding proteins or does not prevent production of enzymes which break down GAG-binding proteins. If qPCR had been more successful, identifying changes to GAG linking

proteins or MMPs may have elucidated this reason. Additional biological stimulants which enhance GAG retention or reduce their expression may better improve PL-based treatments.

Between, IC, talus and tibia, K-C led to higher GAGs in the pellet, and less GAGs in the media. However, K-K showed less GAGs in the pellet. This suggests there are some differences between the healthy and OA tissue that K-C is able to mitigate, but not K-K. As ankle MSCs showed an osteogenic response in both Chapter 3 and 4, they may potentially be less able to commit to chondrogenic differentiation as discussed in previous work, with a precommitment to osteogenic differentiation as shown by Ilas *et al.*^{85,317,375}. Whilst overall, the positive control, C showed the most GAG production in the pellet, least GAG in media and relatively strong GAG retention, C is not a viable treatment for clinical use due to containing animal components. Of the various clinically-available options, K-K showed the highest GAG synthesis in IC, and relatively high GAGs in talus and tibia. Additionally, K-K treatment showed the highest GAG retention in the IC, as well as talus and tibia. K-preconditioning largely showed strong results, and would be relatively easy to add *in vivo*. However, as PL showed the largest amounts of GAG released into media, and 50% PL was used in K differentiation medium, this may have had either synergist effects on GAG production, or led to more GAG release than would've happened otherwise.

To see if preconditioning was effective in talus and tibia as well, these were compared to earlier results in chapter 4. In K-C conditions, for both tibia and talus, 2 of 3 donors showed higher GAG synthesis after treatment with C. This was not true for PL-C. This gives some evidence that preconditioning with K may boost GAG synthesis in talar or tibial MSCs. Preconditioning with PL or K have both been shown to be effective in the past, however, at least with PL, it has been shown the time the biological stimulant was available for and when it was removed was important. Rikkers *et al.* showed that whilst 1% of 5% PL effectively increased GAG synthesis by 2-fold when used for just preconditioning, however its use in 3D showed 0.1-fold of the GAGs seen in the positive control redifferentiation medium³²⁸. As 50% PL was used in differentiation medium, this may have had an effect. Preconditioning is thought to improve MSC differentiation properties through epigenetic modification, by removing methylation from relevant genes, allowing their expression, but has also been shown to affect MSC exosomes as well to enhance cartilage repair^{143,378}. Preconditioning in other cases has been enhanced by the addition of mechanical forces, which could improve upon the positive results seen here¹⁹⁷.

To better understand the pellet ECM structure, to see if GAGs were successfully deposited, both histology for toluidine blue and immunohistochemistry for relevant proteins was attempted. Unfortunately, pellets were again fragile, and due to coronavirus new equipment was used for pellet cryo-sectioning or paraffin embedding, as such many pellets were not possible to Section.

Toluidine blue worked on a few pellets and were shown. These showed GAG deposition and a clear typical pellet structure. Immunohistochemistry was attempted, but this was unsuccessful. Proteins were positively identified by DAB staining, but pellets were broken down and the data was not of sufficient quality to be presented here. Pellets did show evidence of chondrogenic activity by GAG staining.

In summary, this chapter has shown that FA could be a potential model for cartilage synthesis with MSCs demonstrating chondrogenic morphology and GAG deposition, however further optimisation is required. Additionally, it was shown that K preconditioning aids of IC, talar and tibial MSCs, increasing the size of pellets relative to those cultured in just C as seen in Chapter 4, however Chapter 4 cells were P3 and therefore potentially have lost some chondrogenic capacity³⁶⁸. Additionally, K and PL for differentiation in 3D showed formation of chondrogenic pellets and GAG synthesis within the pellet and its release into the media. Of note however, is that whilst in IC pellets, the majority of GAGs were retained in the pellet, in the OA talar and tibial samples, a large proportion of GAGs were released into the media, suggesting there is a lack of link proteins to bind them within the pellet, potentially due to enzymatic activity or lack of synthesis, or simply that pellets were smaller and could not retain GAGs. Gene expression in IC pellets showed elevated expression of chondrogenic genes in the positive control relative to PL. K-treatment successfully inhibited gene expression of osteogenic, stromal, angiogenic and cartilage-degrading enzymes. Moving forward, there needs to be optimisation of RNA isolation to better be able to understand gene expression changes, particularly in relation to enzymatic activity based on the pellet degradation seen in OA talar and tibial MSC chondrogenic pellets. Additionally, optimisation of histology would provide better insight into the ability of K and PL to generate 'hyaline-like' cartilage, or if they encourage a more fibrocartilage-like structure. However, K-K showed a clinically relevant treatment option with elevated GAG production, GAG retention in the pellet but also increased GAG in the media, and therefore offers a promising treatment option with further work, particularly to understand the relative importance of GAG retention, but also the effect on chondrogenic gene expression needs to be undertaken.

7. Chapter 7 – Discussion and Conclusions

OA has remained one of the long-standing barriers to independency during aging, and therapies from many angles have been attempted with limited success. Total joint replacement is still the therapy with the best outcomes, offering 20 or more years mobility in other joints, with less success in the ankle just to its complexity¹⁴⁷. Whilst a plethora of regenerative therapies exist, particularly in the ankle, the majority do not show sustained repair for more than 5 years, leaving limited options available. This thesis has investigated specific OA behaviour in the ankle to better understand the changes, as well as investigated the resident repair-capable regenerative cells, MSCs, and their behaviour to further elucidate why repair may be hindered by scar tissue formation. Additionally, the effect of various biological stimulants on their behaviour to suppress osteogenesis and improve chondrogenesis has been investigated to guide development of enhanced regenerative therapies, with an aim of adding an injection to the already common microfracture practice to better improve treatment outcomes, using an *in vitro* model of preconditioning and differentiation treatments.

This thesis confirms existing work that there are large scale bone changes, with relationships to cartilage lesions as found in the hip, but yet to be demonstrated in the ankle, with key morphological behaviours likely relating to microfracture^{101,219,225}. It additionally identifies MSC presence with potential to form bone, cartilage and fat using the ISCT panel utilised in hip and knee, but for the first time in distal tibia and talus^{85,91,101,219}. This work expands on existing data which shows differences in differentiation capacity based on MSC location, not only between bone and cartilage but also by joint^{85,219,287,299}. Additionally, it confirms that MSCs from OA are likely to be predisposed to osteogenesis after isolation from OA based on increased calcium deposition during osteogenic assays and uncultured MSC morphology^{85,87}. Investigation of current biological stimulants being utilised for cartilage repair therapies supported existing evidence that K at 10 μ M concentration can initiate expression of chondrogenic marker ACAN during preconditioning, as well as suppress RUNX2 expression in 3D and increase GAG deposition and retention in pellet culture, as supposed by other work^{141,143,144,324}. However, whilst this work supported PL preconditioning in that it increased cell growth and retained differentiation, it did not support PL for chondrogenesis in 3D, rather it appeared to support general differentiation capacity, which may explain the variety of published results on chondrogenesis, with some showing increases and others decreases, which may be further explained by work which suggests platelet concentration can affect chondrogenesis^{136,140,328}. This was partially mitigated by K preconditioning, which increased GAG retention. This work additionally supports the use of human serum for MSC culture, as found by other literature, showing increased MSC growth rate, enhanced differentiation capacity and less fibroblastic-like morphology^{331,379}.

This thesis is the first to histologically investigate the effect of OA upon talocrural bone and cartilage in explants removed directly from fusion surgery of the talocrural joint, as well as to relate these changes to bone-resident cells including MSCs and osteocytes, and overlying cartilage changes. Existing work on donor tissue taken post-mortem has investigated donated whole tibial and talar bones, demonstrating track and tram lesions, mostly localised on the anterior of the cartilage, relating to loss of GAGs demonstrated by Safranin O staining, with associated SBP tidemark duplication²⁰⁵. Additionally, work has previously shown that there is increased BV/TV in talus compared to tibia, but also further increasing in OA BV/TV near the joint surface in tibia^{240,380}. This work shows for the first time there is an additional increase in BV/TV in the talus at the surface, as well as loss in BV/TV away from the joint surface. Whilst this disagrees with the work from Harnroongroj *et al.*, who had higher donor numbers, their work used lower resolution CT which may have masked some bone changes, and was performed on patients who did not yet need operation, as such were not yet at end-stage OA, as such will have had more limited bone changes³⁸⁰. This work is the first in the ankle to combine this with histological investigation of cartilage damage by OARSI staining, which has been previously performed in the knee²¹⁹. MSCs associated with cartilage damage as well as osteogenic cells, which has been previously shown in the hip, therefore suggesting in OA that MSCs are involved in the sclerotic response seen in OA⁸⁵. Therefore in order for cartilage repair to be realised, new treatments which suppress bone formation such as K are required.

This thesis has for the first time proven that MSC presence in the distal tibia and talus of the talocrural joint, and characterised them, according to the standard ISCT criteria. This is a standard practice which has already shown MSC presence elsewhere, including the knee, hip and calcaneus²¹⁹. MSCs showed typical tri-potentiality into bone, cartilage and fat, with both tibia and talus showing increased osteogenesis and slightly increased chondrogenesis, and talus showing greatly reduced adipogenesis relative to non-OA IC controls. This work also investigated relationships between different differentiation capacities, showing that osteogenesis and chondrogenesis have a negative relationship as shown in other work, but less clear trends between other combinations^{290,308}.

This work has also shown MSC preconditioning in 2D has positive effects on MSC chondrogenesis, as shown previously, in particular showing that K has some benefits including increased ACAN expression, and 3D culture that had been preconditioned showing improved GAG synthesis and retention relative to the positive control, particularly in IC MSCs^{143,197,320,323,324,378}. However, OA MSCs seemed less responsive. Despite K-preconditioning causing talar and tibial pellets to be larger after C differentiation, there was reduced GAG in the IC pellets compared to earlier results of Chapter 4 utilising P3 MSCs which had been

differentiated towards chondrogenesis (Section 4.3.18-19). As pellets showed little GAG retention, this likely relates to the osteogenic behaviour seen by both histology in Chapter 3 and uncultured MSC morphology seen in Chapter 4. Therefore, there still needs to be further work to investigate Biological Stimulants which may reduce osteogenic behaviour. Removal of PL from K-differentiation mediums may better suppress osteogenesis, or combination with other stimulants such as TGF- β as performed in other work may better improve chondrogenesis¹⁴⁴. However, it seems that use of preconditioning is key, as the same work showed little to no chondrogenic response after K-treatment of micro-pellets alone¹⁴⁴.

Large scale bone and cartilage changes are known to be commonplace in OA, with the altered biomechanics leading to perpetuation of disease³⁸¹. Whilst it is unknown if cartilage or bone changes occur first, it is known that both undergo alterations in their structure, leading to the cartilage being less able to divert load, and the exposure of the bone surface leading to joint pain due to the highly vascularised nature of subchondral bone which is suddenly absorbing greater loads, with evidence of neovascularisation within the bone, worsening the situation³⁷⁶. Whilst MSCs have been cited to be involved in bone synthesis in the hip, as well as being known to be present in the bone and being thought involved in repair, especially for being utilised in regenerative therapies, their behaviour in different joints is poorly studied^{85,243}. This work furthers the results of Ilas *et al.* to suggest MSCs are likely related to the bone formation response in OA, which is likely driven by load-sensing cells in bone responding to the increased loading after cartilage loss to drive a bone formation response^{85,382}. This bone is formed rapidly, at therefore is not getting remodelled as required, as shown by picosirius red staining in this study, as well as the worsened biomechanical properties demonstrated in other work²⁴⁹. Whilst microfracture has shown some ability to improve this, repeated microfracture leads to necrosis of lower bone, as such cannot be used as a consistent treatment^{30,84}. This study has demonstrated links between cartilage damage, MSC presence, BV/TV and SBPT, showing that the behaviour of all 4 in the OA process is related, and all need to be addressed for suitable treatment. MSCs respond to their local environment, according to biological signals received, the hardness of material they rest upon, and prior signals as shown by preconditioning altering MSC behaviour^{180,306,331,344,375}. Therefore, it is likely that for true joint repair, there needs to be methods which allow bone and cartilage to return to their original structure and turnover, which likely requires MSCs and potentially other related resident cells to receive a sustained signal to reduce osteogenesis and synthesis new cartilage. As the OA process progresses, these bone and cartilage changes become more widespread, and so it is likely that treatments will need to target early-stage OA, such as being limited to bone marrow lesions as typically seen¹⁵⁵.

This work has shown the potential of talar and tibial bone resident MSCs to undergo cartilage differentiation but also osteogenic differentiation. Biological stimulants for this process mostly only include PRP (PL), K or TGF- β , which have been discussed earlier, and are still not routinely used for cartilage regenerative therapies despite existing clinical results^{324,361}. There does however exist a plethora of scaffolds which have shown positive effects on chondrogenesis, indeed as well for talocrural repair. These have shown the ability to suppressing osteogenesis and recruit resident cells for repair. Some, such as the ChondroGide[®], are clinically approved, however they still do not show long term success over 5 years in over 50% of patients^{155,383}. Whilst studies have shown efficacy in patients under 40, this limits the treatment and doesn't vary greatly from the results of microfracture alone which has shown high success rates in small lesions of younger patients^{155,383}. MSCs have shown the ability to repair cartilage to a near hyaline-like level for 2 years, however as underlying biomechanical changes have yet to be fixed, as well as issues of new cartilage integrating with old cartilage, this repair is not sustained. The addition of stimulants in this study, as well as a more thorough investigation of microfracture to determine the cells involved, may be able to better improve outcomes and improve our understanding of what occurs during microfracture. By combining the use of K with scaffolds which have already shown good outcomes by preventing reduce osteogenic or ECM-degrading enzyme activity may lead to better treatment outcomes^{142,366}.

This study utilised a basic method of 3D culture, using centrifugation to compress MSCs into a pellet. Whilst a commonly used method in this field that has been used in much of the cited literature, a more complex scaffold with additional functions, such as mechanical properties which match the chondrogenic response of MSCs and that of nearby cartilage, would show more reliable outcomes for response to K or other stimulants. Whilst FA used in this study showed a chondrogenic MSC morphology as well as GAG deposition, the scaffold did not last long enough for the planned experiment. Whilst a reported benefit of FA is that it is resorbed quickly, it needs to be sustained long enough that cartilage repair can begin to a sufficient level that it can be integrated with the local environment, as well as since the joint will likely be loaded fairly shortly, the scaffold needs a level of rigidity. As such, other scaffolds, particularly with a focus on ones which have passed clinical trial, are likely a better model of study for the response in 3D to K, PL and other stimulants.

This study has added a large amount of novel information on the effects of end-stage OA on the structure of the ankle, resident bone MSC behaviour, and their response to novel biological stimulants utilised experimentally and clinically within the field, by both preconditioning and in 3D. Importantly, this study has shown that MSCs are linked with the osteogenic response in OA, but despite that retain a strong level of chondrogenesis, greater than non-diseased IC MSCs. MSCs responded similarly to biological stimulants K and PL after preconditioning, with K showing increased chondrogenic gene expression. With additional 3D culture, K suppressed expression of bone-related gene RUNX2, and enhanced both the production of GAGs in both the pellet and media, but also increase the retention in the pellet. This retention is likely key to cartilage repair, based on the idea that if GAGs are not adhered within the cartilage, they will not aggregate, for the critical function of water retention to manage joint loading. This study has created new questions to be answered:

- 1) Does MSC differentiation potential differ between OA and non-diseased sites, or of different stages of the disease, by investigating healthy and OA donor samples
- 2) Are MSCs directly related to bone changes by paired immunohistochemistry for different osteogenic cell and MSC markers
- 3) Does preconditioning present markers of MSCs pre-committed to chondrogenesis
- 4) Does K alone better improve the chondrogenic capacity than with PL
- 5) What is the effect of K on gene expression of 3D cultured MSCs by qPCR, which could be attempted on an alternate scaffold, or an optimise pellet digestion
- 6) Would alternate scaffolds such as FA or commercial scaffold better enhance chondrogenic repair and inhibit osteogenic gene expression

This study is limited by the scarcity of samples. With only 3-4 samples per experiment, key differences between results may have been masked or enhanced. To advise future work, I would therefore recommend that they have a better ability to collect samples, by approaching additional surgical sites to recruit more patients to the study. However, as surgery moved towards the use of less bone, it would also be important to recruit patients receiving total ankle replacement. Additionally, the lack of healthy controls meant it was hard to identify if changes were joint or disease specific. However, obtaining MSCs from healthy ankle tissue is unlikely, considering the rarity of the tissue, requiring complex ethics, as frozen tissue cannot be used, and so would likely have to be from amputation. Therefore, developing non-invasive joint

imaging methods to investigate OA changes and MSC behaviour after regenerative therapies, or development of animal models, would be potential avenues.

8. APPENDIX

8.1. Undecalcified Resin Histology

8.1.1. Dehydration and Infiltration

URH utilises the rapid polymerisation of a methyl-methacrylate resin monomer to form a hard plastic, which will allow relatively thin Sections of bone to be sectioned and then ground down. For the monomer of the embedding resin to be able to permeate the bone, the water needs to be fully removed. The monomer also needs to be fully dispersed within the tissue before polymerisation. Technovit 7200 VLC resin was used, and in OA can show the microarchitecture of bone ³⁸⁴.

Firstly, the samples were kept in neutral buffered formaldehyde for 2 days. The NBF was removed, and the samples transferred into histology cassettes, which were placed into 250ml of 60% ethanol in distilled water for 36 hours and agitated by shaker at 40 rpm. This was transferred to and repeated for gradual increases of 250ml ethanol concentrations including 80%, 96%, 100% and a duplicate of 100%. After this, the cassette was transferred to 250ml 30% Technovit 7200 VLC in 100% ethanol (ratio of 30:70), placed into the dark to prevent monomer polymerisation, and left for 36 hours with 40 rpm agitation. This was repeated for 250ml of Technovit:ethanol ratios of 50:50, 70:30 and a 100% Technovit solution. Once completed, the cassette was placed into 250ml 100% Technovit solution and pulled into a vacuum. This was left in the dark for 7-20 days, with agitation at 40 rpm.

8.1.2. Embedding of Sample into Resin

To be able to Section the bone, the sample needs to be fully embedded in resin polymer. Following infiltration, the sample was orientated within a large embedding mould and packing beads applied to reduce resin used. Within a fume hood, Technovit 7200 resin was used to cover the sample with some excess. The resin was then cured over 8 hours in a Light Polymerisation Unit. The sample was subsequently removed from the device and left to cure in daylight.

8.1.3. Preparation of Embedding Sample for Sectioning

To allow the sample to be sectioned, the sample was adhered to slides. Coarse grinding paper (Exakt) was attached to the micro-grinding system (Exakt) and used to roughen the slide (Exakt) to be used to aid sample adherence. The slide was cleaned in 100% ethanol, and attached to the vacuum adhesive press (Exakt) by engaging the vacuum. Technovit 4000 cement (Exakt) was then prepared in a fume hood, using 2.5 ml of syrup 1, 1.25 ml of syrup 2, and after mixing 5 ml of powder was added. This was mixed, and then poured onto the concave surface of the embedded block. This was attached to the lower portion of the vacuum press, and the upper portion with the slide attached lowered onto the sample with compression until adhered. The slide and sample were removed, and the face of the resin block was then ground down using the micro-grinding system, with the slide adhered to the vacuum of the system, until the sample was exposed. A micrometer was used to confirm that the two sides of the sample block were parallel. A second slide was then attached to the vacuum adhesive press. Within the fume hood, Technovit 7210 resin was applied thinly to the exposed face of the sample, and the sample attached to the lower arm of the press. The upper arm was allowed to compress the second slide onto the sample, and left to cure the resin for 10 minutes with the device closed.

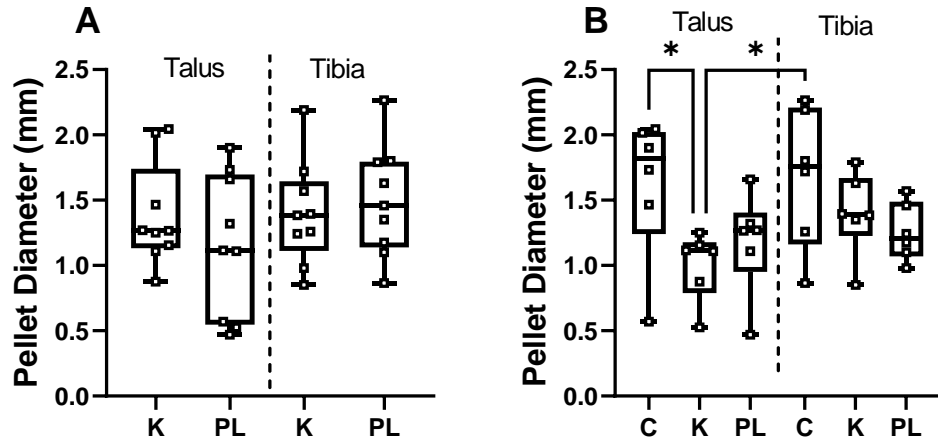
8.1.4. Cutting of Thick Sample Sections

In order to start producing a Section of sample of suitable thickness, the thinnest Section that can be cut by blade is taken first. The sample is first clamped into the bone saw (Exakt). Water is set to run down the blade, and the blade is set to oscillate at a speed of 8 units, cutting at a thickness of 250µm. The sample is allowed to pass through the blade via weighted platform, pulling the block down. Once cutting completed the device turned off and Sections taken.

8.2. Separated Preconditioning and Differentiation Results for Talus and Tibia

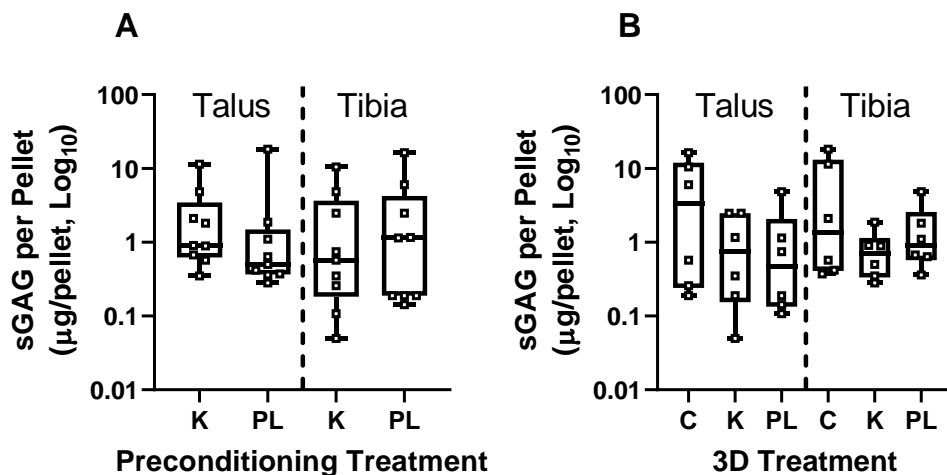
In Chapter 6, graphs showing the effects of both preconditioning and differentiation only were shown, to prevent over complication of the results. These graphs are shown here.

Firstly, pellet diameter as affected by preconditioning (SFig. 8.3.1A) and by differentiation media (SFig. 8.3.1B) is shown.



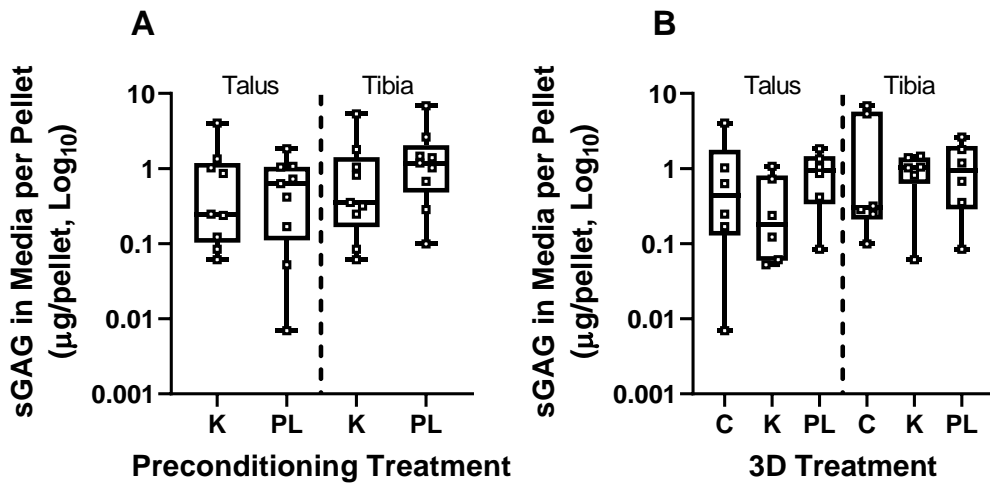
Supplementary Figure 8.3 1 Effect of Preconditioning using K or PL and 3D treatment with C, K or PL or diameter of chondrogenic pellets produced by talar or tibial MSCs after 14 day culture (N=3). A Effect of preconditioning media on talar and tibial MSC chondrogenic pellet diameter. B Effect of 3D treatment medium on talar and tibial MSC pellet diameter. Technical replicates were averaged and only biological replicates are shown. Graphs shown median± range with all data points. Significance was tested for using a non-parametric Friedman test. Significance was set at * p<0.05.

Next, GAG per pellet is shown following preconditioning (SFig. 8.3.2A) and differentiation (SFig. 8.3.2B).



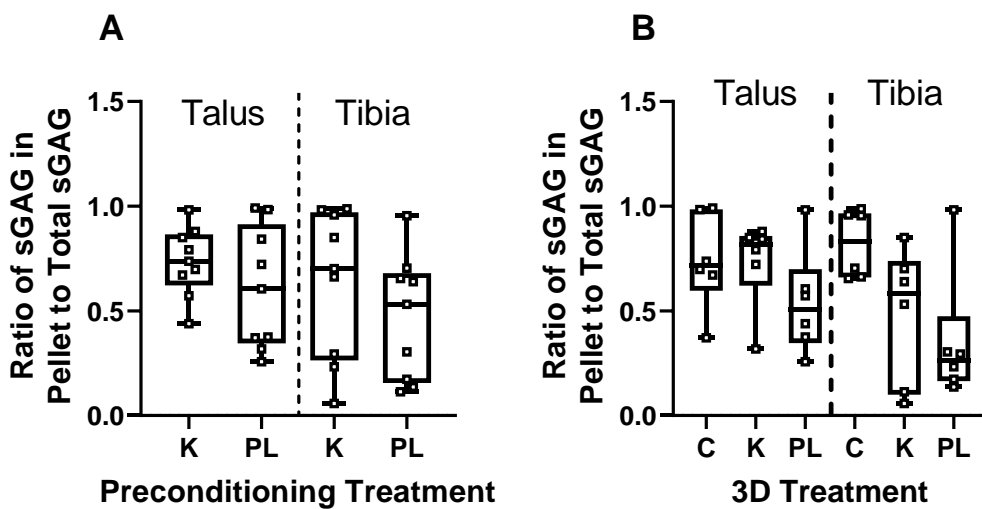
Supplementary Figure 8.3 2 GAG Content of Pellets from Distal Tibial and Talar MSC Cultures, after K or PL Preconditioning for 2 Weeks and Differentiation in C, K or PL for 3 Weeks (N=3). A The effect of preconditioning upon GAGs produced within pellets. B The effect of differentiation media upon GAGs produced within pellets. For all graphs, technical replicates were averaged and therefore only biological replicates are shown. Graphs shown median± range with all data points.

Next, GAG in media per pellet is shown following preconditioning (SFig. 8.3.3A) and differentiation (SFig. 8.3.3B).



Supplementary Figure 8.3.3 GAG Content of Media from Distal Tibial and Talar MSC Cultures, after K or PL Preconditioning for 2 Weeks and Differentiation in C, K or PL in Pellets for 3 Weeks (N=3). A GAG in media after preconditioning with K or PL on final GAG content after differentiation. B Effect of K, PL or C as a 3D treatment medium on GAGs released into medium. For all graphs, technical replicates were averaged and therefore only biological replicates are shown. Graphs shown median \pm range with all data points.

Lastly, GAG retained in pellet of total GAG is shown following preconditioning (SFig. 8.3.4A) and differentiation (SFig. 8.3.4B).



Supplementary Figure 8.3.4 Ratio of GAGs Retained in the Pellet to Total GAGs in Distal Tibia and Talus, of Pellets Preconditioned with K or PL for 2 Weeks and then Cultured in 3D Pellets for 3 Weeks (N=3). A Effect of K or PL preconditioning upon GAG retention on Talus and Tibial MSC cultures. B Effect of K, PL or C differentiation treatment upon GAG retention on Talus and Tibial MSC cultures. For all graphs, technical replicates were averaged and therefore only biological replicates are shown. Graphs shown median \pm range with all data points.

8.3. Reagents, Stocks and Buffers

8.3.1. Antibodies

Supplementary Table 8.1 Antibody Conjugates used for Flow Cytometry					
Target	Antibody Class	Fluorophore	Clone	Manufacturer	Catalogue Number
<i>Positive Markers</i>					
CD73	IgG1κ	R-phycoerythrin (PE)	AD2	Miltenyi Biotec	130-095-182
CD90	IgG1	Peridinin Chlorophyll protein (PerCP)-Vio700	REA897	Miltenyi Biotec	130-114-864
CD105	IgG1	Fluorescein Isothiocyanate (FITC)	43A4E1	Miltenyi Biotec	130-098-774
<i>Negative Markers</i>					
CD14	IgG1κ	VioGreen	REA599	Miltenyi Biotec	130-110-525
CD19	IgG1κ	VioGreen	LT19	Miltenyi Biotec	130-098-226
CD34	IgG1κ	VioGreen	AC136	Miltenyi Biotec	130-113-183
CD45	IgG1κ	VioGreen	REA747	Miltenyi Biotec	130-110-638
HLA-DR	IgG1κ	VioGreen	REA805	Miltenyi Biotec	130-111-795
<i>Isotype Controls</i>					
Mouse	IgG1	R-phycoerythrin (PE)	MCA1210	BioRad	MCA928PE
Mouse	IgG1	Peridinin Chlorophyll protein (PerCP)-Vio700	MOPC-21	BD Biosciences	552834
Mouse	IgG1	Fluorescein Isothiocyanate (FITC)	MCA1210	BioRad	MCA928F
Mouse	IgG1	VioGreen	MOPC-21	BD Biosciences	583025

Supplementary Table 8.2 Antibodies used for Immunohistochemistry

Host Species	Antibody Class	Antibody Target	Clone	Manufacturer	Dilution	Catalogue Number
Mouse	IgG1 κ	CD271	ME20.4	Invitrogen	1:200	14-9400-82
Rabbit	IgG1	CD56	EPR2566	Abcam	1:300	ab133345
Rat	IgG2a	E11	NZ1	Merck Millipore	1:200	14-9381-82

8.3.2. Reagents

Supplementary Table 8.3 Laboratory Reagents		
Reagent	Manufacturer	Catalogue Number
Acetone	Fisher Scientific	15927996
Acrytol Mounting Medium	Generon	21730018-1
Alginic Acid Sodium Salt	Sigma	A1112-100G
Alizarin Red	Sigma	A5533-25G
AdipoDIFF	Miltenyi Biotech	130-091-677
Antibody diluent	Abcam	S080983-2
Calcium Chloride	Sigma	C1016-500G
Calcium kit	Sigma	MAK022
ChondroDIFF	Miltenyi Biotech	130-091-679
Citrate	Sigma	3861-20ML
DAPI	Sigma	<u>28718-90-3</u>
DMEM (High Glucose)	Gibco/Life Tech	61965-059
DMEM (Low Glucose)	Gibco/Life Tech	21885025
DMEM	ThermoFisher	61965-026
DMSO	Sigma	D2660-100ml
DNase	Sigma	DN25-10MG
DPX	Sigma	06522-100ML
Eosin	VWR International	EM-R03040-74
Ethanol	Fisher Scientific	E/065DF/25
Fast Green	Alfa Aesar	A16520.06
Fetal Calf Serum (FCS)	Thermo Fisher	FCS-SA
Fibrinogen Type 1	Sigma	F8630-1G

Supplementary Table 8.3 Laboratory Reagents

Formaldehyde	Sigma	F5554-4L
Glacial Acetic Acid	Fisher Scientific	33026
Haemotoxylin (Mayer's)	VWR International	EM1.05175.2500
Hydrochloric Acid	Fisher Scientific	10316380
Isopropanol	Fisher Scientific	67-63-0
Kartogenin	Sigma	SML0370-5MG
Methylated Spirits	Biostain Ready Reagents	GPS1000-K
Methylene Blue	Sigma	M4159-25G
Modified Weigert's Iron Haemotoxylin	Atom Scientific	RRSP72-E, RRSP73-E
Naphthol	Sigma	861-10ML
Neutral Buffered Formaldehyde	Biostain Ready Reagents	RRFF4000-G
Nile Red	Sigma	19123-10MG
OCT	VWR International	361603E
Oil Red O	Sigma	O0625-25G
OsteoDIFF	Miltenyi Biotech	30-091-678
Paraffin	Sigma	327212
Phosphate Buffered Saline (Calcium Free)	Sigma	14190-144
Phosphate Buffered Saline (tablets)	Fisher Scientific	10209252
Penicillin Streptomycin (PS)	Thermo Fisher	15140-22
Platelet Lysate	StemCell Technologies	6960
Preamplification MasterMix	Fluidigm	100-5580

Supplementary Table 8.3 Laboratory Reagents

Reverse Transcription Master Mix	Fluidigm	100-6298
Safranin O	Merck Life Sciences	1159480025
Saponin	Merck Life Sciences	SAE0073-25G
Scott's Tap Water	Leica Biosystems	3802900
Sodium Hydroxide Pellets	Fisher Scientific	424335000
StemMACS	Miltenyi Biotech	130-091-680
Sterile PBS	ThermoFisher	D8537-500ml
Technovit 4000 Cement	Exact	51090
Technovit 7200 VLC resin	Exakt	51000
Technovit 7210 VLC glue	Exakt	51100
Thrombin	Merck Life Sciences	T4648-1KU
Toluidine Blue	Sigma	<u>198161</u>
Trypan Blue (0.4%)	Sigma	T8154
Trypsin	ThermoFisher	15400054
Xylene	Sigma	534056
Collagenase	Worthington Biochemicals	LS004156
EDTA	Fisher Scientific	D/0700/53
Cell Lysis Buffer	Cell Signalling Technologies	9803S
FACS Buffer	ThermoFisher	A9647, 40-2006-01
Trypan Blue	Sigma	
Triton-X100	Sigma	X100
Nuclease-free water	Sigma	W4502

8.3.3. Solutions and Buffers

Supplementary Table 8.4 Solutions and Buffers

Solution	Details
Acidified Water	5 ml Glacial Acetic Acid in 1L of dH ₂ O
Collagenase (600U/mL)	Collagenase was prepared at a concentration of 600 units/ml in 1% P/S, 20% FCS, DMEM mixture.
EDTA	In 1L dH ₂ O, 186g EDTA powder was added and NaOH pellets added to allow EDTA to dissolve under agitation, and adjusted to pH 7.4 using HCl
FACS Buffer	0.5% BSA and 0.1% Sodium Azide in PBS
Freezing Media	10% DMSO in FCS
Alginate Acid	2.4% sodium alginate w/v in Calcium Free PBS (sterilised by filter)
Methylene Blue	1% methylene blue in borate buffer (10mM, pH8.8)
TE Buffer	10mM, 1 mM EDTA adjusted to pH 8
Tris-Buffered Saline	24g Tris and 88g NaCl in 1L PBS at pH 7.6
Fibrinogen	30mg/ml in calcium free PBS (sterilised by filter)
Fibrin Alginate	1.2% sodium alginate, 15 mg/ml in calcium free PBS prepared sterile
Calcium Chloride	102 mM in calcium free PBS
Thrombin	50U/ml in dH ₂ O
CaCl ₂ Thrombin Solution	2 mM CaCl ₂ with 5U/ml thrombin in dH ₂ O
Cell culture mediums	All cell culture mediums were prepared with 1% P/S

Supplementary Table 8.4 Solutions and Buffers

DMEM	For chapter 3-4, DMEM was prepared with 10% FCS. In chapter 5-6, DMEM was prepared with 10% HS
DNase	1 mg/ml in sterile PBS, sterile filtered
Safranin O	0.1% w/v in dH ₂ O
Fast Green	0.05% w/v Fast Green in 1 ml water. 0.02% for TRAP stain
Acetic Acid (1%)	1% V/V glacial acetic acid in dH ₂ O
Citrate-acetone fixative	2:3 citrate to acetone
Alizarin Red	40 mM in H ₂ O, 342 mg in 2.5 ml H ₂ O, pH to 4.1 with 10% ammonium hydroxide
Nile Red	1 µg/ml
DAPI	1 µg/ml
Saponin	0.2% in dPBS
Oil Red O	0.5% W/V in Propan-2-ol diluted 2:3 in PBS
Toluidine Blue	0.1% in 50% dH ₂ O 50% propan-2-ol for pellet and bead staining. 0.1% in dH ₂ O for preconditioning well stains

8.3.4. Consumables

Supplementary Table 8.5 Laboratory Consumables

Consumable	Manufacturer	Catalogue Number
Cell Strainer (40µm)	Corning	431750
Control Line Fluid (48:48)	Fluidigm	89000020
Control Line Fluid (96:96 for FlexSIX)	Fluidigm	89000021
CoolCell LX	Biocision	BCS-405
Coverslip (HiQa 22 x 40)	CellPath	SAB-2240-03A
Coverslip (SUPA MEGA WHITE)	CellPath	SAF-4864-02A
Cryovials (1.8 mL)	Thermo Scientific	366656
Embedding Mould (Single) 16 mm deep	Exakt	41450
Envision+ Dual Link System-HRP and DAB kit (Dako, Agilent, CA)	Agilent	K4065
FACS Tubes	Corning	35204
Falcon Tubes (1.5 ml, 50mL)	Corning	430790, 430828
Filters (For syringe (0.22, 0.44 microns))	Sigma	SLMPL25SS SLHVM33RS
FlexSIX Gene Expression Interfluidic Chip	Fluidigm	100-6308
48.48 Dynamic Array™ IFC for Gene Expression	Fluidigm	BMK-M-48.48
Grinding Papers	Exakt	K320,K500,K800,K1000, K1200

Supplementary Table 8.5 Laboratory Consumables

Microcentrifuge Tubes	Sigma	EP0030123611-500EA
Needle (19G, 1.5 inches)	Fisher Scientific	10234154
Packing Beads	Exakt	51330
Petri Dishes	SLS	PET3007
Pipette Tips (10 μ L, 20 μ L, 1000 μ L)	Rainin	RT-10F, RT-20F, RT-200F RT-1000F
Picosirius Red Staining Kit	Sigma	ab150681
Polishing Papers	Exakt	K2500, P2000
Polymerase Chain Reaction Tube Strips and Caps	Sigma	BR781326
Sample Pots	Medfor	PJB0250D
Scalpel	Swann Morton	511
Screw top conical microcentrifuge tubes	Fisher Scientific	12350353
Single Cell RNA Isolation Kit	Norgen Biotek	51800
Slides, Large	Exakt	41510
Strippete (10mL, 2.5 ml, 50mL)	Corning	4051, 4101, 4251
Super Frost Histology Slide	Thermo Scientific	810618
Syringe	Fisher Scientific	15809152
Tissue Culture flasks (25cm ³ , 75cm ³)	Corning	430639, 430825
Tissue Culture Round Dishes	Corning	430196

8.3.5. Equipment

Supplementary Table 8.6 Details of Equipment Used in Research Methodology

Equipment	Manufacturer	Catalogue Number/Model
Attune 2 Laser System	Invitrogen	Attune 2
Attune Cytometric Software	Invitrogen	V2.1.0
Axiolmager 2	Zeiss	Axiolmager 2
Balance	Mettler Toledo	AL54
BioMark	Fluidigm	BMKHD-BMKHD
Bone Cutting Forceps (Double Action) - Straight	Narang Medical Limited	353.01
Bone Saw	Exakt	Exakt 310
Centrifuge	Eppendorf Centrifuge	5810R
CKX41/BX45 Microscope	Olympus	CKX41/BX45
CO ₂ Incubator InCuStage	Sanyo	InCuStage
Cytation 5 Imaging Plate Reader	Agilent	Cytation 5
Dehydration and Infiltration system	Exakt	Exakt 510
Dental X-Ray Machine	Carestream Dental	CS2200
EVOS Microscope	ThermoFisher	EVOS M5000
Freeze Dryer	SciQuip	Christ Alpha 1-2 LDplus
Freezer (-20°C)	Scientific Laboratory Supplies	LabCold
Freezer (-80°C)	Panasonic	VIP Series -86 Ultra Low Temperature Upright Freezer

Supplementary Table 8.7 Details of Equipment Used in Research Methodology

Fridge (4°C)	Zanussi	Electrolux
Gilson Pipette	Gilson	P10, P20, P200, P1000
GX Microscope	GT Vision	GX
Haemocytometer	Hawksley	BS7.48
Histology Cassettes	Scientific Laboratory Supplies	HIS0096
Hot Plate	Stuart Scientific	SH3
HX Loader	Fluidigm	HX
Hypoxic Incubator	Sanyo	MCO-18AiC
Indentation Rig	Made in house	N/A
Infinity 1 Camera	Lumenera	Infinity 1
Infinity Image Acquisition Software	Lumenera	V6.5.4
Instron-3365 Rig	Instron	3365
Leica Aperio T2	Leica Biosystem	T2
Light Polymerisation Unit	Exakt	Exakt 520
Linear Variable Differential Transducer	ElectroScience	060-1896-02
Measuring and Control System (Grinder)	Exakt	Exakt AW 110
Micro Grinding System	Exakt	Exakt 400 CS
Micro-CT100	ScanCo Medical	mCT 100
Micrometer	Beslands	N/A
Microtome	Leica	RM2235
NanoDrop 1000	ThermoFisher	1000

Supplementary Table 8.8 Details of Equipment Used in Research Methodology

Nikon Eclipse Ti2-E Camera	Nikon	Ti2-E
Nuance Multispectral Imaging System	Caliper Lifesciences	N/A
PAP pen	Sigma	Z377821-1EA
Precision Adhesive Press	Exakt	Exakt 402
Scanner	Epson	Epson Perfection 3590 Photo
SkyScan 1278 mCT	Bruker	1278
Tissue Processor	Leica	ASP200
Vacuum Adhesive Press	Exakt	Exakt 491
Water Bath	Leica	SUB6/HI1210


8.3.6. Kits

Supplementary Table 8.9 Kits Used

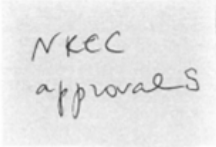
Kit Name	Manufacturer	Product Code
Blyscan Sulphated GAG Assay Kit	Biocolour Life Science Assays	B1000
Calcium Colorimetric Assay Kit	Sigma	MAK022
TRAP kit	Sigma	387A-1KT
XTT Assay	Sigma	11465015001

8.4. Ethical Approval

Ethical approval for ankle fusion sample work is shown first. Directly below is approval of the substantial amendment to allow mCT of tissue.



Health Research Authority
 Yorkshire & The Humber - Leeds West Research Ethics Committee
 Room 001, Jarrow Business Centre
 Rolling Mill Road
 Jarrow
 Tyne and Wear
 NE32 3DT
 Tel: 0207 104 8087



30 March 2016

Dr Elena Jones
 Associate Professor in Rheumatology
 University of Leeds, Leeds Institute of Rheumatic and Musculoskeletal Medicine
 Wellcome Trust Brenner Building
 St James's University Hospital
 Leeds
 LS9 7TF

Dear Dr Jones

Study title: Biology of mesenchymal stem cells and their use in tissue engineering
REC reference: 07/Q1205/27
Protocol number: NA
Amendment number: Minor Amendment 1
Amendment date: 29 March 2016

Thank you for your letter of 29 March 2016, notifying the Committee of the above amendment.

Summary of amendment

This amendment has been submitted to correct typographical errors with the Participant Information Sheets and to alter the word 'patient' to 'participant' as per the Committee's request. The consent forms have been amended to reflect the retention of tissue and the fact that participant medical notes may be looked at by the responsible individuals from the University of Leeds and regulatory authorities.

The Committee does not consider this to be a substantial amendment as defined in the Standard Operating Procedures for Research Ethics Committees. The amendment does not therefore require an ethical opinion from the Committee and may be implemented immediately, provided that it does not affect the approval for the research given by the R&D office for the relevant NHS care organisation.

IRAS Project ID:	
Short Study Title:	Biology of mesenchymal stem cells and their use in tissue repair
Amendment No./Sponsor Ref:	Substantial Amendment 4, 16/05/2018
Amendment Date:	07 June 2018
Amendment Type:	Substantial Non-CTIMP

I am pleased to confirm **HRA and HCRW Approval** for the above referenced amendment.

You should implement this amendment at NHS organisations in England and Wales, in line with the conditions outlined in your categorisation email.

Next, ethics for non-diseased human ankle donor tissue is shown.

The Secretariat
University of Leeds
Leeds, LS2 9JT
Tel: 0113 3434873
Email: ResearchEthics@leeds.ac.uk



UNIVERSITY OF LEEDS

Claire Brockett and Miss Lekha Koria
Faculty of Engineering
University of Leeds
Leeds, LS2 9JT

**MaPS and Engineering joint Faculty Research Ethics Committee (MEEC FREC)
University of Leeds**

12 June 2019

Dear Claire and Lekha

Title of study Characterising the properties of subchondral bone in the
arthritic ankle.
Ethics reference MEEC 18-027

I am pleased to inform you that the application listed above has been reviewed by the MaPS and Engineering joint Faculty Research Ethics Committee (MEEC FREC) and following receipt of your response to the Committee's initial comments, I can confirm a favourable ethical opinion as of the date of this letter. The following documentation was considered:

Document	Version	Date
MEEC 18-027 Ethical_Review_Form_04-19_LKoria_v2	2	24/04/2019
ANKLE_CONSENT_FORM_V1	1	24/04/2019
ANKLE_PATIENT_INFO_SHEET_V6_270319	6	24/04/2019
R1.3 General Human Tissue Risk Assessment	2	24/04/2019
MEDCURE Application and Agreement	1.0	24/04/2019
MEDCURE Donor Consent	1.0	24/04/2019
MEDCURE Letter of Intent	1.0	24/04/2019
SOP 11_01_issue3_Transportation_of_human_tissue_off campus	3.0	24/04/2019
SOP 11_02_issue2_movement on campus	2.0	24/04/2019
MEEC 18-027 RISK11_1_issue2_the use of human tissue	2.0	01/03/2019

Please notify the committee if you intend to make any amendments to the information in your ethics application as submitted at date of this approval as all changes must receive ethical approval prior to implementation. The amendment form is available at <http://ris.leeds.ac.uk/EthicsAmendment>.

Please note: You are expected to keep a record of all your approved documentation and other documents relating to the study, including any risk assessments. This should be kept in your study file, which should be readily available for audit purposes. You will be given a two week notice period if your project is to be audited. There is a checklist listing examples of documents to be kept which is available at <http://ris.leeds.ac.uk/EthicsAudits>.

Lastly, ethical approval for iliac crest tissue is shown.



Health Research Authority

NRES Committee Yorkshire & The Humber - Leeds East

Yorkshire and Humber REC Office
First Floor, Millside
Mill Pond Lane
Meanwood
Leeds
LS6 4RA

Tel: 0113 3050108
Fax:

12 April 2012

Prof Peter Giannoudis
Consultant
Department of Trauma and Orthopaedics
St James's University Hospital
LS9 7TF

Dear Prof Giannoudis

Study title: Biological properties of Mesenchymal Stem Cells in Fracture Healing
REC reference: 06/Q1206/127
Amendment number: 3/1
Amendment date: 11 April 2012

Thank you for submitting the above amendment, which was received on 12 April 2012. It is noted that this is a modification of an amendment previously rejected by the Committee (our letter of 22nd February 2012 refers).

The modified amendment has been considered on behalf of the Committee by the Vice-Chair.

Ethical opinion

I am pleased to confirm that the Committee has given a favourable ethical opinion of the modified amendment on the basis described in the notice of amendment form and supporting documentation.

Approved documents

The documents reviewed and approved are:

Document	Version	Date
Parental Agreement - Consent Form	1.1	23 March 2012
Participant Consent Form: Patient Consent Form 16 - 17 years old	1.0	23 March 2012
Participant Consent Form: Children Assent Form	1.0	01 February 2012
Participant Information Sheet: Patient Information Sheet 16 - 17 years old	1.0	23 March 2012
Participant Information Sheet: Parental Information Sheet	1.1	23 March 2012
Participant Information Sheet: Children Information Sheet	1.1	23 March 2012
Protocol	6.0	19 December 2011
Modified Amendment		11 April 2012

9. Work-cited Publications

1. Arthritis Research UK. Osteoarthritis in General Practice. 2013.
2. Michael JM, Golshani A, Gargac S, Goswami T. Biomechanics of the ankle joint and clinical outcomes of total ankle replacement. *J Mech Behav Biomed Mater.* 2008;1(4):276-294.
3. Gray H. *Gray's anatomy: with original illustrations by Henry Carter.* Arcturus Publishing; 2009.
4. Neumann D. *Kinesiology of the Musculoskeletal System.* 3 ed: Mosby; 2016.
5. Brockett CL, Chapman GJ. Biomechanics of the ankle. *Orthop Trauma.* 2016;30(3):232-238.
6. Giannini S, Buda R, Cavallo M, et al. Cartilage repair evolution in post-traumatic osteochondral lesions of the talus: from open field autologous chondrocyte to bone-marrow-derived cells transplantation. *Injury.* 2010;41(11):1196-1203.
7. Irwin RM, Shimozone Y, Yasui Y, Megill R, Deyer TW, Kennedy JG. Incidence of Coexisting Talar and Tibial Osteochondral Lesions Correlates With Patient Age and Lesion Location. *Orthop J Sports Med.* 2018;6(8):2325967118790965.
8. Buda R, Vannini F, Castagnini F, et al. Regenerative treatment in osteochondral lesions of the talus: autologous chondrocyte implantation versus one-step bone marrow derived cells transplantation. *Int Orthop.* 2015;39(5):893-900.
9. Badekas T, Takvorian M, Souras N. Treatment principles for osteochondral lesions in foot and ankle. *Int Orthop.* 2013;37(9):1697-1706.
10. Medina McKeon JM, Hoch MC. The Ankle-Joint Complex: A Kinesiologic Approach to Lateral Ankle Sprains. *J Athl Train.* 2019;54(6):589-602.
11. Berquist TH. *Radiology of the Foot and Ankle.* 2 ed: Lippincott Williams & Wilkins; 2000.
12. Cailliet R. *Foot and Ankle Pain.* 3 ed: F.A. Davis Company; 1997.
13. Athanasiou KA, Niederauer GG, Schenck RC, Jr. Biomechanical topography of human ankle cartilage. *Ann Biomed Eng.* 1995;23(5):697-704.
14. Donatelli RA. *The Biomechanics of the Foot and Ankle.* 2 ed: F.A. Davis Company; 1995.
15. Boschetti F, Pennati G, Gervaso F, Peretti GM, Dubini G. Biomechanical properties of human articular cartilage under compressive loads. *Biorheology.* 2004;41(3-4):159-166.
16. Berry JL, Thaeler-Oberdoerster DA, Greenwald AS. Subchondral pathways to the superior surface of the human talus. *Foot Ankle.* 1986;7(1):2-9.
17. Sophia Fox AJ, Bedi A, Rodeo SA. The basic science of articular cartilage: structure, composition, and function. *Sports Health.* 2009;1(6):461-468.
18. Kuettner KE, Cole AA. Cartilage degeneration in different human joints. *Osteoarthritis Cartilage.* 2005;13(2):93-103.
19. Rolaufts B, Williams JM, Grodzinsky AJ, Kuettner KE, Cole AA. Distinct horizontal patterns in the spatial organization of superficial zone chondrocytes of human joints. *J Struct Biol.* 2008;162(2):335-344.
20. Bhosale AM, Richardson JB. Articular cartilage: structure, injuries and review of management. *Br Med Bull.* 2008;87:77-95.
21. Simkin PA. Consider the tidemark. *J Rheumatol.* 2012;39(5):890-892.
22. Roudier MP M, P.A., Simkin, P.A. Tidemark Duplication In Osteoarthritis: Evidence Of Incremental Progression [Abstract]. Paper presented at: 2013 ACR/ARHP Annual Meeting 2013; San Diego, C.A.
23. Burr DB, Gallant MA. Bone remodelling in osteoarthritis. *Nat Rev Rheumatol.* 2012;8(11):665-673.
24. Eyre D. Collagen of articular cartilage. *Arthritis Res.* 2002;4(1):30-35.
25. Roughley PJ, Mort JS. The role of aggrecan in normal and osteoarthritic cartilage. *J Exp Orthop.* 2014;1(1):8.
26. Shepherd DE, Seedhom BB. Thickness of human articular cartilage in joints of the lower limb. *Ann Rheum Dis.* 1999;58(1):27-34.

27. DeSmet AA, Dalinka MK, Alazraki N, et al. Chronic ankle pain. American College of Radiology. ACR Appropriateness Criteria. *Radiology*. 2000;215 Suppl:321-332.
28. Treppo S, Koepp H, Quan EC, Cole AA, Kuettner KE, Grodzinsky AJ. Comparison of biomechanical and biochemical properties of cartilage from human knee and ankle pairs. *J Orthop Res*. 2000;18(5):739-748.
29. Mow VC, Kuei SC, Lai WM, Armstrong CG. Biphasic creep and stress relaxation of articular cartilage in compression? Theory and experiments. *J Biomech Eng*. 1980;102(1):73-84.
30. Kraeutler MJ, Kaenkumchorn T, Pascual-Garrido C, Wimmer MA, Chubinskaya S. Peculiarities in Ankle Cartilage. *Cartilage*. 2017;8(1):12-18.
31. Aurich M, Squires GR, Reiner A, et al. Differential matrix degradation and turnover in early cartilage lesions of human knee and ankle joints. *Arthritis Rheum*. 2005;52(1):112-119.
32. Dang Y, Cole AA, Homandberg GA. Comparison of the catabolic effects of fibronectin fragments in human knee and ankle cartilages. *Osteoarthritis Cartilage*. 2003;11(7):538-547.
33. Eger W, Schumacher BL, Mollenhauer J, Kuettner KE, Cole AA. Human knee and ankle cartilage explants: catabolic differences. *J Orthop Res*. 2002;20(3):526-534.
34. Chubinskaya S, Kuettner KE, Cole AA. Expression of matrix metalloproteinases in normal and damaged articular cartilage from human knee and ankle joints. *Lab Invest*. 1999;79(12):1669-1677.
35. Li G, Yin J, Gao J, et al. Subchondral bone in osteoarthritis: insight into risk factors and microstructural changes. *Arthritis Res Ther*. 2013;15(6):223.
36. Milz S, Putz R. Quantitative morphology of the subchondral plate of the tibial plateau. *J Anat*. 1994;185 (Pt 1):103-110.
37. Florencio-Silva R, Sasso GR, Sasso-Cerri E, Simoes MJ, Cerri PS. Biology of Bone Tissue: Structure, Function, and Factors That Influence Bone Cells. *Biomed Res Int*. 2015;2015:421746.
38. Teitelbaum SL. Bone resorption by osteoclasts. *Science*. 2000;289(5484):1504-1508.
39. Kular J, Tickner J, Chim SM, Xu J. An overview of the regulation of bone remodelling at the cellular level. *Clin Biochem*. 2012;45(12):863-873.
40. Garg P, Mazur MM, Buck AC, Wandtke ME, Liu J, Ebraheim NA. Prospective Review of Mesenchymal Stem Cells Differentiation into Osteoblasts. *Orthop Surg*. 2017;9(1):13-19.
41. Lu XL, Huo B, Chiang V, Guo XE. Osteocytic network is more responsive in calcium signaling than osteoblastic network under fluid flow. *J Bone Miner Res*. 2012;27(3):563-574.
42. Coughlin TR, Kennedy OD. The role of subchondral bone damage in post-traumatic osteoarthritis. *Ann N Y Acad Sci*. 2016;1383(1):58-66.
43. Park JS, Chu JS, Tsou AD, et al. The effect of matrix stiffness on the differentiation of mesenchymal stem cells in response to TGF-beta. *Biomaterials*. 2011;32(16):3921-3930.
44. Gao Y, Liu S, Huang J, et al. The ECM-cell interaction of cartilage extracellular matrix on chondrocytes. *Biomed Res Int*. 2014;2014:648459.
45. Cao L, Lee V, Adams ME, et al. beta-Integrin-collagen interaction reduces chondrocyte apoptosis. *Matrix Biol*. 1999;18(4):343-355.
46. Amin AR, Di Cesare PE, Vyas P, et al. The expression and regulation of nitric oxide synthase in human osteoarthritis-affected chondrocytes: evidence for up-regulated neuronal nitric oxide synthase. *J Exp Med*. 1995;182(6):2097-2102.
47. Robey PG, Fedarko NS, Hefferan TE, et al. Structure and molecular regulation of bone matrix proteins. *J Bone Miner Res*. 1993;8 Suppl 2:S483-487.
48. Legate KR, Wickstrom SA, Fassler R. Genetic and cell biological analysis of integrin outside-in signaling. *Genes Dev*. 2009;23(4):397-418.
49. Prasadam I, Farnaghi S, Feng JQ, et al. Impact of extracellular matrix derived from osteoarthritis subchondral bone osteoblasts on osteocytes: role of integrinbeta1 and focal adhesion kinase signaling cues. *Arthritis Res Ther*. 2013;15(5):R150.

50. Maldonado M, Nam J. The role of changes in extracellular matrix of cartilage in the presence of inflammation on the pathology of osteoarthritis. *Biomed Res Int*. 2013;2013:284873.
51. Lodish H, Berk, A., Zipursky, S.L., Matsudaira, P., Baltimore, D. and Darnell, J. *Molecular Cell Biology*. 4th ed. New York: W. H. Freeman; 2000.
52. Mitterhauser M, Toegel S, Wadsak W, et al. Binding studies of [18F]-fluoride and polyphosphonates radiolabelled with [99mTc], [111In], [153Sm] and [188Re] on bone compartments: verification of the pre vivo model? *Bone*. 2005;37(3):404-412.
53. Hwang J, Bae WC, Shieu W, Lewis CW, Bugbee WD, Sah RL. Increased hydraulic conductance of human articular cartilage and subchondral bone plate with progression of osteoarthritis. *Arthritis Rheum*. 2008;58(12):3831-3842.
54. Botter SM, van Osch GJ, Clockaerts S, Waarsing JH, Weinans H, van Leeuwen JP. Osteoarthritis induction leads to early and temporal subchondral plate porosity in the tibial plateau of mice: an in vivo microfocal computed tomography study. *Arthritis Rheum*. 2011;63(9):2690-2699.
55. Upton AR, Holding CA, Dharmapatni AA, Haynes DR. The expression of RANKL and OPG in the various grades of osteoarthritic cartilage. *Rheumatol Int*. 2012;32(2):535-540.
56. Siegler S, Toy J, Seale D, Pedowitz D. The Clinical Biomechanics Award 2013 -- presented by the International Society of Biomechanics: new observations on the morphology of the talar dome and its relationship to ankle kinematics. *Clin Biomech (Bristol, Avon)*. 2014;29(1):1-6.
57. Sturnick D, Constantine, D. and Saito, G.H. The Function Axis of Rotation of the Ankle Joint during Simulated Gait. *Foot and Ankle Ortho*. 2017;2(3).
58. Lundberg A, Svensson OK, Nemeth G, Selvik G. The axis of rotation of the ankle joint. *J Bone Joint Surg Br*. 1989;71(1):94-99.
59. Burdett RG. Forces predicted at the ankle during running. *Med Sci Sports Exerc*. 1982;14(4):308-316.
60. van den Bogert AJ, Read L, Nigg BM. An analysis of hip joint loading during walking, running, and skiing. *Med Sci Sports Exerc*. 1999;31(1):131-142.
61. Calhoun JH, Li F, Ledbetter BR, Viegas SF. A comprehensive study of pressure distribution in the ankle joint with inversion and eversion. *Foot Ankle Int*. 1994;15(3):125-133.
62. Panero E, Gastaldi L, Rapp W. Two-Segment Foot Model for the Biomechanical Analysis of Squat. *J Healthc Eng*. 2017;2017:9652948.
63. Horisberger M, Hintermann B, Valderrabano V. Alterations of plantar pressure distribution in posttraumatic end-stage ankle osteoarthritis. *Clin Biomech (Bristol, Avon)*. 2009;24(3):303-307.
64. Valderrabano V, Nigg BM, von Tscharner V, Stefanyshyn DJ, Goepfert B, Hintermann B. Gait analysis in ankle osteoarthritis and total ankle replacement. *Clin Biomech (Bristol, Avon)*. 2007;22(8):894-904.
65. Dyrby C, Chou LB, Andriacchi TP, Mann RA. Functional evaluation of the Scandinavian Total Ankle Replacement. *Foot Ankle Int*. 2004;25(6):377-381.
66. Tuan RS. Stemming cartilage degeneration: adult mesenchymal stem cells as a cell source for articular cartilage tissue engineering. *Arthritis Rheum*. 2006;54(10):3075-3078.
67. Pittenger MF, Mackay AM, Beck SC, et al. Multilineage potential of adult human mesenchymal stem cells. *Science*. 1999;284(5411):143-147.
68. Smith JR, Hayflick L. Variation in the life-span of clones derived from human diploid cell strains. *J Cell Biol*. 1974;62(1):48-53.
69. Bruder SP, Jaiswal N, Haynesworth SE. Growth kinetics, self-renewal, and the osteogenic potential of purified human mesenchymal stem cells during extensive subcultivation and following cryopreservation. *J Cell Biochem*. 1997;64(2):278-294.
70. Le Blanc K, Mougiakakos D. Multipotent mesenchymal stromal cells and the innate immune system. *Nat Rev Immunol*. 2012;12(5):383-396.

71. Pittenger MF, Discher DE, Peault BM, Phinney DG, Hare JM, Caplan AI. Mesenchymal stem cell perspective: cell biology to clinical progress. *NPJ Regen Med.* 2019;4:22.
72. Jones E, English A, Churchman SM, et al. Large-scale extraction and characterization of CD271+ multipotential stromal cells from trabecular bone in health and osteoarthritis: implications for bone regeneration strategies based on uncultured or minimally cultured multipotential stromal cells. *Arthritis Rheum.* 2010;62(7):1944-1954.
73. Friedenstein AJ, Deriglasova UF, Kulagina NN, et al. Precursors for fibroblasts in different populations of hematopoietic cells as detected by the in vitro colony assay method. *Exp Hematol.* 1974;2(2):83-92.
74. Caplan AI. Mesenchymal stem cells. *J Orthop Res.* 1991;9(5):641-650.
75. Gomez-Salazar M, Gonzalez-Galofre ZN, Casamitjana J, Crisan M, James AW, Peault B. Five Decades Later, Are Mesenchymal Stem Cells Still Relevant? *Front Bioeng Biotechnol.* 2020;8:148.
76. Ghazanfari R, Li H, Zacharaki D, Lim HC, Scheduling S. Human Non-Hematopoietic CD271(pos)/CD140a(low/neg) Bone Marrow Stroma Cells Fulfill Stringent Stem Cell Criteria in Serial Transplantations. *Stem Cells Dev.* 2016;25(21):1652-1658.
77. Horwitz EM, Le Blanc K, Dominici M, et al. Clarification of the nomenclature for MSC: The International Society for Cellular Therapy position statement. *Cytotherapy.* 2005;7(5):393-395.
78. Hosseiniyan Khatibi SM, Kheyrolahzadeh K, Barzegari A, Rahbar Saadat Y, Zununi Vahed S. Medicinal signaling cells: A potential antimicrobial drug store. *J Cell Physiol.* 2020;235(11):7731-7746.
79. Caplan AI. Medicinal signalling cells: they work, so use them. *Nature.* 2019;566(7742):39.
80. Galleu A, Riffo-Vasquez Y, Trento C, et al. Apoptosis in mesenchymal stromal cells induces in vivo recipient-mediated immunomodulation. *Sci Transl Med.* 2017;9(416).
81. Weiss ARR, Dahlke MH. Immunomodulation by Mesenchymal Stem Cells (MSCs): Mechanisms of Action of Living, Apoptotic, and Dead MSCs. *Front Immunol.* 2019;10:1191.
82. Lin W, Xu L, Zwingenberger S, Gibon E, Goodman SB, Li G. Mesenchymal stem cells homing to improve bone healing. *J Orthop Translat.* 2017;9:19-27.
83. Xia H, Liang C, Luo P, et al. Pericellular collagen I coating for enhanced homing and chondrogenic differentiation of mesenchymal stem cells in direct intra-articular injection. *Stem Cell Res Ther.* 2018;9(1):174.
84. Zedde P, Cudoni S, Giachetti G, et al. Subchondral bone remodeling: comparing nanofracture with microfracture. An ovine in vivo study. *Joints.* 2016;4(2):87-93.
85. Ilas DC, Baboolal TG, Churchman SM, et al. The osteogenic commitment of CD271+CD56+ bone marrow stromal cells (BMSCs) in osteoarthritic femoral head bone. *Sci Rep.* 2020;10(1):11145.
86. da Silva Meirelles L, Chagastelles PC, Nardi NB. Mesenchymal stem cells reside in virtually all post-natal organs and tissues. *J Cell Sci.* 2006;119(Pt 11):2204-2213.
87. Ichinose S, Muneta T, Koga H, et al. Morphological differences during in vitro chondrogenesis of bone marrow-, synovium-MSCs, and chondrocytes. *Lab Invest.* 2010;90(2):210-221.
88. Ayala-Cuellar AP, Kang JH, Jeung EB, Choi KC. Roles of Mesenchymal Stem Cells in Tissue Regeneration and Immunomodulation. *Biomol Ther (Seoul).* 2019;27(1):25-33.
89. Isern J, Mendez-Ferrer S. Stem cell interactions in a bone marrow niche. *Curr Osteoporos Rep.* 2011;9(4):210-218.
90. Friedenstein AJ, Chailakhjan RK, Lalykina KS. The development of fibroblast colonies in monolayer cultures of guinea-pig bone marrow and spleen cells. *Cell Tissue Kinet.* 1970;3(4):393-403.
91. Dominici M, Le Blanc K, Mueller I, et al. Minimal criteria for defining multipotent mesenchymal stromal cells. The International Society for Cellular Therapy position statement. *Cytotherapy.* 2006;8(4):315-317.

92. Jones E, McGonagle D. Human bone marrow mesenchymal stem cells in vivo. *Rheumatology (Oxford)*. 2008;47(2):126-131.
93. Baboolal TG, Khalil-Khan A, Theodorides AA, Wall O, Jones E, McGonagle D. A Novel Arthroscopic Technique for Intraoperative Mobilization of Synovial Mesenchymal Stem Cells. *Am J Sports Med*. 2018;46(14):3532-3540.
94. Hatakeyama A, Uchida S, Utsunomiya H, et al. Isolation and Characterization of Synovial Mesenchymal Stem Cell Derived from Hip Joints: A Comparative Analysis with a Matched Control Knee Group. *Stem Cells Int*. 2017;2017:9312329.
95. Sakaguchi Y, Sekiya I, Yagishita K, Muneta T. Comparison of human stem cells derived from various mesenchymal tissues: superiority of synovium as a cell source. *Arthritis Rheum*. 2005;52(8):2521-2529.
96. Kim YS, Lee HJ, Yeo JE, Kim YI, Choi YJ, Koh YG. Isolation and characterization of human mesenchymal stem cells derived from synovial fluid in patients with osteochondral lesion of the talus. *Am J Sports Med*. 2015;43(2):399-406.
97. Li CY, Wu XY, Tong JB, et al. Comparative analysis of human mesenchymal stem cells from bone marrow and adipose tissue under xeno-free conditions for cell therapy. *Stem Cell Res Ther*. 2015;6:55.
98. Centeno CJ, Al-Sayegh H, Freeman MD, Smith J, Murrell WD, Bubnov R. A multi-center analysis of adverse events among two thousand, three hundred and seventy two adult patients undergoing adult autologous stem cell therapy for orthopaedic conditions. *Int Orthop*. 2016;40(8):1755-1765.
99. Kim YS, Koh YG. Injection of Mesenchymal Stem Cells as a Supplementary Strategy of Marrow Stimulation Improves Cartilage Regeneration After Lateral Sliding Calcaneal Osteotomy for Varus Ankle Osteoarthritis: Clinical and Second-Look Arthroscopic Results. *Arthroscopy*. 2016;32(5):878-889.
100. Kim YS, Lee HJ, Choi YJ, Kim YI, Koh YG. Does an injection of a stromal vascular fraction containing adipose-derived mesenchymal stem cells influence the outcomes of marrow stimulation in osteochondral lesions of the talus? A clinical and magnetic resonance imaging study. *Am J Sports Med*. 2014;42(10):2424-2434.
101. Campbell TM, Churchman SM, Gomez A, et al. Mesenchymal Stem Cell Alterations in Bone Marrow Lesions in Patients With Hip Osteoarthritis. *Arthritis Rheumatol*. 2016;68(7):1648-1659.
102. Aigner T, Zien A, Gehrsitz A, Gebhard PM, McKenna L. Anabolic and catabolic gene expression pattern analysis in normal versus osteoarthritic cartilage using complementary DNA-array technology. *Arthritis Rheum*. 2001;44(12):2777-2789.
103. Dowthwaite GP, Bishop JC, Redman SN, et al. The surface of articular cartilage contains a progenitor cell population. *J Cell Sci*. 2004;117(Pt 6):889-897.
104. Hayes AJ, MacPherson S, Morrison H, Dowthwaite G, Archer CW. The development of articular cartilage: evidence for an appositional growth mechanism. *Anat Embryol (Berl)*. 2001;203(6):469-479.
105. Serafini M, Sacchetti B, Pievani A, et al. Establishment of bone marrow and hematopoietic niches in vivo by reversion of chondrocyte differentiation of human bone marrow stromal cells. *Stem Cell Res*. 2014;12(3):659-672.
106. Brown TD, Johnston RC, Saltzman CL, Marsh JL, Buckwalter JA. Posttraumatic osteoarthritis: a first estimate of incidence, prevalence, and burden of disease. *J Orthop Trauma*. 2006;20(10):739-744.
107. Leigh JP, Seavey W, Leistikow B. Estimating the costs of job related arthritis. *J Rheumatol*. 2001;28(7):1647-1654.
108. Saltzman CL, Zimmerman MB, O'Rourke M, Brown TD, Buckwalter JA, Johnston R. Impact of comorbidities on the measurement of health in patients with ankle osteoarthritis. *J Bone Joint Surg Am*. 2006;88(11):2366-2372.
109. UK Clinical Research Collaboration. UK Health Research Analysis. 2015.
110. National Joint Registry. *14th Annual Report 2017*. 2017.

111. Loeser RF. Aging processes and the development of osteoarthritis. *Curr Opin Rheumatol*. 2013;25(1):108-113.
112. van Meurs JB. Osteoarthritis year in review 2016: genetics, genomics and epigenetics. *Osteoarthritis Cartilage*. 2017;25(2):181-189.
113. Saltzman CL, Salamon ML, Blanchard GM, et al. Epidemiology of ankle arthritis: report of a consecutive series of 639 patients from a tertiary orthopaedic center. *Iowa Orthop J*. 2005;25:44-46.
114. Kramer WC, Hendricks KJ, Wang J. Pathogenetic mechanisms of posttraumatic osteoarthritis: opportunities for early intervention. *Int J Clin Exp Med*. 2011;4(4):285-298.
115. Nelson AJ, Collins CL, Yard EE, Fields SK, Comstock RD. Ankle injuries among United States high school sports athletes, 2005-2006. *J Athl Train*. 2007;42(3):381-387.
116. Richmond SA, Fukuchi RK, Ezzat A, Schneider K, Schneider G, Emery CA. Are joint injury, sport activity, physical activity, obesity, or occupational activities predictors for osteoarthritis? A systematic review. *J Orthop Sports Phys Ther*. 2013;43(8):515-519.
117. Sugimoto K, Takakura Y, Okahashi K, Samoto N, Kawate K, Iwai M. Chondral injuries of the ankle with recurrent lateral instability: an arthroscopic study. *J Bone Joint Surg Am*. 2009;91(1):99-106.
118. Gatlin CC, Matheny LM, Ho CP, Johnson NS, Clanton TO. Diagnostic accuracy of 3.0 Tesla magnetic resonance imaging for the detection of articular cartilage lesions of the talus. *Foot Ankle Int*. 2015;36(3):288-292.
119. Roemer FW, Jomaah N, Niu J, et al. Ligamentous Injuries and the Risk of Associated Tissue Damage in Acute Ankle Sprains in Athletes: A Cross-sectional MRI Study. *Am J Sports Med*. 2014;42(7):1549-1557.
120. McGonagle D, Tan AL, Carey J, Benjamin M. The anatomical basis for a novel classification of osteoarthritis and allied disorders. *J Anat*. 2010;216(3):279-291.
121. Hootman JM, Dick R, Agel J. Epidemiology of collegiate injuries for 15 sports: summary and recommendations for injury prevention initiatives. *J Athl Train*. 2007;42(2):311-319.
122. Delco ML, Kennedy JG, Bonassar LJ, Fortier LA. Post-traumatic osteoarthritis of the ankle: A distinct clinical entity requiring new research approaches. *J Orthop Res*. 2017;35(3):440-453.
123. Roudier MP, Manner, P.A., Simkin, P.A., . Tidemark Duplication In Osteoarthritis: Evidence Of Incremental Progression? 2013 ACR/ARHP Annual Meeting; 2013; San Diego, C.A.
124. Shapiro F, Koide S, Glimcher MJ. Cell origin and differentiation in the repair of full-thickness defects of articular cartilage. *J Bone Joint Surg Am*. 1993;75(4):532-553.
125. Pascual Garrido C, Hakimiyan AA, Rappoport L, Oegema TR, Wimmer MA, Chubinskaya S. Anti-apoptotic treatments prevent cartilage degradation after acute trauma to human ankle cartilage. *Osteoarthritis Cartilage*. 2009;17(9):1244-1251.
126. Centres for Disease Control and Prevention. Osteoarthritis. <https://www.cdc.gov/arthritis/basics/osteoarthritis.htm>. Published 2020. Updated 04/05/2020. Accessed 01/06/2020.
127. Eriksen EF. Treatment of bone marrow lesions (bone marrow edema). *Bonekey Rep*. 2015;4:755.
128. Mastbergen SC, Lafeber FP. Changes in subchondral bone early in the development of osteoarthritis. *Arthritis Rheum*. 2011;63(9):2561-2563.
129. National Institute for Health and Care Excellence. *Management of osteoarthritis*. 2017.
130. da Costa BR, Reichenbach S, Keller N, et al. Effectiveness of non-steroidal anti-inflammatory drugs for the treatment of pain in knee and hip osteoarthritis: a network meta-analysis. *Lancet*. 2017;390(10090):e21-e33.
131. Grice J, Marsland D, Smith G, Calder J. Efficacy of Foot and Ankle Corticosteroid Injections. *Foot Ankle Int*. 2017;38(1):8-13.
132. DeGroot H, 3rd, Uzunishvili S, Weir R, Al-omari A, Gomes B. Intra-articular injection of hyaluronic acid is not superior to saline solution injection for ankle arthritis: a

- randomized, double-blind, placebo-controlled study. *J Bone Joint Surg Am.* 2012;94(1):2-8.
133. Migliore A, Giovannangeli F, Granata M, Lagana B. Hylan g-f 20: review of its safety and efficacy in the management of joint pain in osteoarthritis. *Clin Med Insights Arthritis Musculoskelet Disord.* 2010;3:55-68.
 134. Fukawa T, Yamaguchi S, Akatsu Y, Yamamoto Y, Akagi R, Sasho T. Safety and Efficacy of Intra-articular Injection of Platelet-Rich Plasma in Patients With Ankle Osteoarthritis. *Foot Ankle Int.* 2017;38(6):596-604.
 135. Cugat R, Cusco X, Seijas R, et al. Biologic enhancement of cartilage repair: the role of platelet-rich plasma and other commercially available growth factors. *Arthroscopy.* 2015;31(4):777-783.
 136. Klatter-Schulz F, Schmidt T, Uckert M, et al. Comparative Analysis of Different Platelet Lysates and Platelet Rich Preparations to Stimulate Tendon Cell Biology: An In Vitro Study. *Int J Mol Sci.* 2018;19(1).
 137. Wang K, Li Z, Li J, et al. Optimization of the Platelet-Rich Plasma Concentration for Mesenchymal Stem Cell Applications. *Tissue Eng Part A.* 2019;25(5-6):333-351.
 138. Hersant B, Sid-Ahmed M, Braud L, et al. Platelet-Rich Plasma Improves the Wound Healing Potential of Mesenchymal Stem Cells through Paracrine and Metabolism Alterations. *Stem Cells Int.* 2019;2019:1234263.
 139. Hemeda H, Giebel B, Wagner W. Evaluation of human platelet lysate versus fetal bovine serum for culture of mesenchymal stromal cells. *Cytotherapy.* 2014;16(2):170-180.
 140. Altaie A, Baboolal TG, Wall O, Jones E, McGonagle D. Platelet lysate enhances synovial fluid multipotential stromal cells functions: Implications for therapeutic use. *Cytotherapy.* 2018;20(3):375-384.
 141. Johnson K, Zhu S, Tremblay MS, et al. A stem cell-based approach to cartilage repair. *Science.* 2012;336(6082):717-721.
 142. Chen CY, Li C, Ke CJ, Sun JS, Lin FH. Kartogenin Enhances Chondrogenic Differentiation of MSCs in 3D Tri-Copolymer Scaffolds and the Self-Designed Bioreactor System. *Biomolecules.* 2021;11(1).
 143. Liu C, Li Y, Yang Z, Zhou Z, Lou Z, Zhang Q. Kartogenin enhances the therapeutic effect of bone marrow mesenchymal stem cells derived exosomes in cartilage repair. *Nanomedicine (Lond).* 2020;15(3):273-288.
 144. Music E, Klein TJ, Lott WB, Doran MR. Transforming growth factor-beta stimulates human bone marrow-derived mesenchymal stem/stromal cell chondrogenesis more so than kartogenin. *Sci Rep.* 2020;10(1):8340.
 145. Medda S, Al'Khafaji IM, Scott AT. Ankle Arthroscopy With Microfracture for Osteochondral Defects of the Talus. *Arthrosc Tech.* 2017;6(1):e167-e174.
 146. Jones WG, El-Jawhari JJ, Brockett CL, Korla L, Ktistakis I, Jones E. Multipotential stromal cells in the talus and distal tibia in ankle osteoarthritis - Presence, potency and relationships to subchondral bone changes. *J Cell Mol Med.* 2021;25(1):259-271.
 147. Daniels TR, Younger AS, Penner M, et al. Intermediate-term results of total ankle replacement and ankle arthrodesis: a COFAS multicenter study. *J Bone Joint Surg Am.* 2014;96(2):135-142.
 148. Wang Y, Li Z, Wong DW, Zhang M. Effects of Ankle Arthrodesis on Biomechanical Performance of the Entire Foot. *PLoS One.* 2015;10(7):e0134340.
 149. Ebalard M, Le Henaff G, Sigonney G, et al. Risk of osteoarthritis secondary to partial or total arthrodesis of the subtalar and midtarsal joints after a minimum follow-up of 10 years. *Orthop Traumatol Surg Res.* 2014;100(4 Suppl):S231-237.
 150. Muir DC, Amendola A, Saltzman CL. Long-term outcome of ankle arthrodesis. *Foot Ankle Clin.* 2002;7(4):703-708.
 151. Maffulli N, Longo UG, Locher J, Romeo G, Salvatore G, Denaro V. Outcome of ankle arthrodesis and ankle prosthesis: a review of the current status. *Br Med Bull.* 2017;124(1):91-112.

152. Koivu H, Kohonen I, Mattila K, Loyttyniemi E, Tiusanen H. Long-term Results of Scandinavian Total Ankle Replacement. *Foot Ankle Int.* 2017;38(7):723-731.
153. Frigg A, Germann U, Huber M, Horisberger M. Survival of the Scandinavian total ankle replacement (STAR): results of ten to nineteen years follow-up. *Int Orthop.* 2017;41(10):2075-2082.
154. Kanatli U, Eren A, Eren TK, Vural A. Treatment of Osteochondral Lesions of the Talus With Cell-free Polymer-based Scaffold in Single-Step Arthroscopic Surgery. *Arthroscopy Techniques.* 2017;6(5):e1727-e1734.
155. Polat G, Ersen A, Erdil ME, Kizilkurt T, Kilicoglu O, Asik M. Long-term results of microfracture in the treatment of talus osteochondral lesions. *Knee Surg Sports Traumatol Arthrosc.* 2016;24(4):1299-1303.
156. Yoon HS, Park YJ, Lee M, Choi WJ, Lee JW. Osteochondral Autologous Transplantation Is Superior to Repeat Arthroscopy for the Treatment of Osteochondral Lesions of the Talus After Failed Primary Arthroscopic Treatment. *Am J Sports Med.* 2014;42(8):1896-1903.
157. Sun J-La, Li L-Lb, Yang J-Xc, Chen Yc, Ma W-L. A comparison of surgical approaches for osteochondral lesions of the talus associated with ankle fractures. *International Journal of Clinical and Experimental Medicine.* 2016;9(11):21780-21786.
158. Brittberg M, Lindahl A, Nilsson A, Ohlsson C, Isaksson O, Peterson L. Treatment of deep cartilage defects in the knee with autologous chondrocyte transplantation. *N Engl J Med.* 1994;331(14):889-895.
159. Pagliuzzi G, Vannini F, Battaglia M, Ramponi L, Buda R. Autologous Chondrocyte Implantation for Talar Osteochondral Lesions: Comparison Between 5-Year Follow-Up Magnetic Resonance Imaging Findings and 7-Year Follow-Up Clinical Results. *J Foot Ankle Surg.* 2017.
160. National Institute for Health and Care Excellence. Joint distraction for ankle osteoarthritis. <https://www.nice.org.uk/guidance/igp538/chapter/3-The-procedure>. Published 2015. Accessed 8th January, 2017.
161. Rodriguez-Merchan EC. Joint Distraction in Advanced Osteoarthritis of the Ankle. *Arch Bone Jt Surg.* 2017;5(4):208-212.
162. Fragomen AT, McCoy TH, Meyers KN, Rozbruch SR. Minimum distraction gap: how much ankle joint space is enough in ankle distraction arthroplasty? *HSS J.* 2014;10(1):6-12.
163. Nguyen MP, Pedersen DR, Gao Y, Saltzman CL, Amendola A. Intermediate-term follow-up after ankle distraction for treatment of end-stage osteoarthritis. *J Bone Joint Surg Am.* 2015;97(7):590-596.
164. Saltzman CL, Hillis SL, Stolley MP, Anderson DD, Amendola A. Motion versus fixed distraction of the joint in the treatment of ankle osteoarthritis: a prospective randomized controlled trial. *J Bone Joint Surg Am.* 2012;94(11):961-970.
165. Xu Y, Zhu Y, Xu XY. Ankle joint distraction arthroplasty for severe ankle arthritis. *BMC Musculoskelet Disord.* 2017;18(1):96.
166. Zhang K, Jiang Y, Du J, et al. Comparison of distraction arthroplasty alone versus combined with arthroscopic microfracture in treatment of post-traumatic ankle arthritis. *J Orthop Surg Res.* 2017;12(1):45.
167. Holton J, Imam M, Ward J, Snow M. The Basic Science of Bone Marrow Aspirate Concentrate in Chondral Injuries. *Orthop Rev (Pavia).* 2016;8(3):6659.
168. Shaikh N, Seah MKT, Khan WS. Systematic review on the use of autologous matrix-induced chondrogenesis for the repair of articular cartilage defects in patients. *World J Orthop.* 2017;8(7):588-601.
169. Ploegmakers JJ, van Roermund PM, van Melkebeek J, et al. Prolonged clinical benefit from joint distraction in the treatment of ankle osteoarthritis. *Osteoarthritis Cartilage.* 2005;13(7):582-588.
170. Tellisi N, Fragomen AT, Kleinman D, O'Malley MJ, Rozbruch SR. Joint preservation of the osteoarthritic ankle using distraction arthroplasty. *Foot Ankle Int.* 2009;30(4):318-325.

171. Intema F, Thomas TP, Anderson DD, et al. Subchondral bone remodeling is related to clinical improvement after joint distraction in the treatment of ankle osteoarthritis. *Osteoarthritis Cartilage*. 2011;19(6):668-675.
172. Marijnissen AC, Hoekstra MC, Pre BC, et al. Patient characteristics as predictors of clinical outcome of distraction in treatment of severe ankle osteoarthritis. *J Orthop Res*. 2014;32(1):96-101.
173. Emadedin M, Ghorbani Liastani M, Fazeli R, et al. Long-Term Follow-up of Intra-articular Injection of Autologous Mesenchymal Stem Cells in Patients with Knee, Ankle, or Hip Osteoarthritis. *Arch Iran Med*. 2015;18(6):336-344.
174. Hauser RA, Orlofsky A. Regenerative injection therapy with whole bone marrow aspirate for degenerative joint disease: a case series. *Clin Med Insights Arthritis Musculoskelet Disord*. 2013;6:65-72.
175. Kim YS, Lee M, Koh YG. Additional mesenchymal stem cell injection improves the outcomes of marrow stimulation combined with supramalleolar osteotomy in varus ankle osteoarthritis: short-term clinical results with second-look arthroscopic evaluation. *J Exp Orthop*. 2016;3(1):12.
176. Solchaga LA, Penick K, Goldberg VM, Caplan AI, Welter JF. Fibroblast growth factor-2 enhances proliferation and delays loss of chondrogenic potential in human adult bone-marrow-derived mesenchymal stem cells. *Tissue Eng Part A*. 2010;16(3):1009-1019.
177. Jayasuriya CT, Chen Q. Potential benefits and limitations of utilizing chondroprogenitors in cell-based cartilage therapy. *Connect Tissue Res*. 2015;56(4):265-271.
178. Fellows CR, Matta C, Zakany R, Khan IM, Mobasheri A. Adipose, Bone Marrow and Synovial Joint-Derived Mesenchymal Stem Cells for Cartilage Repair. *Front Genet*. 2016;7:213.
179. Giannoudis PV, Einhorn TA, Marsh D. Fracture healing: the diamond concept. *Injury*. 2007;38 Suppl 4:S3-6.
180. Mathieu PS, Lobo EG. Cytoskeletal and focal adhesion influences on mesenchymal stem cell shape, mechanical properties, and differentiation down osteogenic, adipogenic, and chondrogenic pathways. *Tissue Eng Part B Rev*. 2012;18(6):436-444.
181. Ma K, Titan AL, Stafford M, Zheng C, Levenston ME. Variations in chondrogenesis of human bone marrow-derived mesenchymal stem cells in fibrin/alginate blended hydrogels. *Acta Biomater*. 2012;8(10):3754-3764.
182. El-Jawhari JJ, Moisley K, Jones E, Giannoudis PV. A crosslinked collagen membrane versus a non-crosslinked bilayer collagen membrane for supporting osteogenic functions of human bone marrow-multipotent stromal cells. *Eur Cell Mater*. 2019;37:292-309.
183. Montalbano G, Toumpaniari S, Popov A, et al. Synthesis of bioinspired collagen/alginate/fibrin based hydrogels for soft tissue engineering. *Mater Sci Eng C Mater Biol Appl*. 2018;91:236-246.
184. Vorwald CE, Gonzalez-Fernandez T, Joshee S, Sikorski P, Leach JK. Tunable fibrin-alginate interpenetrating network hydrogels to support cell spreading and network formation. *Acta Biomater*. 2020;108:142-152.
185. Zhou H, Chen W, Weir MD, Xu HH. Biofunctionalized calcium phosphate cement to enhance the attachment and osteodifferentiation of stem cells released from fast-degradable alginate-fibrin microbeads. *Tissue Eng Part A*. 2012;18(15-16):1583-1595.
186. Valenick LV, Hsia HC, Schwarzbauer JE. Fibronectin fragmentation promotes alpha4beta1 integrin-mediated contraction of a fibrin-fibronectin provisional matrix. *Exp Cell Res*. 2005;309(1):48-55.
187. Neuss S, Schneider RK, Tietze L, Knuchel R, Jahnen-Dechent W. Secretion of fibrinolytic enzymes facilitates human mesenchymal stem cell invasion into fibrin clots. *Cells Tissues Organs*. 2010;191(1):36-46.
188. Alvarez-Barreto JF, Landy B, VanGordon S, Place L, DeAngelis PL, Sikavitsas VI. Enhanced osteoblastic differentiation of mesenchymal stem cells seeded in RGD-functionalized

- PLLA scaffolds and cultured in a flow perfusion bioreactor. *J Tissue Eng Regen Med.* 2011;5(6):464-475.
189. Akilbekova D, Shaimerdenova M, Adilov S, Berillo D. Biocompatible scaffolds based on natural polymers for regenerative medicine. *Int J Biol Macromol.* 2018;114:324-333.
 190. Polat G, Balci HI, Cakmak MF, Demirel M, Sen C, Asik M. Long-term results and comparison of the three different high tibial osteotomy and fixation techniques in medial compartment arthrosis. *J Orthop Surg Res.* 2017;12(1):44.
 191. Fortier LA, Barker JU, Strauss EJ, McCarrel TM, Cole BJ. The role of growth factors in cartilage repair. *Clin Orthop Relat Res.* 2011;469(10):2706-2715.
 192. Mariani E, Pulsatelli L, Facchini A. Signaling pathways in cartilage repair. *Int J Mol Sci.* 2014;15(5):8667-8698.
 193. Blaney Davidson EN, Vitters EL, van den Berg WB, van der Kraan PM. TGF beta-induced cartilage repair is maintained but fibrosis is blocked in the presence of Smad7. *Arthritis Res Ther.* 2006;8(3):R65.
 194. Yausep OE, Madhi I, Trigkilidas D. Platelet rich plasma for treatment of osteochondral lesions of the talus: A systematic review of clinical trials. *J Orthop.* 2020;18:218-225.
 195. Fu P, Chen, S., Ding, Z., Cong, R., Shao, J., Zhang, L., Qian, Q. Mechanical stimulation promotes osteogenic and chondrogenic differentiation of synovial mesenchymal stem cells through BMP-2. *Int J Clin Exp Med.* 2017;10(2):2842-2849.
 196. Gardner OFW, Fahy N, Alini M, Stoddart MJ. Joint mimicking mechanical load activates TGFbeta1 in fibrin-poly(ester-urethane) scaffolds seeded with mesenchymal stem cells. *J Tissue Eng Regen Med.* 2017;11(9):2663-2666.
 197. Lin S, Lee WYW, Feng Q, et al. Synergistic effects on mesenchymal stem cell-based cartilage regeneration by chondrogenic preconditioning and mechanical stimulation. *Stem Cell Res Ther.* 2017;8(1):221.
 198. Carroll SF, Buckley CT, Kelly DJ. Cyclic Tensile Strain Can Play a Role in Directing both Intramembranous and Endochondral Ossification of Mesenchymal Stem Cells. *Front Bioeng Biotechnol.* 2017;5:73.
 199. Cadossi M, Buda RE, Ramponi L, Sambri A, Natali S, Giannini S. Bone marrow-derived cells and biophysical stimulation for talar osteochondral lesions: a randomized controlled study. *Foot Ankle Int.* 2014;35(10):981-987.
 200. Fayyad-Kazan H, Faour WH, Badran B, Lagneaux L, Najjar M. The immunomodulatory properties of human bone marrow-derived mesenchymal stromal cells are defined according to multiple immunobiological criteria. *Inflammation research : official journal of the European Histamine Research Society [et al].* 2016;65(6):501-510.
 201. Vanwanseele B, Lucchinetti E, Stussi E. The effects of immobilization on the characteristics of articular cartilage: current concepts and future directions. *Osteoarthritis Cartilage.* 2002;10(5):408-419.
 202. Sanjai K, Kumarswamy J, Patil A, Papaiah L, Jayaram S, Krishnan L. Evaluation and comparison of decalcification agents on the human teeth. *J Oral Maxillofac Pathol.* 2012;16(2):222-227.
 203. Jones EA, Crawford A, English A, et al. Synovial fluid mesenchymal stem cells in health and early osteoarthritis: detection and functional evaluation at the single-cell level. *Arthritis Rheum.* 2008;58(6):1731-1740.
 204. National Joint Registry. *14th Annual Report.* 2017.
 205. Li J, Jadin K, Masuda K, Sah R, Muehleman C. Characterization of lesions of the talus and description of tram-track lesions. *Foot Ankle Int.* 2006;27(5):344-355.
 206. Saxena A, Eakin C. Articular talar injuries in athletes: results of microfracture and autogenous bone graft. *Am J Sports Med.* 2007;35(10):1680-1687.
 207. Chuckpaiwong B, Berkson EM, Theodore GH. Microfracture for osteochondral lesions of the ankle: outcome analysis and outcome predictors of 105 cases. *Arthroscopy.* 2008;24(1):106-112.
 208. Weber AE, Locker PH, Mayer EN, et al. Clinical Outcomes After Microfracture of the Knee: Midterm Follow-up. *Orthop J Sports Med.* 2018;6(2):2325967117753572.

209. Hsueh MF, Onnerfjord P, Bolognesi MP, Easley ME, Kraus VB. Analysis of "old" proteins unmasks dynamic gradient of cartilage turnover in human limbs. *Sci Adv.* 2019;5(10):eaax3203.
210. Henderson JH, de la Fuente L, Romero D, et al. Rapid growth of cartilage rudiments may generate perichondrial structures by mechanical induction. *Biomech Model Mechanobiol.* 2007;6(1-2):127-137.
211. Domayer SE, Welsch GH, Stelzeneder D, et al. Microfracture in the Ankle: Clinical Results and MRI with T2-Mapping at 3.0 T after 1 to 8 Years. *Cartilage.* 2011;2(1):73-80.
212. Mithoefer K, McAdams T, Williams RJ, Kreuz PC, Mandelbaum BR. Clinical efficacy of the microfracture technique for articular cartilage repair in the knee: an evidence-based systematic analysis. *Am J Sports Med.* 2009;37(10):2053-2063.
213. Longhini ALF, Salazar TE, Vieira C, et al. Peripheral blood-derived mesenchymal stem cells demonstrate immunomodulatory potential for therapeutic use in horses. *PLoS One.* 2019;14(3):e0212642.
214. Eggenhofer E, Luk F, Dahlke MH, Hoogduijn MJ. The life and fate of mesenchymal stem cells. *Front Immunol.* 2014;5:148.
215. McGonagle D, Baboolal TG, Jones E. Native joint-resident mesenchymal stem cells for cartilage repair in osteoarthritis. *Nat Rev Rheumatol.* 2017;13(12):719-730.
216. Knutsen G, Engebretsen L, Ludvigsen TC, et al. Autologous chondrocyte implantation compared with microfracture in the knee. A randomized trial. *J Bone Joint Surg Am.* 2004;86(3):455-464.
217. Hevesi M, Bernard C, Hartigan DE, Levy BA, Domb BG, Krych AJ. Is Microfracture Necessary? Acetabular Chondrolabral Debridement/Abrasion Demonstrates Similar Outcomes and Survival to Microfracture in Hip Arthroscopy: A Multicenter Analysis. *Am J Sports Med.* 2019;47(7):1670-1678.
218. Sekiya I, Ojima M, Suzuki S, et al. Human mesenchymal stem cells in synovial fluid increase in the knee with degenerated cartilage and osteoarthritis. *J Orthop Res.* 2012;30(6):943-949.
219. Sanjurjo-Rodriguez C, Baboolal TG, Burska AN, et al. Gene expression and functional comparison between multipotential stromal cells from lateral and medial condyles of knee osteoarthritis patients. *Sci Rep.* 2019;9(1):9321.
220. Ilas DC, Churchman SM, Baboolal T, et al. The simultaneous analysis of mesenchymal stem cells and early osteocytes accumulation in osteoarthritic femoral head sclerotic bone. *Rheumatology (Oxford).* 2019;58(10):1777-1783.
221. Zamli Z, Robson Brown K, Sharif M. Subchondral Bone Plate Changes More Rapidly than Trabecular Bone in Osteoarthritis. *Int J Mol Sci.* 2016;17(9).
222. Schneider CA, Rasband WS, Eliceiri KW. NIH Image to ImageJ: 25 years of image analysis. *Nat Methods.* 2012;9(7):671-675.
223. Doube M, Klosowski MM, Arganda-Carreras I, et al. BoneJ: Free and extensible bone image analysis in ImageJ. *Bone.* 2010;47(6):1076-1079.
224. Schmitz N, Laverty S, Kraus VB, Aigner T. Basic methods in histopathology of joint tissues. *Osteoarthritis Cartilage.* 2010;18 Suppl 3:S113-116.
225. Aho OM, Finnila M, Thevenot J, Saarakkala S, Lehenkari P. Subchondral bone histology and grading in osteoarthritis. *PLoS One.* 2017;12(3):e0173726.
226. Waldstein W, Perino G, Gilbert SL, Maher SA, Windhager R, Boettner F. OARSI osteoarthritis cartilage histopathology assessment system: A biomechanical evaluation in the human knee. *J Orthop Res.* 2016;34(1):135-140.
227. Pritzker KP, Gay S, Jimenez SA, et al. Osteoarthritis cartilage histopathology: grading and staging. *Osteoarthritis Cartilage.* 2006;14(1):13-29.
228. Patel V, Issever AS, Burghardt A, Laib A, Ries M, Majumdar S. MicroCT evaluation of normal and osteoarthritic bone structure in human knee specimens. *J Orthop Res.* 2003;21(1):6-13.

229. Pastoureau P, Leduc S, Chomel A, De Ceuninck F. Quantitative assessment of articular cartilage and subchondral bone histology in the meniscectomized guinea pig model of osteoarthritis. *Osteoarthritis Cartilage*. 2003;11(6):412-423.
230. Hayman AR. Tartrate-resistant acid phosphatase (TRAP) and the osteoclast/immune cell dichotomy. *Autoimmunity*. 2008;41(3):218-223.
231. Seol JW, Lee HB, Kim NS, Park SY. Tartrate-resistant acid phosphatase as a diagnostic factor for arthritis. *Int J Mol Med*. 2009;24(1):57-62.
232. Versus Arthritis. *The State of Musculoskeletal Health 2019*. 2019.
233. Bigueti CC, Cavalla F, Tim CR, et al. Bioactive glass-ceramic bone repair associated or not with autogenous bone: a study of organic bone matrix organization in a rabbit critical-sized calvarial model. *Clin Oral Investig*. 2019;23(1):413-421.
234. Beane OS, Fonseca VC, Cooper LL, Koren G, Darling EM. Impact of aging on the regenerative properties of bone marrow-, muscle-, and adipose-derived mesenchymal stem/stromal cells. *PLoS One*. 2014;9(12):e115963.
235. Kuganederan N. *Biotribology of the Natural Ankle Joint* Institute of Biological and Medical Engineering, University of Leeds; 2018.
236. Taylor S, Wang C, Wright TC, Denny L, Kuhn L. A comparison of human papillomavirus testing of clinician-collected and self-collected samples during follow-up after screen-and-treat. *Int J Cancer*. 2011;129(4):879-886.
237. Latif A. *Characterisation and modelling of spinal facet joints*, University of Leeds; 2011.
238. Peters AE, Akhtar R, Comerford EJ, Bates KT. The effect of ageing and osteoarthritis on the mechanical properties of cartilage and bone in the human knee joint. *Sci Rep*. 2018;8(1):5931.
239. Nakasa T, Adachi N, Kato T, Ochi M. Correlation between subchondral bone plate thickness and cartilage degeneration in osteoarthritis of the ankle. *Foot Ankle Int*. 2014;35(12):1341-1349.
240. Tsegai ZJ, Skinner MM, Gee AH, et al. Trabecular and cortical bone structure of the talus and distal tibia in Pan and Homo. *Am J Phys Anthropol*. 2017;163(4):784-805.
241. Kwan Tat S, Lajeunesse D, Pelletier JP, Martel-Pelletier J. Targeting subchondral bone for treating osteoarthritis: what is the evidence? *Best Pract Res Clin Rheumatol*. 2010;24(1):51-70.
242. Tzaphlidou M. Bone architecture: collagen structure and calcium/phosphorus maps. *J Biol Phys*. 2008;34(1-2):39-49.
243. El-Jawhari JJ, Brockett CL, Ktistakis I, Jones E, Giannoudis PV. The regenerative therapies of the ankle degeneration: a focus on multipotential mesenchymal stromal cells. *Regen Med*. 2018.
244. Zhen G, Wen C, Jia X, et al. Inhibition of TGF-beta signaling in mesenchymal stem cells of subchondral bone attenuates osteoarthritis. *Nat Med*. 2013;19(6):704-712.
245. Bhatla JL, Kroker A, Manske SL, Emery CA, Boyd SK. Differences in subchondral bone plate and cartilage thickness between women with anterior cruciate ligament reconstructions and uninjured controls. *Osteoarthritis Cartilage*. 2018;26(7):929-939.
246. Hartlev LB, Klose-Jensen R, Thomsen JS, et al. Thickness of the bone-cartilage unit in relation to osteoarthritis severity in the human hip joint. *RMD Open*. 2018;4(2):e000747.
247. Finnila MAJ, Thevenot J, Aho OM, et al. Association between subchondral bone structure and osteoarthritis histopathological grade. *J Orthop Res*. 2017;35(4):785-792.
248. Beuf O, Ghosh S, Newitt DC, et al. Magnetic resonance imaging of normal and osteoarthritic trabecular bone structure in the human knee. *Arthritis Rheum*. 2002;46(2):385-393.
249. Dequeker J, Mokassa L, Aerssens J. Bone density and osteoarthritis. *J Rheumatol Suppl*. 1995;43:98-100.
250. Gruber HE. Adaptations of Goldner's Masson trichrome stain for the study of undecalcified plastic embedded bone. *Biotech Histochem*. 1992;67(1):30-34.
251. Kapila SN, Natarajan S, Boaz K, Pandya JA, Yinti SR. Driving the Mineral out Faster: Simple Modifications of the Decalcification Technique. *J Clin Diagn Res*. 2015;9(9):ZC93-97.

252. Gonzalez-Chavez SA, Pacheco-Tena C, Macias-Vazquez CE, Luevano-Flores E. Assessment of different decalcifying protocols on Osteopontin and Osteocalcin immunostaining in whole bone specimens of arthritis rat model by confocal immunofluorescence. *Int J Clin Exp Pathol*. 2013;6(10):1972-1983.
253. Ludin A, Sela JJ, Schroeder A, Samuni Y, Nitzan DW, Amir G. Injection of vascular endothelial growth factor into knee joints induces osteoarthritis in mice. *Osteoarthritis Cartilage*. 2013;21(3):491-497.
254. Zamli Z, Robson Brown K, Tarlton JF, et al. Subchondral bone plate thickening precedes chondrocyte apoptosis and cartilage degradation in spontaneous animal models of osteoarthritis. *Biomed Res Int*. 2014;2014:606870.
255. Panaroni C, Tzeng YS, Saeed H, Wu JY. Mesenchymal progenitors and the osteoblast lineage in bone marrow hematopoietic niches. *Curr Osteoporos Rep*. 2014;12(1):22-32.
256. Quirici N, Soligo D, Bossolasco P, Servida F, Lumini C, Deliliers GL. Isolation of bone marrow mesenchymal stem cells by anti-nerve growth factor receptor antibodies. *Exp Hematol*. 2002;30(7):783-791.
257. Tormin A, Li O, Brune JC, et al. CD146 expression on primary nonhematopoietic bone marrow stem cells is correlated with in situ localization. *Blood*. 2011;117(19):5067-5077.
258. Utsunomiya H, Uchida S, Sekiya I, Sakai A, Moridera K, Nakamura T. Isolation and characterization of human mesenchymal stem cells derived from shoulder tissues involved in rotator cuff tears. *Am J Sports Med*. 2013;41(3):657-668.
259. Henry JP, Bordoni B. Histology, Osteoblasts. In: *StatPearls*. Treasure Island (FL)2020.
260. Cohen L, Dean M, Shipov A, Atkins A, Monsonogo-Ornan E, Shahar R. Comparison of structural, architectural and mechanical aspects of cellular and acellular bone in two teleost fish. *J Exp Biol*. 2012;215(Pt 11):1983-1993.
261. Gobbi A, Karnatzikos G, Kumar A. Long-term results after microfracture treatment for full-thickness knee chondral lesions in athletes. *Knee Surg Sports Traumatol Arthrosc*. 2014;22(9):1986-1996.
262. Zhao H, Qu W, Li Y, et al. Functional analysis of distraction arthroplasty in the treatment of ankle osteoarthritis. *J Orthop Surg Res*. 2017;12(1):18.
263. Diekman BO, Guilak F. Stem cell-based therapies for osteoarthritis: challenges and opportunities. *Curr Opin Rheumatol*. 2013;25(1):119-126.
264. Zachar L, Bacenkova D, Rosocha J. Activation, homing, and role of the mesenchymal stem cells in the inflammatory environment. *J Inflamm Res*. 2016;9:231-240.
265. Huang NF, Chu J, Lee RJ, Li S. Biophysical and chemical effects of fibrin on mesenchymal stromal cell gene expression. *Acta Biomater*. 2010;6(10):3947-3956.
266. Kim I, Lee SK, Yoon JI, Kim DE, Kim M, Ha H. Fibrin glue improves the therapeutic effect of MSCs by sustaining survival and paracrine function. *Tissue Eng Part A*. 2013;19(21-22):2373-2381.
267. Camernik K, Mihelic A, Mihalic R, et al. Comprehensive analysis of skeletal muscle- and bone-derived mesenchymal stem/stromal cells in patients with osteoarthritis and femoral neck fracture. *Stem Cell Res Ther*. 2020;11(1):146.
268. Soncini M, Vertua E, Gibelli L, et al. Isolation and characterization of mesenchymal cells from human fetal membranes. *J Tissue Eng Regen Med*. 2007;1(4):296-305.
269. Rojewski MT, Weber BM, Schrezenmeier H. Phenotypic Characterization of Mesenchymal Stem Cells from Various Tissues. *Transfus Med Hemother*. 2008;35(3):168-184.
270. Bethesda (MD): National Library of Medicine (US) NCfBI. NT5E [Internet]. <https://www.ncbi.nlm.nih.gov/gene/>. Published 2004 Accessed 16/12/2020.
271. Bethesda (MD): National Library of Medicine (US) NCfBI. Eng [Internet]. Published 2004. Accessed 16/12/2020.
272. Bethesda (MD): National Library of Medicine (US) NCfBI. Thy-1 [Internet]. Published 2004. Accessed 16/12/2020.

273. McCorry MC, Puetzer JL, Bonassar LJ. Characterization of mesenchymal stem cells and fibrochondrocytes in three-dimensional co-culture: analysis of cell shape, matrix production, and mechanical performance. *Stem Cell Res Ther.* 2016;7:39.
274. Fafian-Labora JA, Morente-Lopez M, Arufe MC. Effect of aging on behaviour of mesenchymal stem cells. *World J Stem Cells.* 2019;11(6):337-346.
275. Li C, Kilpatrick CD, Smith S, et al. Assessment of Multipotent Mesenchymal Stromal Cells in Bone Marrow Aspirate From Human Calcaneus. *J Foot Ankle Surg.* 2017;56(1):42-46.
276. Zhou BO, Yue R, Murphy MM, Peyer JG, Morrison SJ. Leptin-receptor-expressing mesenchymal stromal cells represent the main source of bone formed by adult bone marrow. *Cell Stem Cell.* 2014;15(2):154-168.
277. Tan K, Zhu H, Zhang J, et al. CD73 Expression on Mesenchymal Stem Cells Dictates the Reparative Properties via Its Anti-Inflammatory Activity. *Stem Cells Int.* 2019;2019:8717694.
278. Pochampally R. Colony forming unit assays for MSCs. *Methods Mol Biol.* 2008;449:83-91.
279. Gothard D, Dawson JI, Oreffo RO. Assessing the potential of colony morphology for dissecting the CFU-F population from human bone marrow stromal cells. *Cell Tissue Res.* 2013;352(2):237-247.
280. Churchman SM, Boxall SA, McGonagle D, Jones EA. Predicting the Remaining Lifespan and Cultivation-Related Loss of Osteogenic Capacity of Bone Marrow Multipotential Stromal Cells Applicable across a Broad Donor Age Range. *Stem Cells Int.* 2017;2017:6129596.
281. Kamaldinov T, Erndt-Marino J, Levin M, Kaplan DL, Hahn MS. Assessment of Enrichment of Human Mesenchymal Stem Cells Based on Plasma and Mitochondrial Membrane Potentials. *Bioelectricity.* 2020;2(1):21-32.
282. Stefkova K, Prochazkova J, Pachernik J. Alkaline phosphatase in stem cells. *Stem Cells Int.* 2015;2015:628368.
283. Liu W, Zhang L, Xuan K, et al. Alkaline Phosphatase Controls Lineage Switching of Mesenchymal Stem Cells by Regulating the LRP6/GSK3beta Complex in Hypophosphatasia. *Theranostics.* 2018;8(20):5575-5592.
284. Bancroft JG, Marilyn. *The Theory and Practice of Histological Techniques.* 5th ed: Churchill Livingstone; 2001.
285. Stern J, Lewis WH. The colorimetric estimation of calcium in serum with ocoresolphthalein complexone. *Clin Chim Acta.* 1957;2(6):576-580.
286. Templeton DM. The basis and applicability of the dimethylmethylene blue binding assay for sulfated glycosaminoglycans. *Connect Tissue Res.* 1988;17(1):23-32.
287. Ganguly P, El-Jawhari JJ, Burska AN, Ponchel F, Giannoudis PV, Jones EA. The Analysis of In Vivo Aging in Human Bone Marrow Mesenchymal Stromal Cells Using Colony-Forming Unit-Fibroblast Assay and the CD45(low)CD271(+) Phenotype. *Stem Cells Int.* 2019;2019:5197983.
288. Aldridge A, Kouroupis D, Churchman S, English A, Ingham E, Jones E. Assay validation for the assessment of adipogenesis of multipotential stromal cells--a direct comparison of four different methods. *Cytotherapy.* 2013;15(1):89-101.
289. Beresford JN, Bennett JH, Devlin C, Leboy PS, Owen ME. Evidence for an inverse relationship between the differentiation of adipocytic and osteogenic cells in rat marrow stromal cell cultures. *J Cell Sci.* 1992;102 (Pt 2):341-351.
290. James AW, Leucht P, Levi B, et al. Sonic Hedgehog influences the balance of osteogenesis and adipogenesis in mouse adipose-derived stromal cells. *Tissue Eng Part A.* 2010;16(8):2605-2616.
291. Sanjurjo-Rodriguez C, Altaie A, Mastbergen S, et al. Gene Expression Signatures of Synovial Fluid Multipotent Stromal Cells in Advanced Knee Osteoarthritis and Following Knee Joint Distraction. *Front Bioeng Biotechnol.* 2020;8:579751.

292. Haasters F, Prall WC, Anz D, et al. Morphological and immunocytochemical characteristics indicate the yield of early progenitors and represent a quality control for human mesenchymal stem cell culturing. *J Anat.* 2009;214(5):759-767.
293. Hamilton DW, Maul TM, Vorp DA. Characterization of the response of bone marrow-derived progenitor cells to cyclic strain: implications for vascular tissue-engineering applications. *Tissue Eng.* 2004;10(3-4):361-369.
294. Wang Y, Huso DL, Harrington J, et al. Outgrowth of a transformed cell population derived from normal human BM mesenchymal stem cell culture. *Cytotherapy.* 2005;7(6):509-519.
295. Muraglia A, Corsi A, Riminucci M, et al. Formation of a chondro-osseous rudiment in micromass cultures of human bone-marrow stromal cells. *J Cell Sci.* 2003;116(Pt 14):2949-2955.
296. Yang YK, Ogando CR, Wang See C, Chang TY, Barabino GA. Changes in phenotype and differentiation potential of human mesenchymal stem cells aging in vitro. *Stem Cell Res Ther.* 2018;9(1):131.
297. Muraglia A, Cancedda R, Quarto R. Clonal mesenchymal progenitors from human bone marrow differentiate in vitro according to a hierarchical model. *J Cell Sci.* 2000;113 (Pt 7):1161-1166.
298. Sekiya I, Larson BL, Smith JR, Pochampally R, Cui JG, Prockop DJ. Expansion of human adult stem cells from bone marrow stroma: conditions that maximize the yields of early progenitors and evaluate their quality. *Stem Cells.* 2002;20(6):530-541.
299. Davies BM, Snelling SJB, Quek L, et al. Identifying the optimum source of mesenchymal stem cells for use in knee surgery. *J Orthop Res.* 2017;35(9):1868-1875.
300. Zhai W, Yong D, El-Jawhari JJ, et al. Identification of senescent cells in multipotent mesenchymal stromal cell cultures: Current methods and future directions. *Cytotherapy.* 2019;21(8):803-819.
301. Sareen N, Sequiera GL, Chaudhary R, et al. Early passaging of mesenchymal stem cells does not instigate significant modifications in their immunological behavior. *Stem Cell Res Ther.* 2018;9(1):121.
302. Kaiser S, Hackanson B, Follo M, et al. BM cells giving rise to MSC in culture have a heterogeneous CD34 and CD45 phenotype. *Cytotherapy.* 2007;9(5):439-450.
303. Pettersson LF, Kingham PJ, Wiberg M, Kelk P. In Vitro Osteogenic Differentiation of Human Mesenchymal Stem Cells from Jawbone Compared with Dental Tissue. *Tissue Eng Regen Med.* 2017;14(6):763-774.
304. Shen C, Yang C, Xu S, Zhao H. Comparison of osteogenic differentiation capacity in mesenchymal stem cells derived from human amniotic membrane (AM), umbilical cord (UC), chorionic membrane (CM), and decidua (DC). *Cell Biosci.* 2019;9:17.
305. Rantalainen T, Nikander R, Heinonen A, Cervinka T, Sievanen H, Daly RM. Differential effects of exercise on tibial shaft marrow density in young female athletes. *J Clin Endocrinol Metab.* 2013;98(5):2037-2044.
306. Gungordu HI, Bao M, van Helvert S, Jansen JA, Leeuwenburgh SCG, Walboomers XF. Effect of mechanical loading and substrate elasticity on the osteogenic and adipogenic differentiation of mesenchymal stem cells. *J Tissue Eng Regen Med.* 2019;13(12):2279-2290.
307. Chen Q, Shou P, Zheng C, et al. Fate decision of mesenchymal stem cells: adipocytes or osteoblasts? *Cell Death Differ.* 2016;23(7):1128-1139.
308. James AW. Review of Signaling Pathways Governing MSC Osteogenic and Adipogenic Differentiation. *Scientifica (Cairo).* 2013;2013:684736.
309. Li H, Haudenschild DR, Posey KL, Hecht JT, Di Cesare PE, Yik JH. Comparative analysis with collagen type II distinguishes cartilage oligomeric matrix protein as a primary TGFbeta-responsive gene. *Osteoarthritis Cartilage.* 2011;19(10):1246-1253.
310. Otto F, Thornell AP, Crompton T, et al. Cbfa1, a candidate gene for cleidocranial dysplasia syndrome, is essential for osteoblast differentiation and bone development. *Cell.* 1997;89(5):765-771.

311. North TE, Stacy T, Matheny CJ, Speck NA, de Bruijn MF. Runx1 is expressed in adult mouse hematopoietic stem cells and differentiating myeloid and lymphoid cells, but not in maturing erythroid cells. *Stem Cells*. 2004;22(2):158-168.
312. Yano F, Ohba S, Murahashi Y, Tanaka S, Saito T, Chung UI. Runx1 contributes to articular cartilage maintenance by enhancement of cartilage matrix production and suppression of hypertrophic differentiation. *Sci Rep*. 2019;9(1):7666.
313. Yoshida CA, Yamamoto H, Fujita T, et al. Runx2 and Runx3 are essential for chondrocyte maturation, and Runx2 regulates limb growth through induction of Indian hedgehog. *Genes Dev*. 2004;18(8):952-963.
314. Levanon D, Bettoun D, Harris-Cerruti C, et al. The Runx3 transcription factor regulates development and survival of TrkC dorsal root ganglia neurons. *EMBO J*. 2002;21(13):3454-3463.
315. Brenner O, Levanon D, Negreanu V, et al. Loss of Runx3 function in leukocytes is associated with spontaneously developed colitis and gastric mucosal hyperplasia. *Proc Natl Acad Sci U S A*. 2004;101(45):16016-16021.
316. Yang YQ, Tan YY, Wong R, Wenden A, Zhang LK, Rabie AB. The role of vascular endothelial growth factor in ossification. *Int J Oral Sci*. 2012;4(2):64-68.
317. Kanawa M, Igarashi A, Ronald VS, et al. Age-dependent decrease in the chondrogenic potential of human bone marrow mesenchymal stromal cells expanded with fibroblast growth factor-2. *Cytotherapy*. 2013;15(9):1062-1072.
318. Akiyama H, Chaboissier MC, Martin JF, Schedl A, de Crombrughe B. The transcription factor Sox9 has essential roles in successive steps of the chondrocyte differentiation pathway and is required for expression of Sox5 and Sox6. *Genes Dev*. 2002;16(21):2813-2828.
319. Wang W, Rigueur D, Lyons KM. TGFbeta signaling in cartilage development and maintenance. *Birth Defects Res C Embryo Today*. 2014;102(1):37-51.
320. Sahu N, Budhiraja G, Subramanian A. Preconditioning of mesenchymal stromal cells with low-intensity ultrasound: influence on chondrogenesis and directed SOX9 signaling pathways. *Stem Cell Res Ther*. 2020;11(1):6.
321. Massague J. TGFbeta signalling in context. *Nat Rev Mol Cell Biol*. 2012;13(10):616-630.
322. Tzamelis I, Fang H, Ollero M, et al. Regulated production of a peroxisome proliferator-activated receptor-gamma ligand during an early phase of adipocyte differentiation in 3T3-L1 adipocytes. *J Biol Chem*. 2004;279(34):36093-36102.
323. Kheirandish M, Gavvani SP, Samiee S. The effect of hypoxia preconditioning on the neural and stemness genes expression profiling in human umbilical cord blood mesenchymal stem cells. *Transfus Apher Sci*. 2017;56(3):392-399.
324. Jing H, Zhang X, Gao M, et al. Kartogenin preconditioning commits mesenchymal stem cells to a precartilaginous stage with enhanced chondrogenic potential by modulating JNK and beta-catenin-related pathways. *FASEB J*. 2019;33(4):5641-5653.
325. Boyette LB, Creasey OA, Guzik L, Lozito T, Tuan RS. Human bone marrow-derived mesenchymal stem cells display enhanced clonogenicity but impaired differentiation with hypoxic preconditioning. *Stem Cells Transl Med*. 2014;3(2):241-254.
326. Choi JR, Pinguan-Murphy B, Wan Abas WA, et al. Impact of low oxygen tension on stemness, proliferation and differentiation potential of human adipose-derived stem cells. *Biochem Biophys Res Commun*. 2014;448(2):218-224.
327. Hildner F, Eder MJ, Hofer K, et al. Human platelet lysate successfully promotes proliferation and subsequent chondrogenic differentiation of adipose-derived stem cells: a comparison with articular chondrocytes. *J Tissue Eng Regen Med*. 2015;9(7):808-818.
328. Rikkers M, Levato R, Malda J, Vonk LA. Importance of Timing of Platelet Lysate-Supplementation in Expanding or Redifferentiating Human Chondrocytes for Chondrogenesis. *Front Bioeng Biotechnol*. 2020;8:804.

329. Kamekura S, Kawasaki Y, Hoshi K, et al. Contribution of runt-related transcription factor 2 to the pathogenesis of osteoarthritis in mice after induction of knee joint instability. *Arthritis Rheum.* 2006;54(8):2462-2470.
330. Spakova T, Plsikova J, Harvanova D, Lacko M, Stolfa S, Rosocha J. Influence of Kartogenin on Chondrogenic Differentiation of Human Bone Marrow-Derived MSCs in 2D Culture and in Co-Cultivation with OA Osteochondral Explant. *Molecules.* 2018;23(1).
331. Tateishi K, Ando W, Higuchi C, et al. Comparison of human serum with fetal bovine serum for expansion and differentiation of human synovial MSC: potential feasibility for clinical applications. *Cell Transplant.* 2008;17(5):549-557.
332. Thaweesapphithak S, Tantrawatpan C, Kheolamai P, Tantikanlayaporn D, Roytrakul S, Manochantr S. Human serum enhances the proliferative capacity and immunomodulatory property of MSCs derived from human placenta and umbilical cord. *Stem Cell Res Ther.* 2019;10(1):79.
333. Wagegg M, Gaber T, Lohanatha FL, et al. Hypoxia promotes osteogenesis but suppresses adipogenesis of human mesenchymal stromal cells in a hypoxia-inducible factor-1 dependent manner. *PLoS One.* 2012;7(9):e46483.
334. Sridharan G, Shankar AA. Toluidine blue: A review of its chemistry and clinical utility. *J Oral Maxillofac Pathol.* 2012;16(2):251-255.
335. Owida HA, De Las Heras Ruiz T, Dhillon A, Yang Y, Kuiper NJ. Co-culture of chondrons and mesenchymal stromal cells reduces the loss of collagen VI and improves extracellular matrix production. *Histochem Cell Biol.* 2017;148(6):625-638.
336. Voga M, Drnovsek N, Novak S, Majdic G. Silk fibroin induces chondrogenic differentiation of canine adipose-derived multipotent mesenchymal stromal cells/mesenchymal stem cells. *J Tissue Eng.* 2019;10:2041731419835056.
337. Kilian KA, Bugarija B, Lahn BT, Mrksich M. Geometric cues for directing the differentiation of mesenchymal stem cells. *Proc Natl Acad Sci U S A.* 2010;107(11):4872-4877.
338. Bistolfi A, Ferracini R, Galletta C, et al. Regeneration of articular cartilage: Scaffold used in orthopedic surgery. A short handbook of available products for regenerative joints surgery. 2017;1.
339. Merlin Rajesh Lal LP, Suraishkumar GK, Nair PD. Chitosan-agarose scaffolds supports chondrogenesis of Human Wharton's Jelly mesenchymal stem cells. *J Biomed Mater Res A.* 2017;105(7):1845-1855.
340. Croisier F, Jérôme C. Chitosan-based biomaterials for tissue engineering. *European Polymer Journal.* 2013;49:780–792.
341. Sultankulov B, Berillo D, Sultankulova K, Tokay T, Saparov A. Progress in the Development of Chitosan-Based Biomaterials for Tissue Engineering and Regenerative Medicine. *Biomolecules.* 2019;9(9).
342. Shepherd DE, Seedhom BB. The 'instantaneous' compressive modulus of human articular cartilage in joints of the lower limb. *Rheumatology (Oxford).* 1999;38(2):124-132.
343. Moshtagh PR, Pouran, B., Weinans, H., Zadpoor, A. The elastic modulus of articular cartilage at nano-scale and micro-scale measured using indentation type atomic force microscopy. *Osteoarthritis and Cartilage.* 2014;22.
344. Xue R, Li JY, Yeh Y, Yang L, Chien S. Effects of matrix elasticity and cell density on human mesenchymal stem cells differentiation. *J Orthop Res.* 2013;31(9):1360-1365.
345. Sun J, Tan H. Alginate-Based Biomaterials for Regenerative Medicine Applications. *Materials (Basel).* 2013;6(4):1285-1309.
346. Hwang CM, Ay B, Kaplan DL, et al. Assessments of injectable alginate particle-embedded fibrin hydrogels for soft tissue reconstruction. *Biomed Mater.* 2013;8(1):014105.
347. Almqvist KF, Wang L, Wang J, et al. Culture of chondrocytes in alginate surrounded by fibrin gel: characteristics of the cells over a period of eight weeks. *Ann Rheum Dis.* 2001;60(8):781-790.

348. Brito IR, Silva GM, Sales AD, et al. Fibrin-alginate hydrogel supports steroidogenesis, in vitro maturation of oocytes and parthenotes production from caprine preantral follicles cultured in group. *Reprod Domest Anim.* 2016;51(6):997-1009.
349. Perka C, Spitzer RS, Lindenhayn K, Sittinger M, Schultz O. Matrix-mixed culture: new methodology for chondrocyte culture and preparation of cartilage transplants. *J Biomed Mater Res.* 2000;49(3):305-311.
350. Pawar SN, Edgar KJ. Alginate derivatization: a review of chemistry, properties and applications. *Biomaterials.* 2012;33(11):3279-3305.
351. Choi S, Kim JH, Ha J, et al. Intra-Articular Injection of Alginate-Microencapsulated Adipose Tissue-Derived Mesenchymal Stem Cells for the Treatment of Osteoarthritis in Rabbits. *Stem Cells Int.* 2018;2018:2791632.
352. Dashtdar H, Rothan HA, Tay T, et al. A preliminary study comparing the use of allogenic chondrogenic pre-differentiated and undifferentiated mesenchymal stem cells for the repair of full thickness articular cartilage defects in rabbits. *J Orthop Res.* 2011;29(9):1336-1342.
353. Olivares-Navarrete R, Lee EM, Smith K, et al. Substrate Stiffness Controls Osteoblastic and Chondrocytic Differentiation of Mesenchymal Stem Cells without Exogenous Stimuli. *PLoS One.* 2017;12(1):e0170312.
354. Silver FH, Bradica G, Tria A. Elastic energy storage in human articular cartilage: estimation of the elastic modulus for type II collagen and changes associated with osteoarthritis. *Matrix Biol.* 2002;21(2):129-137.
355. Lehmann R, Gallert C, Roddelkopf T, Junginger S, Wree A, Thurow K. 3 dimensional cell cultures: a comparison between manually and automatically produced alginate beads. *Cytotechnology.* 2016;68(4):1049-1062.
356. Grabska-Zielinska S, Sionkowska A, Carvalho A, Monteiro FJ. Biomaterials with Potential Use in Bone Tissue Regeneration-Collagen/Chitosan/Silk Fibroin Scaffolds Cross-Linked by EDC/NHS. *Materials (Basel).* 2021;14(5).
357. Kuhn PT, Rozenbaum RT, Perrels E, Sharma PK, Van Rijn P. Anti-Microbial Biopolymer Hydrogel Scaffolds for Stem Cell Encapsulation. *Polymers (Basel).* 2017;9(4).
358. Deepthi S, Jayakumar R. Alginate nanobeads interspersed fibrin network as in situ forming hydrogel for soft tissue engineering. *Bioact Mater.* 2018;3(2):194-200.
359. Lotz MK, Otsuki S, Grogan SP, Sah R, Terkeltaub R, D'Lima D. Cartilage cell clusters. *Arthritis Rheum.* 2010;62(8):2206-2218.
360. Misra S, Hascall VC, Markwald RR, Ghatk S. Interactions between Hyaluronan and Its Receptors (CD44, RHAMM) Regulate the Activities of Inflammation and Cancer. *Front Immunol.* 2015;6:201.
361. Moussa M, Lajeunesse D, Hilal G, et al. Platelet rich plasma (PRP) induces chondroprotection via increasing autophagy, anti-inflammatory markers, and decreasing apoptosis in human osteoarthritic cartilage. *Exp Cell Res.* 2017;352(1):146-156.
362. Patel VR, Amiji MM. Preparation and characterization of freeze-dried chitosan-poly(ethylene oxide) hydrogels for site-specific antibiotic delivery in the stomach. *Pharm Res.* 1996;13(4):588-593.
363. Andersen T, Auk-Emblem P, Dornish M. 3D Cell Culture in Alginate Hydrogels. *Microarrays (Basel).* 2015;4(2):133-161.
364. Guarino V, Caputo T., Altobelli R., Ambrosio L. Degradation properties and metabolic activity of alginate and chitosan polyelectrolytes for drug delivery and tissue engineering applications. *AIMS Materials Science.* 2015;2(4):497-502.
365. Troeberg L, Nagase H. Proteases involved in cartilage matrix degradation in osteoarthritis. *Biochim Biophys Acta.* 2012;1824(1):133-145.
366. Gao Z, Yang X, Jones E, et al. An injectable, self-healing and MMP-inhibiting hyaluronic acid gel via iron coordination. *Int J Biol Macromol.* 2020;165(Pt B):2022-2029.

367. Limraksasin P, Kosaka Y, Zhang M, et al. Shaking culture enhances chondrogenic differentiation of mouse induced pluripotent stem cell constructs. *Sci Rep.* 2020;10(1):14996.
368. Shen C, Jiang T, Zhu B, et al. In vitro culture expansion impairs chondrogenic differentiation and the therapeutic effect of mesenchymal stem cells by regulating the unfolded protein response. *J Biol Eng.* 2018;12:26.
369. Maredziak M, Marycz K, Tomaszewski KA, Kornicka K, Henry BM. The Influence of Aging on the Regenerative Potential of Human Adipose Derived Mesenchymal Stem Cells. *Stem Cells Int.* 2016;2016:2152435.
370. Yang X, Qi Y, Avercenc-Leger L, et al. Effect of nicotine on the proliferation and chondrogenic differentiation of the human Wharton's jelly mesenchymal stem cells. *Biomed Mater Eng.* 2017;28(s1):S217-S228.
371. Bernstein P, Sticht C, Jacobi A, Liebers C, Manthey S, Stiehler M. Expression pattern differences between osteoarthritic chondrocytes and mesenchymal stem cells during chondrogenic differentiation. *Osteoarthritis Cartilage.* 2010;18(12):1596-1607.
372. Ullah M, Hamouda H, Stich S, Sittinger M, Ringe J. A reliable protocol for the isolation of viable, chondrogenically differentiated human mesenchymal stem cells from high-density pellet cultures. *Biores Open Access.* 2012;1(6):297-305.
373. Garcia J, Mennan C, McCarthy HS, Roberts S, Richardson JB, Wright KT. Chondrogenic Potency Analyses of Donor-Matched Chondrocytes and Mesenchymal Stem Cells Derived from Bone Marrow, Infrapatellar Fat Pad, and Subcutaneous Fat. *Stem Cells Int.* 2016;2016:6969726.
374. Solchaga LA, Penick KJ, Welter JF. Chondrogenic differentiation of bone marrow-derived mesenchymal stem cells: tips and tricks. *Methods Mol Biol.* 2011;698:253-278.
375. Armiento AR, Alini M, Stoddart MJ. Articular fibrocartilage - Why does hyaline cartilage fail to repair? *Adv Drug Deliv Rev.* 2019;146:289-305.
376. Mapp PI, Walsh DA. Mechanisms and targets of angiogenesis and nerve growth in osteoarthritis. *Nat Rev Rheumatol.* 2012;8(7):390-398.
377. Fernandes TL, Kimura HA, Pinheiro CCG, et al. Human Synovial Mesenchymal Stem Cells Good Manufacturing Practices for Articular Cartilage Regeneration. *Tissue Eng Part C Methods.* 2018;24(12):709-716.
378. Lin S, Lee WYW, Xu L, et al. Stepwise preconditioning enhances mesenchymal stem cell-based cartilage regeneration through epigenetic modification. *Osteoarthritis Cartilage.* 2017;25(9):1541-1550.
379. Pisciotta A, Riccio M, Carnevale G, et al. Human serum promotes osteogenic differentiation of human dental pulp stem cells in vitro and in vivo. *PLoS One.* 2012;7(11):e50542.
380. Harnroongroj T, Volpert LG, Ellis SJ, Sofka CM, Deland JT, Demetracopoulos CA. Comparison of Tibial and Talar Bone Density in Patients Undergoing Total Ankle Replacement vs Non-Ankle Arthritis Matched Controls. *Foot Ankle Int.* 2019;40(12):1408-1415.
381. Yuan XL, Meng HY, Wang YC, et al. Bone-cartilage interface crosstalk in osteoarthritis: potential pathways and future therapeutic strategies. *Osteoarthritis Cartilage.* 2014;22(8):1077-1089.
382. Jia H, Ma X, Wei Y, et al. Loading-Induced Reduction in Sclerostin as a Mechanism of Subchondral Bone Plate Sclerosis in Mouse Knee Joints During Late-Stage Osteoarthritis. *Arthritis Rheumatol.* 2018;70(2):230-241.
383. Erggelet C, Vavken P. Microfracture for the treatment of cartilage defects in the knee joint - A golden standard? *J Clin Orthop Trauma.* 2016;7(3):145-152.
384. Abraham AC, Pauly HM, Donahue TL. Deleterious effects of osteoarthritis on the structure and function of the meniscal enthesis. *Osteoarthritis Cartilage.* 2014;22(2):275-283.